BEHAVIOUR OF STRUCTURALLY INSULATED PANELS

A Thesis

Submitted in fulfilment of the requirement for the award of the degree of

DOCTOR OF PHILOSOPHY
IN
CIVIL ENGINEERING

UPENDER BISHNOI
Registration No. 901502002

DEPARTMENT OF CIVIL ENGINEERING
THAPAR INSTITUTE OF ENGINEERING AND TECHNOLOGY
(DEEMED UNIVERSITY)
PATIALA-147004
PUNJAB (INDIA)
2024

CERTIFICATE

I, Upender Bishnoi, **hereby declare that the thesis entitled, "Behaviour of Structurally Insulated Panels" submitted to Thapar Institute of Engineering and Technology,** Patiala, in partial fulfilment of the requirement of the award of Degree of Doctor of Philosophy in Civil Engineering is a record of original and independent research work done by me. This thesis has been conducted under the supervision and guidance of **Dr. Naveen Kwatra**, Professor, Department of Civil Engineering, Thapar Institute of Engineering and Technology, Patiala, and **Dr. A.B. Danie Roy**, Assistant Professor, Department of Civil Engineering, Thapar Institute of Engineering and Technology, Patiala. It has not formed the basis for the award of any Degree to any candidate of any university.

U Bishnoi

(Upender Bishnoi)

Registration No. 901502002

This is to certify that the above-mentioned statement made by the candidate is correct to the best of my knowledge.

Dr Naveen Kwatra
Professor,
Department of Civil Engineering
Thapar Institute of Engineering and Technology (Deemed University),
Patiala, Punjab, India

Dr. A.B Danie Roy
Assistant Professor,
Department of Civil Engineering
Thapar Institute of Engineering and Technology (Deemed University),
Patiala, Punjab, India

ACKNOWLEDGEMENT

The Almighty has granted me the precious chance to convey my profound appreciation to my guides for their invaluable assistance and unfailing support during the duration of my research project. My deepest gratitude goes out to my advisors in the civil engineering department at Patiala's Thapar Institute of Engineering and Technology, Dr. Naveen Kwatra, Professor, he has guided me throughout my journey of PhD with his wisdom and experience. He shared the knowledge of the subject which is very useful for the understanding the subject. He helped me to expand my horizon in this field of research. He also made me think practically, that how the research can be useful for the society.

My co-supervisor Dr. A. B. Danie Roy, Assistant Professor, helped me out in every difficult situation and the challenges I faced while achieving my goal. He helped me to search for the answers related to my analysis of results obtained, which otherwise would be very difficult to achieve. He is been very kind to me just as an elder brother guiding his younger brother through the swiftness of different phases of PhD.

Their careful direction, helpful critique, and unfailing support saw me through to the end of the project, and I will be eternally grateful to them. Their methodical approach and unwavering support motivated me to put in extra effort. This thesis would not have been feasible without the indefatigable work of these individuals and their exceptional expertise in the field.

I express my gratitude to Dr. Shruti Sharma, HCED, and Dr. Prem Pal Bansal former HCED for furnishing me with lab facilities and an exceptional academic environment. Additionally, I would like to extend my gratitude to the doctoral committee members, Dr. Rafat Siddique, Dr. Heaven Singh, and Dr. Sandeep Kumar Sharma, for their unwavering encouragement and assistance throughout the experimental process. In addition, I would like to extend my gratitude to the entire supporting staff, with particular recognition to Sh. Ram Sumiran, Mr.

Manreet Singh, and Mr. Hitesh, for their invaluable assistance throughout the experimental setup preparation process. I also appreciate the assistance of the Structure lab. I want to acknowledge Dr. Siva R. Chidambaram, Senior Scientist, CBRI, Roorkee, Uttrakhand for helping me out in my testing of samples by providing me with every piece of equipment possible and also helping me analyze the results.

As they say “It’s all about the Journey, not the destination”, this journey was tough but most satisfying. I would be honored to take this opportunity to express my utmost gratitude to my pillar of strength, my parents, Late Sh. Inderjit Bishnoi and my mother Ms. Suman Bishnoi for always showering their blessings. It will be incomplete without the mention of my wife Mrs. Jyoti Bishnoi, for bearing with me throughout this period. One’s life is filled with joy by my friends, Dr. Kamal Anand and Dr. Kirti Vardhan Singla, Mr. Mandeep Walia, Dr. Tarunbir Singh, Dr. Payal Sachdeva, Dr. Divyashree who has been very supportive throughout technical issues and experimental work. Dr. Sunil Garhwal and would-be doctor Mr. Anil Garhwal helped me a lot in the initial testing phase.

Would be doctors, Mr. Amandeep Singh Sidhu, Mr. Harvinder Singh, Mr. Ankit Kumar, Mr. Akshay Sharma, Mr. Ajay Chalotra, Mr. Pavitar Singh and Mr. Himanshu Guleria for helping me out in the last phase of my PhD. In last, I would like to thank all my PhD colleagues who made this journey wonderful and memorable.

(Upender Bishnoi)

LIST OF PUBLICATIONS

Publication in SCI index journals:

- U. Bishnoi, A.B. Danie Roy, N. Kwatra, Out of plane performance of novel concrete sandwich panel using different geosynthetics, Construction Building Materials. 300 (2021) 124186. (Impact Factor:7.61) https://doi.org/10.1016/j.conbuildmat.2021.124186.
- Upender Bishnoi, A. B. Danie Roy & Naveen Kwatra (02 Nov 2023): In-plane shear behaviour of concrete sandwich panels reinforced with various geogrids, European Journal of Environmental and Civil Engineering (Impact Factor: 2.26)
  DOI: 10.1080/19648189.2023.2276141

ABSTRACT

The transition from conventional practices, such as traditional brick masonry, to contemporary construction methods like concrete sandwich panels is gaining notable traction. This shift not only reflects a growing trend but also signifies a substantial movement towards more advanced and efficient construction techniques in the modern era. The primary aim of the study is to examine the behaviour of concrete sandwich panels reinforced with geosynthetics in terms of out-of-plane, in-plane shear, and compression. Two forms of geosynthetic material are being utilised, specifically plastic uniaxial geogrid (PUG) and polyester biaxial Geogrid (PBG). Two types of mixes have been used to further enhance the understandability of the behaviour of concrete sandwich panels

The flexural behaviour of concrete sandwich panels strengthened with geosynthetics is examined in first phase of this study. The panels are tested under a monotonically increasing load using a hydraulic jack. The load–deflection curves of the panels were examined to evaluate the effect of geosynthetics on the strength, stiffness, and deformability of panels. The result shows that plastic geogrid reinforced sandwich panels enhanced the flexural strength and ductility of panels compared with control specimens. Polyester geo-grid as reinforcement is also found to be relatively better in restoring the deformability and energy absorption of panels. The results show a gain of about 28% in plastic geogrid (SPGG); 36.8% in the case of polyester geogrid (SGi200), in comparison with the control specimen.

In-plane diagonal shear strength of concrete sandwich panels, and the effect of incorporating geogrids on the deformation capability and load-bearing capacity is also reported in the study. In contrast to the control specimen, specimens cast with plastic geogrid had a 13.7% and 26% improvement in shear capacity and load-bearing capability for the two types of micro-concrete mixes used in this study. Diagonal shear specimen containing PUG is effective in improving the concrete sandwich panels' load-bearing capacity, shear capacity, and deformation ability. PBG enhanced the ductility of the concrete sandwich panels.

Axial compression testing of these concrete sandwiched panels supported the above mentioned parameters as PUG containing specimen outperformed the control specimen. On the3 other hand the specimen containing PBG enhanced the deformation capacity of the concrete sandwich panel .the results are supported by the energy dissipation values computed from the area under the curve in the load vs deformation graph.

In second phase of the study two dimensional reinforced concrete frames has been cast using CSP as infill wall and compared with brick masonry as infill wall. Three single bay and

single story RC frame specimens were tested under reversed cyclic lateral loading. It has been found that addition of sandwich panels led to a considerable increase in the lateral stiffness and strength, ductility, energy dissipation capacity.

The 2D RC frame with concrete sandwich panel as an infill wall exhibits greater ductility compared to the brick masonry. The increase in lateral load capacity can be attributed to the enhanced rigidity of the concrete sandwich panel. Furthermore, the calculation of energy dissipation is consistent with the values derived from the hysteresis curve. A comparison is made between a 2D reinforced concrete (RC) frame with a concrete sandwich panel that has a door opening, and a 2D RC frame with a complete concrete sandwich panel infill wall subjected to lateral load. Upon comparing it with the other 2D RC CSP frame, it was seen that the opening resulted in significant deformations of the CSP.

The flexure, diagonal shear and axial compression specimen have been subjected to numerical simulation using CAD software to create the geometry and ANSYS Workbench, a FEM software, to analyse it. The simulation results are highly consistent with the experimental findings.

TABLE OF CONTENTS

LIST OF TABLES

LIST OF FIGURES

ABBREVIATIONS

CSP	Concrete Sandwich Panel
SIP	Structurally Insulated Panels
RC	Reinforced Concrete
2D	Two Dimensional
PUG	Plastic Uniaxial Geogrid
PBG	Polyester Biaxial Geogrid
PBG2	Polyester Biaxial Geogrid Sgi200
PBG3	Polyester Biaxial Geogrid Sgi300
EIFS	External Insulation and Finish System
ICF	Insulated concrete Foams
SWP	Sandwich Wall Panels
EPS	Expanded Polystyrene
PUR	Polyurethane
SFRSCC	Steel Fiber Reinforced Self compacting Concrete
CFRP	Carbon Fiber Reinforced Polymer
BFRC	Basal Fiber Reinforced Composite
BFRP	Basal Fiber Reinforced Polymer
GFRP	Glass Fiber Reinforced Polymer
LGSF	Lighjt Gauge Steel Frame
RCSP	Reinforced Concrete Sandwich Panel
FEA	Finite Element Analysis
FEM	Finite Element Method
HDPE	High Density Polyethylene
FRP	Fiber Reinforced polymer
ACI	American Concrete Institute
FE	Finite Element
AAC	Aerated concrete
FRAC	Foam Reinforced Aerated Concrete
CSWP	Concrete Sandwich Wall Panel
PCSP	Precast Concrete Sandwich Panels

RCSP	Reinforced Sandwich Concrete Panel
DIC	Digital Image Correlation
ECC	Engineered Cementitious Composite
TRC	Textile Reinforced Concrete
URM	Unreinforced Masonry
TRM	Textile Reinforced Mortar
PVA	Polyvinyl Alcohol
CRM	Composite Reinforced Mortars pp
PP	Polypropylene
CSIP	Composite Structural Insulated Panels
DSC	Double Steel Shear Connector
FCS	Foamed Concrete Sandwich Walls
SSC	Single Steel Shear Connector
FFRP	Flax Fiber Reinforced Polymer
PIR	Polyisocyanurate
BJR	Bed Joint Reinforcement
FRCM	Fabric Reinforced Cementitious Matrix
CSP-ISF	Concrete Sandwich Panel- Infilled Steel Frames
MD	Machine Direction
CMD	Cross Machine Direction
WWM	Welded Wire Mesh
SP	Sandwich Panel
LVDT	Linear Variable Differential Transformer
UTM	Universal Testing Machine
DOF	Degree of Freedom
CAD	Computer Aided Design
ITZ	interfacial Transition zone
Fck`	Compression resistance to deformation
E_c	Modulus of Elasticity of Concrete
Py	Yield Load
Pu	Ultimate Load
Δy	Deflection at yield

LIST OF UNITS

kN	Kilo Newton
mm	Millimeter
cm	Centimeter
kN.mm	Kilo Newton millimeter
N	Newton
MPa	Mega Pascal
kg/m^3	Kilogram per cubic meter
min	Minutes
sec	Second
GPa	Giga Pascal
%	Percent

Chapter 1

Introduction

1.1 General

In this world of changing technologies, time is a very precious commodity. When talking about construction, it is even more precious. Various new construction techniques have been introduced in the market to challenge the conventional method of construction (laying brick by brick). Easy and fast construction is the requirement of today's world, hence technologies such as light gauge steel frame (LGSF), concrete sandwich panels (CSP), etc. are being used. Sandwich panel is one such method of rapid construction. These sandwich panels have been in use since the early 1930s in the North American continent. They gained popularity in the late 1970s. India is currently the fastest-growing economy in the world and for that infrastructure is the major key to sustaining it. So India is also adopting these new emerging construction techniques. The availability of affordable housing is a significant indicator of the financial and social empowerment of a nation's population. India's urban population in the year 2022 was 508 million and it is expected to reach 675 million in the year 2035, if this trend continues then the urban population is expected to reach 2.2 billion by 2050 (United Nations, 2022; World Bank, 2023).

According to recent research, there is a significant deficit of housing dwellings in both urban and rural areas, amounting to roughly 70 million units (Shanker Singh & Narayan Pandey, 2012) . The high demand for affordable housing units can be attributed to factors such as rapid urbanization, population growth, and a significant shortage of residential houses. Meeting the demand for housing units within a limited timeframe poses a significant challenge when relying on traditional building materials such as burnt clay bricks, stone blocks, timber, cement, sand, and reinforcement, as well as conventional construction systems like load-bearing walls and framed structures. The time-consuming nature of construction using these conventional methods further exacerbates the difficulty in fulfilling the housing demand promptly. Given the existing limitations, there arises a necessity for exploring alternative construction systems that possess qualities such as rapidity, cost-effectiveness, energy efficiency, durability, and disaster resilience. These attributes are crucial to facilitate the provision of secure and affordable housing options. The availability of resources for conventional building materials is limited. The increasing demand for a particular product or

service has both direct and indirect consequences. These consequences include cost escalation, which refers to the direct impact on the price of the product or service due to increased demand. Additionally, there is the indirect consequence of rapid and irrational utilization, which refers to the accelerated and irrational consumption patterns resulting from the increased demand. Moreover, this phenomenon will result in the depletion of valuable topsoil, the destruction of forests, and the degradation of the environment.

In a seminal study conducted by Lee et al. (2006), the authors delineated the key attributes that define the optimal technologies for the forthcoming construction industry. These attributes encompass affordability, energy efficiency, durability, safety, economic viability, cultural acceptability, rapid applicability, adaptability, environmental sustainability, non-proprietary nature, ease of maintenance, and reproducibility in diverse markets. By identifying and emphasizing these characteristics, Lee et al. (2006) provide a comprehensive framework for the development and implementation of future construction technologies. Further studies have also been conducted in same context by O'Hegarty et al. (2021). Considering the aforementioned attributes, the utilization of cast-in-situ/precast reinforced sandwich panels and composite panels in construction exhibits considerable potential as a viable technique for forthcoming building projects. Sandwich composite panels typically consist of a central layer, referred to as the 'core', composed of a low-strength material. This core is sandwiched between two outer layers, known as 'wythes', which are made of high-strength skin materials. The purpose of this configuration is to provide enhanced structural integrity and protection to the core material. The inclusion of reinforcement or wire mesh within the wythes of a structure is a variable factor that may or may not be present. The determination of core thickness and type is influenced by thermal resistance and design temperatures, while the thickness of wythes is primarily dictated by structural considerations. The primary purpose of wythes in construction is to fulfil several essential functions, including load resistance, reinforcement coverage, durability, connector anchorage, and surface finish. These functions collectively contribute to the overall structural integrity and performance of the construction system. In typical construction practices, it is common for the thickness of the wythes to be comparatively lesser than that of the core.

The sandwich panels have been used as partition walls i.e. a non-load-bearing member (Ferreira et al., 2023). But now as the technology advanced they are used as a structural load-bearing member. For the sandwich panel to possess structural integrity, there must be a

connecting element that joins the wythes and allows the entire panel to function as an integrated unit. The rigid behaviour of CSP is due to the welded wire mesh and the shear connectors.

A shear connector is an element that connects the wythes and ensures the composite behaviour of the panel or concrete sandwich panel (CSP). Different types of shear connectors have been used in the past. The type and orientation of the shear connector are responsible for the degree of composite action of the concrete sandwich panel. Various types of connectors that have been used previously by many different researchers are either steel or polymer-based. Different polymers used as shear connectors are basalt fiber-reinforced polymer (BFRP), glass fiber-reinforced polymer (GFRP), fiber-reinforced polymer (FRP), and carbon fiber-reinforced polymer (CFRP) (Gu & Lu, 2023a). The orientation of these shear connectors plays a vital role in the overall performance of concrete sandwich panels under different loading conditions. Concrete sandwich panels have started gaining popularity as they can be erected easily and are less time-consuming than the conventional method of laying bricks. In a reinforced frame brick masonry wall is considered a non-structural member, CSP is a replacement for such walls first. In a few parts of the country, low-rise buildings have been constructed by using these concrete sandwich panels, and beams and columns have been eliminated from the structure. It is very difficult to imagine living in a building with no beams and columns as it is different from the conventional way of building a structure. Different research is going on these concrete sandwich panels and their extensive use is being promoted due to the reliable results obtained in the research.

1.2 Conventional Materials

Traditionally, building materials used in the construction are rock, mud, clay, cement blocks, concrete, and cement mortar bricks.

- *Fired Clay Bricks:* Fired bricks undergo a high-temperature firing process within a kiln, resulting in enhanced durability. In the typical composition of brick, the primary constituents are Silica, Alumina, Lime, Iron oxide, and Magnesia. These ingredients are responsible for the structural and chemical properties exhibited by brick materials. Silica, commonly sourced from sand, contributes to the overall strength and durability of the brick due to its high melting point and resistance to deformation. Alumina, derived from clay, aids in enhancing the plasticity and workability of the brick during the manufacturing process. Lime acts as a fluxing agent, facilitating the fusion of other components.

- *Mud Brick (Adobe Brick):* Unfired bricks, commonly referred to as mud bricks, are a type of construction material produced by combining a moist soil composition containing clay with reinforcing elements such as straw or comparable binders. The specimens undergo an air-drying process until they reach a state suitable for utilization.
- *Stone Bricks:* The utilization of this particular technology has been observed for an extensive duration. Stone masonry, a traditional construction technique, encompasses two primary types: ashlar masonry and rubble masonry. Ashlar masonry refers to the precise arrangement of cut and dressed stones, resulting in a uniform and aesthetically pleasing appearance. On the other hand, rubble masonry involves the use of irregularly shaped stones, typically in their natural form, creating a more rustic and organic look.
- *Concrete Blocks:* Concrete bricks, commonly referred to as blocks, are typically characterized by their pale grey hue. The construction material utilized in their fabrication consists of a dry, finely graded aggregate concrete mixture. This mixture is meticulously placed within robust steel molds and subjected to vigorous vibration and compaction techniques. The cured process of the finished blocks involves the utilization of low-pressure steam. Concrete blocks exhibit a significantly broader spectrum of shapes and dimensions in comparison to clay bricks, while also offering a more extensive selection of face treatments. When constructed with an appropriate proportion of cement, these structures exhibit a high level of suitability for challenging environmental conditions, such as wet environments and applications involving the retention of soil or other materials. Concrete blocks exhibit comparable thermal and sound resistance, as well as fire resistance, to other bricks of equivalent density.

1.3 Masonry structures

Brick masonry is a robust construction method where bricks are bound together using cement mortar, forming a durable structure. It is adept at accommodating minor ground movements caused by differential settlement of foundations. Known for its historical durability and resilience against weathering, brick masonry is a cost-effective choice that can be easily constructed with semi-skilled labor. Repairing damaged sections involves removing the affected area and rebuilding with new bricks. Under regular gravity loads, masonry performs well; however, it faces challenges under extreme conditions like earthquakes, often leading to partial or total collapse and significant loss of lives.

Several factors contribute to the vulnerability of masonry structures. Their brittle nature, combined with substantial self-weight, makes them prone to sudden and unpredictable

failure, leaving occupants with insufficient time to seek safety. In developing countries, variations in the crushing strength of locally available bricks further impact the reliability of masonry. Failures primarily occur against horizontal forces, causing flexure due to out-of-plane bending and shear due to in-plane bending (Figure 1.1). Masonry's inability to resist tensile stresses induced by these forces results in sudden collapse. Cracks develop along bed joints in flexure and diagonally due to in-plane forces. Past earthquakes in various parts of India have documented such failures, emphasizing the need for caution when using brick masonry, particularly in earthquake-prone regions.

Figure 1. 1: Failure of masonry walls (a) In-plane failure of wall of District court building at Bhuj (Dubey, R.N., 2011); (b) Diagonal cracks in the short pier in Zila Panchayat building at Bhuj (Dubey, R.N., 2011)

Common issues happen with buildings made of bricks that don't have any extra support. One major problem is when the walls that are supposed to stand against sideways shaking during an earthquake end up bending and cracking, causing them to fall. This happens a lot in buildings made of bricks without extra support. The walls can break at the corners and in the middle, forming vertical cracks. This is called out-of-plane failure. It's a big problem for buildings made without any extra strengthening. One reason this happens is that the bricks are not attached well to the roof, and the bricks and the material holding them together are not strong enough to handle the sideways shaking. The walls end up breaking because they can't handle the pressure. This type of problem is more likely to happen higher up in the building and can cause parts of the outer wall to fall off or crack. It's not as common in the lower parts of the building.

Sometimes, the walls of a building can bend and crack in a different way when there's an earthquake. This happens when the walls are supposed to stand against the shaking, but they

end up bending and cracking inside the building. The bending can be horizontal or diagonal, forming cracks in the wall. This is called in-plane failure. For walls made without extra support, cracking can be more common, especially in the shape of an "X." This is because the walls can't handle the bending and shear forces well. The cracks show where the walls are not strong enough to handle repeated shaking, and this can lead to the whole wall falling. Luckily, if the building shakes only a little or for a short time, the walls might not collapse completely. However if the cracks become too severe, the walls might not be able to hold the weight of the building. Cracks often happen more in the lower parts of the building, especially in short pillars or slender pillars that rock back and forth.

During an earthquake, the forces that affect buildings come from two directions, which means each part of a building has to deal with forces pushing and pulling in both directions. For certain parts of a building made without extra support (URM elements), there can be cracking that happens when the building shakes. This cracking is especially weaker when the building is pushed or pulled from the sides (out-of-plane direction) compared to the original, uncracked condition. This means that when the building shakes, certain parts might not be as strong in one direction, making them more vulnerable to damage.

1.4 Modern Building Methods

In light of recent advancements in building technology, numerous novel materials have emerged to construct walls in buildings, taking into consideration the limitations of traditional approaches. Materials other than conventional materials used in structural engineering can be classified into different categories:

1. Variable-density concrete panels: To optimize thermal storage capabilities, enhance insulation properties, and ensure the production of a high-quality end product, the variable-density concrete panel concept was introduced. The variable density concrete panel, as depicted in Figure 1.2, is fabricated utilizing a singular concrete mix that undergoes vibration to attain the desired characteristics:

- Lightweight insulating top (outside) layer with low thermal conductivity providing good insulation
- Heavy/normal weight material, dense bottom (inside) layer with high specific heat to provide thermal mass and sufficient strength for construction handling and to withstand service loads.

2. EIFS (External Insulation and finish system): First, EPS sheets with the appropriate thickness and density—typically 20 kg/m^3 and above—are fastened to the building's exterior. As the sheets are being finished on the exterior of the walls, an adhesive known as "Base Coat," a polymer-mixed cement, is utilized. Supplemental fasteners and adhesives can secure the sheets to the wall surface. After affixing EPS sheets to the entire surface, a trowel is used to apply a uniform base layer to the EPS. A fiber-wire mesh is utilized on the surface of the base coat.

While wet, fiber mesh is easily attached to the surface. For complete mesh embedding in the base coat, an additional coat of 'base coat' is equally put over the wire mesh. The fiber-wire mesh strengthens the EPS surface. The surface hardens and resembles a wall surface poured with cement after a day. On this surface, an external primer is then applied. The finish coat, the second major part of this method, is an acrylic substance that gives the wall a textured appearance (Figure 1.3).

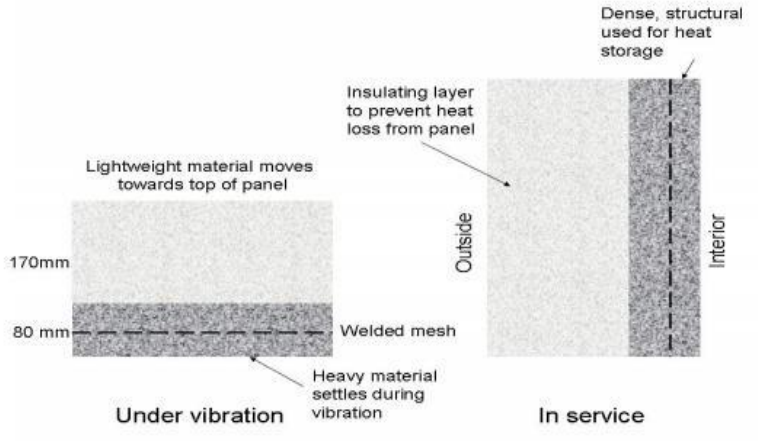

Figure 1.2**:** Illustration of variable density concrete panel (Mackechnie et al., 2007)

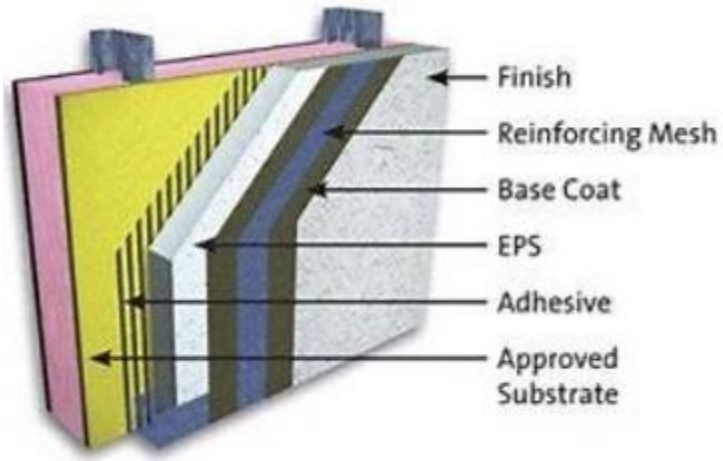

Figure 1.3: Illustration of EIFS (External Insulation and Finish System) (Almasri et al., 2021)

3. ICF (Insulated concrete foams): ICFs are box-shaped expanded polystyrene (EPS) items with open tops and bottoms. The upper and lower edges possess interlocking characteristics, resulting in a secure connection when stacked on each other. The wall cavity is filled with concrete after the ICF (insulated concrete forms) are positioned to create the wall. A specific duration is allocated for the concrete to solidify before pouring the subsequent layer on top. The rebar can be positioned in horizontal and vertical orientations and secured with ties before pouring the concrete. This enhances the wall's lateral stability. Once the wall hollow is filled with concrete, the outside and interior EPS surfaces can be completed using various methods. GFRC (Glass Fibre Reinforced Cement) finish, which uses a fiber wire mesh, can be used for wall surface finishing. A polymer-modified cement paste, excluding sand, is applied thinly onto the surface using a trowel.

4. Sandwich Wall Panels (SWPs): Structural insulated panels (SIPs) are a high-performance building system for residential and light commercial construction. The panels consist of an insulating foam core sandwiched between two structural facings. Typically, sandwich panels consist of wythes made from either concrete or concrete-based polymers, reinforced with wire mesh, bars, fibers, and polymer textiles. The selection of the Wythe material and its thickness are determined by factors such as the magnitude of the load to be withstood, the desired durability, and the required level of fire resistance. Sandwich panels are constructed using various types and strengths of concrete, including normal concrete (NC), foamed concrete (FC), self-compacting concrete (SCC), high-performance concrete (HPC), high-performance fiber reinforced concrete (HPFRC), glass-reinforced concrete (GPC), reactive powered concrete (RPC), and ultra-high performance concrete (UHPC).

The compressive strength of the concrete used in the wythes ranges from 8 MPa for FC to 193 MPa for UHPC. Textile-reinforced concrete has been employed as a solution to address the issue of durability. Textile materials are resistant to corrosion, although they have a high cost. Different types of sandwich panels and connector types are described in Table 1.1.

1.5 Reinforced concrete sandwich panel

A reinforced concrete sandwich panel is a composite construction element consisting of two outer layers of concrete, known as the faces, separated by a core material that enhances its structural performance. The faces typically serve as the load-bearing components, while the core contributes to the panel's stiffness, insulation, or other desired properties (O’ Hegarty et

al., 2021). Reinforcement, often in the form of steel bars or mesh, is integrated into the concrete to enhance its tensile strength and overall durability. These panels are widely used in construction for applications such as walls, floors, and roofs due to their versatility, strength, and thermal insulation properties.

Table 1.1 Composite sandwich panel details

S No.	Core material	Type of wythe	Connector types and material	Author
1.	Expanded Polystyrene (EPS)	Precast, pre-stressed concrete	CFRP (Carbon Fiber Reinforced Polymer)	(Frankl, 2008)
2.	Expanded Polystyrene (EPS)	Shotcrete concrete with 3mm diagonal galvanized, steel welded wire mesh	Galvanized steel wire truss	(Ricci et al., 2013)
3.	Polyurethane (PUR)	SFRSCC (Steel Fiber Reinforced Self – compacting concrete)	GFRP (glass fiber reinforced polymer)	(Lameiras et al., 2013)
4.	Polystyrene foam (EPS)	Glass-fibre reinforced magnesia cement boards	Only adhesive layer, no shear connectors	(Smakosz & Tejchman, 2014)
5.	Expanded Polystyrene (EPS)	Ferro-cement layers reinforced with one layer of woven wire mesh	Steel wires	(Hafiza et al., 2015)
6.	Polyurethane (PUR)	TRC (Textile Reinforced concrete) or UHPFRC (ultra-high performance fiber reinforced concrete)	Syspropin made up of GFRP	(Shams et al., 2015)

The manufacturing process of reinforced concrete sandwich panels involves casting the outer layers of concrete with the embedded reinforcement around the core material. The core can be made from various materials like foam, lightweight aggregates, or other composite materials, depending on the specific requirements of the application. The resulting structure combines the benefits of the individual components, creating a strong and efficient construction material. Reinforced concrete sandwich panels find use in both residential and commercial buildings, offering advantages such as reduced weight, improved thermal insulation, and faster construction times compared to traditional building methods.

1.6 Procedure of construction using concrete sandwich panel

EPS panels with a standardized width of 1.2 m are manufactured in a factory. The length of these panels can vary between 2.8 m and 4.5 m, depending on the specific requirements for the height or span of the building. A single person may easily carry and handle one EPS panel. Expensive site equipment, such as cranes and hoisting devices, is unnecessary for the installation of EPS structures. Light footings, such as strip footing or mat foundation, can be used by the building plan to reduce the overall weight. The vertical reinforcement, also known as dowel bars, is intentionally left in place to secure the wall panels (Refer to Figure 1.4). The EPS panels are positioned in a manner that the vertical reinforcement is put between the mesh and polystyrene, and the alignment of the wall is carried out. Rebar dowels can be installed on an existing foundation slab using drilling. Additionally, alternative techniques such as metal channels or U-shaped welded wire mesh can be employed.

The installation of panels often commences from the corners (Refer to Figure 1.5). Initially, two panels are positioned to create a corner and securely fastened together, preferably employing a pneumatic fastening tool. Right-angled welded wire mesh is affixed to the inside and outside corners and securely fastened to the panel mesh. Openings for doors and windows can be created either before or following the installation of panels. After the hole is finished, a piece of appropriate mesh is typically positioned at an angle both above and below the corners to avoid the formation of cracks. In certain instances, a U-shaped mesh is employed to strengthen the perimeters of door and window openings. Following the installation of wall panels, the slab/roof panels are subsequently positioned. The slab/roof panels are upheld by shoring until the top and bottom mortar have fully solidified. Reinforcement can be incorporated into ribbed panels to support long-span slabs. Reinforced concrete beams are installed to ensure seamless integration at the junction between the wall and the slab. After the panels have been firmly fastened, the installation process can be completed. The space between the polystyrene sheet and the layer of wire mesh provides an optimal position for enclosing electrical conduits and water lines.

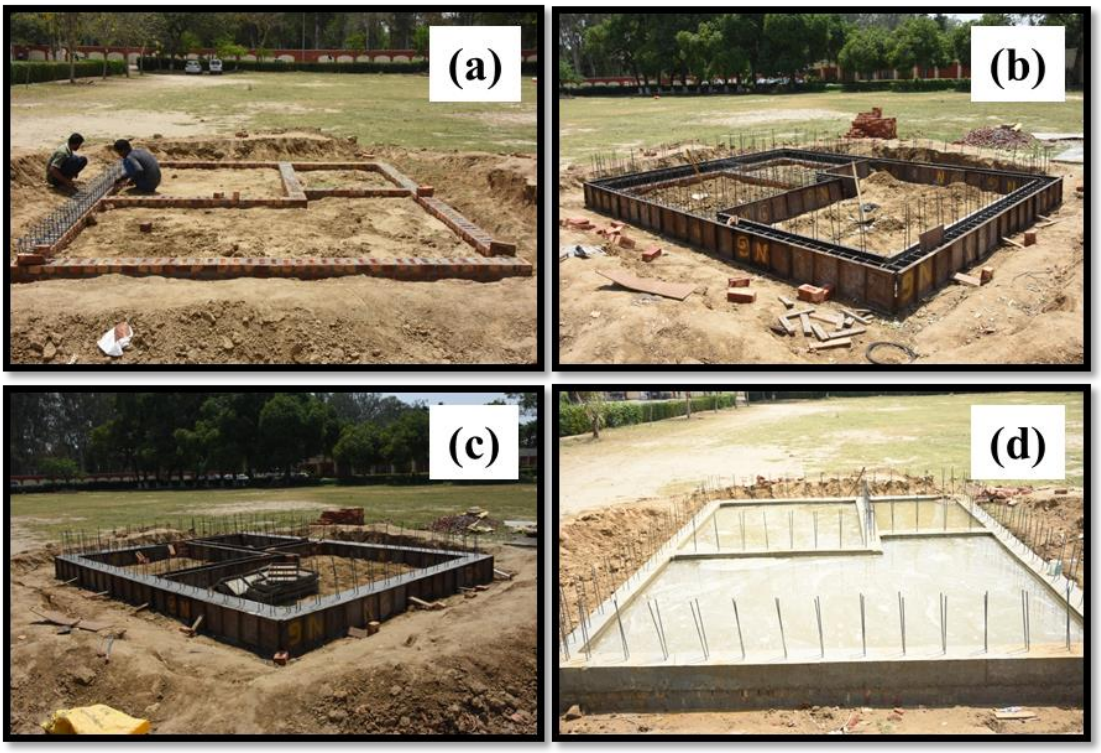

Figure 1. 4: Construction of building using CSP (a) foundation being laid; (b) shuttering for plinth beam; (c) concreting of plinth beam; (d) dowel bars erected on plinth beam

Figure 1. 5: Shuttering and concreting on EPS (a) Erection of panels; (b) erect panels with roof slab; (c) plastering of sandwich panels; (d) final building

There are several methods available to cover the panels with concrete. Concrete can be applied either manually or mechanically using either the wet technique (mortar pump) or the

dry process (gun) known as shotcrete. The thickness of concrete often ranges, although it is generally twice the distance between the polystyrene face and the cover mesh. To guarantee protection against corrosion, the steel mesh must be encased in a layer of concrete that is at least 20 mm thick in a typical environment. In a hostile environment, it is necessary to augment the thickness of the concrete cover.

1.7 Composite action of concrete sandwich panel

The structural response of reinforced concrete structural members (RCSPs) under different stress circumstances relies on the combined behaviour of their constituent elements. RCSPs are classified into three categories: fully composite, partial composite, and non-composite (O' Hegarty et al., 2019). This classification is based on the mechanism of longitudinal shear stress transfer, which involves shear connectors and friction between the wythe and core surfaces. In fully composite panels, both wythes work together to resist the loads. In partial composite action, the connectors are unable to fully transfer longitudinal shear stress. In non-composite panels, the connectors cannot transfer longitudinal shear stress and the wythes act independently (Figure 1.6).

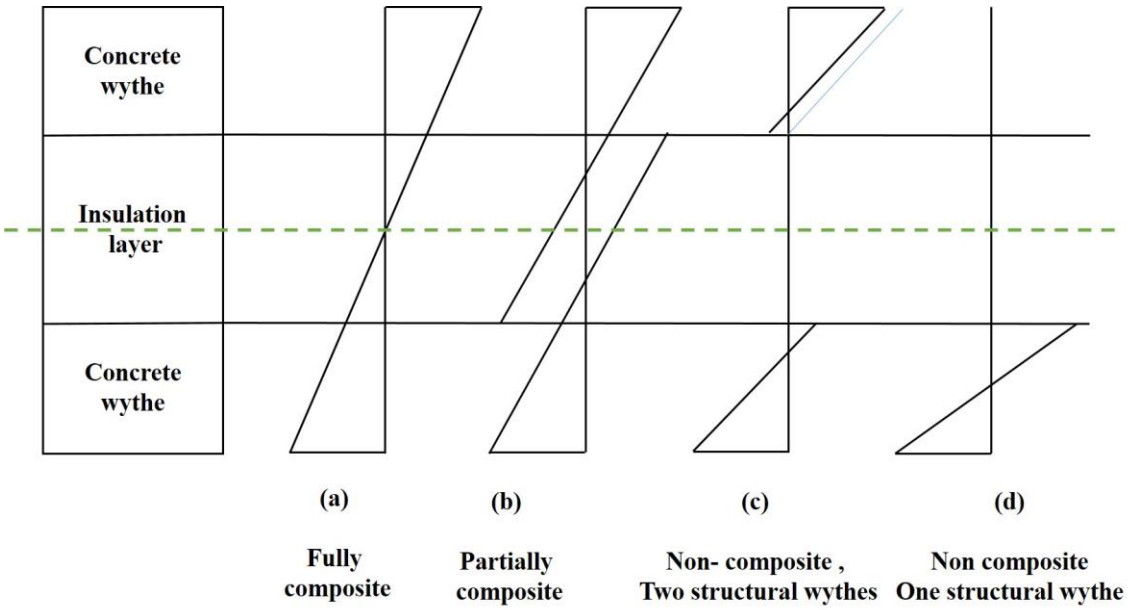

Figure 1. 6: Strain distribution of precast composite sandwich panels (Mugahed Amran et al., 2018)

1.8 Flexural Behaviour of Concrete Sandwich Panel

Reinforced concrete sandwich panels represent a versatile and efficient structural system that exhibits unique behaviour under flexural loading. These panels typically consist of two outer concrete layers (known as wythes) separated by an insulating core material. The outer layers are reinforced with steel bars to enhance the structural integrity and load-bearing capacity of the panels. The use of sandwich panels in construction offers advantages such as improved thermal insulation, reduced weight, and enhanced durability.

1. *Flexural Loading Behaviour:*

The flexural behaviour of reinforced concrete sandwich panels is primarily characterized by their bending stiffness. The outer concrete layers resist tensile and compressive forces, while the insulating core contributes to the overall stiffness of the panel. The combination of these elements results in a structural system that efficiently resists flexural loading. As the panel is subjected to flexural loads, the outer concrete layers experience tensile and compressive stresses. The reinforcement within these layers helps to control and distribute these stresses, preventing the formation of extensive cracks. The panel peak ultimate strength is a crucial parameter determined by the failure of either the concrete or the steel reinforcement. Reinforced concrete sandwich panels often exhibit ductile behaviour under flexural loading. This ductility allows the panel to undergo significant deformation before reaching failure. The ability to absorb energy through plastic deformation enhances the overall functioning in terms of resisting large and sustained loads in the panel.

2. *Influence of Core Material:*

The insulating core material plays a vital role in the behaviour of the sandwich panel. While it primarily serves to provide thermal insulation, it also contributes to the overall stiffness of the panel. The choice of core material can influence factors such as the panel's weight, thermal conductivity, and resistance to shear forces. Shear transfer between the two wythes through the core material is a critical aspect of flexural behaviour. Effective shear transfer enhances the overall strength and stability of the panel. The shear strength of the core material and the bond between the core and the concrete layers are crucial considerations.

3. *Construction and Design Considerations:*

The arrangement and detailing of reinforcement in the outer layers are essential for optimizing the flexural behaviour. Properly designed reinforcement helps control cracking,

improves strength, and ensures a ductile response. The overall thickness and aspect ratio of the panel influence its flexural performance. Thicker panels may exhibit higher bending stiffness, while the aspect ratio (length-to-thickness ratio) affects the panel's slenderness and stability. Understanding how loads are distributed between the two wythes is critical for designing reinforced concrete sandwich panels. Careful consideration of load paths and distribution mechanisms ensures that the panel functions as an integral and efficient structural element.

In summary, reinforced concrete sandwich panels demonstrate a complex yet efficient behaviour under flexural loading. Their composite nature, combining the strength of concrete and steel with the insulating properties of a core material, makes them an attractive option for various construction applications. Proper design and construction practices are essential to maximize the performance and structural integrity of these panels in flexural conditions.

1.9 In-plane shear behaviour of the concrete sandwich panel

The in-plane shear behaviour of concrete sandwich panels is a critical aspect of their structural performance. In-plane shear refers to the deformation and resistance to forces applied parallel to the plane of the panel. Concrete sandwich panels are composed of two concrete wythes separated by an insulating core, and understanding their in-plane shear behaviour is essential for designing structurally sound and stable constructions. Here are key considerations regarding the in-plane shear behaviour of concrete sandwich panels:

1. *Shear Transfer Mechanisms:*

The in-plane shear behaviour relies significantly on the efficiency of shear transfer mechanisms between the two concrete wythes. Shear connectors, such as shear studs or connectors embedded in the insulating core, facilitate the transfer of shear forces between the layers. Proper detailing and installation of shear connectors are crucial for ensuring the structural integrity of the panel. The bond between the concrete layers and the insulating core is essential for effective shear transfer. Adequate bond strength ensures that the two wythes act together as a cohesive unit, resisting shear forces and preventing delamination.

2. *Shear Strength and Failure Modes:*

In-plane shear loading can induce diagonal cracks in the concrete layers. The orientation and spacing of these cracks are influenced by the material properties, reinforcement details, and shear transfer mechanisms. Proper detailing of reinforcement can help control the width and spacing of diagonal cracks. The shear strength of the individual concrete wythes is

a critical parameter in the in-plane shear behaviour. The presence of reinforcement in the concrete layers contributes to both shear strength and ductility, allowing the panel to withstand shear forces without sudden failure.

3. Effect of Core Material:

The insulating core material also plays a role in the in-plane shear behaviour. Depending on its properties, the core may contribute to the overall shear resistance of the panel. Additionally, the stiffness and strength of the core material can influence the panel's response to in-plane shear forces. The shear modulus of the core material affects the overall stiffness of the panel. A stiffer core can enhance shear resistance but may also influence the distribution of shear forces between the wythes.

4. Design and Construction Considerations:

Proper shear reinforcement, such as horizontal shear reinforcement in the form of stirrups or other detailing, is essential for controlling and distributing shear forces within the concrete layers. This reinforcement enhances the shear capacity and ductility of the panel. The geometric characteristics of the panel, such as its thickness, aspect ratio, and overall dimensions, can influence in-plane shear behaviour. Design considerations should account for these factors to ensure the stability and effectiveness of the panel under shear loading.

Understanding and appropriately addressing the in-plane shear behaviour of concrete sandwich panels are crucial for designing resilient and durable structures. Engineers must consider shear transfer mechanisms, material properties, and reinforcement details to optimize the panel's performance under in-plane shear forces. Additionally, adherence to proper construction practices and quality control measures is essential for realizing the intended shear-resistant characteristics of concrete sandwich panels in real-world applications.

1.10 Axial compression behaviour of the concrete sandwich panel

The axial compression behaviour of concrete sandwich panels is an important consideration in structural engineering, especially when designing building elements subjected to vertical loads. Concrete sandwich panels consist of two concrete wythes separated by an insulating core, and their axial compression behaviour is influenced by factors such as material properties, geometric configuration, and detailing. Here are key points to understand about the axial compression behaviour of concrete sandwich panels:

1. *Load-Carrying Mechanism:*

Concrete sandwich panels primarily resist axial compression loads through the combination of the compressive strength of the outer concrete wythes and the load-bearing capacity of the insulating core. The load-carrying mechanism involves both the compressive resistance of the concrete and the bearing capacity of the core material. Proper shear transfer mechanisms and bonding between the two concrete wythes and the core material are critical to ensure that the panel acts as a cohesive unit under axial compression. Effective interaction allows the panel to distribute axial loads between the layers.

2. *Material Properties:*

The compressive strength of the concrete in the outer wythes significantly influences the axial compression behaviour. High compressive strength is desirable to support larger axial loads. The use of high-strength concrete or additional reinforcement can enhance the compressive strength of the panels. The properties of the insulating core, such as its compressive strength and modulus of elasticity, play a role in axial compression behaviour. A strong and stiff core contributes to the overall axial load-carrying capacity of the panel.

3. *Geometric Configuration:*

The thickness of the concrete sandwich panel is an important parameter affecting axial compression behaviour. Thicker panels generally exhibit higher axial load-carrying capacity, but the overall design should consider both structural requirements and thermal considerations. The aspect ratio, defined as the ratio of the panel height to its width, can influence the panel's buckling behaviour under axial compression. Proper consideration of aspect ratio helps avoid instability issues.

4. *Reinforcement and Detailing:*

The inclusion of vertical reinforcement within the concrete wythes enhances the axial load-carrying capacity and ductility of the panel. The reinforcement resists tensile forces induced by axial loads and helps control cracking. Proper detailing of connections, including the attachment of the panel to the supporting structure, is essential for ensuring the integrity of the panel under axial compression. Adequate anchorage and connection details prevent premature failure modes.

5. Buckling Considerations:

Axial compression behaviour should consider the potential for buckling, especially in taller panels. Adequate bracing and detailing can enhance the buckling resistance of the panel. Engineers must assess both local and global stability to ensure that the panel remains stable under axial compression. This involves evaluating the resistance to buckling and deformation at different locations within the panel.

Understanding the axial compression behaviour of concrete sandwich panels is crucial for their effective use in structural applications. Engineers must carefully consider material properties, geometric configurations, and reinforcement details to design panels that can safely and efficiently carry axial loads in various construction scenarios. Additionally, compliance with relevant design codes and standards is essential to ensure the structural integrity of concrete sandwich panels in practice.

1.11 Cyclic loading two-dimensional reinforced concrete frame

Earthquakes are naturally occurring disasters that bring a huge loss of life and property. Recent earthquakes in Turkey and Syria in February 2023 have brought unimaginable destruction. Such incidents have again bound the structural engineers' community to rethink and do intensive research on each and every parameter again. Over the last two decades, India also experienced many earthquakes, and due to this seismic activity buildings are destroyed and the risk of life is also very high. The earthquake also highlights the inadequacy of current building techniques, which may be used to analyze the region's seismic risk and establish a framework for improved preparedness in the case of future earthquakes (Halder et al., 2021). Back in 2001, Bhuj, a place in India experienced the devastating effects of an earthquake resulting in a huge loss of life and property ((Humar et al., 2001; Jagadish et al., 2003)). Buildings collapsed and the failure of infill masonry walls in Reinforced concrete (RC) frames was extensively observed. A similar failure of walls was also observed during the earthquake that came in Assam and Mizoram in India (Halder et al., 2021). The previous unfortunate events of the earthquake which shook Nepal (2015) and a few parts of India raised a question about the safety of the inmates of the building (Bastin & Sharma, 2017). An earthquake is an uncertain activity that is beyond human control. So there is an extensive need to ensure the safety of inmates living in a building when such incidents occur. To ensure such things, intensive experimental testing is required to encounter such seismic occurrences (de Sousa et al., 2022). Researchers have done extensive research on strengthening the brick masonry infill

wall (Arslan et al., 2022; Manos et al., 2021; Sakr et al., 2021a;). This strengthening of the infill wall is costly and laborious. There is no standardised guideline available for strengthening these different structures as well. Brick masonry requires brick that is made in a kiln, emitting anthropogenic CO_2 in the environment. The world is headed towards achieving zero carbon emissions and so is India. India is to achieve its target of zero emissions by the year 2070, for that more sustainable construction methods are needed and at the same time the construction has to be rapid (Rissman et al., 2020). As in today's modern world, time is of utter importance, so light and fast construction are gaining popularity i.e. light gauge steel frames, concrete sandwich panels (CSP), etc. So fast construction methods are desired (de Sousa et al., 2022; Hashemi et al., 2018a). Cyclic loading and monotonic loading are the testing methods that create a virtual earthquake effect and also provide sufficient data to understand the behaviour of a Reinforced Concrete (RC) 2D frame. Conventional construction methods can be replaced by the concrete sandwich panel for brick masonry. CSP has a core of expanded polystyrene (EPS) and welded wire mesh on both faces attached with shear connectors. The two wythes can be mortar or micro-concrete, based on the design.

These CSPs are nowadays being used in place of brick masonry as they are easy to install and take less time than conventional methods. They are also structurally sound and many researchers have found that their load-bearing capacity is also at par with conventional techniques ((de Sousa et al., 2022; Hashemi et al., 2018). Considering the seismic data of the northern part of India (Halder et al., 2021), there is a dire need for detailed experimental testing of such new techniques to be more sure of the behaviour of these CSPs as infill. From experiences of past seismic activities, it can be seen that the infill wall plays a quite significant role in the structural frame (Halder et al., 2021). Not considering the effect of infill walls is not intelligent, especially in earthquake-prone areas, so testing experimentally as well as numerically is critical. Many researchers have tested frames under cyclic loading (de Sousa et al., 2022; Hashemi et al., 2018a). Hashemi (2017) tested concrete sandwich panel-infilled steel frames and observed that sandwich panels results into increase in the strength and lateral stiffness, , capacity of energy dissipation and ductility (Hashemi et al., 2018). Jung & Aref (2005) used polymer matrix composite as infill in steel frame and observed that buckling resistance increased in out-of-plane behaviour (Jung & Aref, 2005)). Sakr et al. (2021a) investigated the effect of partially bonded carbon fiber reinforced polymer (CFRP) on masonry infilled RC frames retrofitted with CFRP and observed the strength was significantly enhanced (Sakr et al., 2021a). de Sousa et al. (2022) assessed the behaviour of RC frames strengthened

with composite sandwich panels by (quasi-static) in-plane cyclic loading and found that load-carrying capacity improved significantly. Structural integrity was maintained by the sandwich panel and very little damage was observed for higher drift values. Manos et al. found out that the strength of the masonry panel can be enhanced by the use of thermos insulating attachments (Manos et al., 2021). Arslan et al. (2022) demonstrated the mechanical behaviour of walls fortified with plasters containing varying percentages of fibre has significantly improved as compared to non-plastered and regular cement plastered brick walls.

Experimental cyclic loading tests on a 2D RC frame with masonry infill walls provide valuable insights into the behaviour of structures under seismic conditions. These experiments contribute to the development of improved design guidelines and construction practices for earthquake-resistant buildings. These above-mentioned details act as a guide for conducting a quasi-static analysis of a two-dimensional reinforced concrete frame.

1.12 Finite element analysis of concrete sandwich panel

Finite Element Analysis (FEA) is a powerful numerical method used to simulate and analyze the behaviour of complex structures, including concrete sandwich panels. The analysis involves dividing the structure into smaller, interconnected elements to approximate the physical behaviour of the entire system. Here's a step-by-step guide on how Finite Element Analysis can be applied to study concrete sandwich panels:

Step-1. Geometry and Material Properties:

- **Model Creation:** Develop a three-dimensional (3D) geometric model of the concrete sandwich panel using specialized FEA software. Define the dimensions, and thicknesses of the concrete wythes and the insulating core, and any other relevant geometric details.
- **Material Properties:** Assign material properties to each component of the sandwich panel. This includes the modulus of elasticity, Poisson's ratio, and density for the concrete layers and the core material. Nonlinear material properties may also be considered for concrete in large deformations.

Step-2. Mesh Generation:

- **Element Type and Size:** Choose appropriate finite elements for modeling each component (e.g., solid elements for concrete, shell elements for thin layers, etc.).

Generate a mesh by dividing the geometry into a network of elements. The size and type of elements should be selected based on the expected behaviour of the structure.

- **Mesh Refinement:** Perform mesh refinement to ensure accurate results. This involves adjusting the size of elements in critical areas, such as regions with high-stress gradients or areas of anticipated failure.

Step-3. Boundary Conditions:

- **Support Conditions:** Apply appropriate boundary conditions to represent the structural support and loading conditions. This may include fixing certain degrees of freedom at points where the panel is supported or applying distributed loads and point loads.
- **Loading Conditions:** Define the loading scenarios that the panel will experience. This could include axial compression, in-plane shear, or other loading conditions depending on the specific analysis goals.

Step-4. Material and Geometric Nonlinearities:

- **Material Nonlinearities:** If applicable, account for material nonlinearities, such as concrete cracking or plastic deformation. Implement material models that capture the nonlinear behaviour of concrete under various loading conditions.
- **Geometric Nonlinearities:** Consider geometric nonlinearities, especially if the panel undergoes large deformations. This may involve accounting for changes in geometry as the structure deforms.

Step-5. Solver Settings:

- **Solver Selection:** Choose an appropriate solver within the FEA software. Implicit or explicit solvers may be used depending on the nature of the analysis (e.g., quasi-static or dynamic).
- **Convergence Criteria:** Set convergence criteria for the solution, ensuring that the analysis reaches a stable and accurate solution. Adjust parameters such as iteration limits and tolerance levels.

Step-6. Analysis and Post-Processing:

- **Perform Analysis:** Run the finite element analysis to obtain results. The software will provide information on the distribution of stresses, displacements, and other relevant parameters within the concrete sandwich panel.
- **Post-Processing:** Interpret the results and visualize them through contour plots, graphs, or animations. Evaluate critical areas of stress concentration, deformation patterns, and failure modes.

Step-7. Validation and Sensitivity Analysis:

- **Validation:** Compare the FEA results with analytical solutions, experimental data, or real-world observations to validate the accuracy of the simulation.
- **Sensitivity Analysis:** Perform sensitivity analyses by varying input parameters to understand their impact on the structural response. This helps identify key factors influencing the behaviour of the concrete sandwich panel.

Step-8. Optimization and Design Iterations:

- **Optimization:** Use FEA to explore different design alternatives and optimize the structural performance of the concrete sandwich panel. This may involve adjusting material properties, layer thicknesses, or reinforcement details.
- **Design Iterations:** Based on the analysis results, iterate the design to enhance structural efficiency, address potential issues, and meet design requirements.

Finite Element Analysis provides valuable insights into the structural behaviour of concrete sandwich panels, allowing engineers to optimize designs, assess performance under various loading conditions, and ensure the reliability and safety of structures in practical applications.

1.13 Geosynthetics

Geogrids are geosynthetic materials used in civil engineering and construction applications. These are of two types, namely, plastic uniaxial geogrids and polyester biaxial geogrids. Both plastic uniaxial geogrids and polyester biaxial geogrids play important roles in geotechnical engineering applications such as to reinforce soil structures, improve load distribution, and enhance overall stability. The choice between them depends on specific project requirements, cost considerations, and the desired performance characteristics in terms

of reinforcement and stability. Engineers typically evaluate factors such as soil conditions, loading conditions, and project specifications when selecting the appropriate geogrid for a given application.

Plastic uniaxial geogrids and polyester biaxial geogrids can be distinctly characterized as shown in Table 1.2:

Table 1.2: Types of Geogrid

S.No.	Property	Plastic Uniaxial Geogrid	Polyester Biaxial Geogrid
1.	**Material**	• Typically made from high-density polyethylene (HDPE) or polypropylene (PP) materials. • These plastics provide high tensile strength, durability, and resistance to environmental factors such as UV radiation and chemical degradation.	• Made from high-strength polyester yarns, providing excellent tensile strength and modulus. • Polyester resists corrosion and biological degradation.
2.	**Orientation**	• Uniaxial geogrids have reinforcement primarily in one direction (longitudinal). • The grid structure consists of intersecting ribs, forming openings that facilitate soil interaction.	• Biaxial geogrids have reinforcement in two perpendicular directions (both longitudinal and transverse). • The grid structure is characterized by intersecting ribs, forming a square or rectangular pattern.
3.	**Function and Applications**	• Soil Reinforcement • Retaining Walls • Slope Stabilization	• Soil Stabilization • Subgrade Improvement
4.	**Installation**	• Uniaxial geogrids are typically installed with their primary reinforcement direction aligned with the expected direction of force or movement. • Installation involves placing the geogrid within or on the soil and securing it in place.	• Biaxial geogrids can be installed in any orientation, offering flexibility in construction applications. • Installation involves placing the geogrid within or on the soil, securing it, and ensuring proper connection to the structure.
5.	**Benefits**	• Cost-effective	• High tensile Strength

		• Ease of Installation	• Versatility • Durability

1.14 Gaps in research area

The use of sandwich panels in the construction industry has gained a tremendous popularity. Such methods of construction provide efficiency in terms of structural strength, thermal insulation, sound insulation, durability and serviceability. Though many types of sandwich panels are being used across the globe, the present study focused mainly on the load bearing concrete sandwich panels. There are many areas in which extensive and in-depth study is needed to better understand the behaviour of concrete sandwich panels. Some of the gaps found from the previous literature are as follows:

- Multiple studies have sought to test sandwich panels constructed of various materials under varying loading situations, and some of them have documented the brittle breakdown of the panels.
- Limited literature is available on the use of geogrids in concrete to enhance the strength, deformability, energy dissipation and displacement ductility factors. As per the limited literature, properties that geogrids possess have been found to very useful to enhance the strength and other properties of the concrete.
- Masonry strengthened with welded wire mesh is not just inefficient in resisting seismic forces, but it also requires substantial labour and presents challenges during installation.
- Many researchers have ignored the influence of openings in the infill walls, but structural testing can account for this.
- Limited literature has been documented on the behaviour of a two-dimensional reinforced concrete frame with concrete sandwich panel infill under seismic stresses. Understanding the behaviour of the panel can be highly beneficial.
- Literature has not been reported with openings in wall in the behaviour of panels with vertical and horizontal in-plane forces which are influenced by the overall dimensions and openings in the structure.

1.15 Objectives

The main objectives of the study are:

- To study the behaviour of concrete sandwich panels with different grid materials under out-of-plane loading and horizontal in-plane shear loading and in compression testing.
- To study the behaviour of 2D frame with sandwich panel as infill masonry wall, by performing static loading test for various openings in wall.
- Analytically simulating and comparing the experimental observation

1.16 Research significance

This study has provided in-depth insights into the use of concrete sandwich panels as infill wall in 2D RC frame and their behaviour under cyclic loading. Other structural parameters such as flexure, diagonal in-plane shear and axial compression would provide a better understanding of such panels under various loading conditions. The use of geogrids as an additional reinforcement enhances the strength and overall deforming capability under various loading conditions. The study would be helpful in encouraging the use these concrete sandwich panels as a replacement of conventional building construction systems.

1.17 Organisation of thesis

This thesis has followed following orientation:

Chapter 1 presents the basic idea behind the origin of this study, namely, how the construction industry has evolved from conventional materials and erection techniques to new EPS panels and their installation. Also, the various behaviour of panels in different loading conditions has been discussed, with the introduction of geo-grid usage in this EPS panel system. Research gaps have been found based on the discussion presented in Chapters 1 and 2, and objectives have been set for the proposed study. Finally, research significance concludes this chapter.

Chapter 2 presents a detailed literature review of the recent works related to EPS panel performance in flexural loading, diagonal shear loading, compression loading, and their applicability in 2D-frame systems. With these recent works, the focus has been kept on surveying the FEM software applicability in validating the behaviour of EPS panels.

Chapter 3 presents the experimental program i.e. the methodology of the out-of-plane, in-plane, and axial compression testing and the testing procedure of a dimensional reinforced concrete frame with concrete sandwich panel and brick masonry as infill wall.

Chapter 4 presents the results of the out-of-plane in-plane and axial compression in the form of load versus deformation graphs, failure pattern, energy dissipation, and deflection ductility factor.

Chapter 5 presents the behaviour of a 2D RC frame with a concrete sandwich panel as infill and brick masonry as infill. The comparison between both of them is done through the S-curve. Energy dissipation has also played an important role in justifying the ductility of the frames.

Chapter 6 presents the numerical simulation of experimental results. the software used is ANSYS Workbench. Out-of-plane and the in-plane specimen has been modeled and tested by using the FEM software.

Chapter 7 presents the summary of all the chapters. This chapter contains the conclusion drawn from each parameter. Combining all the results and deducing the outcome of the thesis.

References

Chapter 2

Literature Review

2.1 General

The modern era of changing technologies many researchers are working on different techniques to bring about a huge change in the construction industry to make construction more rapid and durable. Replacing the conventional methods is not an easy task, but these new techniques of rapid construction are gaining popularity. Concrete sandwich panel is one such method which can be used to replace the brick masonry. It has been observed in many studies that the sandwich panels are the future of construction industry. Techniques are being developed to make them cheaper, so that these can be used as a replacement and would me more effective and durable. The structural capacity of these panels is greater than the brick masonry as reported by many researchers. So it would be wise to use these concrete sandwich panels as a replacement for brick masonry. This chapter of the thesis deals with the literature already published in the field of sandwich panels. The behaviour of the concrete sandwich panel is discussed in terms of flexure behaviour, in-plane shear and axial compression behaviour. The literature review on reinforced concrete frames is also presented.
In order to achieve this the chapter is further divided into four parts.

2.2 Flexural behaviour

Salmon & Einea (1995) performed extensive trials on tall sandwich panels measuring up to 9m in length. These panels included both FRP connectors and steel truss connectors. In addition, they performed flexural testing on compact precast concrete sandwich panels of 2.44 metres in length, featuring a solitary row of FRP bent bar positioned along the panel's central axis. The tests yielded an approximation of the level of composite action facilitated by the FRP connector.

Khorami & Ganjian (2011) explored the utilization of Agricultural Waste Fibres (AWF), specifically bagasse, wheat, and eucalyptus fibers, in the production of Fiber Cement Boards (FCB). Different fiber contents (2% and 4% by weight of Portland cement) were tested, and the impact of silica fume on the flexural behavior of FCB was investigated. Results indicate that the flexural characteristics of FCBs are influenced by various factors such as fiber type,

length, diameter, aspect ratio, and texture. Increasing fiber content from 2% to 4% enhances the maximum flexural strength in all groups. Additionally, the incorporation of silica fume improves flexural strength across the board.

Carbonari et al. (2013) assessed the bending strength of PSP with 90 connectors, examining it under various boundary circumstances. To achieve this objective, empirical trials were conducted utilising full-scale slabs featuring either hinged or partially fixed ends, which were exposed to either concentrated or distributed loading. The tests were conducted on individual isotactic slabs and on continuous slabs supported by walls constructed with PSP. The acquired results facilitated the identification of potential failure mechanisms and the development of a simplified analytical formulation to estimate the maximum load that the panels can withstand.

Khorami & Ganjian (2011) explored The research focuses on developing environmentally friendly construction materials by using recycled waste cardboard in fiber cement board production. The study comprises three phases: first, exploring the flexural behavior with varying fiber content (1–14%); second, determining the optimal 8% fiber content for highest flexural strength; and third, investigating the impact of nanosilica fume and limestone powder on specimens with 8% fiber content. The results indicate that incorporating 10% limestone powder and 3% nanosilica fume enhances the flexural strength of the cement composite board, emphasizing the potential for sustainable and cost-effective construction materials.

Smakosz & Tejchman (2014) conducted bending tests on panels composed of expanded polystyrene (EPS) foam core and glass fibre facings reinforced with magnesium-cement. They noticed that the failure of these panels occurred as a result of tensile failure in the bottom facing.

Chen et al. (2015) observed the impact of the FRP connector on the flexural behaviour of the panels in terms of stiffness, strength, and suitability for roof/floor constructions. Three groups of concrete panels were constructed, each with different FRP shear plate connectors: continuous, segmental, and discrete. Two additional solid concrete panels were used as baselines. The panels underwent bending tests until failure and the study discovered that the FRP shear plate can effectively transfer shear between the concrete layers, creating a composite panel that meets ACI requirements for roof/floor applications. The type of shear connector used significantly influenced the strength and stiffness of the panels. Continuous and segmental connectors outperformed discrete connectors. The FE model developed in the study accurately predicted the degree of composite action, allowing for the assessment of panel behaviour. The

specially designed FRP connectors, with their anchoring schemes, demonstrated successful shear force transfer between concrete wythes.

Dey et al. (2015) explored the mechanical behaviour of textile-reinforced aerated concrete sandwich panels under static and low-velocity dynamic loading. Two types of aerated concrete, AAC and FRAC, form the core, while Alkali Resistant Glass textiles reinforce the skin layer. The research evaluates two composite configurations and observes that externally bonded textiles significantly enhance properties. Dynamic flexural strength is up to four times greater than static strength, with polypropylene fibers increasing toughness by 25%. The study emphasizes the positive impact of textile reinforcement on load carrying, flexural stiffness, and energy absorption. Overall, these construction materials offer manufacturing efficiency, a moderate weight–strength ratio, and thermal efficiency.

Raj et al. (2015) examined the flexural loading on sandwich panel consisting of BFRC (Basalt Fiber Reinforced Composite). The panel comprises top and bottom skins made of BFRC mix with profile sheet flanges to resist flexure. The panel is constructed using a combination of prefabrication and cast-in-situ processes. With an ultimate flexural strength of 26 kN, the panel exhibits ductile behaviour and 200% ductility over the deflection. A numerical study assesses the connection integrity between the skin and core, demonstrating that improved connections enhance both the strength and stiffness of the panel. The finite element analysis results align well with the experimental findings. The construction methodology, combining prefabrication and cast-in-situ, optimizes formwork usage and reduces transportation costs. The study emphasizes the potential for enhanced panel performance through improved connection mechanisms between the skin and core.

Daniel Ronald Joseph et al. (2019) experimental and analytical studies carried out to understand and compare flexural behaviour of concrete sandwich panels under two different loading conditions such as punching and four-point bending.

Kang & Kim (2016) introduced design models for insulated concrete sandwich wall panels (SWPs) incorporating Glass Fiber Reinforced Polymer (GFRP) grids to enhance structural performance. The models address both ultimate and serviceability limit states, offering mean-prediction models for ultimate and cracking moments. Capacity factors, statistically determined to consider uncertainties, are integrated into the design models. Two calibrated capacity factors, 0.5 for ultimate limit state and 0.78 for serviceability limit state, ensure structural safety. A unified capacity factor, based on a nominal ultimate moment, streamlines the design process, automatically meeting both ultimate and serviceability

requirements. The application of GFRP grids brings structural advantages, offering a new design option, improved safety, and superior heat loss reduction properties compared to conventional materials like carbon steel and concrete.

Leng & Song (2017) explored the flexural and shear behaviour of steel-concrete-steel (SCS) sandwich slabs. Six slabs with varying geometries were loaded at their center and studied for deformation, strain, and cracking patterns. Two main failure modes were observed: flexural yielding triggered by the bottom steel plate, and shear punching of the concrete core. Interestingly, even after initial failures, the slabs' load-carrying capacity increased due to the stiffening effect of the top steel plate and the membrane action of the bottom one. Notably, the top steel plate significantly contributed to shear resistance even after cracking. A theoretical model predicting the load capacity of SCS slabs under concentrated loads was developed, considering flexural, shear, and tie bar contributions. Overall, the study suggests SCS slabs offer excellent ductility for both flexural and shear forces, making them promising for high-strength structures.

Chithambaram & Kumar (2017) investigated the flexural behaviour of bamboo-based ferrocement slab panels reinforced with chicken wire mesh layers. Twelve slab panels, with and without 15% cement replacement by fly ash, are tested under uniformly distributed loads. Results indicate similar first crack and ultimate loads for both types of slabs, with the ultimate load approximately twice the first crack load. Bamboo strips contribute significantly to the ultimate load capacity. The study suggests that this ferrocement system, using bamboo and fly ash, is suitable for low-cost roofing in rural and suburban areas, offering environmental benefits by utilizing waste materials without compromising structural integrity.

Hopkins et al. (2017) employed a non-linear explicit dynamic finite element model to investigate the static response to typical flexural loading and the dynamic response to blast loading. The concrete was modelled using a damaged plasticity model, which took into account the nonlinear material properties in both compression and tension. To emulate the static behaviour, the temporal loading control was implemented on the FE model to decelerate the loading rate and accurately capture the reaction. It may be inferred that, despite its smaller weight, the insulated concrete sandwich panel demonstrates a rather strong performance when subjected to blast stress, comparable to that of the solid panel. Hence, the utilisation of insulated concrete sandwich panels has great potential for constructing both traditional and blast-resistant buildings.

Gu & Lu (2023b) investigated the distinct effects of flexural and shear connector damages on global structural stiffness, proposing a method to identify these damages accurately using vibration tests and a genetic algorithm-based finite element model updating procedure. Results demonstrate successful separation and accurate identification of flexural and shear link parameters.

REMARKS

Extensive research has been conducted on composite panels for roofs and floors, focusing on different materials and connectors to improve their flexural behaviour. Research has demonstrated the effectiveness of FRP connectors in transferring shear, the improved load capacity with textile reinforcement, and the low-cost, eco-friendly option provided by bamboo-ferrocement. Using GFRP grids in insulated panels enhances the overall structural performance and helps to minimise heat loss. On the other hand, BFRC panels are known for their excellent ductility, making them a great choice for flooring applications. Through extensive analysis of various conditions, we were able to gain valuable insights into the failure mechanisms and create accurate analytical models for estimating loads. Overall, composite panels provide a highly efficient and sustainable option for roofs and floors, offering significant performance and weight benefits.

2.3 In-plane shear behaviour of sandwich wall panels

Pantelides et al. (2008) examined precast/prestressed concrete sandwich panels, which include of two concrete layers separated by a rigid insulating foam layer. These panels are commonly employed as walls or slabs in thermal insulation applications. The thermal efficiency is reduced due to the thermal bridge effect caused by commonly used connections, such as steel trusses or concrete stems, that penetrate the insulation layer between the two wythes. The conducted experiments in this study demonstrate that hybrid GFRP/steel reinforced sandwich panels have the ability to endure external forces in a direction perpendicular to the plane, while also offering resistance to lateral forces between the two layers of concrete.

Gara et al. (2012) conducted diagonal compression experiments on square specimens with various configurations to examine the response of panels to horizontal in-plane forces. The tested panels were composed of in situ concrete with an EPS core. The core was supported by welded wire mesh on both sides and connected by pin or non-shear connectors on both sides

of the core. The diagonal compression tests were conducted on both plain wall panels and panels having transversal stiffening walls, as depicted in Figure 2.1.

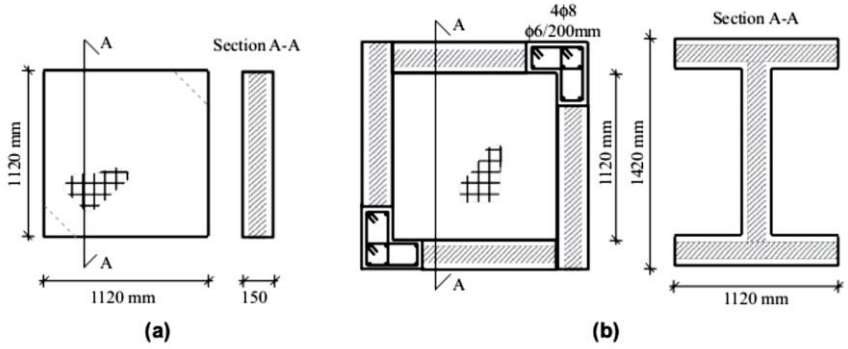

Figure 2. 1: a) Wall Panel b) Transversally stiffened panel. (Gara et al., 2012)

Choi et al. (2015) documented the in-plane shear characteristics of insulated concrete sandwich wall panels (CSWP) that were strengthened with corrugated glass fiber-reinforced polymer (GFRP) shear connection. The test findings demonstrated that the addition of corrugated GFRP shear connection greatly enhanced the in-plane shear strength. Additionally, their study examined how increasing the depth at which shear connectors are embedded can effectively prevent the pull-out of these connectors. Furthermore, they found that removing the adhesive force of insulation materials has a tendency to reduce the in-plane shear strength.

Hamed (2016) examined the structural performance of load-bearing Pre-stressed Concrete Sandwich Panels (PCSPs) by creating a theoretical model. The model incorporates the axial and bending stiffness of the RC layers, the shear and normal stiffness of the insulation layer, and the elastic flexibility of the diagonal truss connectors. The findings indicate that the occurrence of cracks in a reinforced concrete (RC) layer can result in a substantial decrease in the overall rigidity of the sandwich panel. Additionally, it can cause a significant decline in the composite behaviour due to the potential spread of cracks throughout the entire thickness of the RC layer, which experiences both axial tension and bending moments.

Hodicky et al. (2015) analysed the combined behaviour of 46 segments that resemble precast concrete sandwich panels (PCSPs) by utilising a fibre reinforced polymer (FRP), especially a carbon fiber-reinforced polymer (CFRP), grid/rigid foam as a shear mechanism. The research presented in this paper focused on conducting experiments to investigate the impact of different parameters on the shear flow strength of the CFRP grid/foam system. The experimental findings of this study work demonstrate that augmenting the gap between vertical lines of CFRP grid leads to a rise in the overall shear flow strengths. This is attributed to the

increased bonded contact area between the rigid foam and the concrete surface. Nevertheless, the total shear stresses decreased as a result of the increased surface area at this interface.

Ahmad & Singh (2021) analysed the structural response of Reinforced Concrete Sandwich Panels (RCSP) containing an Expanded Polystyrene (EPS) core when subjected to axial and in-plane shear loads. A total of fourteen specimens undergo testing, with six specimens exposed to axial compression and eight specimens submitted to diagonal compression. The panels are composed of prefabricated corrugated EPS core, welded wire mesh, and orthogonal shear connectors. The technique of Digital Image Correlation (DIC) is utilised for the purpose of quantifying displacements and strains. The study outlines the failure mechanism, fracture growth, maximum axial load capacity, shear strength within the plane, and stress-strain behaviour. Analytical comparisons demonstrate a strong correlation between the axial load capacity achieved via experiments and the predictions made through analysis. However, the shear strength shown in experiments surpasses the estimations derived from design codes for reinforced concrete. The axial response during compression tests has a linear trend to the point of failure, where the load resistance is mostly governed by the concrete section. Diagonal compression tests demonstrate the presence of cracks that experience tension along the vertical diagonal, indicating complete composite behaviour. Shear strength predictions derived from design code models for solid reinforced concrete (RC) walls are determined to be overly cautious, particularly for thicker samples. The study highlights the significance of conducting further tests to establish dependable correlations for shear strength and acknowledges the utility of results obtained from small-scale specimens in constructing analytical or empirical models for full-scale walls.

Behera & Nanda (2021) examined the enhancement of the structural integrity of brick masonry prisms and panels by employing geogrid reinforcement inserted inside the brick mortar. Compressive strength testing were performed on prisms, whereas diagonal compression tests were undertaken on panels with two different reinforcement patterns. Geogrid-reinforced prisms demonstrated a significant 32.7% enhancement in compressive strength as compared to prisms that were not reinforced. The reinforced brick panels exhibited enhanced resistance to crushing loads, in-plane shear forces, lateral forces, and ductility, with the greatest improvement noted in the strengthening of the bed joints. Diagonal compression testing demonstrated a significant 108% enhancement in crushing load for bed joint reinforcement, and a notable 20% improvement for bed and head joint reinforcement. Enhanced mortar strength led to the display of enhanced failure modes in the reinforced panels.

The in-plane shear strength had a substantial increase, namely a 108% increase for bed joint reinforcement. The geogrid bed joint reinforcement significantly increased the lateral strength of the panel by 45% compared to panels without reinforcement. Both categories of geogrid-reinforced panels demonstrated enhanced rigidity and flexibility in comparison to panels without reinforcement, with the most significant improvements recorded in panels reinforced with geogrid bed. The cost analysis revealed that the unit prices of unreinforced and reinforced walls are comparable, with a difference of no more than 6.5%. This suggests that strengthening walls is a feasible option for new structures and an economically efficient strategy for mitigating earthquake disasters in brick masonry.

Cheng et al. (2020) examined the shear behaviour of masonry walls enhanced with several fiber-reinforced substances, fiber-reinforced polymer (FRP), textile-reinforced concrete (TRC). Twenty masonry wall specimens underwent in-plane shear testing, and the obtained data was examined to determine failure mechanisms, shear strength, pseudo-ductility, and energy dissipation. The study revealed that unreinforced and mortar-strengthened masonry walls displayed a characteristic of being brittle, whereas walls strengthened using FRP, ECC, and TRC exhibited enhanced ductility and reduced brittleness. The shear strength boost of TRC and ECC was found to be similar, with FRP showing a little smaller enhancement. The computed shear values for TRC, ECC, and FRP were more cautious than the observed values. The study indicates that masonry walls reinforced with TRC demonstrate enhanced ductility and energy dissipation, rendering them a highly effective method for seismic strengthening.

Dong et al. (2021) examined the ability of carbon and glass textile-reinforced mortar (TRM) composites, which were reinforced with short and water-dispersible polyvinyl alcohol (PVA) fibres, to enhance the diagonal shear performance of masonry (URM- unreinforced masonry walls) walls. A total of ten specimens, consisting of a reference sample and several single or double-sided reinforced configurations, were subjected to testing. The findings demonstrated that the increased TRM composites significantly improved the masonry walls' deformation and bearing capability. Incorporating short PVA fibres into the matrix reduced early failures, such as spalling and delamination, and enhanced overall efficiency. The study introduces non-dimensional metrics (α and β) to assess the efficiency and enhancement ratios of various TRM composites. The results indicate that the enhanced TRM composites significantly improve the bearing capacity.

Zoppo et al. (2019) investigated the effectiveness of reinforced plasters and Composite Reinforced Mortars (CRM) in enhancing the in-plane shear capacity of tuff masonry walls.

Thirty-two single-leaf tuff masonry panels underwent diagonal compression tests, with various strengthening configurations, matrix compositions, and grid properties. Results indicated that single-sided strengthening increased shear capacity by 42% to 85%, while double-sided strengthening achieved a higher increase from 138% to 288%. The cement content in the matrix influenced the response, with reduced cement content leading to lower shear capacity and energy dissipation. The study highlights the importance of grid properties, showing that GFRP 40 × 40 grid exhibited superior strengthening effectiveness.

Remarks

In conclusion, the diverse studies on structural elements, ranging from sandwich panels to masonry walls, reveal innovative approaches to enhance their mechanical performance and resilience. The use of hybrid materials, such as GFRP/steel reinforcements in sandwich panels, and the exploration of various strengthening techniques, including geogrid reinforcement and fiber-reinforced materials for masonry walls, demonstrate a commitment to optimizing structural behaviour. These investigations contribute valuable insights into improving load-bearing components, considering factors like thermal efficiency, shear strength, and deformation characteristics. The findings underscore the importance of employing advanced materials and methodologies for creating robust, durable, and adaptable structural systems, essential for the evolving demands of construction and seismic mitigation.

2.4 Compression behaviour of sandwich panels

Benayoune (2007) conducted an experimental study to examine the ultimate strength characteristics of precast concrete sandwich panels (PCSP) subjected to eccentric loading, utilising steel truss shear connections (Figure 2.2). The PCSPs experienced a 38% loss in ultimate strength as the slenderness ratio increased from 10 to 20. The panels underwent testing with the lower end secured and the upper end fastened. This was presumed to replicate the final conditions of the panel when utilised in a one-story structure.

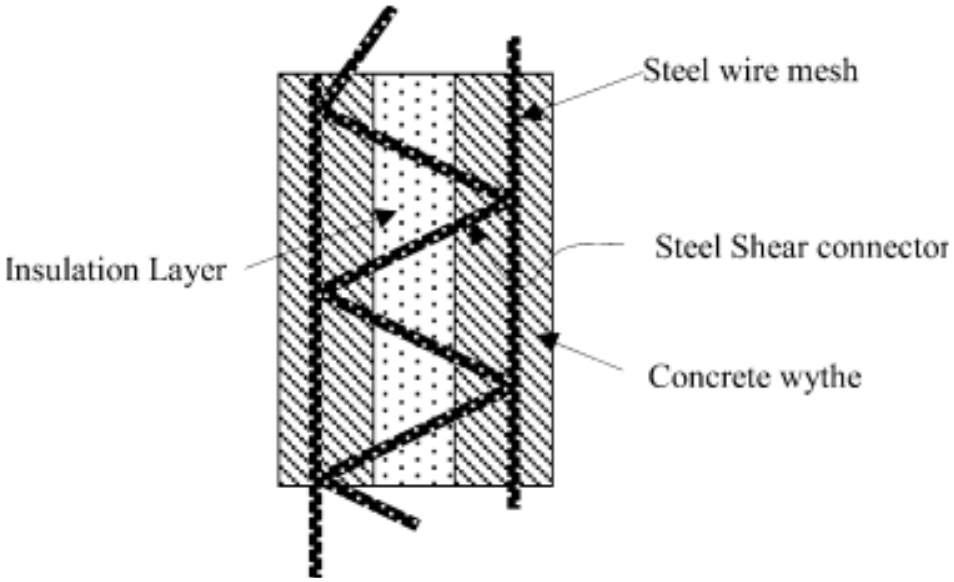

Figure 2. 2: Precast Sandwich Panel with truss shaped shear connector (Benayoune, 2007)

Gara et al. (2012) performed compression tests on full-scale panel specimens constructed with concrete wythes and EPS core. These specimens had varying slenderness ratios and were subjected to both axial and eccentric loads. The objective of the study was to investigate the response of the panels to vertical in-plane forces. The utilisation of non-shear connectors to link the inner and outer wythes resulted in a somewhat composite behaviour, which was ensured by the presence of polystyrene and strengthened beams at the ends of the panel. The experimental testing and numerical calculations revealed that the tested panels achieved a partial level of composite behaviour, despite the absence of shear connectors in the internal layer (Figure 2.3).

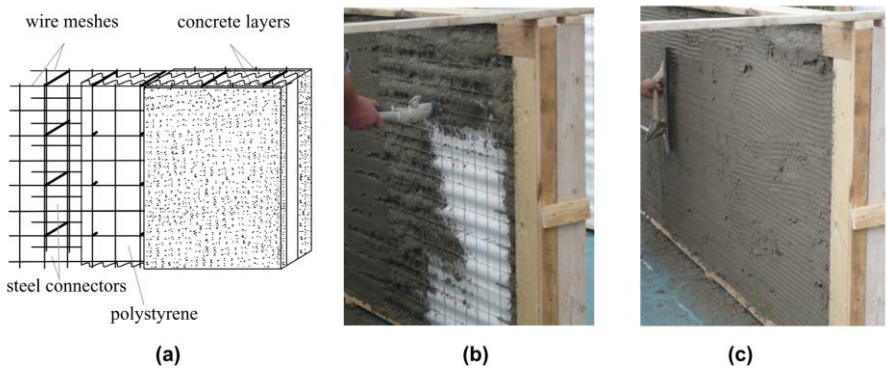

Figure 2. 3: Casting of corrugated EPS panels a) Schematics of the components b) Concrete spraying up to the mesh c) Concrete spraying up to the final thickness. (Gara et al., 2012)

Mousa & Uddin (2012) examined the structural characteristics of a novel type of Composite Structural Insulated Panels (CSIPs) designed for load-bearing wall purposes. These panels were constructed using a cost-effective orthotropic thermoplastic glass/polypropylene (glass-PP) laminate as the outer layer and Expanded Polystyrene Foam (EPS) as the inner core. An extensive experimental investigation was done to investigate the response of CSIP walls to eccentric loading. Three CSIP panels were subjected to full-scale testing. It was noticed that the panels experienced localised de-bonding between the core and facesheets on the side that was under maximum compression. This failure mode is referred to as compression-induced wrinkling of the facesheet, resulting from a rapid localised buckling of the facesheets.

Smakosz & Tejchman (2014) conducted a series of experiments to examine the tensile strength, flexibility, and mode of failure of panels composed of expanded polystyrene (EPS) foam core and glass fibre facings reinforced with magnesium-cement. During the compression testing, it was noticed that the failure occurred as a result of the facings being crushed, without any occurrence of local or overall buckling of the facing.

Tomlinson & Fam (2016b) conducted 38 push-through tests on a precast concrete insulated sandwich panel design utilising both angled and horizontal connectors. The performance of connectors made of basalt fiber-reinforced polymer (BFRP) and steel was evaluated and compared. Typically, when subjected to tension, larger-diameter BFRP connectors tend to be pulled out, whereas under compression, they tend to be crushed. The smaller-diameter BFRP connectors experienced failure due to tension rupture and compression buckling. The connector angle and diameter positively correlated with the increase in strength and stiffness.

Tomlinson & Fam (2016a) created a computational model to forecast the behaviour of partially composite load-bearing concrete sandwich panels subjected to axial loads applied to the structural wythe at any eccentricity. The degree of composite action is substantially impacted by the length of the panel. Longer panels exhibit greater composite behaviour due to the increased shear transfer between the wythes at the midpoint, compared to shorter panels with the same connection arrangement. Nevertheless, the total capacity of the panel to withstand axial forces reduces as the length increases due to the increasing influence of slenderness effects.

Mohamad et al. (2017) investigated the structural performance of precast foamed concrete sandwich walls (FCS) that were reinforced with double steel shear connectors (DSC) and subjected to axial load. The study investigates the impact of the slenderness ratio (H/t) on

wall behaviour and compares the impacts of double shear connectors to single steel shear connectors (SSC). Finite element analysis (FEA) is used to model and simulate different wall layouts with varying H/t ratios. The findings indicate that an increase in the H/t ratio leads to a decrease in the ultimate load and an increase in the maximum horizontal deflection. Walls made of Fibre Cement Siding (FCS) and Double Skin Concrete (DSC) can withstand more loads and experience less bending than walls made of Single Skin Concrete (SSC). This demonstrates that FCS and DSC walls are well-suited for use as load-bearing walls in construction.

CoDyre & Fam (2017) investigated the axial compressive strength of sandwich panels using flax fiber-reinforced polymer (FFRP) skins with different thicknesses and layer counts. The purpose was to explore FFRP skins as a potential substitute for glass fiber-reinforced polymer (GFRP) skins. The panels are equipped with polyisocyanurate (PIR) foam cores of varying densities. A total of 78 column specimens were subjected to concentric axial compression tests. Panels containing three layers of FFRP showed the same axial strength as panels with only one layer of GFRP, regardless of the length of the panel and the density of the core. Increasing the core density by two or three times led to significant increases in peak load. The conventional decrease in peak load with increasing panel length was particularly noticeable at greater core densities. Panels exceeding a length of 1,250 mm exhibited global buckling, whilst shorter panels suffered from localised failures. The failure mechanism was affected by the length of the panel, resulting in the occurrence of skin buckling and core shear failures, particularly in panels with thicker skins and greater core densities. Greater core densities not only amplified maximum loads but also permitted greater post-peak stresses and lateral deflections prior to secondary failure.

Remarks

In summary, the studies investigate the structural behaviour of various composite panels used in load-bearing applications. From CSIPs with glass-PP laminate facesheets to panels with EPS foam and glass fiber facings, and precast concrete insulated sandwich panels with different connectors, these studies enhance our understanding of failure modes, strength, and deformability in innovative structural systems. The use of materials like BFRP, steel connectors, and FFRP skins showcases versatility. Additionally, the impact of slenderness ratios and connector layouts on overall performance has been thoroughly examined. These findings underscore the significance of material properties, connector types, and panel

dimensions in optimizing the structural response of composite panels for resilient and efficient load-bearing structures.

2.5 Behaviour of 2D Frames

Asteris (2003) explored the influence of masonry infill panel openings on the stiffness and redistribution of action effects in infilled frames subjected to lateral loads. A finite element technique is employed for the analysis, considering parameters such as the position and percentage of the opening in one-story one-bay frames and extending the investigation to multi-storey frames. The findings reveal that increasing opening percentage results in a substantial decrease in lateral stiffness, and the opening position affects the overall action between the frame and infill. In multi-storey buildings, infill walls significantly contribute to frame stiffness and lateral resistance. The study emphasizes the impact of infills on shear forces in frame columns, particularly noting higher shear forces in frames with soft ground stories.

Stavridis & Shing (2010) tackled the difficulties in assessing the seismic behaviour of masonry-infilled reinforced concrete (RC) frames by creating and fine-tuning nonlinear finite-element models. The modelling methodology integrates smeared and discrete crack methodologies to accurately represent various failure modes, such as mixed-mode fracture of mortar joints and shear failure of reinforced concrete elements. An organised calibration methodology for material parameters is introduced and verified using experimental data. The models effectively capture nonlinear behaviour, precisely forecasting strength and failure processes. The study evaluates the responsiveness to modelling parameters, emphasising the significance of calibrated factors, namely those associated with the initial shear strength of concrete, brick, and mortar joints, with mortar joint qualities having the greatest impact.

Sadek & Lissel (2013) investigated the seismic performance of concrete masonry walls through tests on eight squat specimens subjected to simulated seismic loads. The walls include an Unreinforced Masonry (URM) control wall and others reinforced with different configurations of Bed Joint Reinforcement (BJR), such as steel-ladder shaped BJR, Geogrid, and Glass Fibre Reinforced Polymer (GFRP). The study demonstrates enhanced seismic performance, including increased energy dissipation and in-plane flexural strength, due to various BJR types. The results indicate up to an 85% improvement in lateral capacity with the use of BJR. However, the stiffness of walls with bed joint reinforcement decreases, leading to sliding failure in most cases. Geogrid and GFRP materials, when used as bed joint reinforcement, show increased energy absorption and improved seismic performance. The

study recommends the use of GFRP and Geogrid materials as bed joint reinforcement, highlighting their corrosion resistance and the recyclable and cost-effective nature of Geogrid. Overall, both materials exhibit an average percentage increase in lateral capacity of 54.7%, with the grid shape of Geogrid providing the best improvement.

Furtado et al. (2015) studied the in-plane behaviour of infill masonry walls and its interaction with the surrounding frames. The experimental test setup was presented, including all the instrumentation and loading conditions. It was observed a continuous increase of the in-plane strength until 0.25% of drift, after which the strength got stable.

N. Jayaramappa (2015) carried out an experimental investigation on the behaviour of a 2D single bay two storey reinforced concrete (RC) frame with brick infill. The proposed model is subjected to lateral load at each storey level and their performance was assessed based on load carrying capacity and deflection. Analytical study was also conducted for the similar frame and the results were compared with experimental study.

Brodsky & Yankelevsky (2017) examined the behaviour of common infilled masonry reinforced concrete (RC) frame buildings during intense events. The progressive bending of the frame caused by the absence of a column support can be limited by the structural strength of the masonry infill wall and its ability to work together with the surrounding reinforced concrete frame. The findings demonstrate that the presence of brick infill walls significantly enhances the ability of the frame to withstand vertical loads, in comparison to a frame without any infill walls. On average, the resistance is increased by around 280%, with certain cases showing an increase of up to 500%.

Sagar et al. (2019) investigated the performance of masonry-infilled reinforced concrete (RC) frames strengthened with fabric-reinforced cementitious matrix (FRCM) under bidirectional loading. Six single-story, single-bay half-scale RC frames were tested with varying FRCM configurations, including different fabric application modes, the presence of mechanical anchors, and fabric orientations. The bidirectional loading protocol involved slow cyclic in-plane drifts and ground motion-induced out-of-plane loading. Findings reveal that direct fabric application outperformed sandwich application, exhibiting superior bond characteristics and stress redistribution. Mechanical anchors enhanced the bidirectional response, limiting infill separation and improving energy dissipation. The study underscores the effectiveness of FRCM strengthening in preserving structural integrity and out-of-plane stability in masonry-infilled RC frames.

Hashemi et al. (2018b) examined the seismic behaviour of Concrete Sandwich Panel-Infilled Steel Frames (CSP-ISF) in the horizontal direction using both experimental and numerical analysis. Four steel frame specimens of significant size, consisting of one frame without any additional material and three frames with varying proportions of CSP infill, were subjected to reversed cyclic lateral loading during testing. The use of sandwich panels led to enhanced lateral stiffness, strength, ductility, energy dissipation capacity, and equivalent viscous damping ratio of the steel frames. The maximum shear capacity was verified using analytical methods, demonstrating excellent correspondence with experimental findings. The introduction presents the proposed performance levels for structural performance in Performance-based Analysis. The numerical model accurately forecasts the nonlinear characteristics of CSP-ISFs, confirming the model's resilience in relation to experimental findings.

Ha et al. (2018) examined the performance of Reinforced Concrete (RC) frames that were reinforced with L-type Precast Concrete (PC) wall panels when subjected to cyclic stresses. The technique entails substituting brick walls with windows within reinforced concrete frames containing robust and stiff precast concrete infills. The method utilises dowels, which are anchors placed after the fact, to securely attach PC wall panels to RC frames. Six complete, single-bay, single-story reinforced concrete frames were built and subjected to reverse cyclic stress. To reinforce the frames, four L-shaped precast wall panels were utilised. The findings demonstrate substantial enhancements in the frames' ability to resist lateral forces, rigidity, and capacity to absorb and dissipate energy. The proposed seismic retrofitting technique is considered highly beneficial for low-rise structures that have windows. It enhances the buildings' ability to withstand seismic activity, while still allowing for the presence of openings. Additionally, this technique is cost-effective and efficient in terms of construction. The study offers valuable insights into the determinants that impact the overall flexural strength of reinforced concrete (RC) columns and L-type precast (PC) wall panels. It highlights the significance of horizontal dowels, the thickness of PC wall panels, and reinforcement in this regard.

Rao & Poluraju (2020) examined the efficiency of full-scale precast Reinforced Concrete (RC) sandwich slim walls when subjected to reversed cyclic loads. Eight precast slender walls, designed with differing aspect ratios and characteristics, were subjected to lateral incremental monotonic and cyclic stress utilising a displacement control system. The study assesses the performance of the walls by comparing the lateral load to the lateral displacement,

analysing cracking patterns, measuring displacement ductility, evaluating stiffness deterioration, and quantifying energy dissipation. The experimental findings, which were compared to predicted lateral strength values from different codes of practice, demonstrate that the inclusion of extra longitudinal reinforcement and end stiffeners greatly enhances the lateral strength, resistance to cracking, stiffness, ductility, and ability to dissipate energy of precast sandwich slender walls subjected to lateral cyclic loading. The walls that are designed with these additions demonstrate slight boosts in stiffness when subjected to lateral loading, and their seismic base shear capacity is similar to that of typical RC walls. The results indicate that precast sandwich slim walls, when combined with supplementary reinforcement and stiffeners, have the ability to endure significant lateral stresses. This makes them well-suited for use in seismic applications inside regions characterised by high levels of seismic activity.

Sakr et al. (2021b) examined the experimental and numerical responses of retrofitted masonry infilled reinforced concrete (RC) frames. They tested the use of either fully bonded or partially bonded diagonal carbon fibre reinforced polymers (CFRP) strips under cyclic loads. Five 1/2-scaled, one-bay, one-storey non ductile reinforced concrete (RC) frames were built and examined. The frames were evaluated in three different conditions: bare, infilled with reference materials, and retrofitted with x-cross carbon fibre reinforced polymer (CFRP) sheets. Two methods of retrofitting were used: fully bonded CFRP strips and partially bonded CFRP strips. The study conducts a comparison between retrofitted specimens and reference specimens, analysing inter-storey drift, lateral load capacity, energy dissipation capacity, stiffness, and observable damages. The study's findings indicate that the suggested retrofitting approaches greatly improve the ability of reinforced concrete frames to withstand earthquakes. The numerical model used in the study accurately predicts the results of the experiments.

Einea (1992) experimentally studied the performance of PICS boards with FRP bent bars as shear linkers under pull-off force (through-depth shear force). The push-off force analysis is done to see the performance of these structural boards under the combined action of flexure and axial force. The analysis for push-off analysis determines the performance for two parameters that are bond strength of shear linkers with a concrete top and bottom wythe and the middle insulated (EPS) core and the resistance of shear linkers against the deformation force which leads these linkers to buckle.

Hodicky et al. (2015) showed that shear flow in PICS panels is highly dependent on the spacing of the shear linkers. They observed that the shear flow increases with the increase in

spacing of shear linkers and decreased with the increase in middle core depth and it was also observed that for PICS specimens, EPS middle core performed better than XPS middle sheet.

Gara et al. (2012) conducted the axial, eccentric and diagonal compression on these PICS panels with straight shear connectors. The author also has performed experiment on panels with different EPS core thicknesses. The authors reported that all the panels tested behaved as semi-composite elements, and increasing panel thickness was necessary for increased load-carrying capacity. The panels also showed a high capacity for stress redistribution due to the metallic mesh inside the concrete layers. In this paper FEM analysis is done using the software ANSYS workbench in push-off loading, axial and diagonal compression and the results are obtained from the FEM simulation

Ronald et al. (2019) observed the effect of depth of middle EPS sheet, the clear gap between the wythes, presence/absence of the EPS core and number of shear connector lines influence the through-depth shear behaviour and resistance to deformation of the PICS panels. They stated that the through-depth shear resistance of the PICS panels increases with reduction in thickness of the EPS middle sheet and reduction in clear gap between the wythes.

Remarks

In conclusion, the reviewed studies provide a comprehensive understanding of the complex interactions and behaviours associated with various structural systems, ranging from masonry-infilled frames to retrofitted reinforced concrete structures and innovative panels like Precast Insulated Concrete Sandwich (PICS) boards. These investigations utilize experimental, numerical, and analytical approaches to explore seismic performance, retrofitting strategies, and the influence of design parameters on structural behaviour. The findings contribute valuable insights into enhancing the resilience, load-carrying capacity, and energy dissipation capabilities of diverse structural elements. As the research landscape continues to evolve, the collective knowledge gained from these studies paves the way for improved design practices and the development of robust, sustainable, and resilient structures in the face of dynamic forces and seismic events.

2.6 Analysis of concrete sandwich panel through FEM software

Einea et al. (1994) experimentally studied the performance of PICS boards with FRP bent bars as shear linkers under pull-off force (through-depth shear force). The push-off force analysis is done to see the performance of these structural boards under the combined action of flexure and axial force. The analysis for push-off analysis determines the performance for two

parameters that are bond strength of shear linkers with a concrete top and bottom wythe and the middle insulated (EPS) core and the resistance of shear linkers against the deformation force which leads these linkers to buckle.

Hodicky et al. (2015) showed that shear flow in PICS panels is highly dependent on the spacing of the shear linkers. They observed that the shear flow increases with the increase in spacing of shear linkers and decreased with the increase in middle core depth and it was also observed that for PICS specimens, EPS middle core performed better than XPS middle sheet.

Gara et al. (2012) conducted the axial, eccentric and diagonal shear on these PICS panels with straight shear connectors. The author also has performed experiment on panels with different EPS core thicknesses. The authors reported that all the panels tested behaved as semi-composite elements, and increasing panel thickness was necessary for increased load-carrying capacity. The panels also showed a high capacity for stress redistribution due to the metallic mesh inside the concrete layers. In this paper FEM analysis is done using the software ANSYS workbench in push-off loading, axial and diagonal compression and the results are obtained from the FEM simulation

Ronald et al. (2019) noted the influence of centre EPS sheet, the distinct space between the wythes, the wythes, the presence or absence of the EPS core, and the number of shear connector lines all had an impact on the shear behaviour and resistance to deformation of the PICS panels. The shear resistance of the PICS panels increases when the thickness of the EPS middle sheet decreases and the clear gap between the wythes decreases.

Huang et al. (2020) presented an Explicit Nonlinear and Plastic Analysis Model (ENPAM) designed for Steel–Concrete–Steel (SCS) panels. ENPAM considers concrete behaviour under biaxial stresses and the post-yield characteristics of steel plates, providing a comprehensive simulation of stress redistribution during plastic flow after steel plate yielding. The model's accuracy is demonstrated through comparisons with experimental data and Finite Element Modeling (FEM) for SCS panels subjected to various loading conditions, showcasing its ability to capture post-yielding behaviour, strength, loading processes, and ductility. ENPAM's predictions align well with experimental and FEM results, indicating its efficacy in simulating SCS panel behaviour, especially in scenarios involving complex nonlinear processes.

Colombo et al. (2018) explored sandwich beams with Textile Reinforced Concrete (TRC) layers and expanded polystyrene (EPS) insulation using analytical and numerical models. Validated through experiments, the analytical model proves reliable with conservative

predictions for slender beams. The Finite Element (FE) model, incorporating a Crushable Foam model for EPS, aligns well with experiments, capturing global response. The perfect bond assumption works initially but fails to simulate high ductility, especially at the TRC/EPS interface. The FE model predicts experimental results but conservatively underestimates load in the plastic branch for slender beams.

Djamai et al. (2017) explored sandwich beams with Textile Reinforced Concrete (TRC) layers and expanded polystyrene (EPS) insulation using analytical and numerical models. Validated through experiments, the analytical model proves reliable with conservative predictions for slender beams. The Finite Element (FE) model, incorporating a Crushable Foam model for EPS, aligns well with experiments, capturing global response. The perfect bond assumption works initially but fails to simulate high ductility, especially at the TRC/EPS interface. The FE model predicts experimental results but conservatively underestimates load in the plastic branch for slender beams.

Jensen et al. (2020) introduced a novel mechanics-based model (MBM) for partially composite concrete sandwich wall panels designed exclusively in the elastic range. The MBM, suitable for practical design, incorporates out-of-plane loading, axial loading, thermal deformation, and asymmetric geometry and loading. Validation against experiments shows good agreement for deflections and thermal bowing. A parametric study and comparison to finite element analysis (FEA) demonstrate the MBM's robustness, handling different scenarios such as openings, eccentric dead loads, and asymmetric panels. The study addresses the absence of a well-accepted design method in the literature outside finite element analysis.

Khatibi et al. (2023) explored the flexural behaviour of Box-Profile (BP) shear connectors in composite steel–concrete-steel (SCS) structures. Nine beam specimens are tested, and geometric parameters' effects on flexural strength are analyzed. Increasing shear connector width enhances beam rigidity but leads to slot weld failure. Concrete core strength above 40 MPa doesn't improve behaviour. Beams with specific geometric parameters exhibit higher composite behaviour. Numerical modeling and nonlinear finite element method (FEM) validation are performed, revealing insights into shear connector arrangement and concrete core strength contributions. The study suggests the potential use of Nelson studs and considers future research directions.

Latour et al. (2021) investigated the potential applications of metal foams, known for their attractive mechanical properties, in civil engineering, specifically focusing on double-skin composite sandwich panels made of steel sheets and aluminum foam for civil structures.

Experimental tests and finite element simulations are conducted to assess the performance of these panels. Thinner aluminum foam panels exhibit greater sensitivity to defects, suggesting a preference for thicker panels. Preliminary design guidelines are derived for multistory steel buildings, showcasing potential weight reduction and enhanced sustainability with the use of steel-to-aluminum foam sandwich panels. The study emphasizes the need for further experimental tests to characterize debonding resistance for different adhesives and provides insights into foam density effects on panel flexural resistance, stiffness, and ductility within a specific range.

Ngo & Nguyen (2023) investigated the behaviour of thin-walled TRC structures connected by bolts, with a focus on open box panel members for various applications such as walls, floors, and roofs. Three types of connections—moment joints, shear joints, and half-box connections—are examined. The study identifies that the bearing capacity of TRC structures is significantly influenced by the bolt-to-edge distance. The location and type of cracks in moment joints depend on the number of bolts used. Half-box connections experience damage at the bolted side, with cracks around steel bolts leading to failure at approximately 74% and 70.6% of the original panel's bearing capacity. The bolted connection is identified as the weakest link, necessitating improvements in bolt structure or increased rib thickness to enhance bearing capacity. Finite element models developed in the ATENA software accurately replicate load-carrying capacities, load-deflection relationships, and failure modes for both panels and connections.

Proença et al. (2020) investigated the acoustic performance of composite sandwich panels designed for building floors. Experimental, numerical, and analytical approaches were employed. The panels exhibited overall low acoustic performance, requiring additional sound insulation measures. Numerical simulations agreed well with experimental data, capturing the coincidence effect. Finite element analysis proved useful in estimating airborne sound transmission, and analytical predictions aligned with experimental results, affirming the method's applicability. Impact sound pressure levels estimated through the analytical method demonstrated good agreement with experimental results, indicating its efficiency without relying on time-consuming standardized testing.

Serpilli et al. (2021a) found that experimental and numerical findings demonstrated the efficiency of sprayed concrete with no evident splitting from the insulation layer. The shear tests, including diagonal compression and shear with constant compression, show stress redistribution and semi-composite behaviour till rupture. The shear capacity of RC sandwich

panels is comparable to conventional RC walls. Nonlinear finite element analysis approximates the experimental trends well, emphasizing the structural potentialities of RC sandwich panels for load-bearing and shear walls.

Ye et al. (2021) investigated the blast behaviour of Precast Concrete Sandwich Panels (PCSPs) through numerical analyses and experimental validation. A three-dimensional finite element model is developed and validated with explosion tests. A simplified numerical model is proposed to validate dynamic response calculations under blast loads. Comparisons with reinforced concrete (RC) slabs show that PCSPs exhibit weaker blast resistance. The study suggests that narrow connector spacing enhances blast resistance, and the theoretical model reliably predicts PCSPs' dynamic response, highlighting their vulnerability to blast loads compared to RC slabs. Further research is recommended, considering novel connector materials.

Yuan et al. (2023) studied blast mitigation for protective structures through an innovative multilayer sandwich wall. The wall comprises two steel wire mesh-reinforced geopolymer-based high-performance concrete layers and a metallic tube core layer. Experimental and numerical investigations are conducted under a 1.0 kg contact explosion, exploring factors such as layer thickness. Findings reveal that well-designed sandwich walls exhibit excellent anti-blast performance, with the rear G-HPC layer significantly influencing results. Adjusting layer thicknesses enhances anti-blast performance. The study provides insights into energy absorption and supporting resistance, and while promising, scale effects should be considered in practical applications.

Zhao et al. (2023) investigated the blast resistance of C-shaped doubled steel concrete slabs (C-DSCS) with L-shaped connectors, utilizing the concrete's compressive strength and arch-like load-bearing capacity. Experimental and numerical analyses under near-field explosion explore dynamic behaviours and energy dissipation. The C-DSCS exhibits good integrity and withstands the explosion without severe destruction. Concrete and bottom steel plate are primary energy-consuming components, dissipating over 78% of explosive energy. L-shaped connectors contribute to energy absorption, effectively reducing maximum deflection with decreased connector spacing. The study provides a foundation for theoretical analysis and design methods for C-DSCS under close-in explosion scenarios.

Gu & Lu (2023a), through numerical simulations, studied the feasibility of distinguishing between different types of damage in a structural health monitoring and damage identification process using vibration information like natural frequencies and mode shapes.

Alharthi et al. (2023) investigated the flexural behavior of hollow concrete beams reinforced with GFRP bars featuring longitudinal openings of various sizes and shapes. Seven beams were tested, including solid GFRP-RC beams, hollow GFRP-RC beams with circular and square holes (constituting 6-15% of the cross-sectional area), and one hollow steel-RC beam with a 9% longitudinal hole. An analytical model for the flexural capacity of hollow beams was also developed, and it accurately predicted cracking behavior.

Remarks

In summary, these diverse studies contribute valuable insights into innovative structural materials and systems, spanning metal foams, Textile Reinforced Concrete, and geopolymer-based high-performance concrete. The integration of experimental, numerical, and analytical approaches highlights the need for comprehensive analysis in ensuring structural integrity. As the field evolves, these findings pave the way for advancements in structural engineering, addressing challenges such as blast resistance, acoustic performance, and the behaviour of novel materials. The collective research encourages further exploration and development towards resilient, efficient, and sustainable structural solutions.

Closing remark

This chapter dealt with the literature review of the concerned area of research i.e. the concrete sandwich panels. From literature it can be understood that the new emerging techniques are gaining popularity over the conventional building methods. Moreover the literature also give a sense of relief that these sandwich panels can be used as a structural member. Various researchers have performed various test on these panels made up of different materials and noted their response. These studies have been very helpful in achieving the objective decided for this thesis.

Chapter 3

Experimental Program

3.1 General

This chapter provides a thorough and detailed summary of the experimental program. The first step is a comprehensive analysis of the characteristics of various materials employed in the project. This chapter provides the mix proportions for the manufacture of micro concrete. Furthermore, this document also covers the details on the preparation of specimens, as well as the techniques for casting and curing. This text discusses the methodology used to analyse the behaviour of concrete sandwich panels (CSP) when subjected to various loading conditions. The process of casting the 2D RC frame with CSP as an infill wall and the arrangement for conducting the test have been described.

3.2 Materials

3.2.1 Cement

Ordinary Portland cement of grade 53 conforming to BIS: 8112-1989 has been used and is comparable to ASTM C150-17. To reduce the impact of switching brands, a fresh batch of cement from the same brand has been utilized. The results of the physical properties of cement are mentioned in Table 3.1.

Table 3. 1: Physical properties of cement

Characteristics	**Test values obtained**	**Permissible values given in IS 12269-2013**
Standard Consistency (%)	32	---
Fineness of cement as retained on 90-micron sieve (%)	0.7	---
Specific Gravity	3.12	---
Setting Time (minutes) (a) Initial Setting time (b) Final Setting Time	 116 minutes 305 minutes	 30 min (minimum) 600 min (maximum)
Compressive Strength (MPa) (a) 3 days (b) 7 days (c) 28 days	 29 39.5 57	 27 37 53

3.2.2 Fine Aggregates

Two types of fine aggregates are used in the present study. It includes the conventional river sand and stone dust. The details of both the materials used as fine aggregates are presented in the following sections:

3.2.3 River Sand

Locally available river sand fulfilling the requirements of BIS 383 (2016) was used as fine aggregates. The physical properties of the aggregates were obtained by testing as per the relevant codal provisions and the values are provided in Table 3.2.

The sieve analysis results of fine aggregates used in the present study are presented in Table 3.3. From sieve analysis results (Table 3.4), it can be seen that the percentage passing of fine aggregates satisfied the Zone III recommendations and codal provision.

Table 3. 2: Physical properties of river sand

Characteristic	**Natural River Sand**	**Standard followed**
Specific gravity	2.49	BIS 2386 Part III- 1963
Water absorption	2.1	BIS 2386 Part III- 1963
Fineness modulus	2.26	BIS 2386 Part III- 1963
Bulk density (kg/m3)	1510	---
Specific surface area (m2/g)	0.210	---
Grading Zone	Zone III	BIS 383-2016

Table 3. 3: Chemical composition of river sand

Constituent (%)	River Sand
CaO	5.73
SiO_2	77.39
Al_2O_3	8.38
Fe_2O_3	2.39
SO_3	-
MgO	0.70
K_2O	0.02
Na_2O	0.005

Table 3. 4: Sieve analysis results for sand with some replacement of stone dust

IS-Sieve size (mm)	Weight retained (%)	Cumulative weight retained (%)	Weight passing (%)	IS limits for Zone III
4.75 mm	8.5	99.15	.85	100
2.36	292	69.95	30.05	90-100
1.18	224.5	47.5	52.5	85-100
600 µm	119.5	35.55	64.45	75-100
300 µm	142.5	21.4	78.6	65-79
150 µm	115	9.9	90.1	-
Pan	-	-	-	-
Total	-	-	316.55	-

3.2.4 Stone Dust

Stone dust was obtained from the stone crushing units located in Ramgarh, district Panchkula, Haryana as part of the data collection process for this study. The specimen was obtained in a desiccated state and underwent a sieving process prior to its incorporation into the concrete mixture.

The findings pertaining to the sieve analysis of stone dust have been presented in Table 3.5. The specific gravity of stone dust was determined to be 2.50, indicating its relative density compared to water. Additionally, the water absorption of the stone dust was found to be 0.5%, indicating its ability to absorb water when exposed to it.

3.2.5 Coarse Aggregate

Coarse aggregate refers to the portion of the concrete mix that is retained on the sieve (4.75 mm) during the process of sieving. Coarse aggregates can vary in size, and those with a size less than 6 mm (Figure 3.1) (typically in the range of 4.75 mm to 6 mm) are often referred to as "fine" or "small" coarse aggregates.

These smaller coarse aggregates are commonly used in specific concrete applications, including certain types of lightweight or high-strength concrete or micro concrete (Table 3.6).

Table 3. 5: Sieve analysis results for stone dust

IS-Sieve size (mm)	**Weight retained (%)**	**Cumulative weight retained (%)**	**Weight passing (%)**	**IS limits for Zone III**
4.75	41.5	95.9	4.1	100
2.36	166.5	79.3	20.7	90-100
1.18	169	62.4	37.6	85-100
600 µm	115.5	50.9	49.1	75-100
300 µm	160	34.9	65.1	65-79
150 µm	163	18.6	81.4	-
Pan	183	-	-	-
Total	-	-	258	-

Figure 3. 1: Aggregate size less than 6 mm

Table 3. 6: Physical properties of coarse aggregate

Properties	Coarse Aggregate		
	6 mm	10 mm	20mm
Specific Gravity	2.65	2.65	2.63
Water absorption (%)	1.31	1.4	1.38

3.2.6 Geogrids

Plastic geogrid was procured locally and Polyester geogrid was supplied by Strata Grid India Private Limited and shown in Figure 3.2. The mechanical properties of wire mesh and EPS are shown in Table 3.9. Plastic uniaxial geogrid (PUG) and polyester biaxial geogrid (PBG2 and PBG3) have been provided by Strata Grid India Private Limited, as illustrated in Figure 3.2. Plastic Geogrid is a uniaxial geogrid, Figure 3.2(a) and 3.2(c). Polyester biaxial geogrid (PBG2 and PBG3) is a biaxial geogrid having two weaving directions. One is the machine direction (MD) and the other is the cross-machine direction (CMD), Figure 3.2(b) and 3.2(d). The machine direction has 200 kN/m^2 as the average tensile strength for PBG2 and 300 kN/m^2 as the tensile strength for PBG3, whereas cross-machine direction ribs have the tensile strength of 30 kN/m^2.

3.2.7 EPS and WWM

The core of the sandwich panel consists of expanded polystyrene having density of 15 kg /m^3. It also consist of welded wire mesh on both the sides of the eps connected with truss shaped shear connectors., The properties of EPS and WWM are mentioned in Table 3.7.

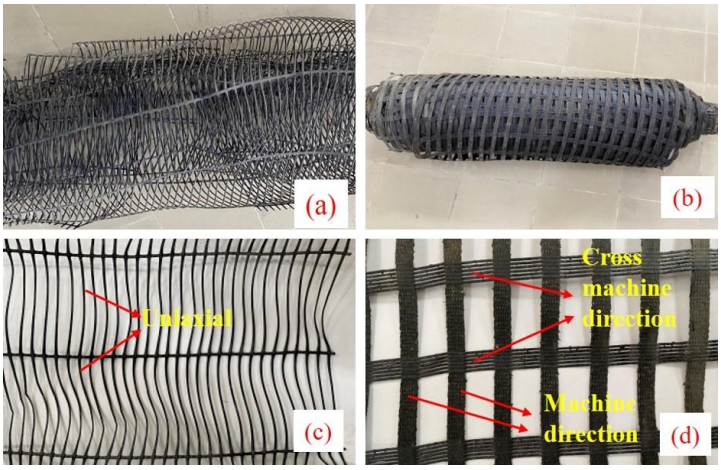

Figure 3. 2: Geosynthetics (a) Plastic uniaxial geogrid roll; (b) Polyester biaxial geogrid roll; (c) Plastic uniaxial geogrid; (d) detail of polyester biaxial geogrid.

Table 3. 7: Properties of Wire Mesh and EPS

Galvanised Steel Specification	Expanded Polystyrene Specification
Wire diameter : 3 mm	Density : 15 kg/m^3
Tensile strength : 88 kg/mm^2	Grade : fire resistant
Low carbon steel with hot dipped zinc coating	Thickness : 50 mm

3.3 Mix proportions

Two types of mix have been used M1 (cement and fine aggregate ratio is 1:3) conforming to IS 13935 (2009) standard & M2 (1:2:3), (cement, fine aggregate and aggregate size less than 6 mm) conforming to IS : 2386 (Part I) (1963) and IS 456 (2000) standards. A similar mix proportion was reported by Padalu et al. (2018) and Vishnu et al. (2017). Ordinary Portland cement conforming to IS 8112 (2013) standards are used in the present study and the fine aggregate conforming to BIS 383 (2016) standards. The water to cement ratio used in the study for all specimens is 0.5. Locally available stone dust is used as a partial replacement for coarse sand of zone II, and the fine aggregate passing through 4.75 mm sieve and retaining on 2.36 mm sieve have been used; so, 3 part is further divided into 1.2:0.6:1.2 to prepare M1 mix in which 1.2 is coarse sand (zone II), 0.6 is the aggregate size having less than 4.75 mm and 1.2 is stone dust. The ratio of mix M2 used for casting is 1:2:3 (1 part of cement, 2 parts of fine sand, and 3 parts of aggregate having size < 6 mm). The average compressive strength of M1 is 29.5 MPa at 28 days whereas M2 is 24 MPa as per BIS 516 (1959) standards. However, the strength difference in both the mixes is significant this may be due to the larger surface area of stone dust present in M1. The water absorption value of stone dust obtained is 3.3 as per BIS 1124 (1974) standard, stone dust was used as a partial replacement of fine aggregate as its capacity to absorb water is higher than that of fine aggregate thereby decreasing the effective water-cement ratio hence increases the strength.

3.4 Methodology of concrete sandwich panel testing

3.4.1 Flexure testing

A total of sixteen specimens are cast and tested to evaluate the flexural behaviour of the CSPs. The geometrical properties of the specimens are shown in Table 1. The minimum thickness of the wythe required for a load-bearing panel is 35 mm as per the guidelines mentioned by Building Materials and Technology Promotion Council (BMTPC) (“Manual for Expanded Polystyrene (EPS) Core Panel System and Its Field Application Sponsored By Ministry of Housing and Urban Poverty Alleviation , Government of India,” 2017). The thickness of each wythe in the present study is 40 mm for all specimens.

Table 3. 8: Details of Material Used

Specimen id	Specimen Size (L × B × H)mm	Material	Mix
SPC1	1300 × 600 × 130	Welded Wire Mesh (WWM)	M1 (1 : 3*) (C : FA)
SPGG		WWM + PUG	
SPSgi200		WWM + PBG2	
SPSgi300		WWM + PBG3	
SP1C		Welded Wire Mesh (WWM)	M2 (1 : 2 : 3**) (C : FA : CA)
SP1GG		WWM + PUG	
SP1Sgi200		WWM + PBG2	
SP1Sgi300		WWM + PBG3	

* FA (fine aggregate) consisting of stone dust, fine sand and coarse sand (retained on 2.36 mm sieve)

** Aggregate size less than 6mm; SPC= Sandwich Panel (Control); SPGG= Sandwich Panel Geogrid (Plastic); SPSgi200= Sandwich Panel containing Sgi200; SPSgi300= Sandwich Panel containing Sgi300; PUG: Plastic uniaxial geogrid; PBG: Polyester Biaxial Geogrid; PBG2: Sgi 200; PBG3: Sgi 300.

3.3.1.1 Fabrication and Casting

The specimens are cast horizontally using steel formwork. The cover blocks are used to maintain the concrete cover of 25 mm before placing the EPS core having the welded wire mesh (WWM). A rich cement slurry is spread on the EPS core so that the mix could bind with the EPS. A layer of a mix (M1/M2) has been plastered on it up to a depth of 15 mm (i.e. the gap between EPS core and WWM) and the specimen is left for drying (2 hours). The surface is made rough so that the next layer of 25mm of mix (M1/M2) binds completely with the previous layer and the respective 40 mm thickness of one wythe is achieved (Figure 3.3). Then after the casting of the upper wythe, the mould is left for drying so that when it is toppled over to cast the lower wythe, it stays intact.

A similar procedure for casting of the specimen with geogrids as mentioned in Table 2 is followed. The top layer of the respective mix is put up to a depth of 15 mm then geogrid (Figure 3.4) is laid on the first layer and tied with the WWM using cable ties (non-corrosive) Fig. 3(b). The rest of the thickness i.e. 25 mm wythe is achieved by pouring the mix. The side supports are cast using M20 grade concrete (1:1.5:3) as per the IS 10262:2019 (IS 10262, 2019). All the specimens are cured until the testing age. All the cross section details of the concrete sandwich panels are also shown in Figure 3.5 – 3.9.

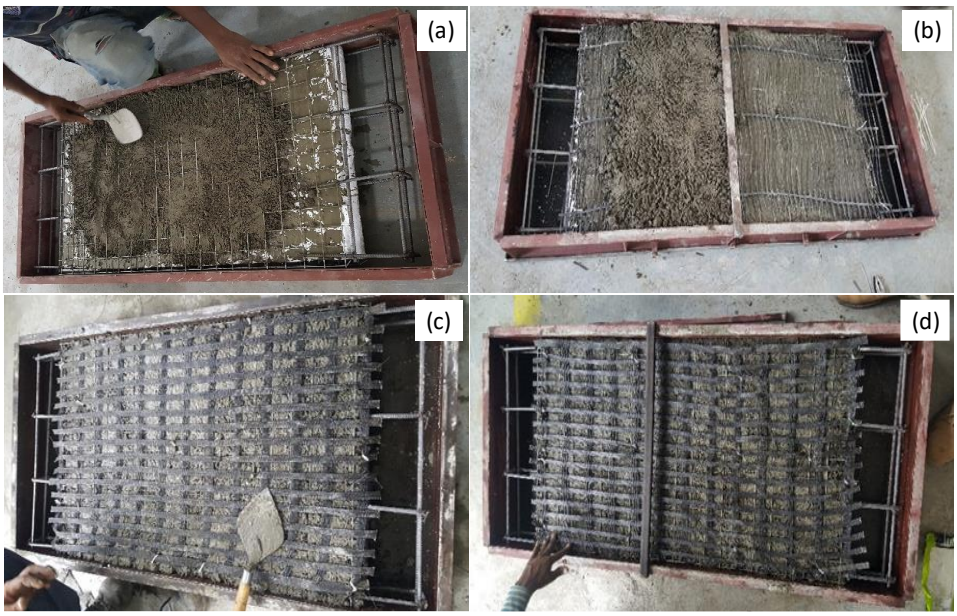

Figure 3. 3: Initial stages of casting of CSP (a)Control Specimen; (b) Plastic Geogrid with WWM; (c) Sgi 200 with WWM; (d) Sgi300 with WWM

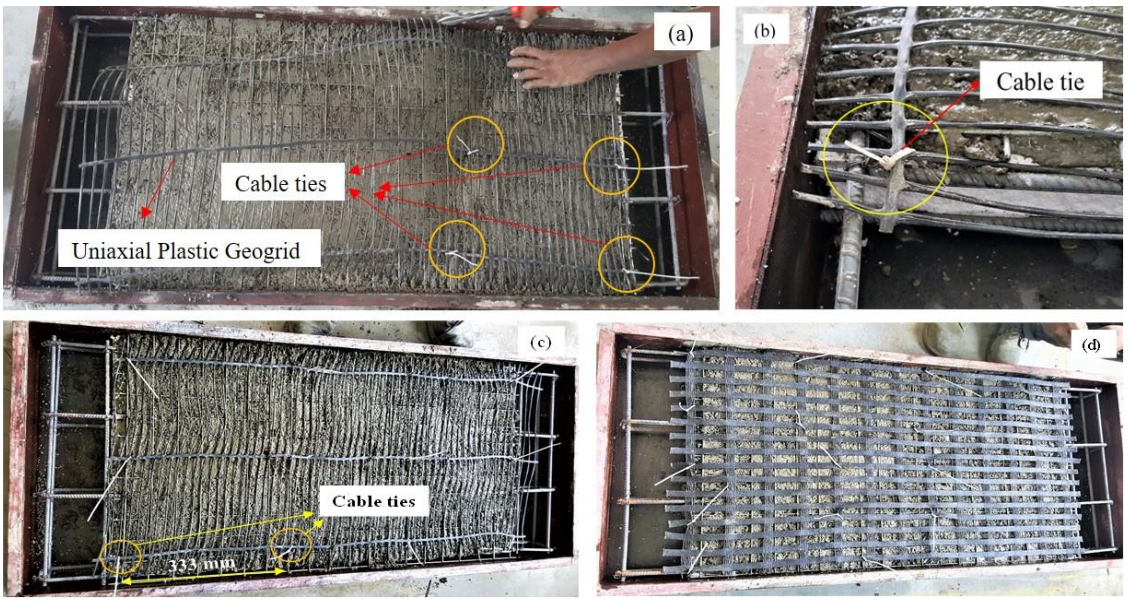

Figure 3. 4: Laying of geogrids(a) Layer of plastic geogrid being attached to welded wire mesh with the help of cable ties; (b) Magnified view of cable tie attached to welded wire mesh (c) Plastic geogrid (SPGG/SP1GG) tied tightly to the welded wire mesh with the help of cable ties (attached at 333 mm distance) to ensure its straightness; (d) Polyester geogrid (Sgi200/Sgi300) being attached to welded wire mesh.

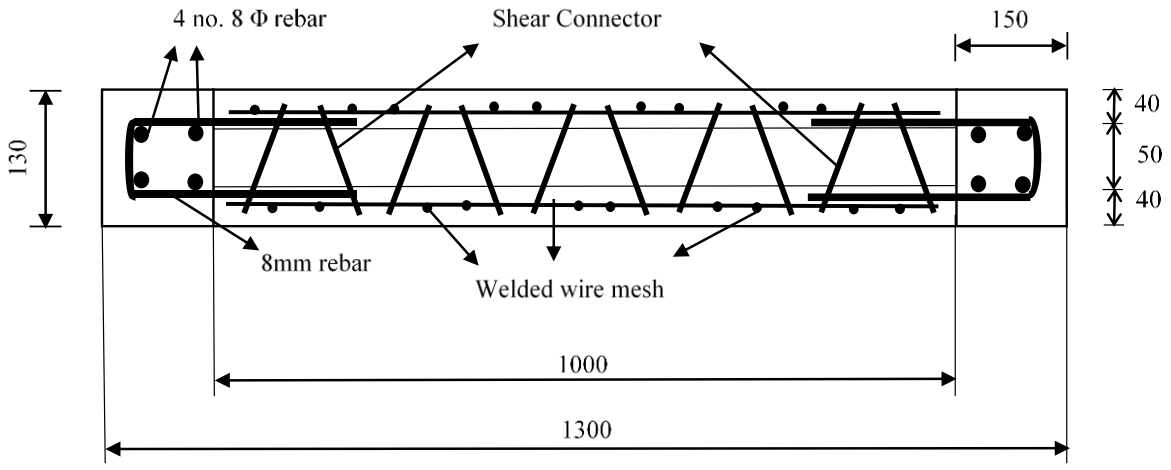

Figure 3. 5: Cross section details of end beam (All dimensions are in mm)

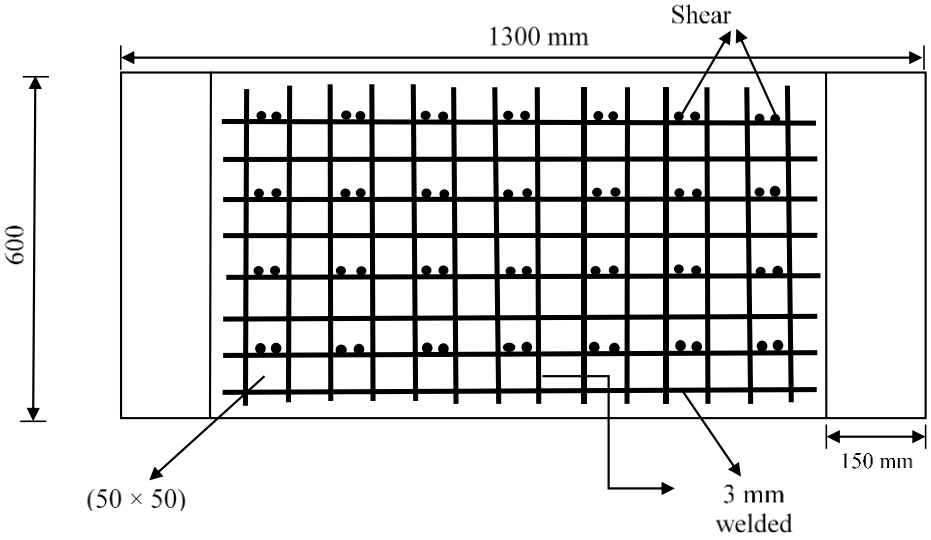

Figure 3. 6: Top view of cross section of CSP

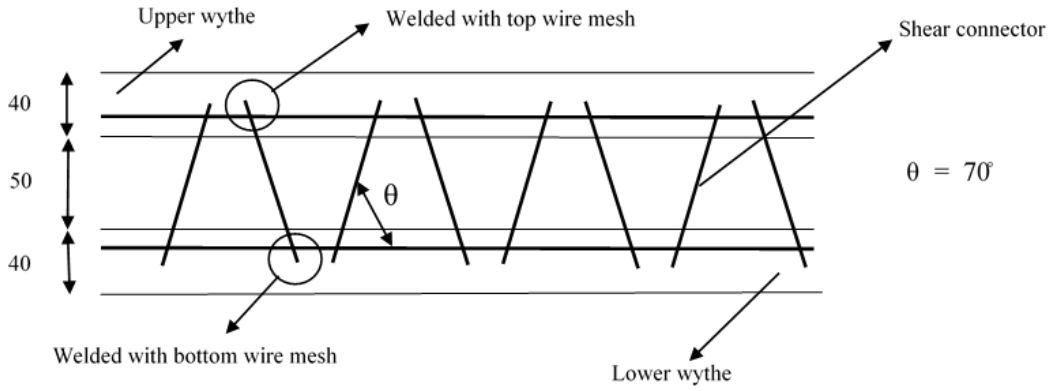

Figure 3. 7: Details of shear connector. (All dimensions are in mm.)

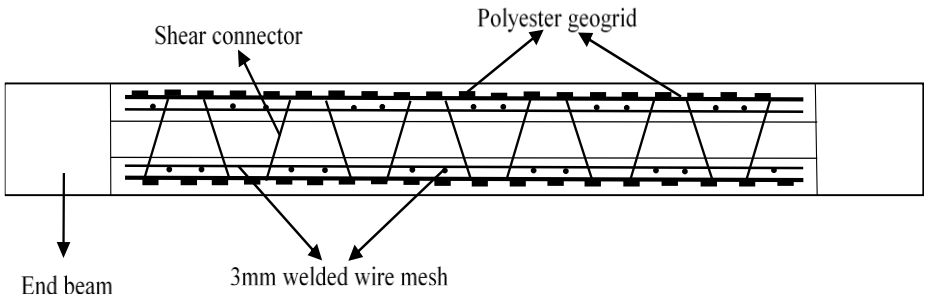

Figure 3. 8: Cross section of CSP strengthened with polyester geogrid (Sgi200 and Sgi300)

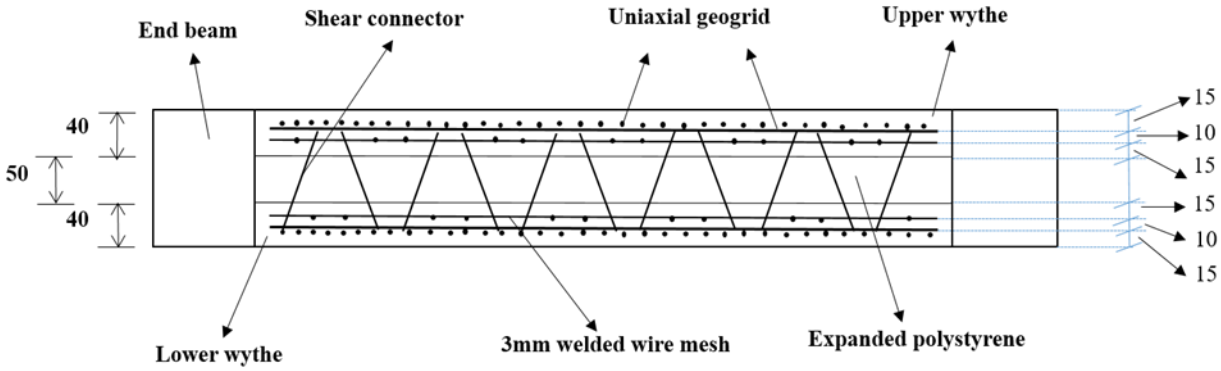

Figure 3. 9: Cross section of CSP strengthened with plastic geogrid (SPGG). (All dimensions are in mm.).

3.3.1.2 Instrumentation and Test setup

All specimens are tested under four-point bending conditions as per the guidelines of ASTM E72 (ASTM E72, 2002). The load is applied by a hydraulic jack of 600-kN capacity. To measure deflection at the mid-span, a 50-mm range Linear Variable Differential Transformer (LVDT) is used. Figure 3.10 and Figure 3.11 represents the instrumentation setup and the schematic diagram for flexural testing respectively. A total of sixteen specimens have been tested in flexure (out of plane).

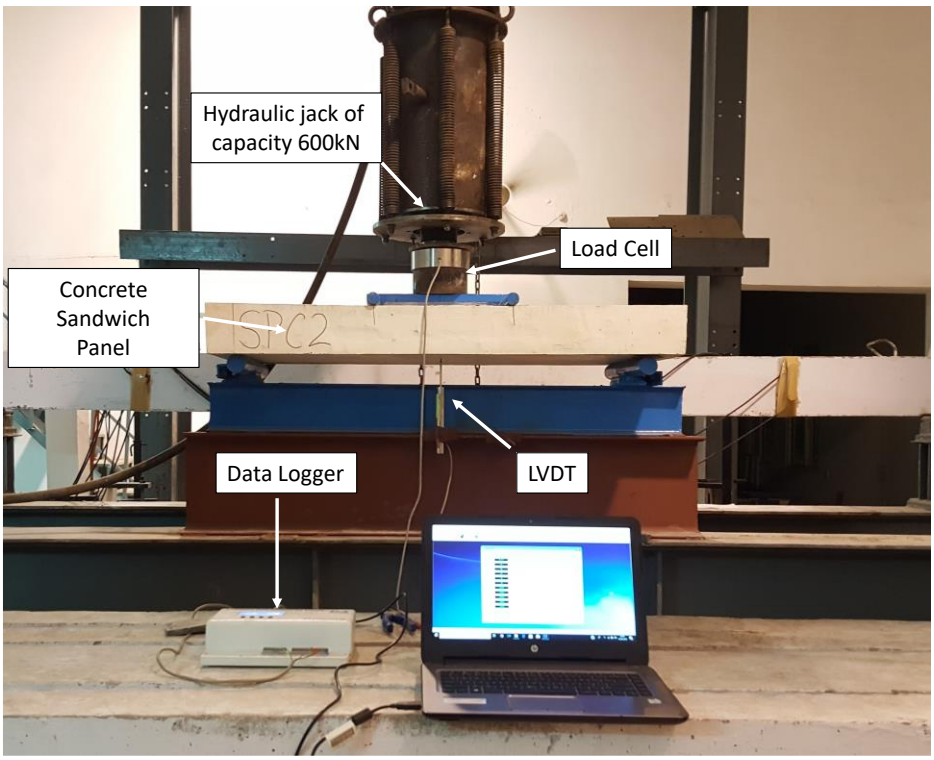

Figure 3. 10: Experimental setup to acquire data using data acquisition system

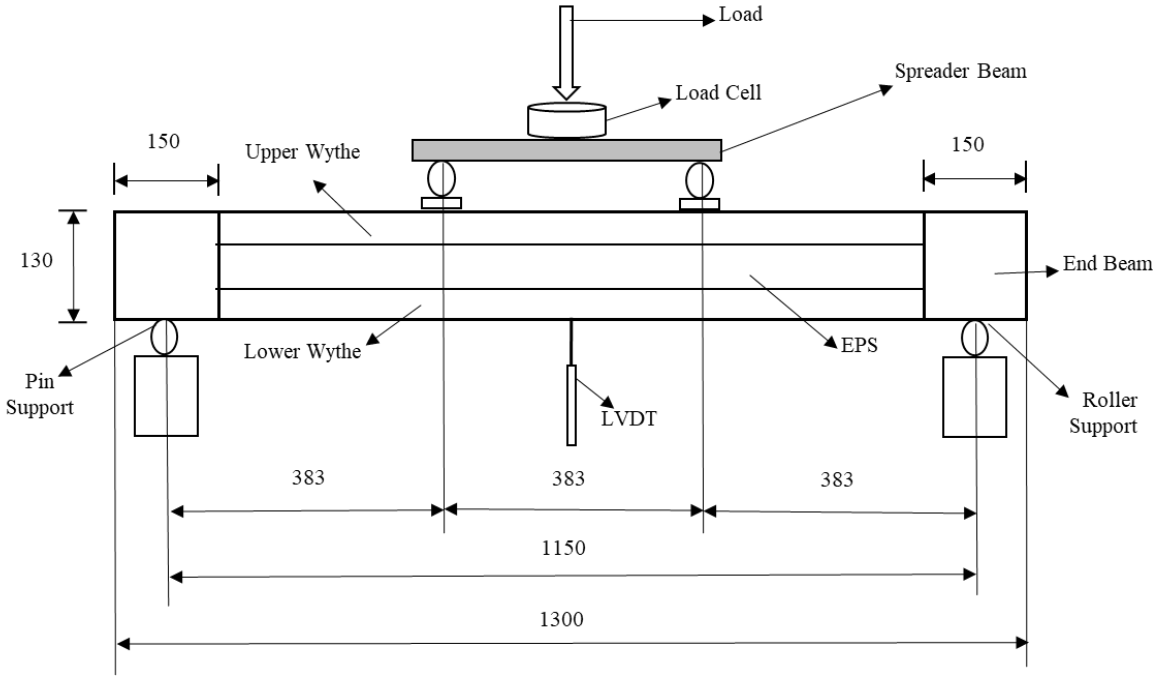

Figure 3. 11: Schematic diagram. (All dimensions are in mm.)

3.4.2 In-plane diagonal shear testing

Sixteen specimens are cast and tested to analyze the CSPs' in-plane diagonal shear behaviour. Two specimens have been cast for each group, and the average of the two has been taken as given in Table 3.9. The specification of the specimens are displayed in Table 1. The

minimum wythe thickness is 35 mm for using CSP as load-bearing structure ('Manual for Expanded Polystyrene (EPS) Core Panel System and Its Field Application Sponsored By Ministry of Housing and Urban Poverty Alleviation , Government of India', 2017). In this investigation, the thickness of each wythe is 40 mm for all specimens. M1 (1:3), as per, IS 13935 (2009) standard, and M2 (1:2:3), per IS : 2386 (Part I) (1963) and IS 456 (2000) standards. A similar mix proportion has been reported by researchers (Padalu et al., 2018; Vishnu et al., 2017). In this investigation, ordinary Portland cement that meets IS 8112 (2013) criteria and fine aggregate that meets BIS 383 (2016) standards have been employed. For all specimens in the research, the water to cement ratio has been maintained at 0.5. Coarse sand is partially replaced by stone dust procured locally, fine aggregate retained on 2.36 mm sieve is used; thus, three parts are further bifurcated into 1.2:0.6:1.2 to prepare M1 mix, where 1.2 being coarse sand, 0.6 being fine aggregate having size less than 4.75 mm, and 1.2 being the stone dust. The casting mix M2 has a 1:2:3 ratio (3 parts coarse aggregate with size of less than 6 mm.

Table 3. 9: Experimental Design

Specimen nomenclature	**No. of specimens**	**Specimen dimensions (L × B × H)mm**	**Reinforcing material**	**Mix**
DS1C	2	600 × 600 × 130	Welded Wire Mesh (WWM)	M1 (1 : 3*) (C: FA)
DS1GG	2		WWM + PUG	
DS1Sgi200	2		WWM + PBG2	
DS1Sgi300	2		WWM + PBG3	
DS2C	2		Welded Wire Mesh (WWM)	M2 (1 : 2 : 3**) (C : FA : CA)
DS2GG	2		WWM + PUG	
DS2Sgi200	2		WWM + PBG2	
DS2Sgi300	2		WWM + PBG3	

* FA (fine aggregate) consisting of stone dust, fine sand and coarse sand (retained on 2.36 mm sieve); ** Coarse Aggregate size less than 6mm; DS: Diagonal Shear; C: Control; PUG: Plastic uniaxial geogrid; PBG: Polyester Biaxial Geogrid; PBG2: Sgi 200; PBG3: Sgi 300; SPSgi200= Sandwich Panel containing Sgi200; SPSgi300= Sandwich Panel containing Sgi300

The mechanical characteristics of the component materials determine how CSP behaves structurally. To evaluate the mechanical characteristics, tests on micro-concrete, welded wire

mesh, plastic uniaxial geogrid (PUG) and polyester biaxial geogrids (PBG2 and PBG3) have been carried out according to ASTM standards.

Each specimen yielded three micro-concrete cubes (70 mm) that have been evaluated for compressive strength using BIS 383 (2016) and BIS 516 (1959). The cubes are allowed to cure for 28 days before being put through the compression test. According to BIS 516 (1959) standards, M1 has a compressive strength of 36.7 MPa and M2 has 28.7 MPa. However, there is a substantial strength difference between the two mixes, which might be attributed to the greater surface area of the stone dust present as a partial replacement of fine aggregate in the mix M1. The test of water absorption gave a value of 3.3 for the stone dust, test performed as per BIS 1124 (1974) standard. Stone dust has been utilized as a partial replacement for fine aggregate because it has a larger ability to absorb water than fine aggregate, lowering the effective water-cement ratio and therefore increasing strength.

Uniaxial tension tests on WWM wire, plastic geogrid and polyester geogrid have been performed according to ASTM A370 (2004); IS13162 (1992) standards to evaluate the mechanical characteristics in tension. The tests have been carried out in a displacement-controlled mode with a loading rate of 0.5 mm/min. Steel formwork is used to cast the specimens horizontally. Before installing the EPS core with the welded wire mesh, movable rods are utilized to maintain a 25 mm depth beneath the welded wire mesh for the bottom wythe, Figure 3.12(a). Slurry prepared by cement and water is applied to the EPS core for the mix to adhere to it. The specimen has been plastered with a mix (M1/M2) to an extent of 15 mm and left to dry (2 hours), Figure 3.12(b). The top surface is scratched such that the following layer of 25 mm mix (M1/M2) adheres entirely to the preceding layer, and 40 mm thickness is achieved. The mould is then left to dry after casting the upper wythe, then it is tipped over to cast the bottom wythe. The technique for casting the specimens incorporated with the geogrids is similar to the control specimen (DS1C AND DS2C), the only difference is that when first layer of the mix (M1or M2) is spread to a depth of 20 mm, then geogrids is laid on top and tied to WWM by using cable ties, Figure 3.12(c) and 3.12(d). The remaining thickness, 20 mm is obtained by spreading the mix on top of geogrids. According to IS 10262 (2019), the top and bottom capping are made of M20 concrete (1:1.5:3), Figure 3.12(e). The specimens are cured for up to 28 days before being tested, Figure 3.12(f). The formation of capping (solid zones) has been achieved through the selective extraction of EPS from the two opposite corners, while retaining the welded wire mesh in its original position. The detail of the top view of the diagonal shear specimen and capping are mentioned in Figure 3.13 and

Figure 3.14. Cross-section details of control specimen and specimen incorporated with geogrids are given in Figures 3.15-3.17. Cable ties used to bind the geogrids with welded wire mesh are shown in Figure 3.18. Details of the shear connector and welded wire mesh spacing are also given in Figure 3.19-3.21. The top view of CSP core is mentioned in Figure 3.22.

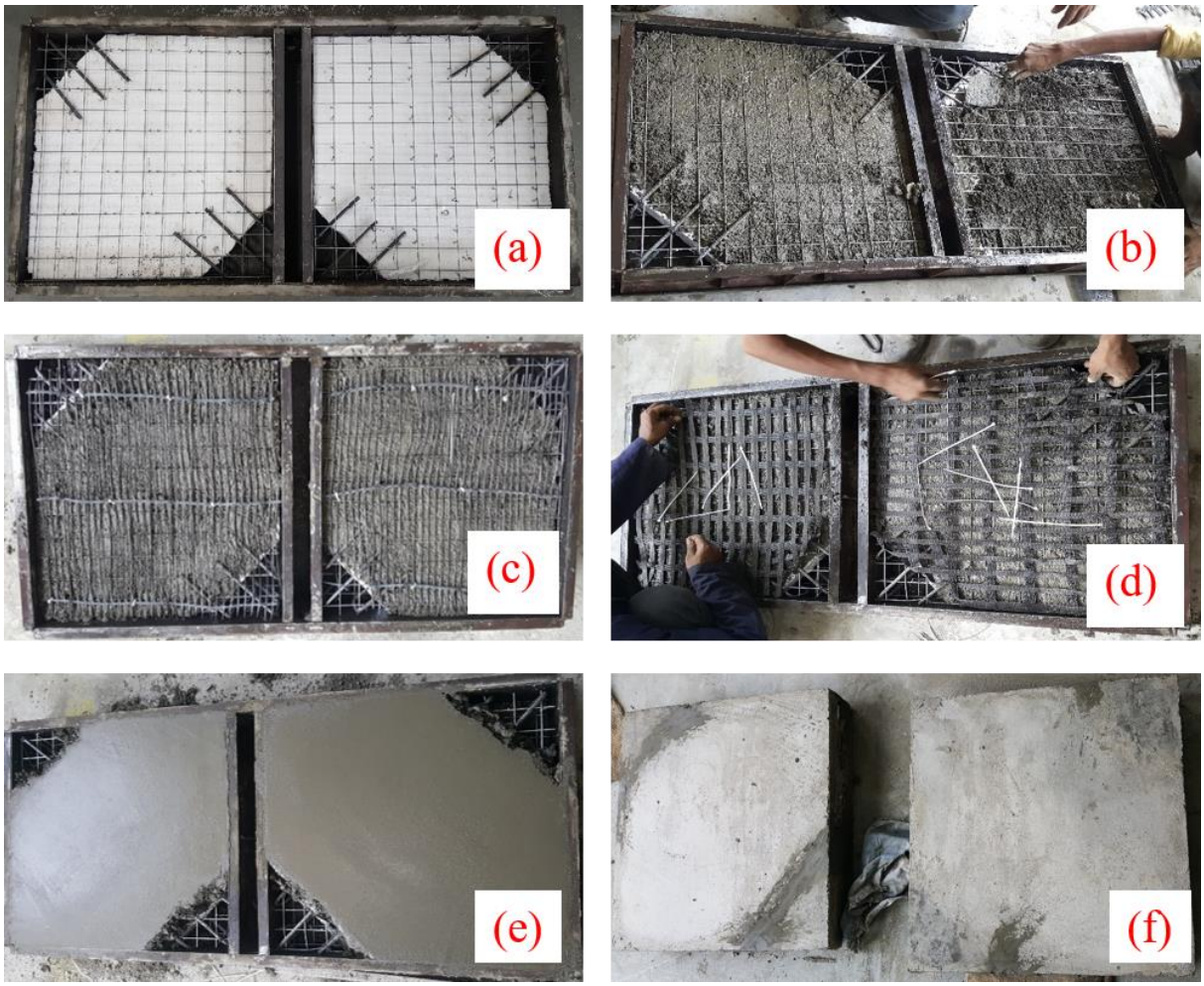

Figure 3. 12: Casting of diagonal shear specimen (a) CSP being placed in the mold; (b) the first layer of top wythe being cast; (c) plastic uniaxial geogrid is being attached to WWM by cable ties; (d) polyester biaxial geogrid is being attached to WWM by cable ties; (e) after laying the final layer of micro-concrete; (f) specimen ready for curing

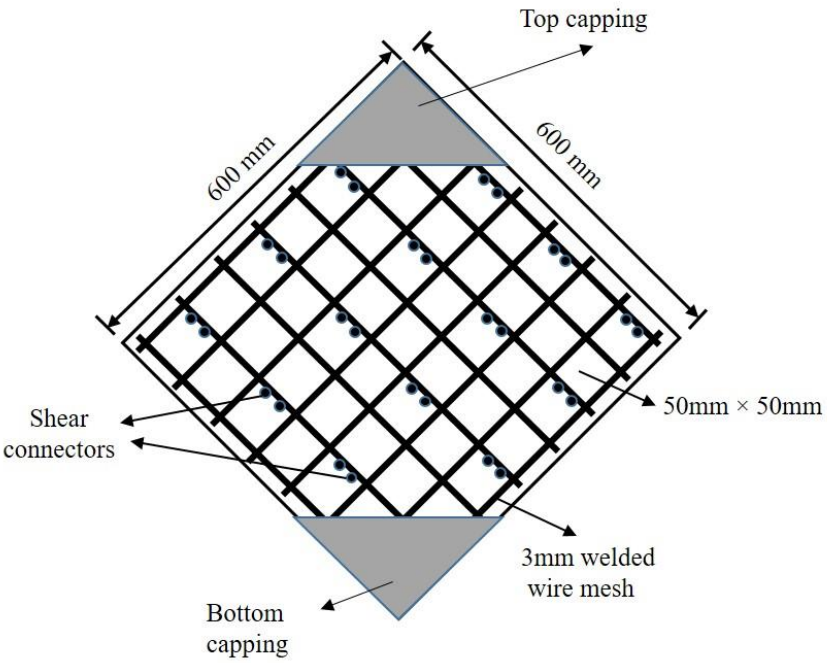

Figure 3. 13: Top view of a diagonal shear specimen

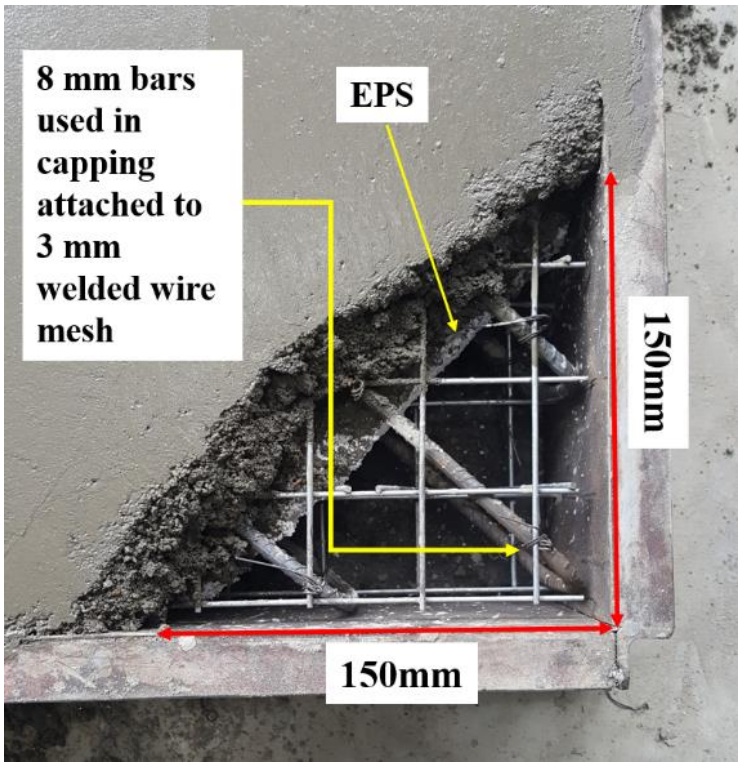

Figure 3. 14: Corner capping detail

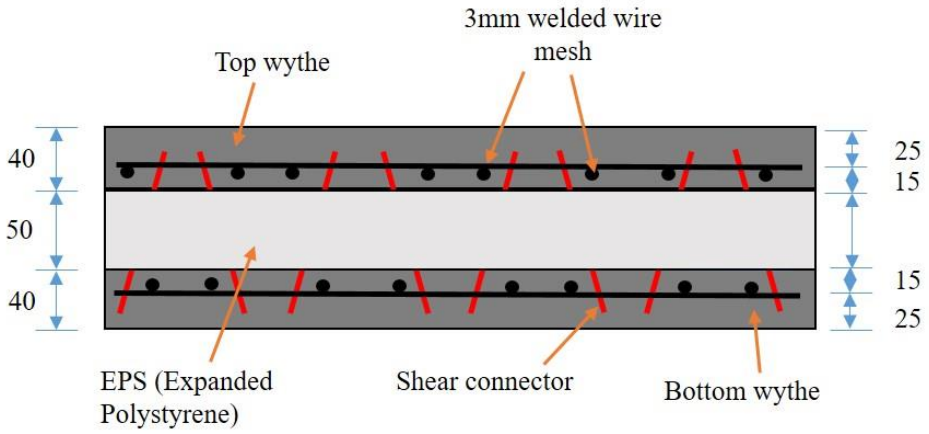

Figure 3. 15: Cross-section details of concrete sandwich panel

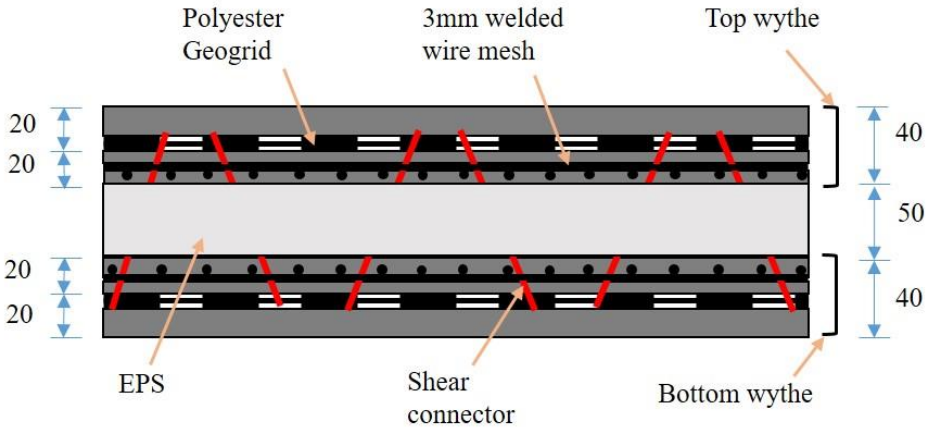

Figure 3. 16: Cross-section details of CSP containing polyester biaxial Geogrid

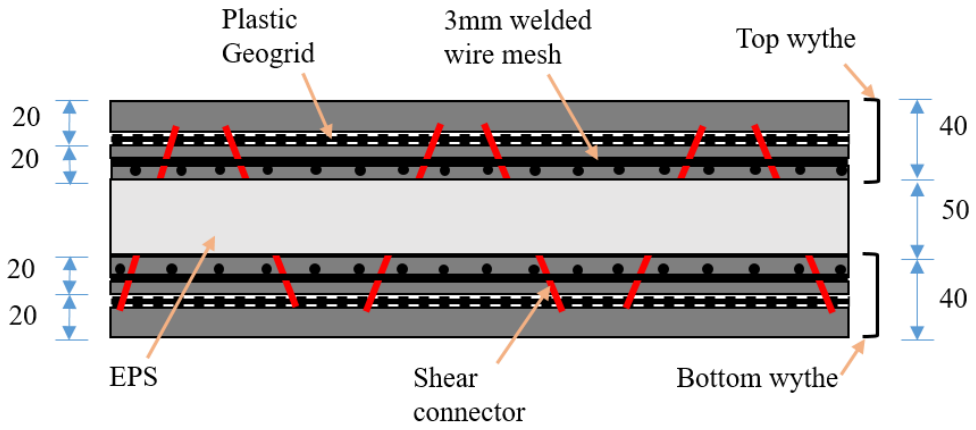

Figure 3. 17: Cross-section details of CSP containing plastic uniaxial geogrid

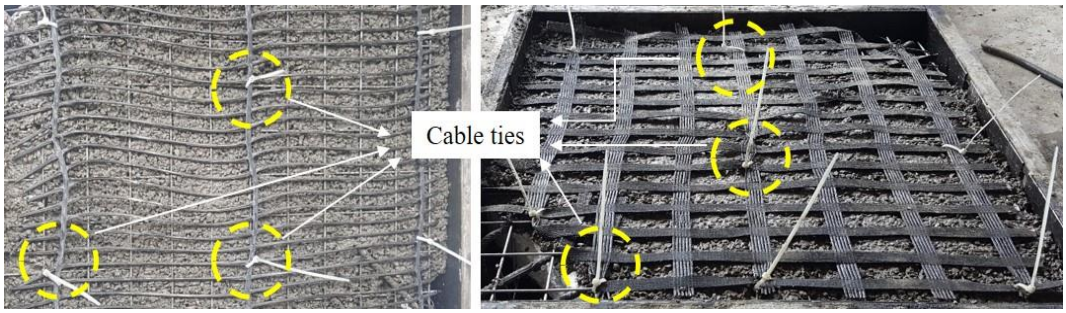

Figure 3. 18: Cable ties used to attach various geogrids with welded wire mesh

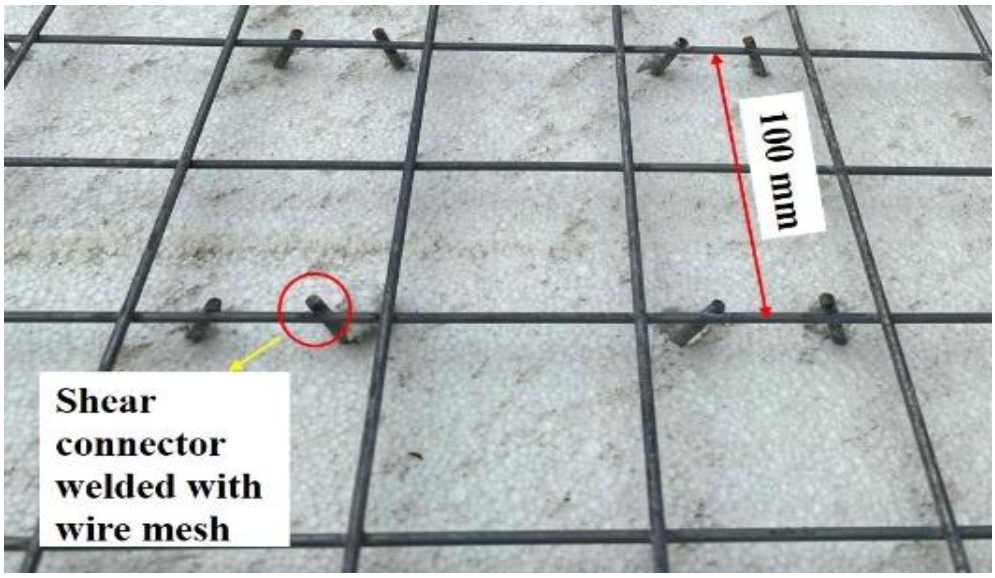

Figure 3. 19: Magnified view of welded wire mesh and shear connector

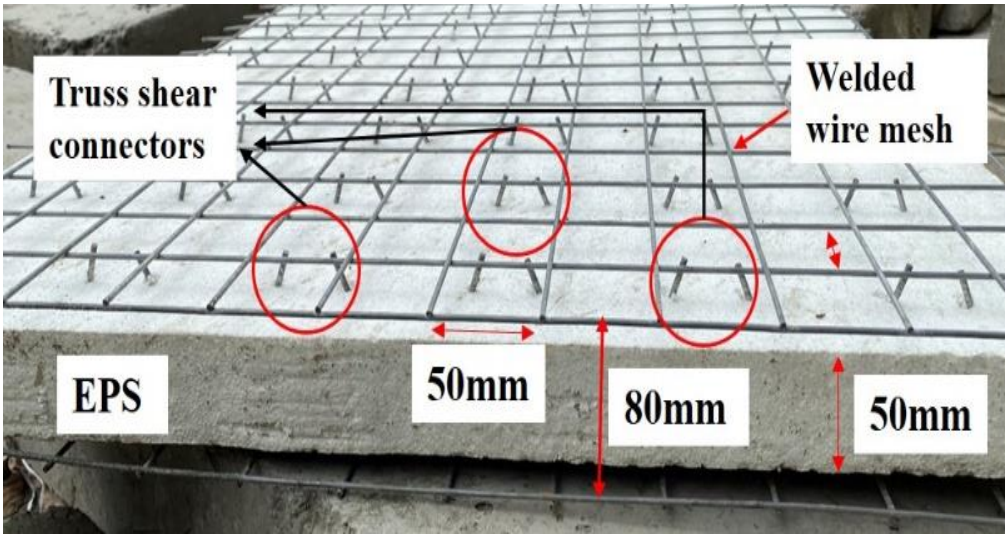

Figure 3. 20: Shear connector details

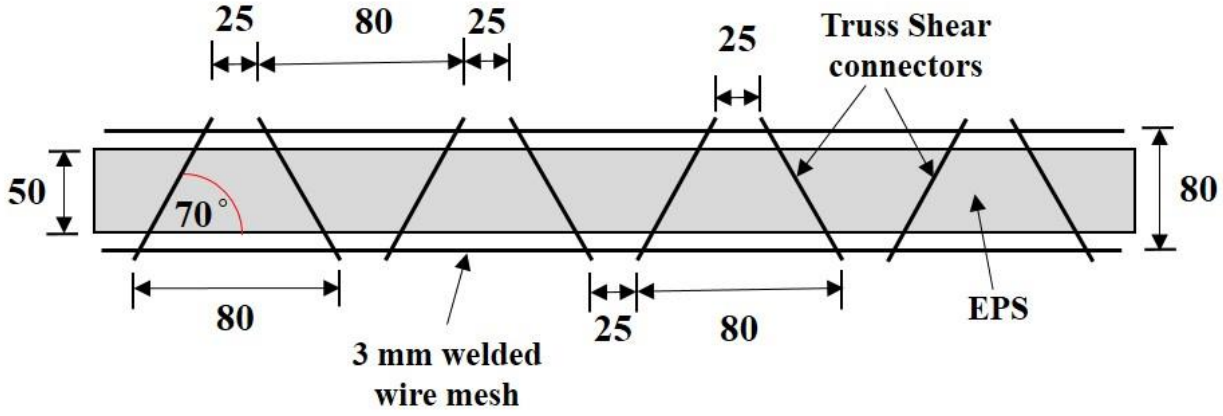

Figure 3. 21: Detail dimension of truss shear connectors (all dimensions are in mm)

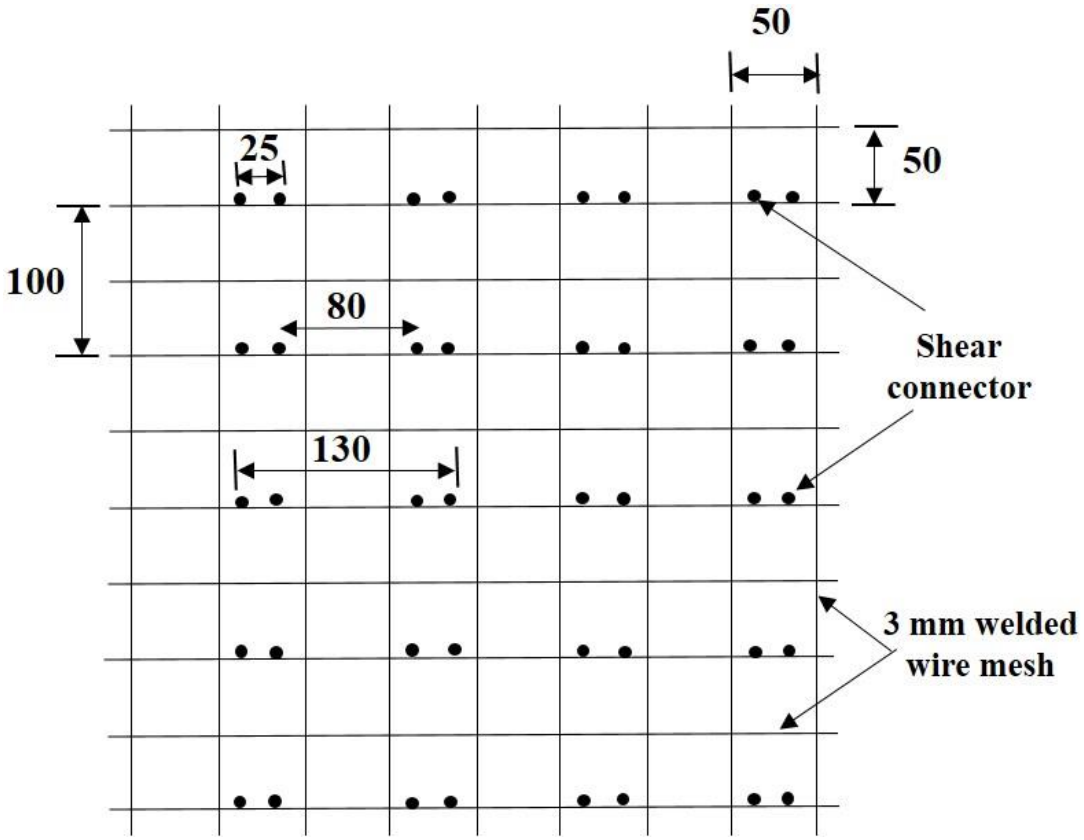

Figure 3. 22: Top view of CSP core (all dimensions are in "mm")

3.3.2.1 Instrumentation and Test setup

All specimens have been tested on a universal testing machine (UTM) having the capacity of 1000kN under compression ASTM E519 (2020). The absence of a universally recognised procedure for conducting diagonal compression tests on concrete sandwich panels, the testing methodology and configuration outlined in ASTM E-519/E-519 M for diagonal

compression testing on masonry have been employed. The diagonal of the specimens has been oriented vertically and has solid corner zones (capping).

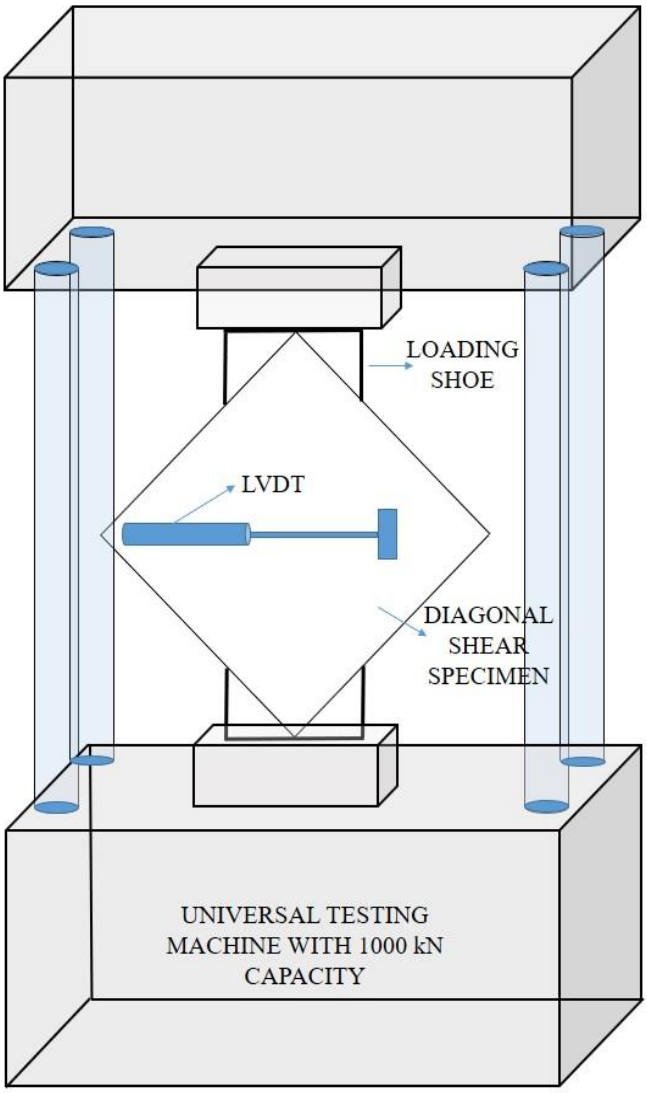

Figure 3. 23: Schematic test set up of diagonal shear testing

Concrete capping has been provided at the top and bottom of the specimen for the diagonal shear test, as in the absence of this capping, the specimen might fail at the loading corner before even transferring the load to the specimen (Ahmad & Singh, 2021; ASTM E 519-02, 2002). Steel loading shoes have been positioned between the loading plates and specimen at both ends of the loaded diagonal. The loading shoes have been implemented to distribute the load evenly and reduce stress concentrations on the sharp edges of the specimen, thereby enhancing its stability during the testing process. The testing of the specimens has been carried out in displacement control mode. Linear Variable Differential Transducer (LVDT) is installed in the middle of the specimen to measure the horizontal crack width. The vertical deflection is

measured by the control setup attached with the displacement-controlled universal testing machine (UTM). To carry out the test, the prepared specimens has been placed with loading shoes between the UTM jaws (Figure 3.23). The net movement of UTM jaws has been considered as the total vertical deformation. Before the commencement of each test, a 10kN seating load was applied to tightly grip the specimen to remove the space between it and the device. The diagram depicted in Figure 3.23 illustrates the instrumentation arrangement utilised for conducting diagonal compression tests.

3.4.3 Axial compression testing

Sixteen specimens are created and tested to assess the in-plane diagonal shear behaviour of the CSPs. A pair of specimens has been chosen for each group, and the average of the two has been documented. Table 3.10 contains the specific information about the specimens. As per the 2017 'Manual for Expanded Polystyrene (EPS) Core Panel System and Its Field Application Sponsored by Ministry of Housing and Urban Poverty Alleviation, Government of India', the load-bearing structure shall have a minimum wythe thickness of 35 mm while utilising CSP. All specimens in this experiment possess a consistent wythe thickness of 40 mm. M1 (1:3) adheres to the IS 13935 (2009) standard, whereas M2 (1:2:3) conforms to the IS : 2386 (Part I) (1963) and IS 456 (2000) standards. The researchers (Padalu et al., 2018) and Vishnu et al. (2017) have documented a similar combination ratio. This study employed standard Portland cement that adheres to the IS 8112 (2013) criteria and fine aggregate that meets the BIS 383 (2016) requirements.

All specimens in the research have continuously maintained a water to cement ratio of 0.5. The usage of locally produced stone dust partially replaces the coarse sand, while the fine aggregate with a particle size that is retained on a 2.36 mm filter is utilised. The three ingredients are divided in a ratio of 1.2:0.6:1.2 to form the M1 mix. The ratio consists of 1.2 parts of coarse sand, 0.6 parts of fine aggregate with a size smaller than 4.75 mm, and 1.2 parts of stone dust. The casting mix M2 comprises a proportion of 1:2:3, with 3 portions of coarse aggregate measuring less than 6 mm in size. Figure 3.24(a) shows the steel mould used for casting of panel. Figure 3.24(b), Figure 3.24(c) and Figure 3.24(d) shows the casting procedure of specimen. Figure 3.25 show the casting of the complete panel and finished surface. The end beams are cast after the completion of the wythe on both sides and compaction of end beam is done by (Refer Figure 3.26). Finished specimen after the casting of both the end beams (Refer Figure 3.27). Specimen are then taken for curing using gunny bags, (Refer Figure 3.28).

Specimens are painted in white after the completion of curing period of 28 days for getting them ready for testing (Refer Figure 3.29).

Table 3. 10 : Details of axial compression specimen

Specimen id	**Specimen Size (L × B × H)mm**	**Material**	**Mix**
WP 1	1300 × 600 × 130	Welded Wire Mesh (WWM)	M1 (1 : 3*) (C : FA)
WP 2		WWM + PUG	
WP 3		WWM + PBG2	
WP 4		WWM + PBG3	
WP I		Welded Wire Mesh (WWM)	M2 (1 : 2 : 3**) (C : FA : CA)
WP II		WWM + PUG	
WP III		WWM + PBG2	
WP IV		WWM + PBG3	

* FA (fine aggregate) consisting of stone dust, fine sand and coarse sand (retained on 2.36 mm sieve); ** Coarse Aggregate size less than 6mm; DS: Diagonal Shear; C: Control; PUG: Plastic uniaxial geogrid; PBG: Polyester Biaxial Geogrid; PBG2: Sgi 200; PBG3: Sgi 300; SPSgi200= Sandwich Panel containing Sgi200; SPSgi300= Sandwich Panel containing Sgi300.

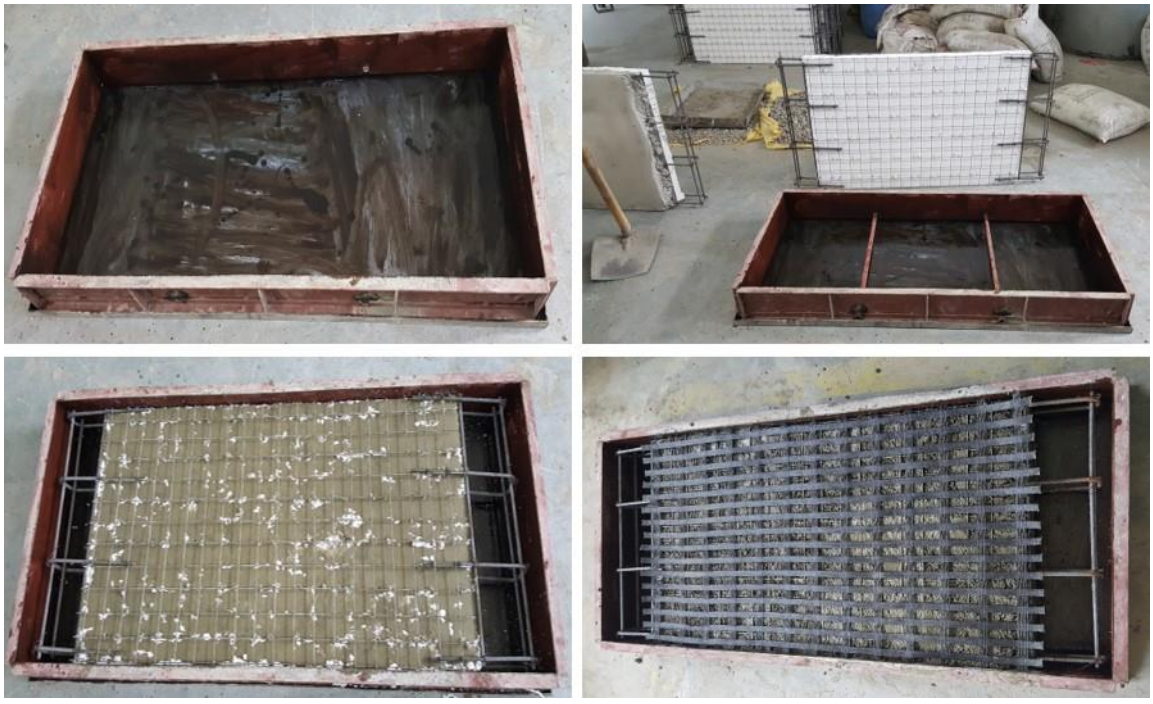

Figure 3. 24: Casting of axial compression specimen (a) Steel mould for casting of specimen; (b) mould with rods to support the panel to help in casting of first layer; (c) rich slurry mix spread over the core of sandwich panel

Figure 3. 25: Spirit level check during wythe casting.

Figure 3. 26: Casting of end beam with M20 mix, a steel rod is being used for compaction of the concrete.

Figure 3. 27: Finished Specimen

Figure 3. 28: Curing of specimens

Figure 3. 29: Paint job of specimen after 28 days curing

3.3.3.1 Experimental test setup

The test has been conducted using a hydraulic machine having the capacity of 5000 kN (Refer Figure 3.30). The sample of CSP was placed on the base plate of the hydraulic jack. Two loading shoes have been placed at both the ends to transfer the load uniformly. A load cell is also placed on top of the loading shoe (Figure 3.31) to monitor the loading. An LVDT (Linear variable differential transducer) has been installed at the mid span. A data logger has been installed to note down the reading obtained from the load cell as well as the LVDT.

A chain pulley arrangement has been used to uplift the specimen at a height of about 1.0 m to place it on the top of the loading jack plate. To ensure safety of the experimental setup, chains have been kept wrapped to the specimen and attached to pulley system.

In the Figure 3.32 it can be observed that the specimen has been clutched into the two opposite ends of the machine. A starting initial load of 10 kN has been applied to the specimen top clutch it properly in the loading shoes and to check if there is a need for any packing to transfer the load uniformly through the specimen.

Figure 3. 30: Experimental test setup

Figure 3. 31: Steel shoes for testing of CSP in axial compression

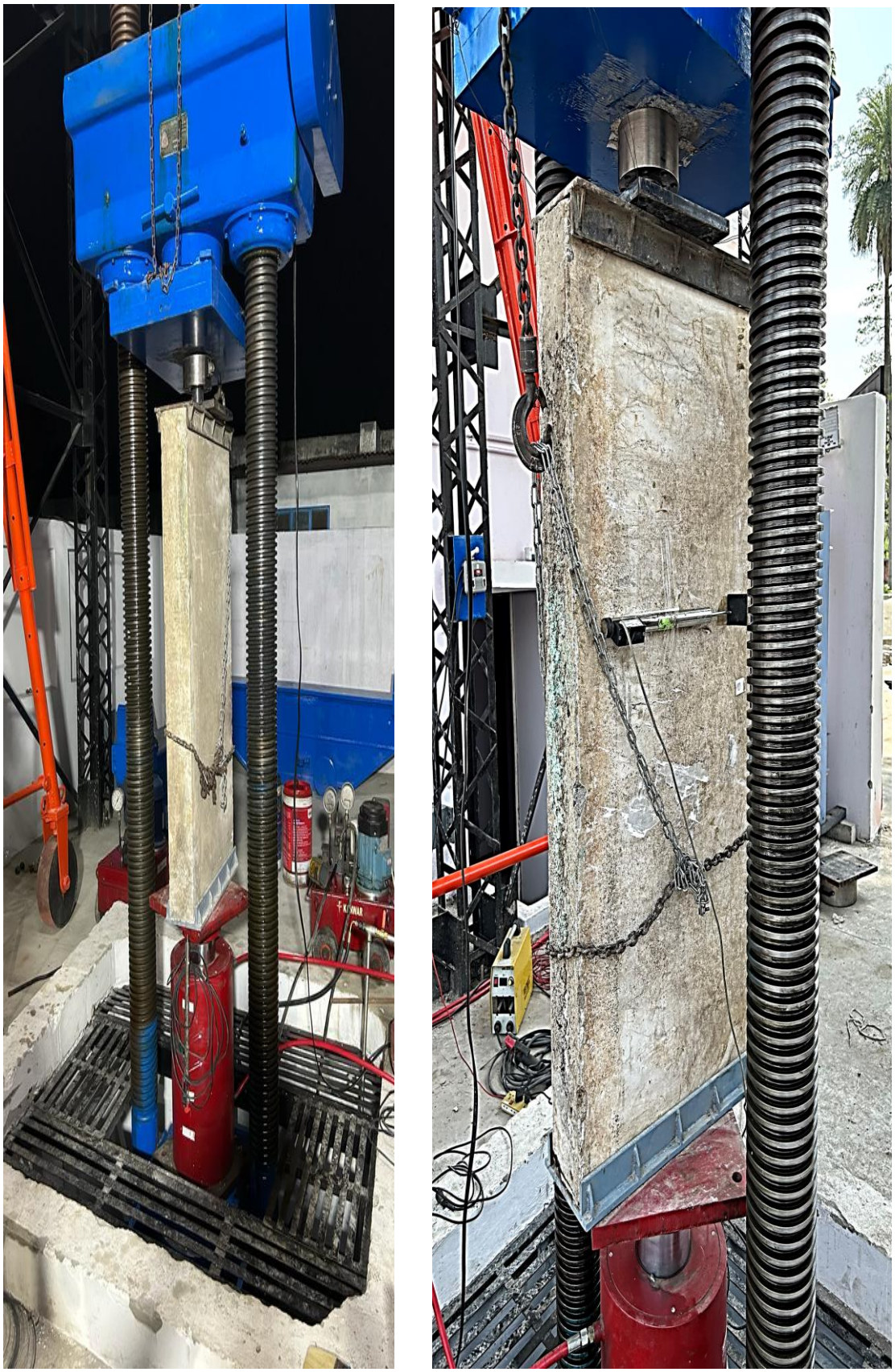

Figure 3. 32: Test setup for axial compression testing with load cell attached the top.

3.5 Methodology of 2D RC frame testing

3.5.1 Casting of 2D RC Frames

The casting of 2D Reinforced Concrete (RC) frames involves the construction process of forming and pouring concrete to create structural elements with two-dimensional configurations. These frames typically consist of columns and beams interconnected to provide stability and support for buildings and structures. The casting process begins with the assembly of formwork, which serves as the mold for the concrete. Reinforcement, usually in the form of steel bars, is strategically placed within the formwork to enhance the structural strength of the concrete elements. Once the formwork and reinforcement are in place, concrete is poured into the mold, ensuring complete filling and proper compaction. After the concrete cures and attains sufficient strength, the formwork is removed, revealing the finalized 2D RC frame. This casting procedure (Figure 3.33) is crucial in ensuring the integrity and durability of the structure. To assure the stability of the column's footing, a robust floor was constructed before casting the 2D RC frames, preventing any displacement. A plate with a thickness of 20mm and dimensions of 280mm x 280mm has been affixed to the sturdy floor using studs. The rebars are welded on top of the plate (Figure 3.33 (a)). The plate was also secured by bolting it through the studs embedded in the robust floor. Stirrups were positioned across the whole length of the rebar (Figure 3.33 (b)). The columns were welded with precision to ensure accurate proportions. A vibrator equipped with a 25 mm diameter needle has been utilised to perform the compaction while concreting M25 concrete. In order to guarantee the removal of the footing girder, additional supports were also installed on the created stubs, which had dimensions of 300 mm x 300 mm.

The experimental program described in this work attempts to evaluate the cyclic behaviour of 2D RC frame specimens by using three alternative specimen configurations : (i) complete sandwich panel, specimen ‘C’ (Figure 3.34); (ii) concrete sandwich panel with an opening, specimen ‘O’ (Figure 3.35); (iii) Brick masonry as infill wall, Specimen ‘B’ (Figure 3.36).

This section contains particular information on total three reinforced concrete (RC) frames which were tested, having concrete sandwich panel and brick masonry as infill. Size of the plinth beam is 150 × 150, top beam 150 × 200 and that of both columns is 150 × 150 (Figure 3.41). Size of the infill is 1200 × 1080 × 130 for concrete sandwich panel (Figure 3.34). Frame with CSP had both the wythes cast with the design mix as 1:2:5 (“Manual for Expanded

Polystyrene (EPS) Core Panel System and Its Field Application Sponsored By Ministry of Housing and Urban Poverty Alleviation , Government of India," 2017).

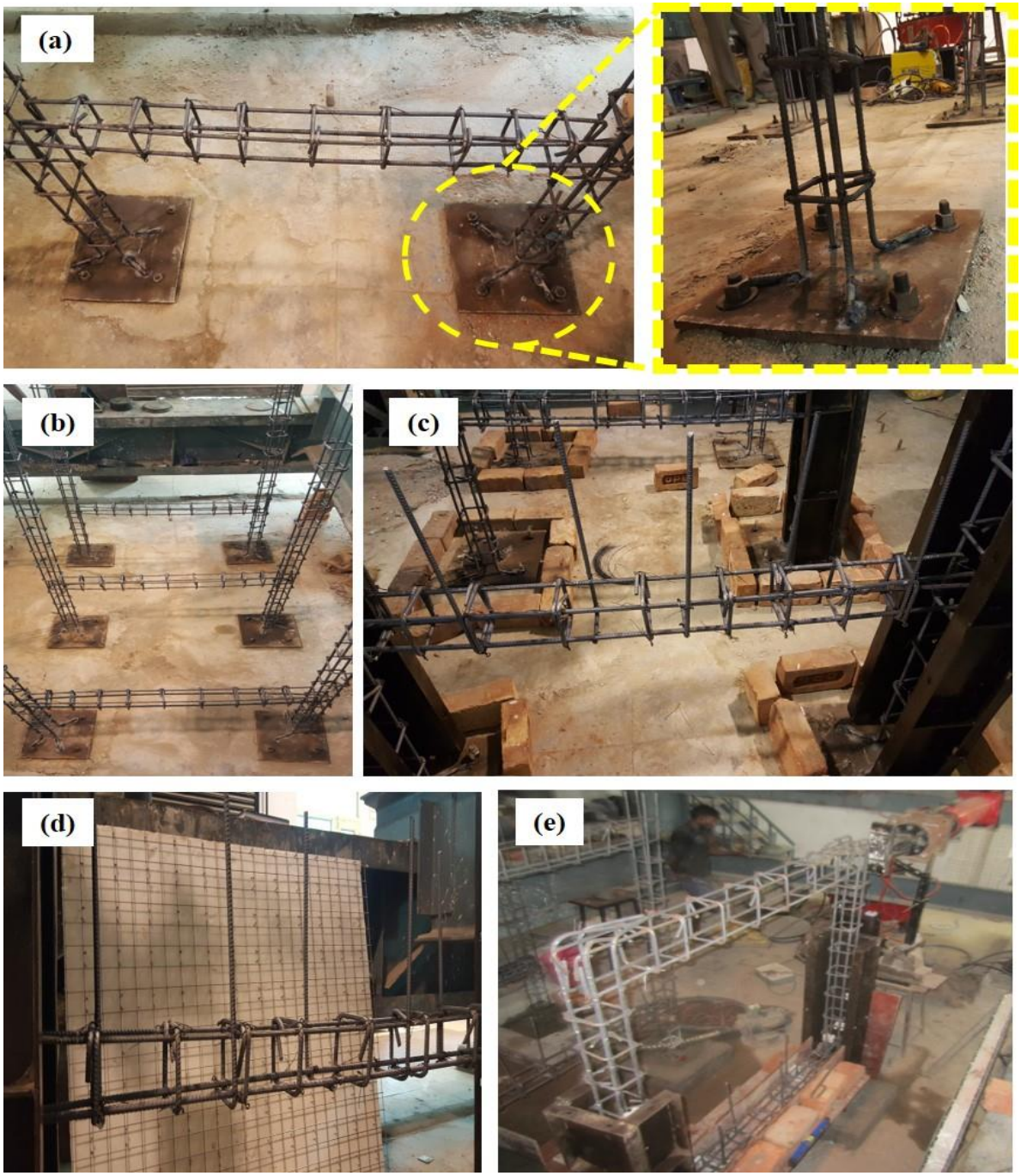

Figure 3. 33: Casting of 2D frames (a) Rebar welded to the steel plate and the magnified view of the plate; (b) skeletal of all the three frames; (c) shuttering plates covering the column reinforcement; (d) dowel bars attached to the reinforcement of the plinth beam; (e) top beam reinforcement attached to the column reinforcement.

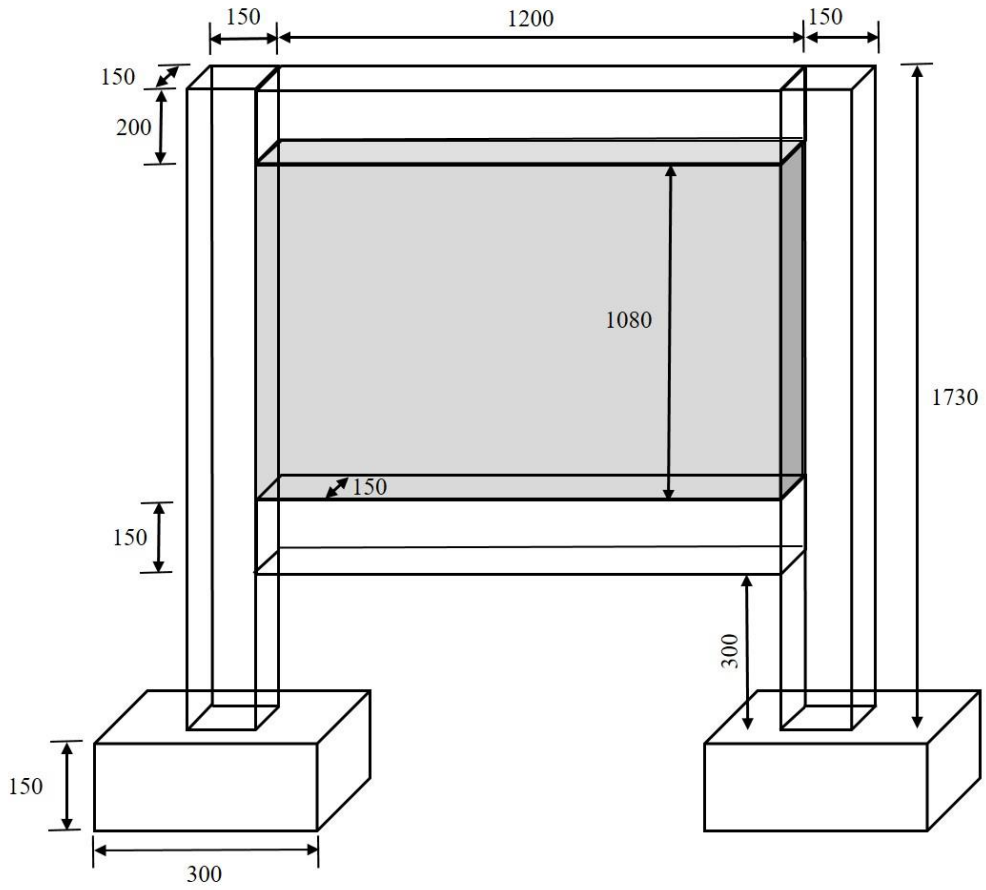

Figure 3. 34: 2D frame with CSP as infill (all dimensions are in mm)

The 2D frames has been designed as per the laboratory geometry restrictions. Similar constrained while designing the 2D frame specimen have been observed by Sousa (2022) in the latest study. Therefore in the present study a scale factor of 1: 3.5 with respect to real-scale dimensions (for geometry of the structural members and the infill wall) has been adopted. RC frame has been cast using M25 and reinforcement of 12 mm diameter bar have been used, reinforcement details are given in Figure 3.41. Dowel bars (Figure 3.33 (c) and Figure 3.33 (d)) have been erected in the plinth beam for the placing and joining of the core of the CSP. Length of the dowel bars is kept 450 mm (‘Manual for Expanded Polystyrene (EPS) Core Panel System and Its Field Application Sponsored By Ministry of Housing and Urban Poverty Alleviation, Government of India’, 2017). After the casting of the frame curing is performed for 28 days. Then the core of CSP is placed as the infill. The dowel bars are tied with the welded wire mesh of the panel with the help of steel wires. (Figure 3.39). Cement slurry is sprayed on the core of the panel before plastering it with micro-concrete. Plastering is done in two stages as the thickness of the wythe is 40 mm (‘Manual for Expanded Polystyrene (EPS) Core Panel System and Its Field Application Sponsored By Ministry of Housing and Urban Poverty

Alleviation , Government of India', 2017). Firstly upto the depth of 20mm and it is left for 2 hours to set and dry and then second layer is plastered on to the first layer, there by achieving the complete thickness of a wythe. Similar procedure is followed for the other wythe.

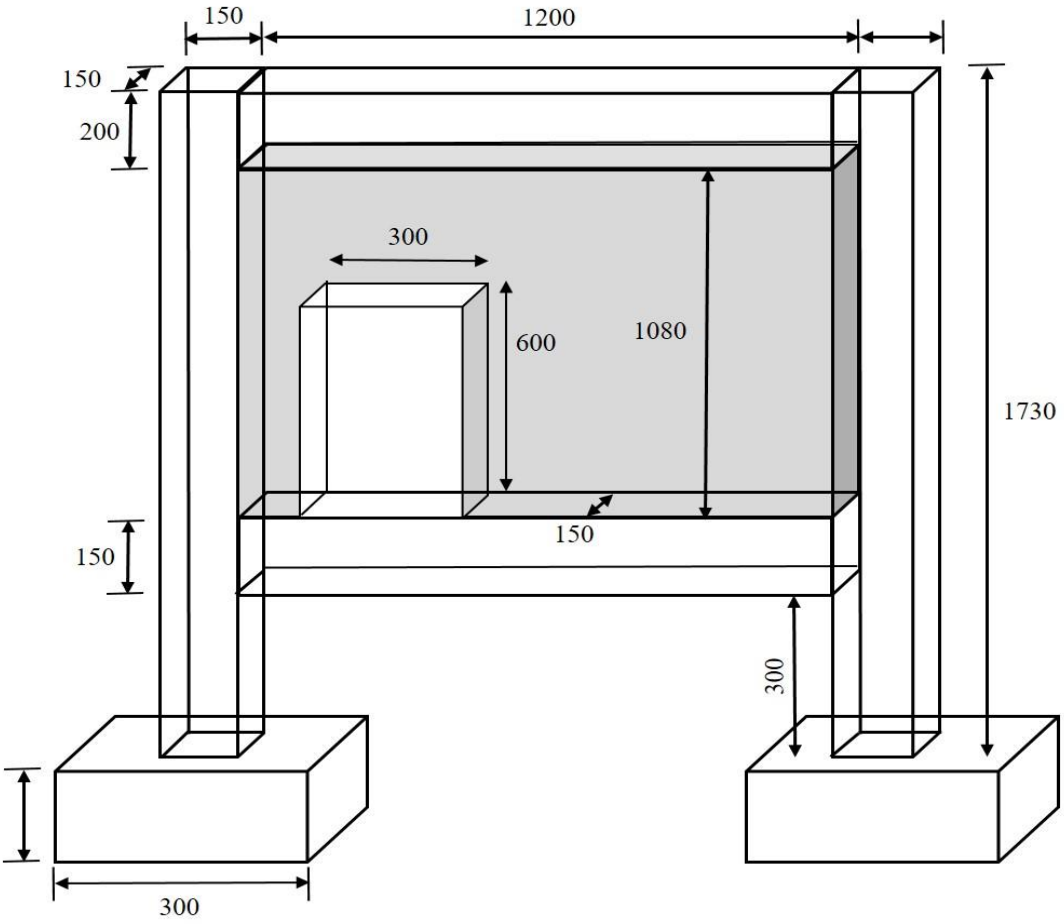

Figure 3. 35**:** 2D frame with door opening (all dimensions are in mm)

The second RC frame is also having CSP as infill, but with an opening. Similar casting procedure is followed in this case as done in first frame. U-shaped wire meshes have been installed to the door opening as additional reinforcement ('Manual for Expanded Polystyrene (EPS) Core Panel System and Its Field Application Sponsored By Ministry of Housing and Urban Poverty Alleviation , Government of India', 2017). Size of the opening is 300 × 600 (Figure 3.35). The U shaped wire mesh is provided to enhance the strength of the edges of the opening so as it should not fail just after applying the load. The third RC frame has brick masonry as infill. Standard bricks procured locally have been used. The mortar used is having the design mix of 1:3 as per IS: 2116 (1980) and IS: 2250 (1981). Size of the brick is 190x90x90 mm as per IS: 2691 (1988).

The compressive strengths of the M25 used to cast the RC frame have been determined with 150 mm cubes as per IS 456 (2000) . The compressive strength of designed concrete used in fabrication of RC frame is 28.35 MPa. The mortar cube cast of micro-concrete showed the compressive strength of 22.60 MPa. The compressive strength of mortar (1:3) used for brick masonry is 22.3 MPa.

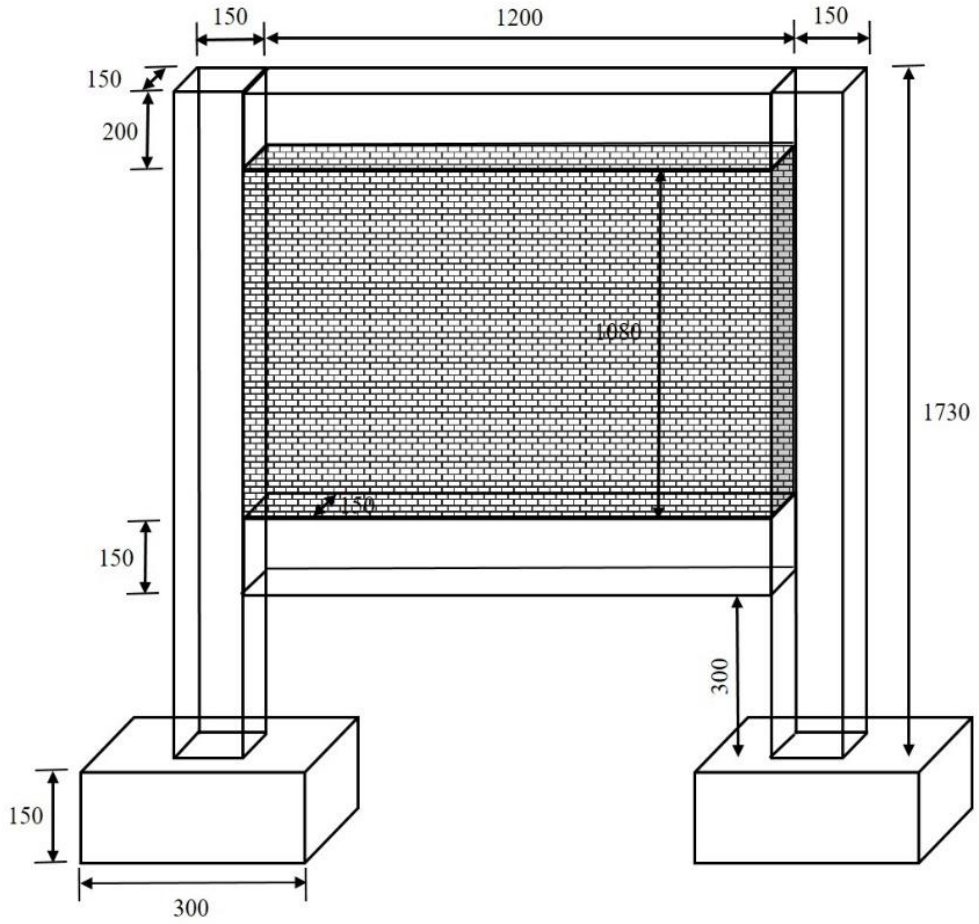

Figure 3. 36**:** 2D frame with brick masonry infill (all dimensions are in mm)

3.5.2 Test setup and instrumentation

Cyclic testing of the RC frame were conducted using the apparatus seen in Figure 3.42. In order to prevent the RC frame from sliding or rising, the reinforcement of the column has been attached with the plate which is further bolted with strong floor. A stub of size 300 mm x 300 mm x 150 mm has been cast over the steel plate of size 270 mm x 270 mm x 25 mm. The hydraulic actuator (capacity of 600 kN) was attached to the reaction wall and lateral in-plane quasi-static loading has been applied, Figure 3.42. The lateral displacement was induced on the upper RC beam by using two steel plates with dimensions of 250 mm x 250 mm x 40 mm,

which were joined by four 50 mm tie rods. Three linear variable differential transducers (LVDTs) have been used having an amplitude of ±50 mm. One LVDT has been installed at the near end (where hydraulic jack was attached with top RC beam), Figure 3.42. Two LVDTs were installed at the far end (Figure 3.40).

Figure 3. 37: Three bare 2D RC frames under going curing with the help of gunny bags

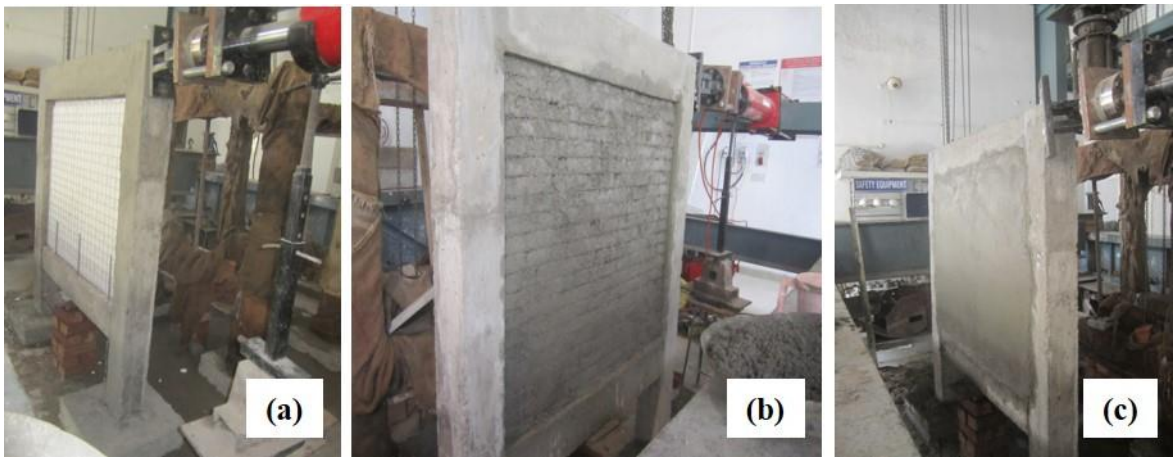

Figure 3. 38: Casting phases of CSP infill wall (a) Core of concrete sandwich panel being installed in the 2D RC frame and attaching with the dowel bars; (b) first layer of plastering being done; (c) final layer of plastering on the same side of panel to achieve the desired thickness of wythe.

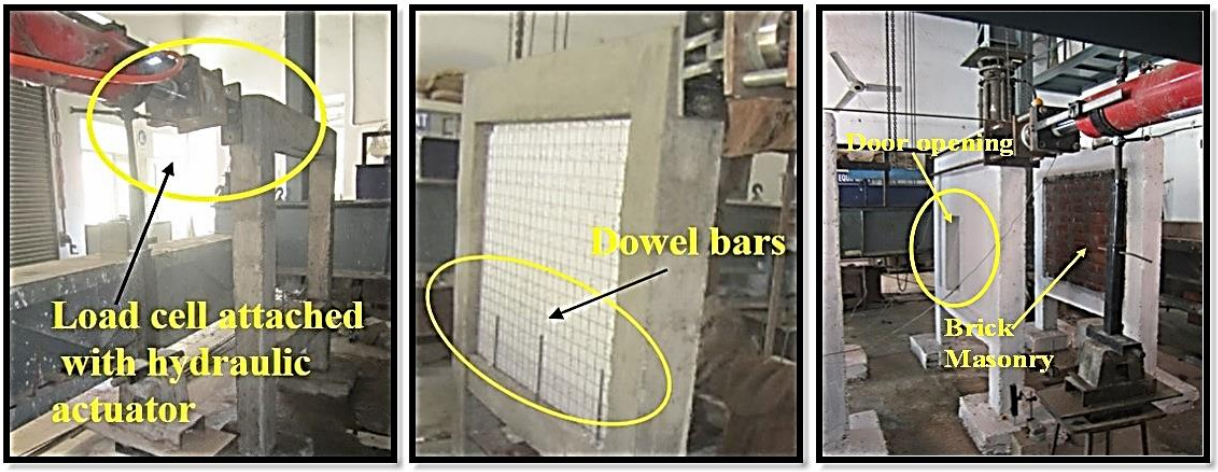

Figure 3. 39**:** Intermediate phase of RC frames (a) Load cell attached with hydraulic jack and placed in position; (b) specimen with concrete sandwich panel being placed in between dowel bars; (c) specimen with door opening and brick masonry as infill

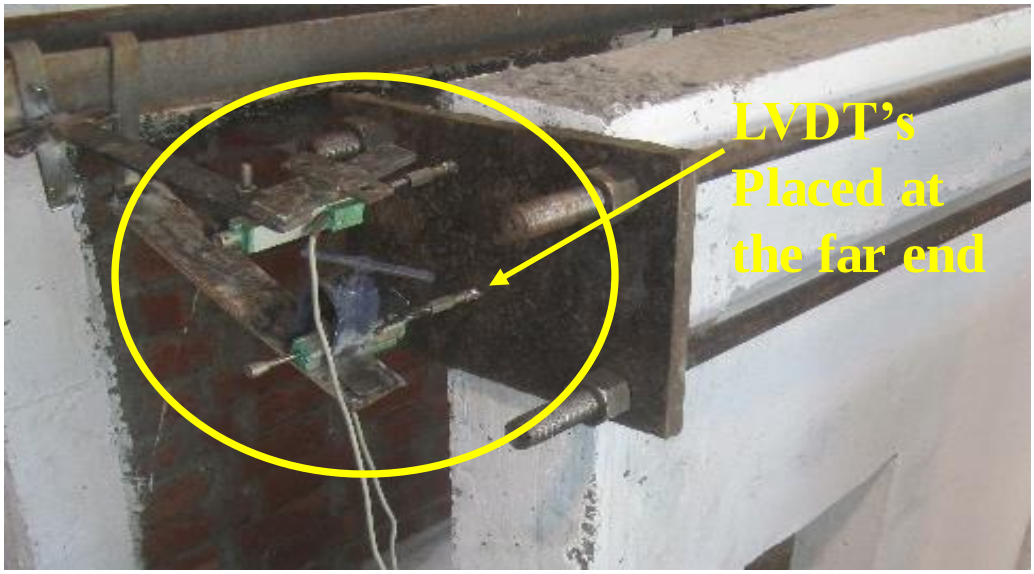

Figure 3. 40**:** LVDT installed at far end of the RC frame

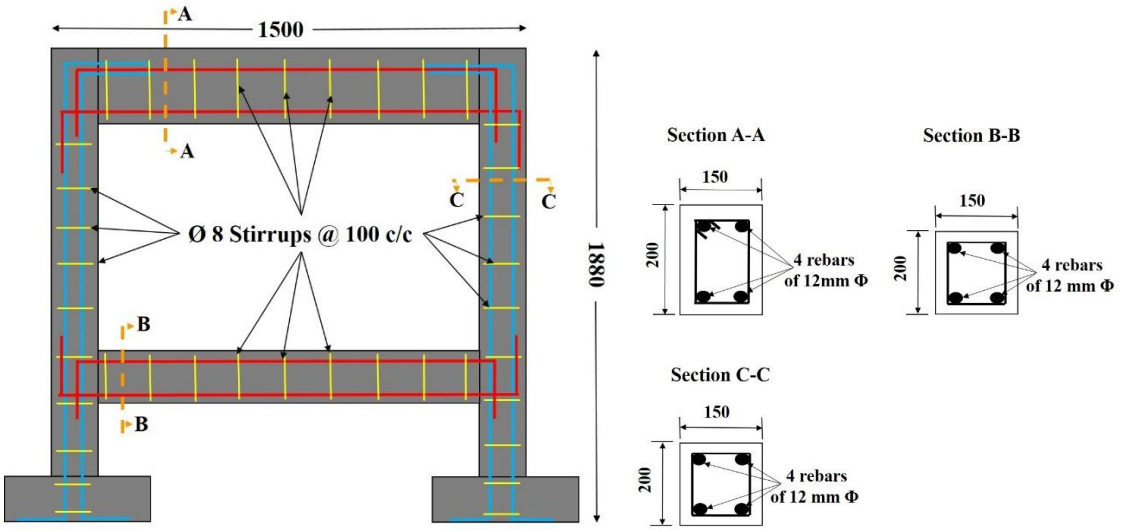

Figure 3. 41**:** Reinforcement details of 2D frame (all dimensions are in mm)

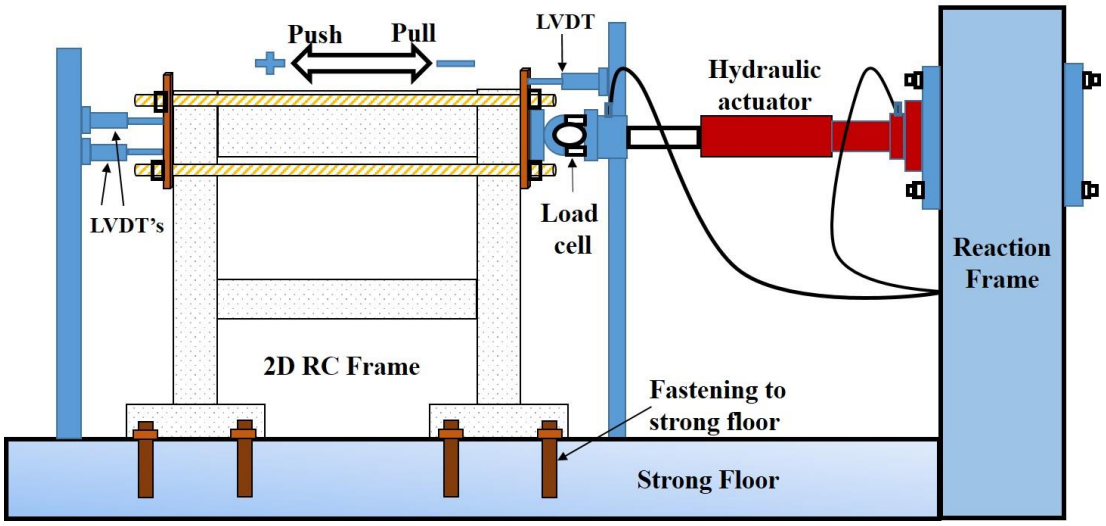

Figure 3. 42**:** Schematic diagram of test setup

3.5.3 Load protocol

Displacement control loading has been enforced by an actuator (Figure 3.43) and monitored by an LVDT during the in-plane quasi-static cyclic testing. Increasing levels of displacement amplitude, which have been pre-established in accordance with the recommendations provided by FEMA 461, are used to determine the adopted displacement protocol, Figure 3.43. The loading process is comprised of a total of twenty phases, the first of which involves a displacement amplitude of 5 mm. Up to a maximum displacement of 50 mm, which equals 2.65% of drift. This continues until the maximum displacement is reached (Figure 3.43). The

displacement rate taken is 0.5mm/s, initially first two cycles are of 5mm each. 3rd and 4th cycle were of 10 mm each and so on up to 50 mm, a total of twenty cycles were completed.

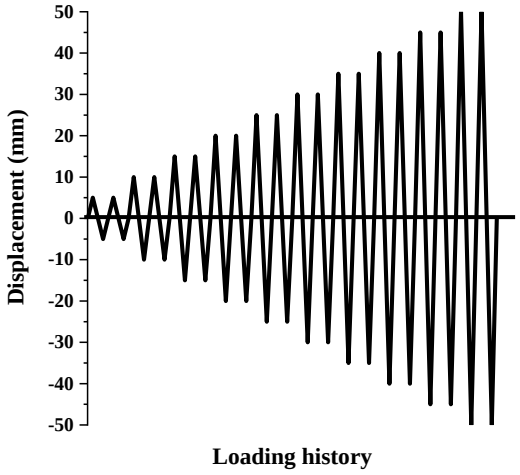

Figure 3. 43: Loading cycle for quasi static cyclic testing

Figure 3. 44: Instrumentation set up for testing (Specimen 'O')

Closing remark

In this part of the thesis, the basics of experiment have been discussed regarding the material as well as the methodology of the objectives in detail. The dimension of specimen cast and the relevant material to use are also mentioned in this section. Detail of every step have been given to understand the procedure of casting and the specimen has to be placed in the instrumentation setup to test. As this chapter is having methodology of all the objectives, so the images of all the specimen and their cross section has been shown.

Chapter 4

In-plane and out-of-plane behaviour of concrete sandwich panels

4.1 General

Concrete sandwich panels (CSPs) are one of the modern-day techniques for rapid construction. Made up of a low-density expanded polystyrene (EPS) core, welded wire mesh on both sides attached with shear connectors, two concrete skins (wythes), as a whole, behave as a single composite. Their popularity against brick masonry is that they are easy to install, lightweight, and reinforced with welded wire mesh making them structurally practicable. Unreinforced masonry is weak when experiencing in-plane and out-of-plane lateral forces; the failure is brittle. The traditional construction of residential houses is being constructed using brick masonry. The brick masonry exhibited excellent compressive strength however the flexural strength during out-of-plane failure is extremely brittle. However, CSPs are being identified for the rapid construction of buildings. The flexural strength of concrete sandwich panels subjected to out-of-plane bending relates to the resistance of the wall subjected to lateral loads (wind, earthquake, or earth pressures) and eccentric load or direct bending due to gravity loading. This chapter discusses results and experimental observations of flexural (out-of-plane), compression (axial), and diagonal compression (in-plane) behaviour with the incorporation of different geogrids.

4.2 Flexural response of CSP's

In this phase of experimentation, the concrete sandwich panel underwent flexural loading, a testing method commonly referred to as four-point bending as mentioned in previous Chapter 3. The testing procedure strictly adhered to the guidelines stipulated in the ASTM E72 code, specifically the ASTM E72 (2002) standard, which outlines the methods for conducting strength tests on panels designed for building construction. The performance of the concrete sandwich panel is measured by the load–deflection curves in terms of peak load capacity, stiffness, energy absorption capacity, failure pattern.

4.2.1 Load-displacement behaviour

It can be observed from Figure 4.1 and Figure 4.2, in SPC1 before the yield load a kink in the curve is observed at 24 kN which is due to crack initiation in the lower wythe of the specimen.

Another significant drop in the curve is observed at 55 kN and it is due to the crack generated near support. After attaining the peak load (57.87 kN) the rigidness in the panel which is due to welded wire mesh is lost and the shear connector weld starts breaking. Hence the decrease in load-bearing capacity is observed and deformation also increases.

In Figure 4.2 and Figure 4.6, specific observations are made for SP1C. Prior to reaching the yield load, a distinctive kink appears in the curve at 22 kN, indicating the initiation of cracks in the lower wythe of the specimen. Another notable drop in the curve is identified at 35 kN, corresponding to the development of a crack near the support region. Upon reaching the peak load (45 kN), the inherent rigidity in the panel, attributed to the presence of welded wire mesh, diminishes, and the welds connecting the shear connectors begin to fracture. The subsequent behaviour of the specimen, occurring after the attainment of the peak load, is characterized by a post-elastic phase observed within the 25 mm to 40 mm range along the extension of the curve. This phase is marked by a decline in load-bearing capacity and a concurrent increase in deformation. The described sequence describes the mechanical response and failure mechanisms exhibited by the SP1C concrete sandwich panel during the four-point bending test. SPC1 attained a peak load of 57.87 kN whereas the SP1C exhibited a peak load of 47 kN. The noticeable difference in peak load is due to the low compressive strength of the M2 mix as reported in preceding chapter 3. However, it is concluded that the M1 mix exhibited high initial stiffness and the post elastic behaviour of the M2 mix is significantly higher.

SPGG specimen (Figure 4.3 and Figure 4.4) after undergoing four point bending test behave linearly upto 25kN and a bend is observed at this load which signifies the breaking of the weld of shear connector, than again there is a steep rise in the curve. Another bend is observed at 33 kN depicting the failure of one more shear connector weld failure. A sharp rise is again observed in the curve, a few kinks are observed at 50kN, 54kN, and 57 kN. This is due to the additional reinforcement of plastic geogrid which came into action after the welded wire mesh was not able to withstand/sustain loads without crack generation. A peak load value of 73.87 kN has been attained. A sharp decline is noted after attaining the peal load. This sudden drop in curve signifies that the welded wire mesh has failed completely. Load is being taken by plastic uniaxial geogrid as it is a stiff plastic material and avoiding the sudden failure of the panel and increasing the ductility. This may be interpreted due to the increased deformation seen in the curve.

In SP1GG (Figure 4.4 and Figure 4.9) first drop in the curve is observed at 25kN, this may due to the transfer of cracks from top wythe to lower wythe through the EPS. It behaves

similar to SP1C as the significant drop in the curve is observed at a value of 45kN (which is very near to the peak value of SP1C) but the curve keeps on rising which is due to the presence of plastic geogrid, which starts bearing the load in combination with welded wire mesh. The bending of the specimen is observed and tension in geogrid is generated. The peak load value achieved is less than the other specimen (SP1GG) due to the low compressive strength of the mix.

SPGG and SP1GG both behaved better than the respective control specimens of the two mixes, M1 and M2. As mentioned in earlier text, M1 has more compressive strength than the M2 mix, which is further supported by the additional reinforcement of plastic uniaxial geogrid. This combination is the reason behind the increased strength of the CSP. Due to the presence of geogrid, the spalling of concrete has also been halted (a feature of geogrid—not to let the material displace).

In SPSGi200 (Figure4.5 and Figure 4.7), the first significant bend occurred at nearly 63 kN. Now as load has gradually reached the value attained by control specimen as mentioned in above text, further load taking capacity is clearly supported by polyester biaxial geogrid and enhanced the strength of the concrete sandwich panel. Again a drop is noticed which explains that at this instant weld of shear connectors have started to lose their strength and geogrid have come into action i.e tension has been generated in it and the further rise in the curve is also noted. After the peak load 78.78 kN is achieved, there is a sudden drop down which constitutes the failure of the specimen, and the post elastic curve runs down steeply. The maximum deformation attained is more than 40 mm which shows the enhanced ductility of the CSP. There is no spalling of concrete also which signifies the bond with concrete wythe.

In SP1Sgi200, the first kink (Figure 4.7 and Figure 4.11) is observed earlier than its counterpart this is surely due to the compressive strength of the mix used. Then again another significant drop-down of the curve is noticed at 45kN and then the rise in peak load is not as its counterpart, this is due to the failure of weld of the shear connector. Declination of the load is observed which constitutes the enlargement of cracks and sudden failure is observed after the peak load is achieved because the joint of the side beam broke after the failure of end beam joint with the CSP.

In SPSgi300, the curve starts to bend at 35 kN which describes that shear connector welds have started losing their strength (Figure 4.8 and Figure 4.10). At 43 kN significant drop is observed which means that load has transferred to the lower wythe of the panel. Now the tension in geogrid has arisen which can be seen from the rise in the curve. SPSgi300 has also

shown the maximum deformation behaviour among all the other materials but the peak load (50.35kN) observed is less because of the debonding of lower wythe from the core. The width of the machine direction rib in Sgi300 is more than SGi200, so due to increased surface area concrete in lower wythe is not able to bind properly and this may have led to the debonding of the layers of wythe. The composite behaviour has been lost and hence the load-bearing capacity decreased.

In SP1Sgi300, a smooth curve is obtained which means that composite behaviour is throughout the same. The polyester geogrid (Sgi300) comes into action and stops the spalling of concrete, as the crack widens. Curve (Figure 4.10 and Figure 4.12) clearly shows the deforming capability (ductile behaviour) because of the presence of Sgi300 and extends the deformation up to 50 mm. From Figure 4.2 it can be observed that mix M2 specimens are showing peak load values less than mix M1 as the compressive strength of M1 is less than M2. The visual observation of all the specimen are mention in Table 4.1. The reason for M1 performing better than M2 is the mix ratio, M1 is having stone dust as a replacement to the fine aggregate which is finer, so its surface area is higher, and hence binding is better which results in increasing the compressive strength than the other ratio, M2 (Refer Figure 4.13 and Figure 4.14).

Table 4. 1: Detailed observation of flexure specimen

S. no.	Specimen ID	Failure of shear connectors at load (kN)	Visual observations	Reference Figure
1	SPC1	First crack initiated at 24 kN. Second shear connector failed at 45 kN. Peak load has been achieved at 57.87 kN.	Flexure crack initiated at the mid span throughout the width of the specimen. Ultimate failure occurred at beneath one of the loading points. Apart from the breaking of the both the wythes, EPS also failed which signifies that load has been transferred uniformly from top to bottom wythe. Shear cracks were also observed near the support. Post elastic behaviour showed the	Figure 4.1 Figure 4.2

			ductility of the concrete sandwich panel.	
2	SPGG	First crack initiated at 26.3 kN. Second shear connector weld failed at 33 kN. At 50 kN, 55kN, 57kN three consecutive bends are observed, which may be attributed to the failure of shear connectors. Peak load achieved is 73.87 kN.	Flexural and shear cracks are observed which start originating at the mid span. The crack which first initiated is under one of the loading points and propagated in a diagonal manner towards the lower wythe. Before the ultimate failure cracks have spread all over the thickness of both the wythes.	Figure 4.3 Figure 4.4
3	SPSgi200	Shear connector failed at 10 kN. Second major crack appeared at 64 kN. Peak load achieved is at 78.78 kN	Flexural cracks are observed beneath both the loading points. Cracks are more in lower wythe than the upper wythe. Ultimate failure is in flexure and maximum peak load is achieved. Post elastic behaviour is also depicting towards the enhanced ductility.	Figure 4.5 Figure 4.7
4	SPSgi300	Shear connector failed at 11 kN. Another connector broke at 40 kN. Peal load achieved is 50.35	Debonding of layer has been observed in this specimen. Though the initial cracking of weld of mesh is noted at a very early stage. Due to this micro cracking inside the panel lead to a weak composite nature of the panel. So it has been able to sustain a peak load less than the control specimen.	Figure 4.10 Figure 4.8

5	SP1C	First bend is noted at 21.76 kN. Then slight increase in the load value is 35 kN.	As this specimen is made up of mix M2 the compressive strength of this mix is less than M1 mix. But the specimen showed more ductility, which can be observed from the curve. Post elastic behaviour is extremely good.	Figure 4.2 Figure 4.6
6	SP1GG	First shear connector failed at 22.5 kN. Second connector at 40 kN. Peak load is achieved at 65.21 kN	Specimen containing the plastic geogrid showed more load taking capacity from the control specimen. Flexural cracks running throughout the width of the specimen. Plastic uniaxial geogrid has enhanced the load capacity as well as deformation capability. Breaking of plastic uniaxial geogrid is also observed.	Figure 4.4 Figure 4.9
7	SP1Sgi200	Initial crack appeared at 11.5 kN. Cracks started widening. Peak load achieved is at 59.20 kN.	Specimen behaved in similar manner as the control specimen. Cracks occurred at the over lapping point where the reinforcement of end beam and panel are joined.	Figure 4.7 Figure 4.11
8	SP1Sgi300	Initial cracking started at 12.5 kN. Second drop is at 41.7 kN. Peak load achieved is at 57.09 kN	Cracks propagated from the loading point towards the lower wythe through EPS. Shear failure dominated this specimen. Initially cracks started beneath the loading point but ultimate failure occurred at near the end beam and panel joint. Breaking of EPS has also been observed.	Figure 4.10 Figure 4.12

Figure 4. 1: Failure of specimen SPC1 at one of the loading points

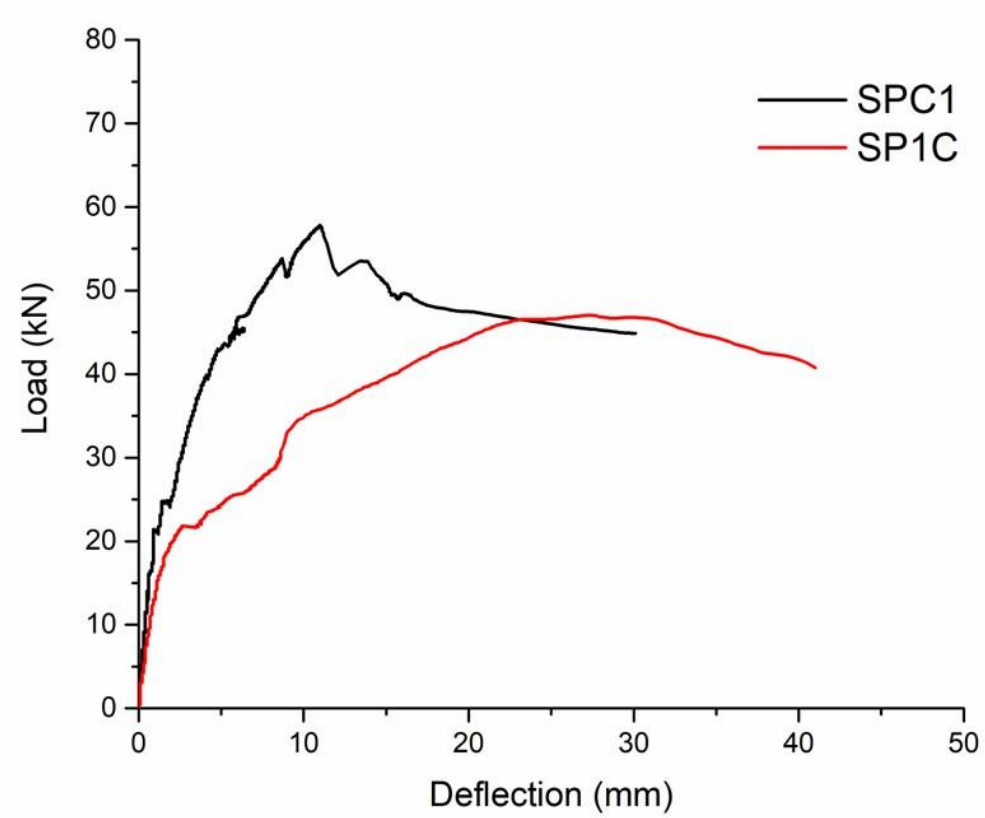

Figure 4. 2: Comparison of both the control specimen of two mixes M1 and M2

Figure 4. 3: Cracks are observed under the loading point throughout the width of the specimen.

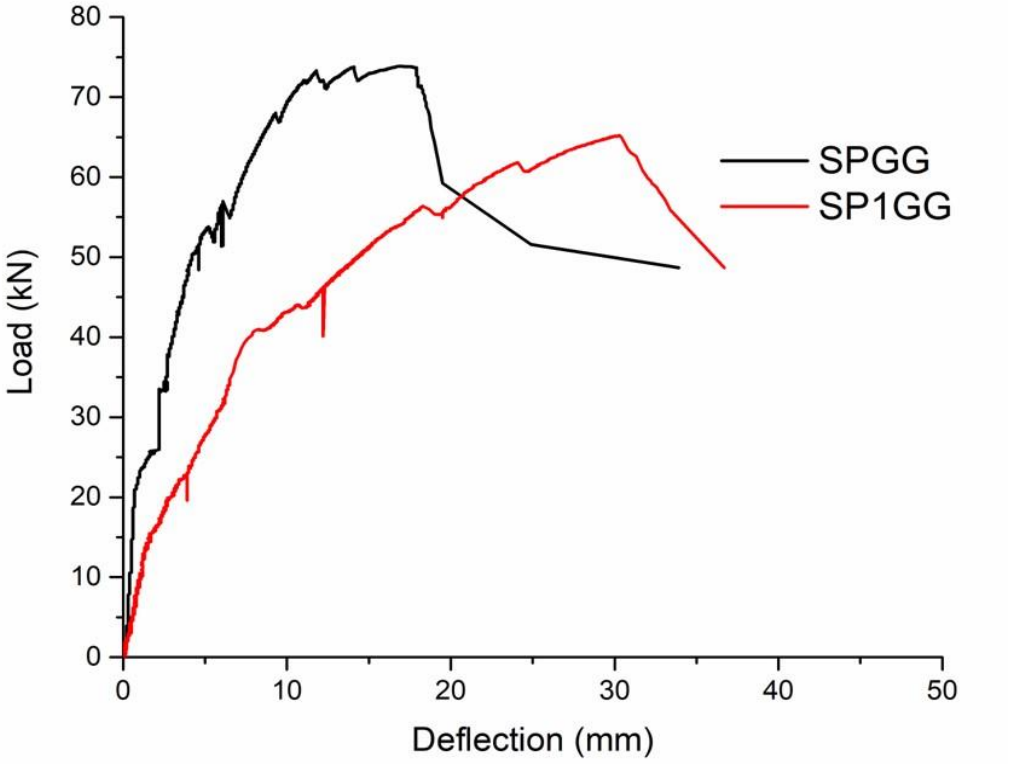

Figure 4. 4: Load vs deflection of SPGG and SP1GG

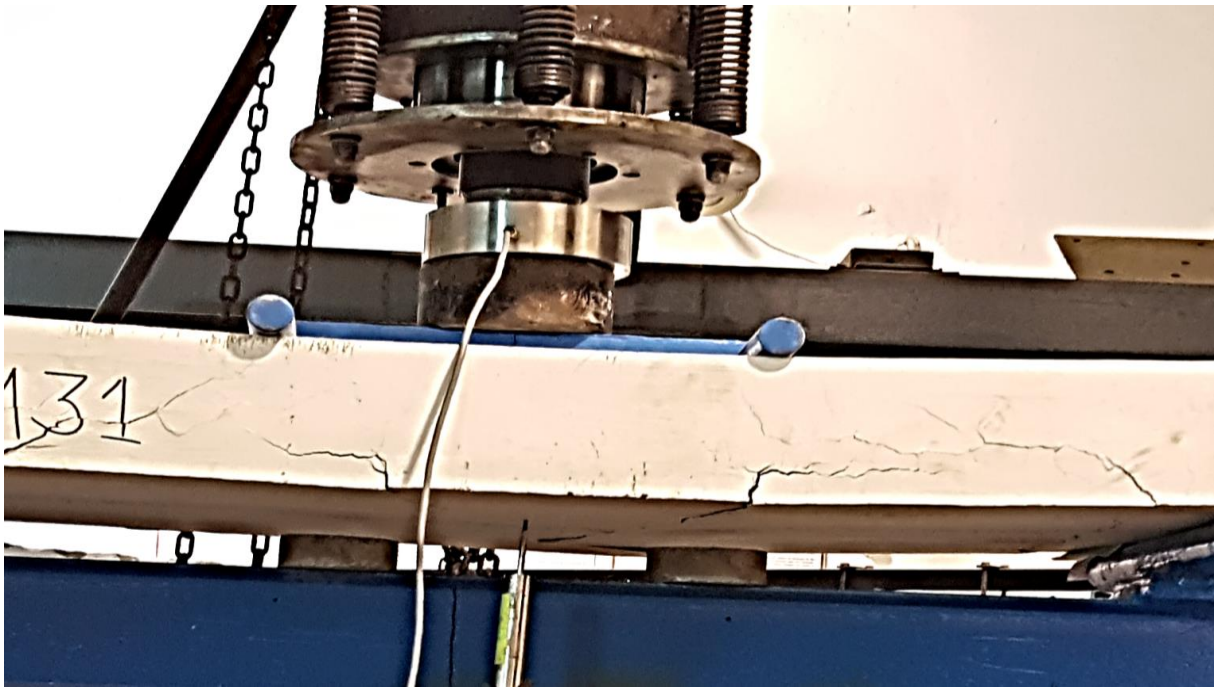

Figure 4. 5: Flexure cracks developing in the mid span

Figure 4. 6: Crack width expansion

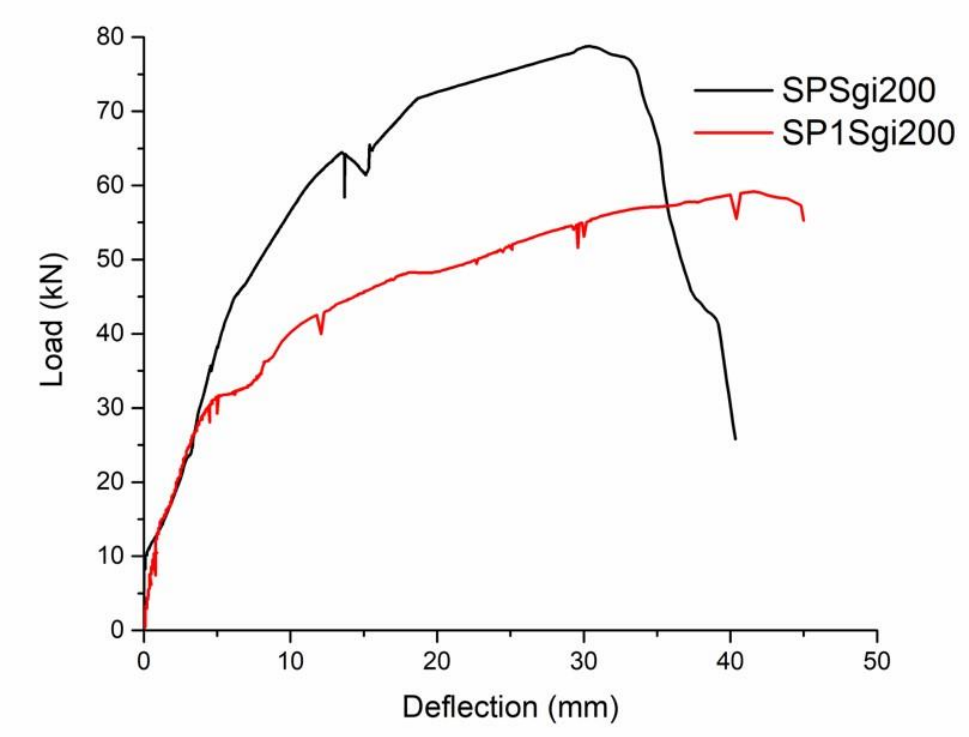

Figure 4. 7: Load vs deflection of SPSgi200 and SP1Sgi200

Figure 4. 8: Flexural crack running throughout the width of the specimen in the bottom wythe

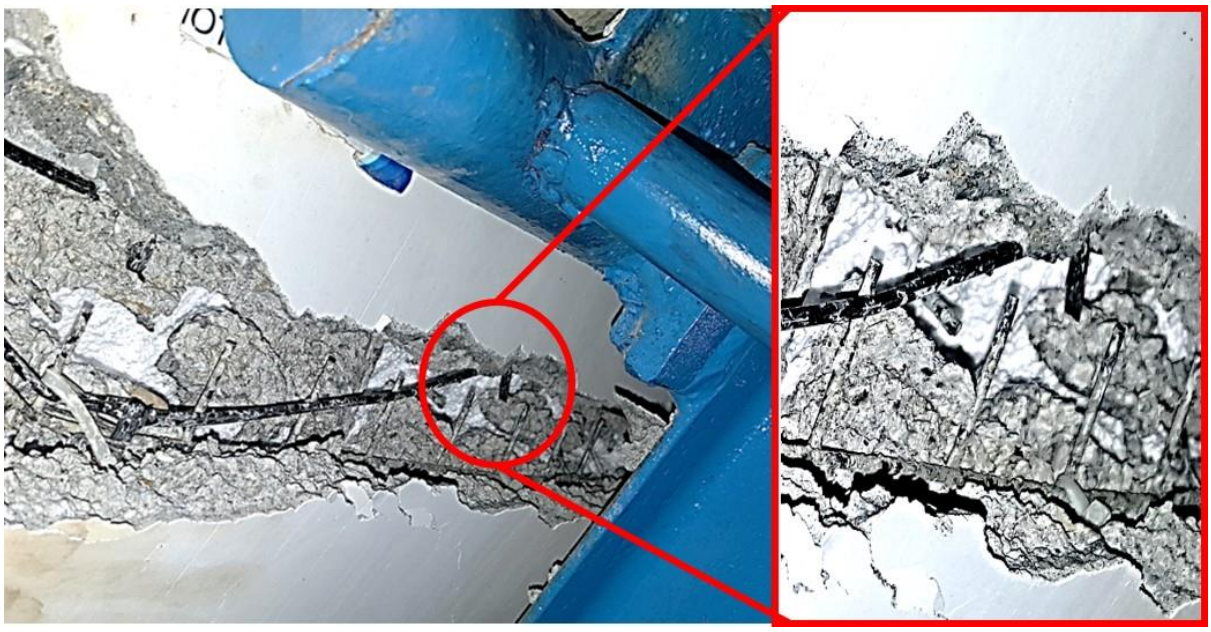

Figure 4. 9: Failure of PUG near the end beam joint

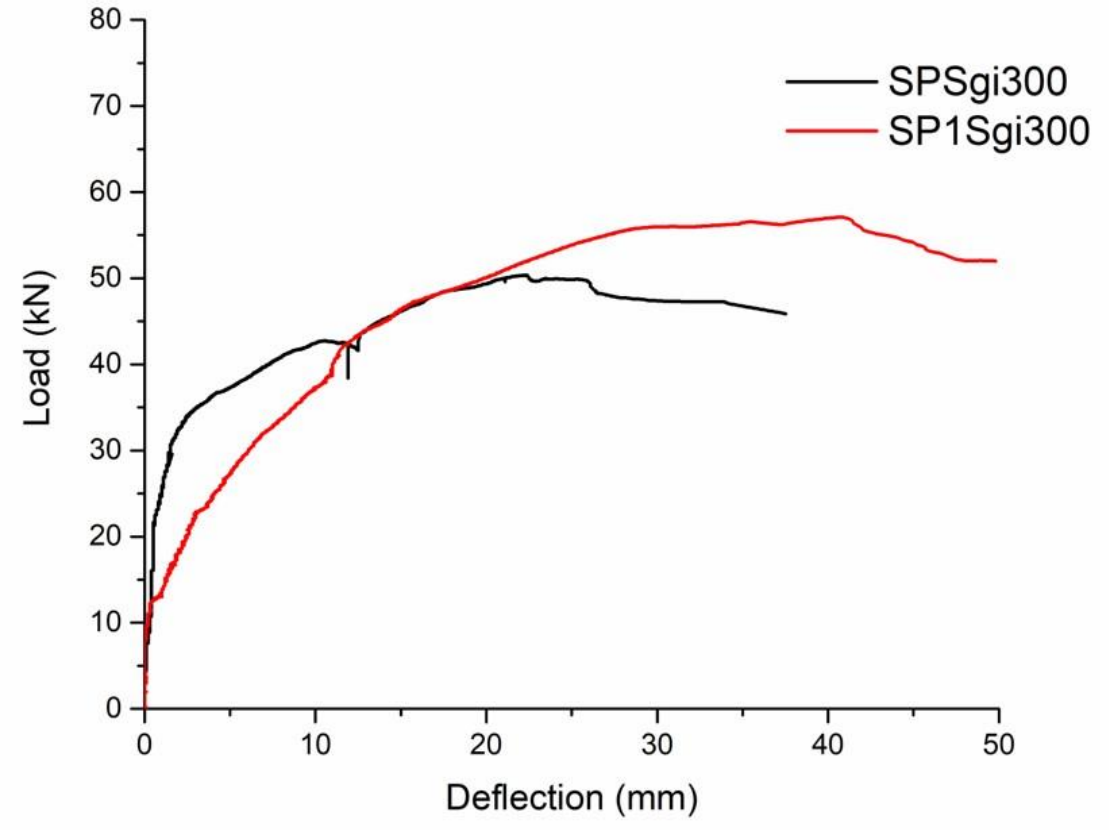

Figure 4. 10: Load vs deflection of SPSgi300 and SP1Sgi300

Figure 4. 11: Initial cracks appeared at the mid span and reaching the ultimate failure near the support

Figure 4. 12: Cracks propagation from the loading point towards the lower wythe through EPS

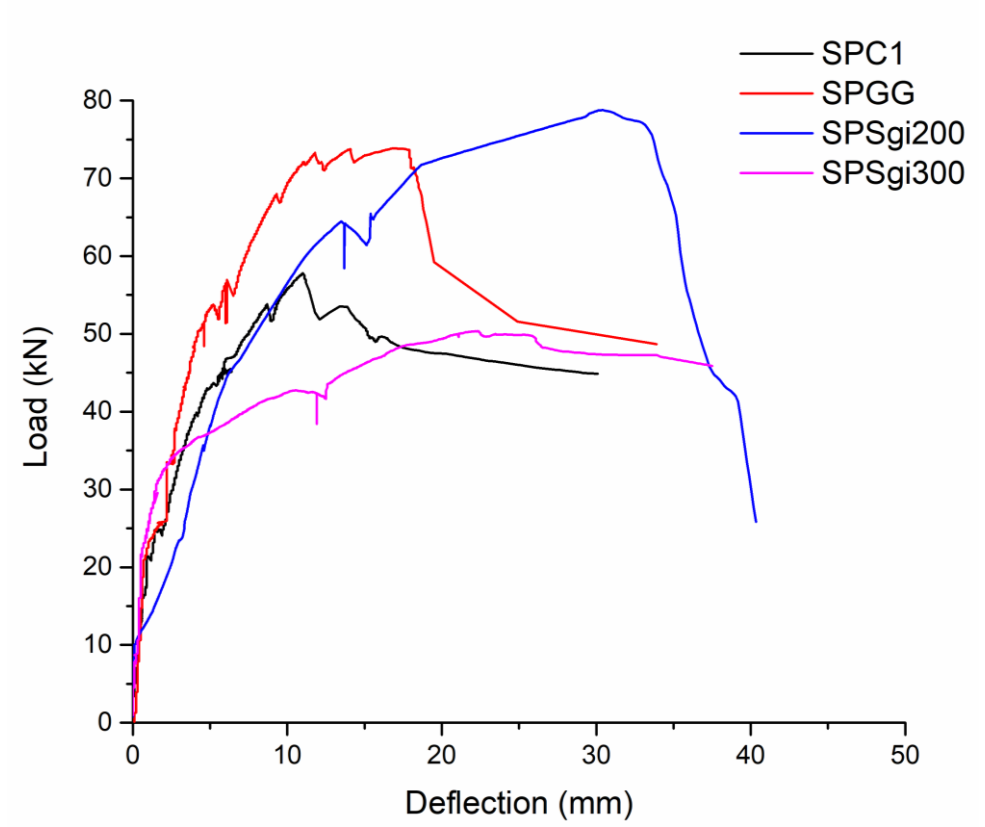

Figure 4. 13: Load versus deformation comparison of M1 specimen

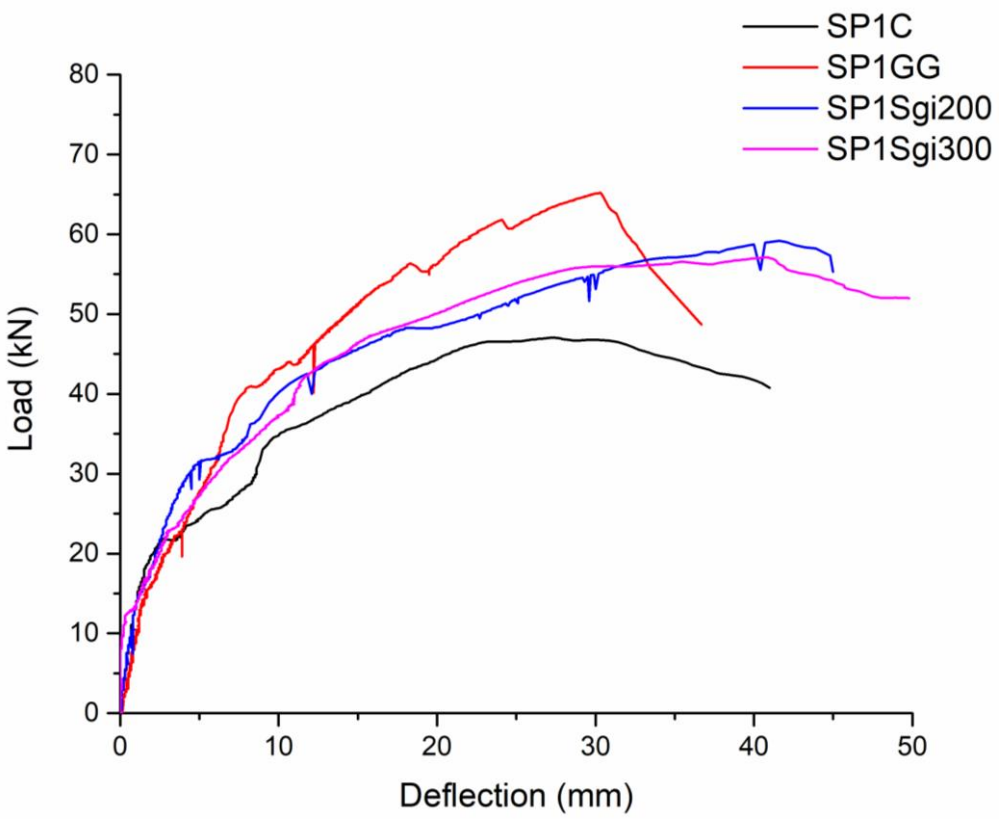

Figure 4. 14: Load versus deformation comparison of the mix M2

4.2.2 Failure pattern

The behaviour of all the specimens is evaluated carefully during the entire testing. The SPC1 specimens failed in flexure and cracks occurred just beneath the loading point and propagate towards the center (Figure 4.15 (a)). The specimens (SP1C) failed in shear (Figure 4.15 (b)) and the deflection observed was less as compared to other mix ratios. The mix M2 is having less compressive strength, so the onset of crack appeared earlier than the mix M1 containing the specimen. The SPGG specimen failed in shear because of the debonding between the layers (Figure 4.15(c)).

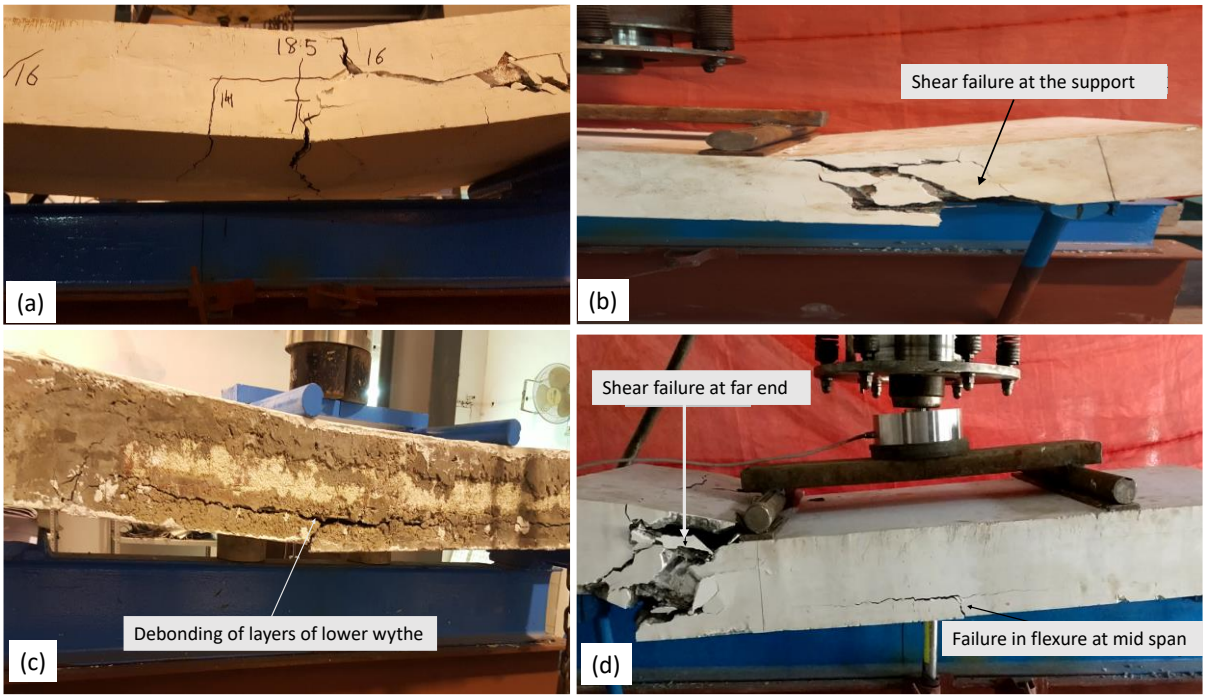

Figure 4. 15: Various flexural failure (a) Failure in Flexure (Out of Plane); (b) Failure in Shear at Support; (c) Debonding failure pattern in SPGG; (d) Failure in Flexure as well as Shear

Also, it has been clear from the post-peak behaviour of SP1GG, that the ductility behaviour has increased but at the same time specimen cracked earlier than SPGG because of the compressive strength of the M1 (i.e SPGG) is higher. Sandwich panel with polyester geogrid i.e SPSgi200 failed in shear and the crack occurred beneath the point load and propagated towards side support. The specimen SP1Sgi200 also failed in shear towards one of the support and cracks propagated through the center but failure occurred at one of the supporting end (Figure 4.15(d)). SPSgi300 failed in flexure and debonding was also observed. The panel cast using polyester geogrid, i.e. SP1Sgi300 which failed in shear but gave extreme ductile

behaviour. From these observations, the failure of the panel can be associated with concrete failure in the bottom wythe due to the combined effect of shear and flexural stresses.

4.2.3 Quantification of Panel stiffness, strength and deformability

The results shown in Tables 4.3 indicate a significant improvement in the ultimate load carrying capacity, stiffness, energy dissipation, and ductility of the concrete sandwich panel because of geogrids added as an additional reinforcement. The results show a gain of about 28% in plastic geogrid (SPGG); 36.8% in the case of polyester geogrid (Sgi200), in comparison with the control specimen. This may be due to the synergistic impact of grid confinement along with welded wire mesh. On the contrary, polyester geogrid (Sgi300) showed 12% less strength than the control specimen due to the debonding of the lower wythe from the core. One of the most important criteria for assessing efficiency is the ductility of sandwich panels. Ductility characterizes the tendency of the panels to deform after yield or dissipate energy. Ductility is the ability of a structure to resist the large deformation in an in-elastic state. In the present study the deflection ductility index $\mu\Delta$ is calculated; it is the ratio of ultimate displacement (Δ_u) to the yield displacement (Δ_y). The energy absorption ductility (μ_E) is also calculated for the control and geogrid containing panels. It is the ratio of the area of the load–deflection diagram up to the ultimate load (E_u) to the yield load (E_y). In terms of energy dissipation capacity (Table 4.3), the deformation capacity has also been evaluated by calculating the area under the load-deformation curve. Higher energy absorption suggests more plastic deformation before failure and therefore a panel with higher energy dissipation capacity will certainly be more ductile. In the SPGG specimens apart from welded wire mesh additional reinforce-ment of plastic geogrid is also there and its contribution can be clearly understood from an increase in the values of ductility and energy dissipation capacity. Higher inelastic deformation exhibited by Polyester geogrid (Sgi200) also shows an increase in ductility. The secant stiffness of the concrete sandwich panels has been determined by the ratio of the maximum peak load to the corresponding deflection. The secant modulus offers a useful comparison of the effect of various geosynthetic materials on the stiffness of the concrete sandwich panel (Table 4.2). A significant loss in stiffness of specimens cast using mix M2 as compared to M1 is observed. It is attributed due to the lesser compressive strength of mix M2 as compared with the M1 mix.

Table 4. 2: Stiffness of flexure specimens

Specimen ID	Mix	Yield Stiffness (kN/mm)	Secant Stiffness (kN/mm)
SPC1	M1	10.2	5.25
SPGG		11.75	4.34
SPSGi200		6.54	2.58
SPSGi300		17.6	2.26
SP1C	M2	3.46	1.71
SP1GG		5.13	2.16
SP1SGi200		4.34	1.42
SP1SGi300		4.33	1.40

4.2.4 Effect of mixes

The compressive strength results of the mix M1 is much better than mix M2. The effect of these mixes can be clearly observed on the specimen strength. Through load deformation curve of all the specimen it shows that M1 mix specimen outperformed the M2 mix specimen.

4.2.5 Effect of Geogrids

The inclusion of geogrids as supplementary reinforcement aims to augment the ductility of the concrete sandwich panel. It has been found from the load versus deformation curves that the specimen containing the geogrids exhibited greater deformation compared to the control specimen of either mix.

Additionally, the plastic uniaxial geogrid increased the strength, while the polyester geogrid improved the deformation capabilities, specifically in terms of post-elastic behaviour.

Closing remarks

The aim behind the flexural testing of the concrete sandwich panels is to observe the performance under four point bending load. The addition of geogrids as an extra reinforcement has enhanced the ductility of the concrete sandwich panel when compared with its counterpart control specimen. Hence it can be said that the addition of geogrids and the variable mixes used

has enhanced the load bearing capacity as well as the ductility of the concrete sandwich panel. The energy dissipation results also suggests the same.

Table 4. 3: Strength and deformability parameters of concrete sandwich panels in flexure

Panel Designation	**Yield load P_y (kN)**	**Ultimate load P_u (kN)**	**Deflection Δy (mm)**	**Δu (mm)**	**Deflection ductility factor $\mu\Delta = \Delta u/\Delta y$**	**Energy E_y (kN.mm)**	**E_u (kN.mm)**	**Energy ductility factor $\mu_E = E_u/E_y$**	**Energy dissipation (kN.mm)**	**Failure mode**
M1 (1:3)										
SPC1	48.00	57.82	4.60	11.00	2.39	121.31	447.86	1.17	447.86	F
SPGG	70.50	73.87	6.00	17.00	2.83	219.44	540.51	2.46	540.51	S & D
SPSgi200	70.00	78.78	10.70	30.42	2.84	396.19	1791.57	4.52	1791.57	F & S
SPSgi300	44.00	50.35	2.50	22.20	8.88	65.78	921.35	14.00	921.35	F
M2 (1:2:3)										
SP1C	45.10	47.07	13.00	27.40	2.10	343.45	973.57	2.83	973.57	S
SP1GG	59.00	65.21	11.50	30.30	2.63	340.80	1412.08	4.14	1412.08	S
SP1Sgi200	54.30	59.20	12.50	41.60	3.32	374.28	1900.07	5.07	1900.07	S
SP1Sgi300	52.00	57.09	12.00	40.60	3.38	339.70	1848.18	5.44	1848.18	S & D

F: Flexural; S: Shear; D: Debonding of layer of wythe

4.3 Diagonal Shear response of concrete sandwich panels

The majority of structures are built with brick masonry, and these unreinforced brittle constructions are unable to withstand lateral thrust caused by earthquake ground motion. Over the last decade, there has been tremendous growth in the demand for masonry structure strengthening. Several reinforcing methods, such as the most popular welded wire mesh (WWM), fibre reinforced polymer (FRP), and engineered cementitious composite (ECC) reinforced mortars and inorganic composites have been proposed to enhance the in-plane behaviour of masonry walls. Although these technologies can increase masonry walls' in-plane deformation and bearing capacity, but still have some shortcomings that must be addressed. In usual practice, the masonry panel is strengthened by attaching the welded wire mesh using shear connectors. On the other hand, CSPs have shear connectors that ensure the composite behaviour of wythes on both sides of the panel. Shear connectors are responsible for the rigid behaviour of CSP. In this section, the concrete sandwich panel has been subjected to diagonal shear loading. Testing has been conducted following the procedure outlined in the ASTM E519 code (ASTM E72, 2002) for the standard methods of performing strength tests on panels used in building construction.

4.3.1 Load-deflection behaviour

The results of diagonal shear specimen obtained experimentally are studied in terms of the effect of the mix, mode of failure, the effect of geogrids**,** initiation of cracks, load carrying capacity, deflection ductility factor, shear strength and energy dissipation.

Under axial compression, concrete expands horizontally, the longitudinal stresses caused by this loading cause tensile strains in the transverse direction, leading to vertical cracks propagation and failure. The lateral expansion is countered by lateral pressure, resulting in a significant increase in both ductility and strength. The cracks formed on the front and back wythes at the same time or one after the other. These fractures began at the top or bottom of the specimen in the solid zones and eventually spread across the full height. The concrete capping does not exhibit a dominant role in the failure pattern, rather it serves as a mechanism for load transfer. Cracks appeared in a diagonal pattern (about the middle of the span), and then the damage occurred at the point of connection between the capping and the EPS. All specimens have been tested until they collapsed or have been reduced to less than 80% of their peak load. Upon comparison of mix M1 specimens, it has been observed that specimen DS1GG exhibits a 13.7% increase in strength. The observed decrease in strength of the specimen that

contained PBG2 and PBG3 can be attributed to inadequate bonding between the layers of the same wythe. The specimens of mix M2 are also compared with one another, and an increase of 26% in load bearing capacity has been noticed in the specimen DS2GG when compared with the specimen DS2C. On the other hand, the compression load was greatly reduced in specimens DS2Sgi200 and DS2Sgi300 due to the bonding of the layer of the same wythe (20 mm thickness of each layer; 40 mm thickness of the total wythe) as well as the width of the strip. A comparative analysis between M1 mix (DS1C) and M2 mix (DS2C) has revealed a 17% rise in the load bearing capacity of the former. An additional increase of 6%, 18%, and 24% has been observed in the PUG, PBG2, and PBG3 specimens, respectively.

The shear stress has been calculated using Eq. (4.1) (ASTM E 519-02, 2002) and the applied force. Table 4.4 lists the specimens' shear strengths.

$$\boldsymbol{\tau = \frac{0.707 \times P}{0.5 \times t \times (L+B)}} \quad 4.1$$

Where, τ = average shear stress; t = thickness of the specimen; L = length of specimen; B = width of specimen; P = diagonal compressive force. Following ACI 318-14(Committee, 2014) shear capacity of CSPs have been calculated using equation 4.2 - 4.4 and related with the maximum shear force endured by the specimens mentioned in Table 3.

$$\mathbf{V_n = V_c + V_s} \quad 4.2$$

$$\mathbf{V_c = (0.27 \times \lambda \times (\sqrt{f'_c}) \times l \times T) + N_u \times (\frac{l}{4 \times L})} \quad 4.3$$

$$\mathbf{V_s = A_V \times f_y \times \frac{l}{s}} \quad 4.4$$

Where, $\mathbf{V_n}$ = Shear capacity of CSP; **T** = total thickness of concrete; **λ** = Modification factor; $\mathbf{N_u}$ = component of axial force; $\mathbf{f'_c}$ = compressive strength of concrete; $\mathbf{V_s}$ = Shear contribution of reinforcement $\mathbf{A_v}$ = Area of shear reinforcement; and **s** = spacing of shear reinforcement $\mathbf{V_c}$ = Shear contribution of concrete; $\mathbf{f_y}$ = yield stress of shear reinforcement; **l** = 0.8L; where **L** = dimension of the specimen.

From IS 456:2000 (IS 456, 2000) shear capacity can be calculated using equations 4.5 and 4.6.

$$\mathbf{S_c = \tau_c \times \delta} \quad 4.5$$

Table 4. 4: Diagonal compression results and shear strength

S no.	Specimen nomenclature	Mix	Diagonal compression load (kN)	Shear capacity (kN)			Average shear strength, τ (MPa) Eq. (1)
				Experimental*	ACI 318-14**	IS 456: 2000***	
1	DS1C	M1	293.65	208.26	189.39	118.53	2.66
2	DS1GG		333.87	236.78	195.17	118.53	3.02
3	DS1Sgi200		232.12	164.62	180.74	111.05	2.10
4	DS1Sgi300		207.37	147.07	177.23	107.64	1.87
5	DS2C	M2	249.12	176.68	175.89	118.53	2.25
6	DS2GG		314.68	223.17	185.19	118.53	2.85
7	DS2Sgi200		196.65	139.46	168.45	113.72	1.78
8	DS2Sgi300		166.35	117.97	164.15	108.37	1.50

$$\boldsymbol{\delta = 1 + \frac{3 P_u}{A_g \times f_{ck}}} \quad 4.6$$

Where, S_c = shear capacity (kN) of CSP; $\boldsymbol{\tau_c}$ = design shear strength (N/mm^2) from the IS 456: 2000; δ = modification factor; P_u = axial compressive force (N); A_g = gross area of concrete section in mm^2; f_{ck} = characteristic compressive strength of concrete (MPa). For the experimental Shear capacity value, the following formula (equation 4.7) have been used to calculate its value

$$V_u = P \sin \Phi \quad 4.7$$

Where V_u represents the shear capacity; P represents the peak load; Φ represents the angle between the line of loading and the shear surface, in this diagonal shear compression case the angle Φ is 45˚ (Ahmad & Singh, 2021). It can be deduced from Table 4.4 that PUG containing specimens outperformed the rest of the specimens in both mixes. The reason behind the increased values of the shear capacity (Serpilli et al., 2021) in PUG (DS1GG and DS2GG) is the stiffness of this material which acted as additional shear reinforcement (Figure 4.17) attached to the welded wire mesh with cable ties. Whereas in the specimens containing PBG2 and PBG3, the width of the strip, both in the machine direction and cross-machine direction

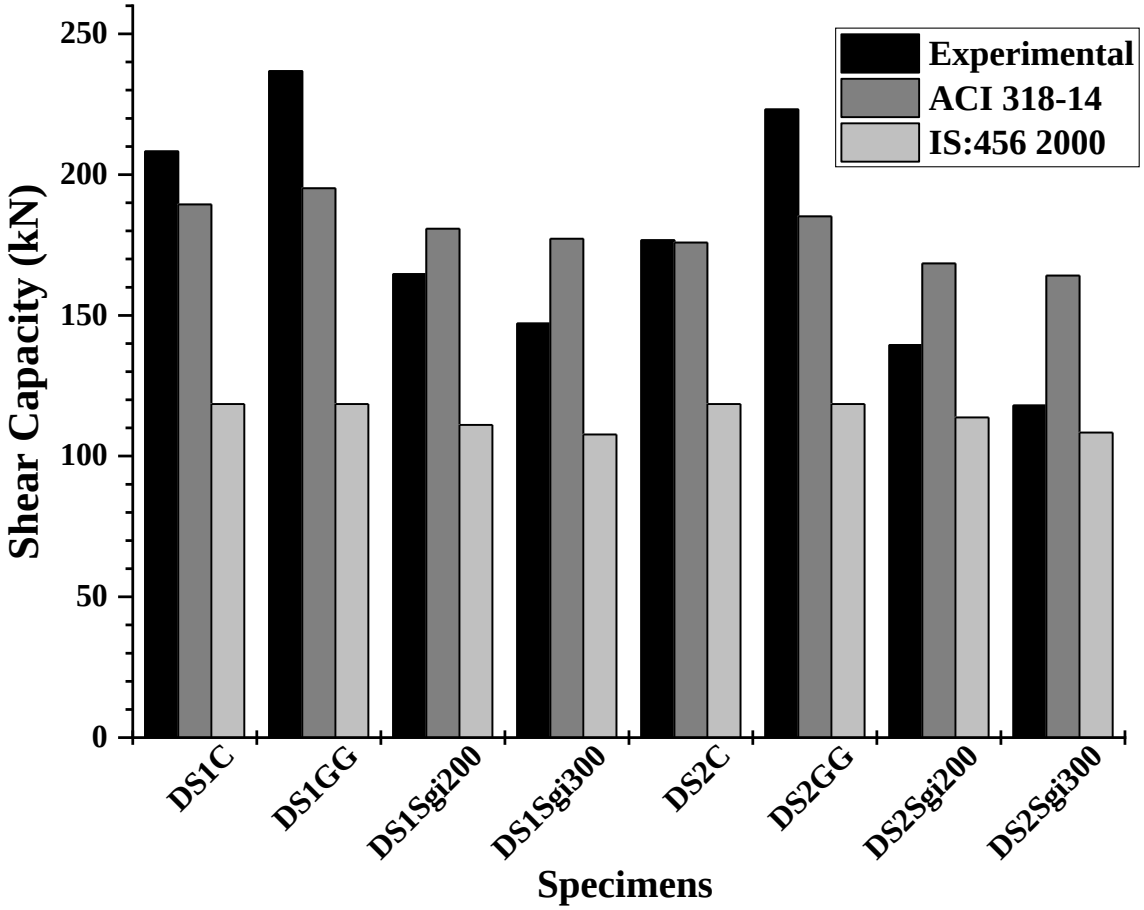

Figure 4. 16: Bar chart representation of shear capacity of all specimens

(Figure 3.2(d)), obstructed the bond between the layers of micro concrete resulting into weak bond formation which clearly explains the decreased values of diagonal compression load when compared with control specimen. The free ends are forced to expand and the only resisting force against this expansion is welded wire mesh and the plastic uniaxial geogrid, which has enhanced the shear capacity of the CSP panel (Siva Chidambaram & Agarwal, 2015). Tensile stresses generating in this direction are resisted by welded wire mesh and three columns of plastic uniaxial geogrid resulting in an increased shear capacity of the panel. Shear capacity values found out using IS 456:2000 (IS 456, 2000) are much less than experimental shear capacity values mentioned in Table 4.4 and Figure 4.16. There is no obvious rationale for this cautious shear strength calculation, and it is most likely due to experimental variabilities. More experiments are needed to determine the more accurate data (Ahmad & Singh, 2021).

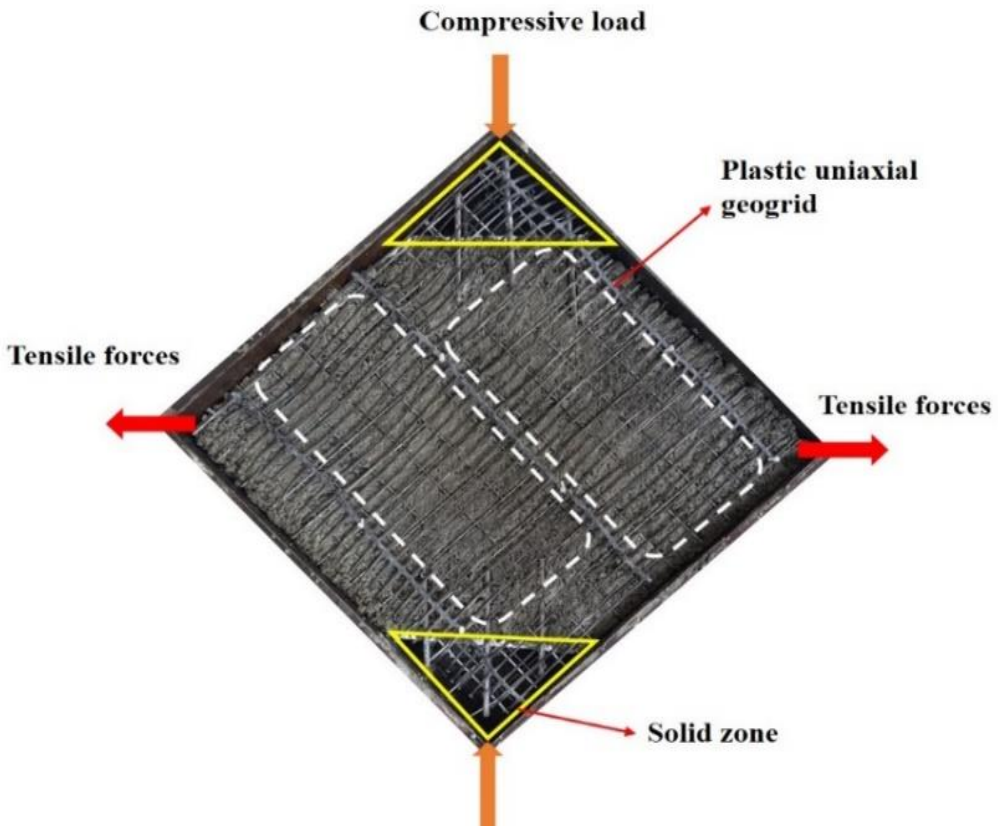

Figure 4. 17: Plastic Uniaxial Geogrid (PUG) specimen detail and direction of forces

4.3.2 Mode of Failure

Both the specimens, DS1C and DS2C, exhibited local concrete crushing at the capping upon application of a diagonal compression force, ultimately leading to failure. The failure of specimen DS1C has been observed at the bottom capping, and concrete spalling has also been noticed, as illustrated in Figure 4.18. The specimen DS2C experienced failure at the top capping, as depicted in Figure 4.19. The two specimens showed composite behaviour, and once the maximum stress has been reached, vertical cracks appeared on the wythe. Diagonal shear failure and local concrete crushing were observed in the DS1GG specimen. At a load of 130kN, the initial crack appeared and subsequently extended vertically from the uppermost section to the lowermost section within the rear wythe. The crack promulgated almost in the middle as a diagonal. The cracks on both wythes at the centre of the panel indicate the specimen's composite character, as seen in Figures 4.20 and 4.21. Similar behaviour has been observed in specimen DS2GG under diagonal compression testing. One of the other observations is the improvement in deformation when the peak load is achieved compared to the DS1GG specimen.

As shown in Figure 4.22, the crack in the specimen DS1Sgi200 began in the front wythe and close to the support, whereas in the opposite wythe, crack propagation was seen from the diagonal's centre to the bottom. The failure of DS1Sgi200 occurred at a lower load magnitude compared to the control specimen. The load value immediately decreases after reaching the peak load. The interlocking mechanism between PBG2 and the wythe may be responsible for the observed abnormalities. The inadequate bonding between the two layers of the same wythe is attributed to the width of the strip in PBG2, depicting the division of layers within the wythe. The result that was seen was that the specimen DS1Sgi200 was unable to show a strength that was comparable to the control specimen. This results from a weak connection that lowers the total adequate thickness.

A diagonal shear failure was observed in DS2Sgi200 (Figure 4.23). The specimen DS2Sgi200 has exhibited similar behaviour to specimen DS1Sgi200. The only different feature of this specimen is the M2 mixture used in its casting, which has a lower compressive strength than the M1 mixture. Diagonal cracks have been observed in the front wythe of the DS1Sgi300 specimen (Figure 4.24) and show no crack on the back wythe. The top capping of the DS2Sgi300 specimen has undergone forced intrusion into the panel, as depicted in Figure 4.25. The potential cause of the failure of the top support could be attributed to the PBG3 bond with the concrete and the bond between the two layers of the same wythe. Concrete spalling has also been observed at the top support located at the back.

The shear capacity is controlled by concrete capping in the case of PBG2 and PBG3 specimens, whereas in the case of PUG specimens, the reinforcement layer controls the shear capacity (Figures 4.26 and Figure 4.27). Based on experimental observation, PBG could not increase load-bearing capacity and shear capacity because of the poor bonding between the two layers of concrete. Due to the more width of the PBG strip (Figure 3.2(d)), it lead to partial bonding between the layers of a wythe. Hence leading to partial debonding of the layer while achieving the peak load. It is recommended to utilise polyester biaxial geogrids (PBG) with narrower strip widths or increased spacing between strips to enhance the interlayer adhesion of the concrete.

4.3.3 Effect of Geogrids

PUG (Plastic Uniaxial geogrid) is a stiff plastic material having thin strips (diameter = 4mm-5mm). While casting the wythe, the binding between the two layers of the same wythe is consistent, and the layers of the wythe act as one composite. The addition of plastic uniaxial geogrid (DS1GG and DS2GG specimens) has enhanced the performance of concrete sandwich

panels (Siva Chidambaram & Agarwal, 2015). Figure 4.16 shows that when an axial compressive load is applied (Daniel Ronald Joseph et al., 2022; Ronald et al., 2017), tensile

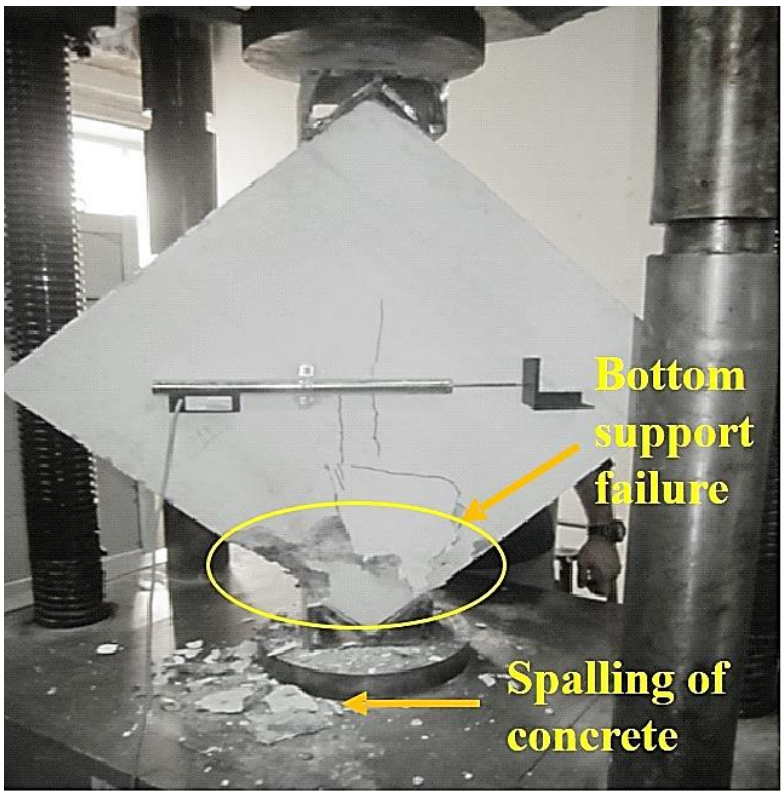

Figure 4. 18: Bottom support failure is observed (DS1C)

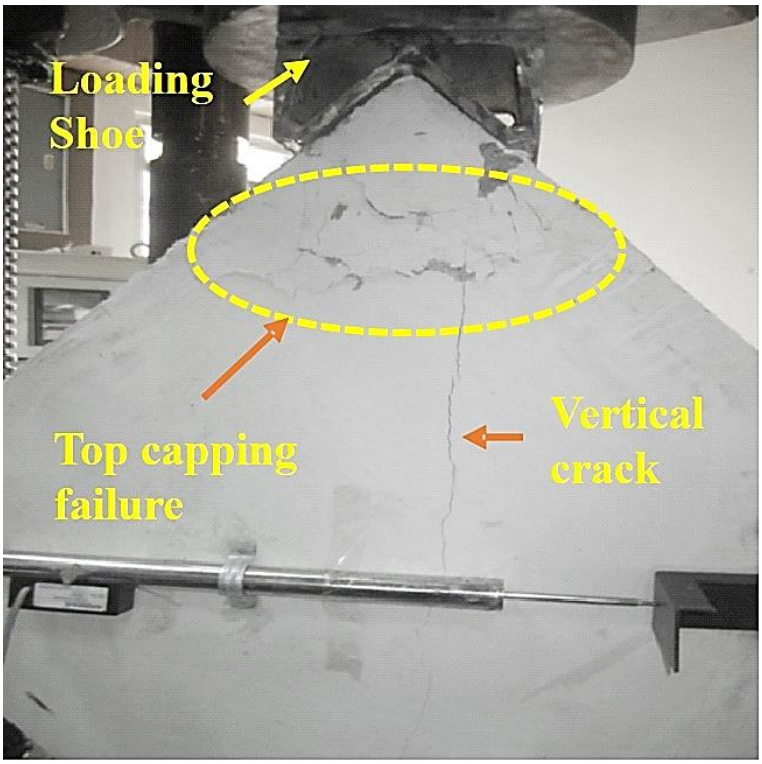

Figure 4. 19: Failure of specimen DS2C

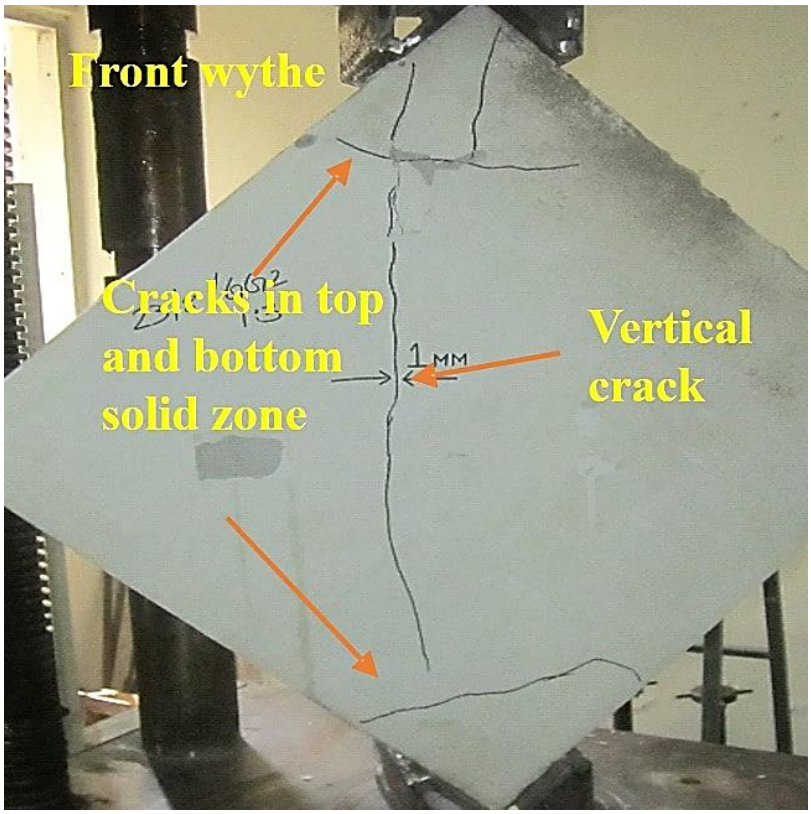

Figure 4. 20: Failure crack pattern of DS1GG

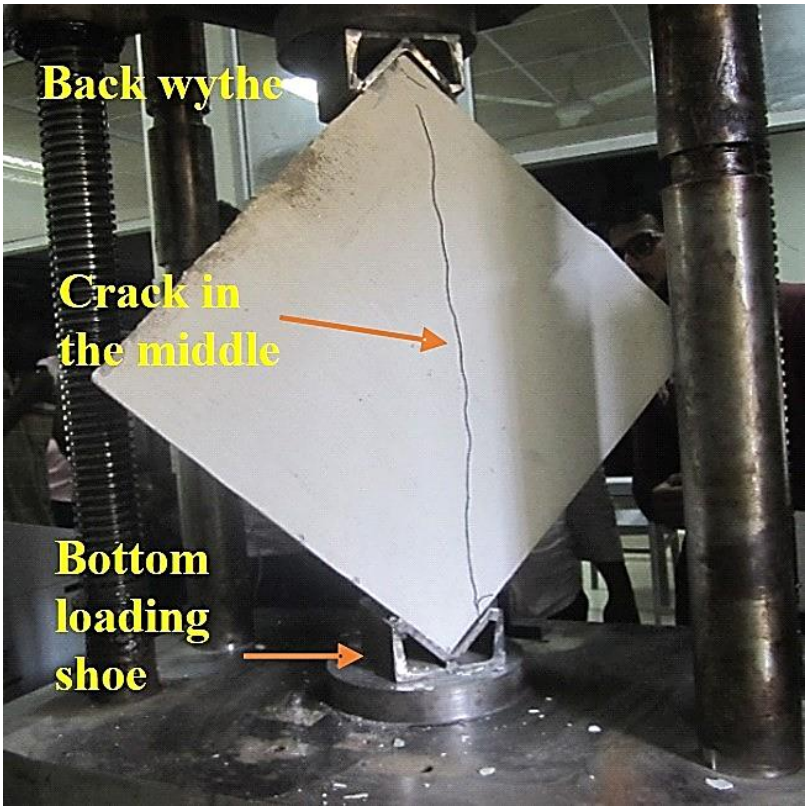

Figure 4. 21: Diagonal shear failure (DS1GG)

forces are generated (Serpilli et al., 2021), and tension is also generated in PUG, thereby increasing the load-bearing capacity (Ronald et al., 2018; Serpilli et al., 2021). Debonding failure has not been observed in the case of PUG and PBG2 (Polyester Biaxial Geogrid) specimens. PBG3 specimens achieved the peak load during the partial debonding. The horizontal crack width also signifies the behaviour of the geogrids incorporated in the concrete sandwich panel (Shelton et al., 2021). Table 4.5 shows that in specimen DS1C, the crack width observed is more than the DS1GG, which implies that the additional reinforcement (PUG) further supported the welded wire mesh against the tensile forces generated due to the axial compressive load.

Crack width in both the specimens containing PBG3 is the largest among all other specimens, which suggests that the bonding between the two layers of the single wythe has been interfered with, by the width of the geogrid. It results in partial debonding as well as bearing less compressive load, thereby increasing the crack width beyond the control specimen.

Figure 4.26-4.27 shows the combined results of mix M1 and M2 load-deformation curves. In Figure 4.17 and Figure 4.26-4.27, it can be seen that DS1GG has the maximum shear capacity and load-bearing capacity among the specimens cast with the M1 mix. Whereas in the case of mix M2 (Figure 4.17 and Figure 4.26-4.27), though DS2GG has shown maximum shear capacity, initial stiffness is observed to be higher in DS2C. This abnormality may be because of the size of the

coarse aggregate used in the M2 mix. The stone dust used in the mix M1 has a larger surface area and acts as a better binder. On the contrary, in the M2 mix, coarse aggregate is of the size range of 4.75mm to 6mm, so these aggregates are not as fine as the stone dust, a partial replacement in mix M1. Thus, the shear capacity values deduced in Table 4.3 and Figure 4.5 clearly show that the M1 mix is better than M2.

4.3.4 Energy dissipation

The results in Table 4.6 demonstrate that adding geogrids as an extra reinforcement significantly improved the CSPs' load-bearing capacity, energy dissipation, ductility, and deflection ductility index. In contrast to the control specimen, the results reveal a gain of around 13.7 % in PUG (DS1GG). This could be because grid confinement and welded wire mesh have a synergistic effect. Due to the partial debonding within the wythe, PBG3 (DS2Sgi300) has shown 33% lower strength than the DS2C.

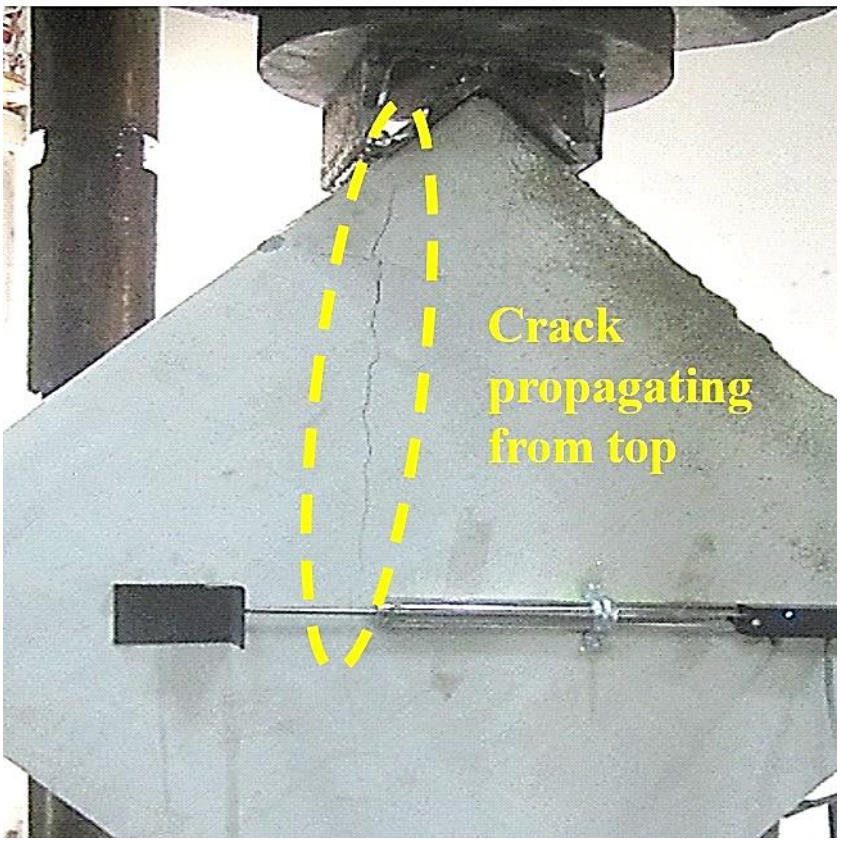

Figure 4. 22: Failure of specimen (DS1Sgi200)

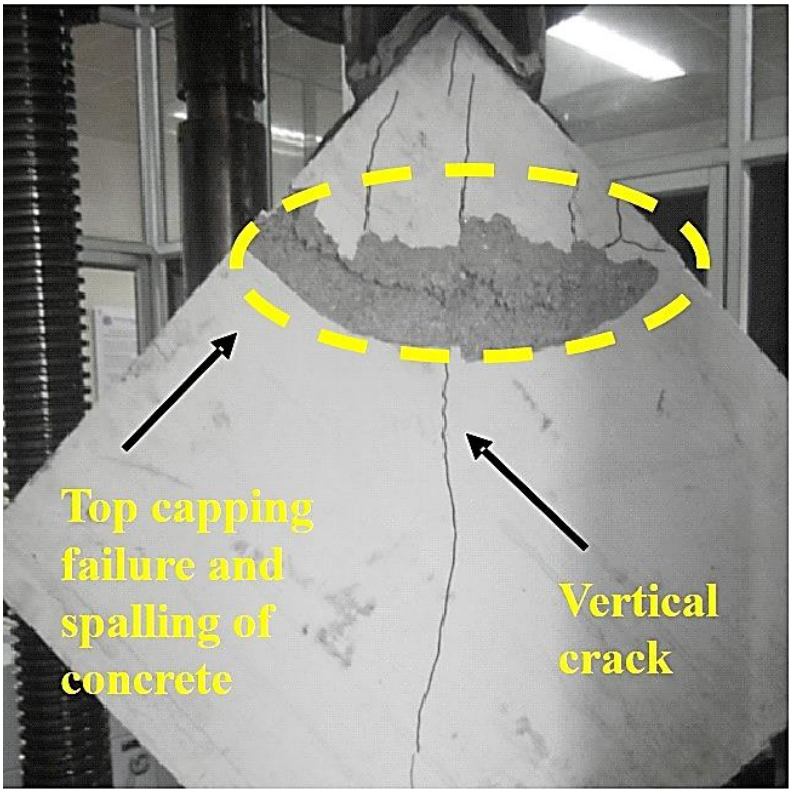

Figure 4. 23: Failure of specimen (DS2Sgi200)

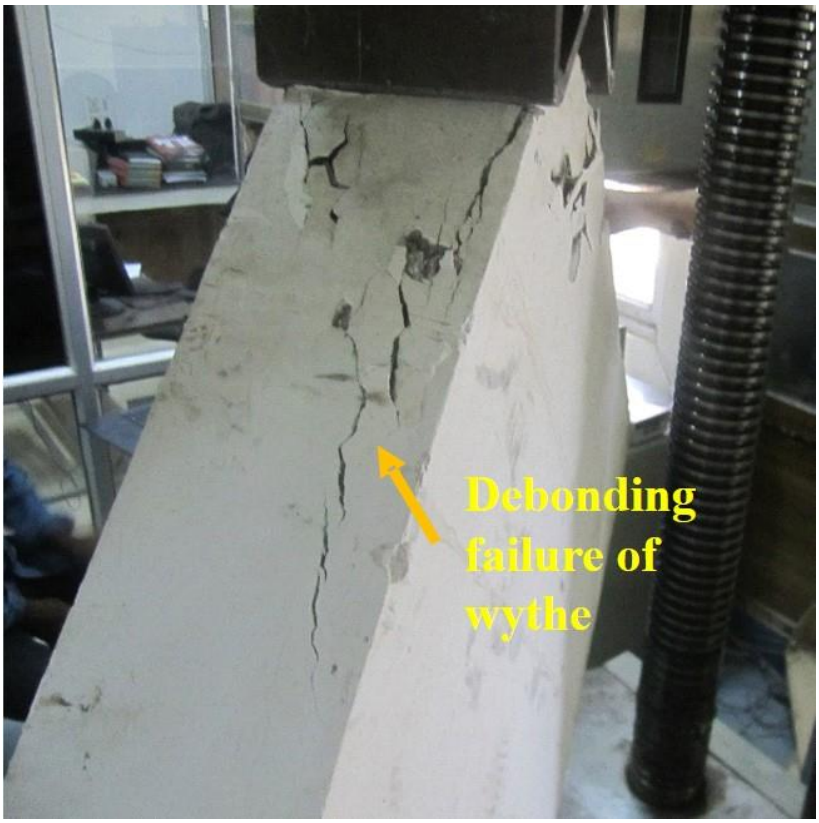

Figure 4. 24: Debonding failure of specimen DS1Sgi300

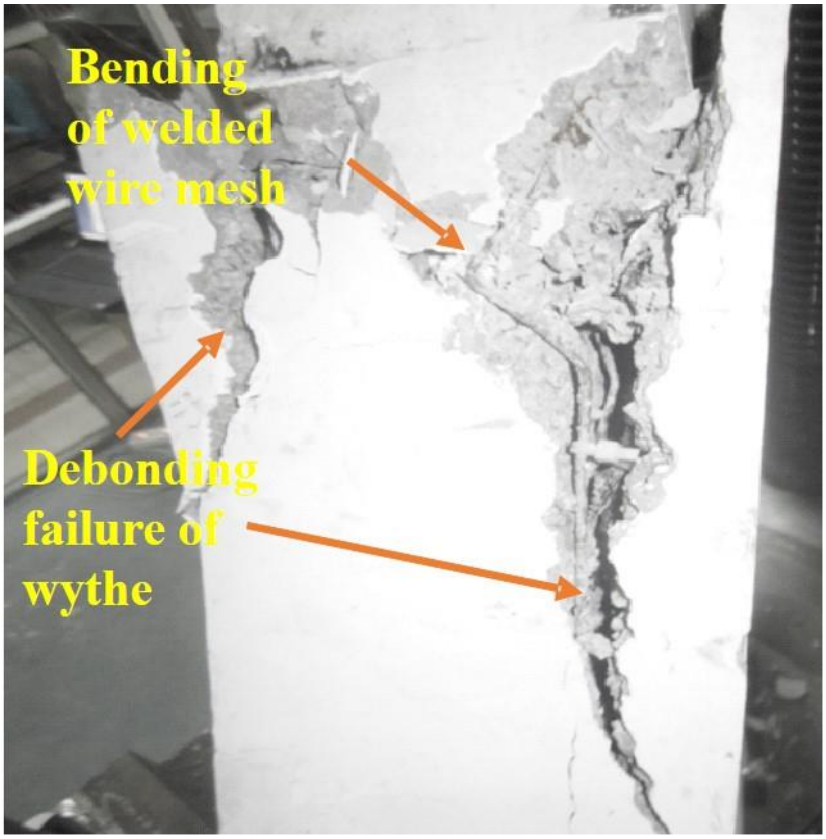

Figure 4. 25: Welded wire mesh failure (DS2Sgi300)

Table 4. 5: Horizontal LVDT reading

S No.	Specimen name	Crack width (mm)
1	DS1C	1.7
2	DS1GG	1.0
3	DS1Sgi200	1.1
4	DS1Sgi300	3.0
5	DS2C	1.3
6	DS2GG	0.5
7	DS2Sgi200	2.2
8	DS2Sgi300	4.2

The ductility of sandwich panels is one of the most essential variables for determining efficiency. The affinity of the panels to distort after they have yielded or dissipated energy is referred to as ductility. The capacity of a structure to tolerate substantial deformation in an inelastic condition is known as ductility (Spadea et al., 1998)). The deflection ductility factor ($\mu\Delta$) is determined in this study; the ratio of ultimate deformation (Δu) to yield deformation (Δ_y). The energy absorption ductility (μ_E), is defined as the ratio of area under the curve of load-deformation up to the ultimate load (E_u) divided by the yield load (E_y) (Bastin & Sharma, 2017).

Energy dissipation capacity mentioned in Table 4.5, the deformation capacity has been calculated by computing the region under the load-deformation graph. More energy absorption implies more post-elastic deformation before the collapse, implying that CSP with greater energy dissipation capacity is undoubtedly ductile (Bastin & Sharma, 2017). Apart from WWM, the influence of PUG reinforcement can be shown in Table 4.5 for DS1GG and DS2GG specimens. Because these geogrids are less expensive than the other strengthening materials (fibre-reinforced polymers), they may be employed as supplementary reinforcement to increase the ductility of CSPs at a lower cost.

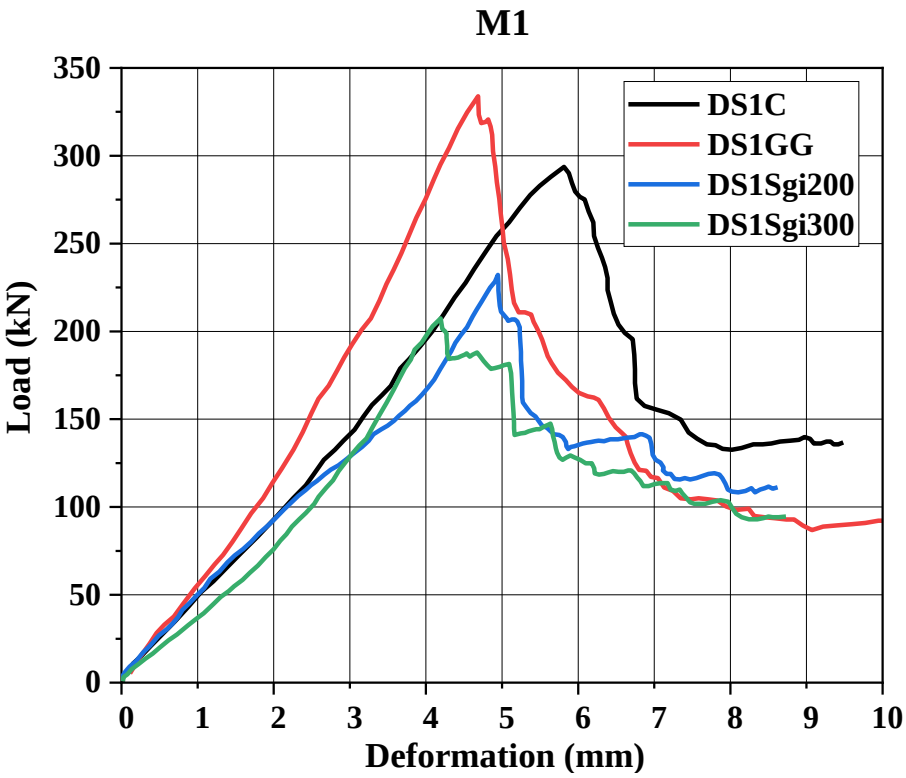

Figure 4. 26: Load vs deformation curve of all M1 specimen

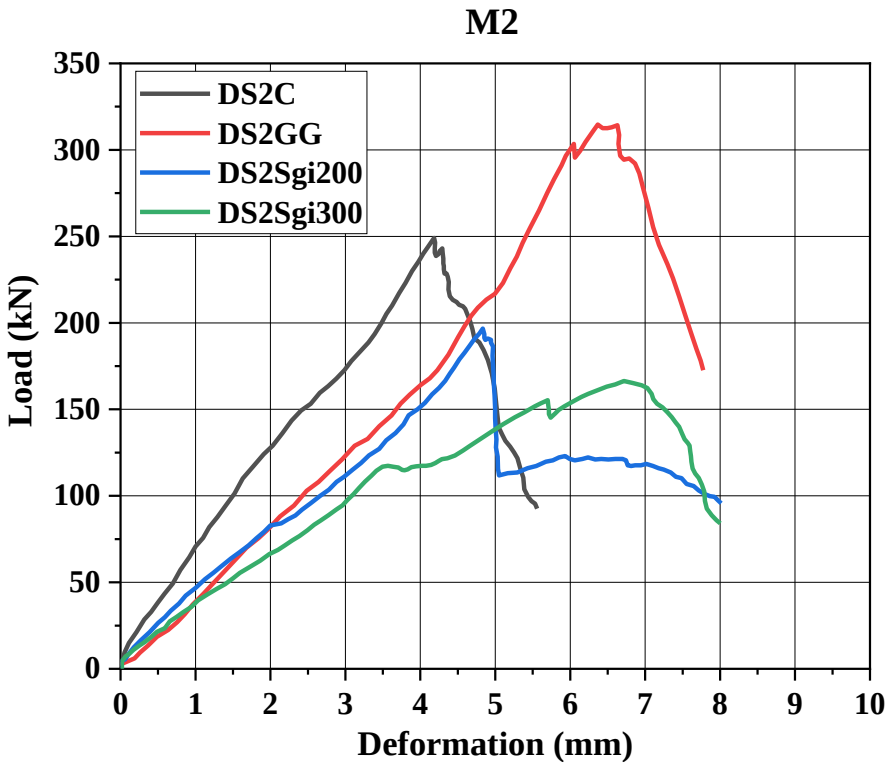

Figure 4. 27: Load vs deformation graph of mix M1 and M2

Closing remark

The aim behind the diagonal shear testing of the concrete sandwich panels is to observe the performance under in-plane loading. The addition of geogrids as an extra reinforcement has enhanced the load bearing capacity of the concrete sandwich panel when compared with its counterpart control specimen. The shear capacity results support the reasoning made from load deformation curves.

Table 4. 6: Strength deformation capabilities of diagonal shear specimen

Panel Designation	**Yield load P_y (kN)**	**Ultimate load P_u (kN)**	**Deflection Δ_y (mm)**	**Δ_u (mm)**	**Deflection ductility factor $\mu\Delta = \Delta u/\Delta y$**	**Energy E_y (kN.mm)**	**E_u (kN.mm)**	**Energy ductility factor $\mu_E = E_u/E_y$**	**Energy dissipation (kN.mm)**	**Failure mode (A,B,D)***
M1 (1:3)										
DS1C	176.19	293.65	3.68	5.82	1.58	318.61	829.76	2.60	829.76	A
DS1GG	200.32	333.87	3.21	4.68	1.45	293.84	703.58	2.39	703.58	A&B
DS1Sgi200	139.27	232.12	3.62	4.94	1.36	252.64	544.80	2.15	544.80	B
DS1Sgi300	124.42	207.37	3.04	4.19	1.37	169.17	377.74	2.23	377.74	B&D
M2 (1:2:3)										
DS2C	149.47	249.12	2.84	4.18	1.47	194.75	538.26	2.76	538.26	A
DS2GG	188.81	314.68	4.65	6.62	1.42	413.61	886.15	2.14	886.15	B
DS2Sgi200	117.99	196.65	3.55	4.82	1.35	209.58	458.61	2.18	458.61	B
DS2Sgi300	99.81	166.35	3.06	6.72	2.19	164.97	652.39	3.95	652.39	A&B

*A: local concrete failure; B: Diagonal shear failure; D: Partial debonding of the wythe

4.4 Axial compression testing

This part of the chapter represents the axial compression testing of the concrete sandwich panels and its various parameters which have been carefully observed and compared. The results of axial compression specimen obtained experimentally are studied in terms of the effect of the mix, mode of failure, initiation of cracks, load carrying capacity, deflection ductility factor, shear strength and energy dissipation.

4.4.1 Load deformation behaviour

Concrete will expand laterally when subjected to axial compression. The longitudinal stresses that are a result of this loading will generate tensile strains in the transverse direction, which will ultimately result in vertical fractures propagating and the material failing. The lateral pressure acts as a check on the lateral expansion, which ultimately leads to a substantial improvement in both the material's ductility and its strength. The formation of cracks occurred either simultaneously or sequentially on both the front and back wythes. The fractures initiated at either the upper or lower regions of the specimen within the solid areas, and subsequently propagated throughout the entire height. The concrete capping functions as a mechanism for transferring loads. Cracks were observed to propagate vertically from the top to the bottom of the span. Additionally, cracks were also observed at the end beams. Every specimen was put through a series of tests either until it was completely destroyed or until its peak load was lowered to less than 80 percent of its original value. The visual observation of all the specimen are mention in Table 4.7.

Table 4. 7: Details of compression specimen

S. no.	Specimen ID	Visual observations	Reference Figure
1	WP 1	Initial stiffness is linear up to a load of 200 kN. Slight deviation is observed in the curve after 3mm deformation, this may be due to crack initiation at micro levels. Another drop is observed at the load of 475 kN. Ultimately a peak load of 711 kN has been achieved. Sudden drop in load and increase in deformation is also observed after the failure. Failure at end beam is observed at the top and a vertical crack is observed in the middle.	Figure 4.28

2	WP 2	Initial vertical crack is generated at 250 kN. Another drop is observed at 501 kN, at this point the vertical crack widening star to occur but it is still taking the load linearly. After surpassing the peak load of control specimen WP 1 there is sudden increase in deformation. The peak load achieved by this specimen is 828.08 kN.	Figure 4.29
3	WP 3	Initial stiffness is the highest among all the specimens which is clearly visible from the blue curve. The bends at 240 kN, 325kN, 375 kN, 450kN signifies the cracks generated in the panel at middle, top end beam, bottom end beam and side of the wythe, respectively. the peak load achieved is 563.75 kN. This is less than the control specimen WP 1, which may be due to the thickness of the polyester biaxial geogrid added as an additional reiforcenent leading to the bond failure of one of the wythes.	Figure 4.30
4	WP 4	This specimen has behaved as the weakest among all the specimen made from mix M1. First bend is achieved at 125 kN. A bend is achieved at 250 kN and 350 kN and the corresponding deformation is 3 mm and 4 mm. the peak load (515.30 kN) achieved is lowest among all the specimens.	Figure 4.31
5	WP I	Stiffness initially achieved is very low. This may be due to the weak strength of the mix M2. There are many micro cracks generated over the panel. Failure at top end beam is observed. The peak load achieved is about 596.19 kN. Steep drop down of curve is also observed.	Figure 4.28
6	WP II	Initial stiffness is the highest among all the specimen. Which can be clearly seen from the curve. There are many kinks in the curve which signifies that shear connectors are losing the strength. Once the specimen reaches the peak load of the control specimen, deformation increases keeping the load constant. Then again rising to achieve a peak load of 747.45 kN	Figure 4.29

7	WP III	Initial curve stiffness matches with stiffness of control specimen. Many kinks are also observed referring to the various crack generation in between the panel. Further due to increase in load gradually the spalling of concrete is observed at the bottom end beam of the CSP panel. Deformation has been enhanced but the failure is almost similar to control in the post elastic nature	Figure 4.30
8	WP IV	This specimen performed the weakest and exhibited multiple crack failure at both the end beams joint as well bond failure, which could be seen from the side of the panel.	Figure 4.31

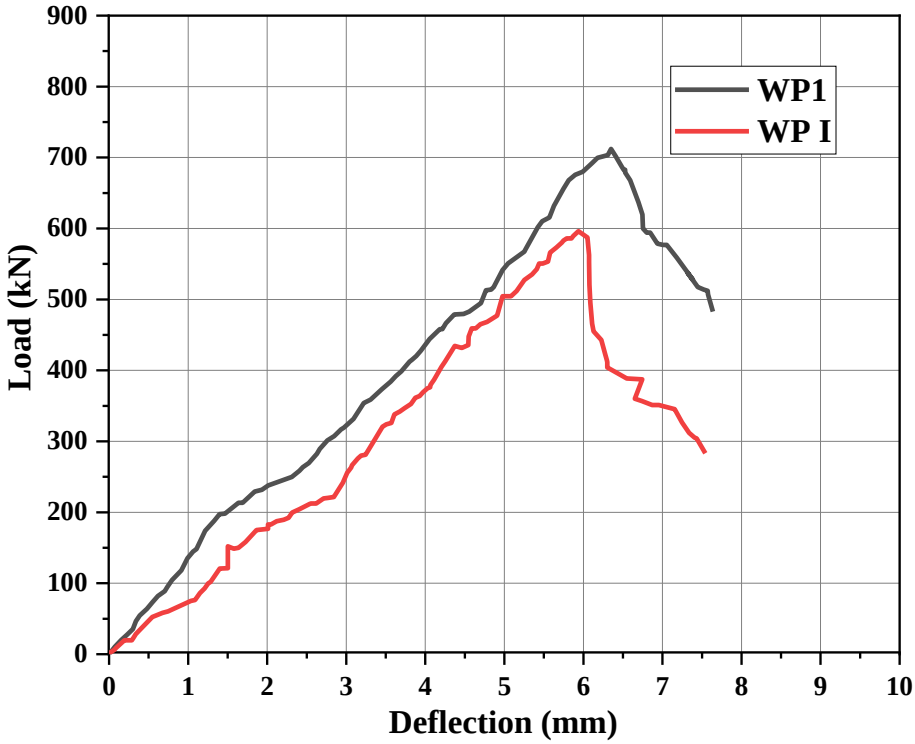

Figure 4. 28: Comparison of both control specimen of mix M1 and M2

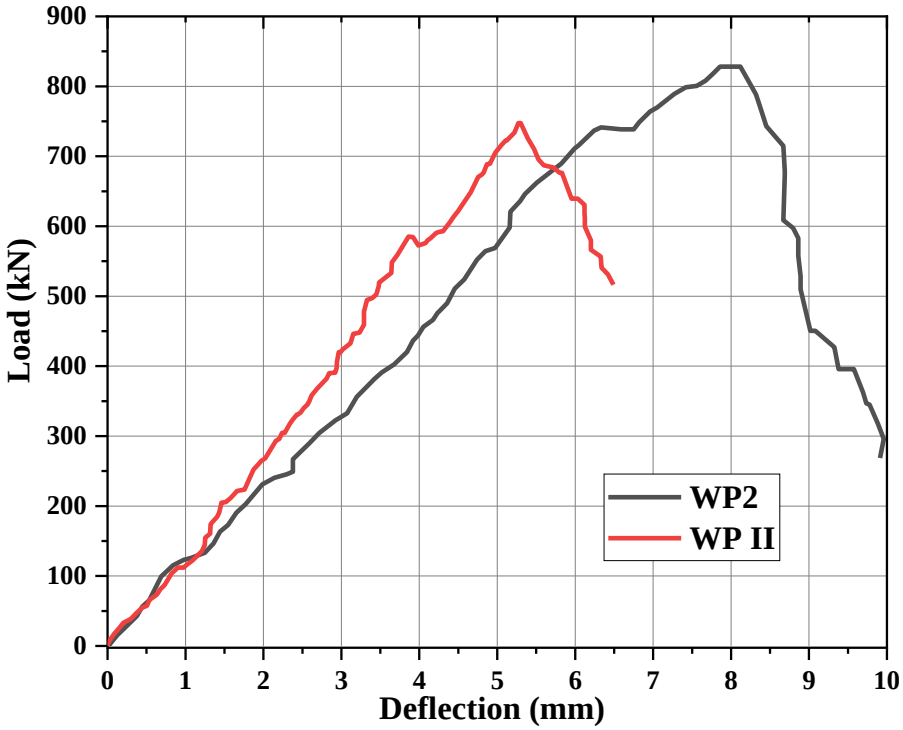

Figure 4. 29: Comparison of both specimen containing PUG

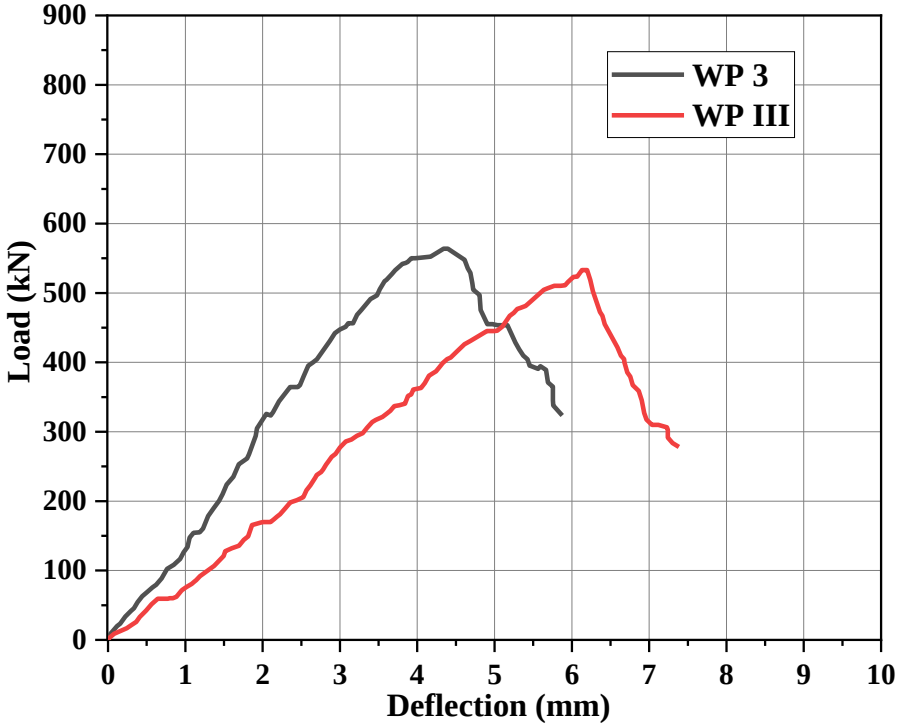

Figure 4. 30: Comparison of both specimen containing PBG (Sgi200)

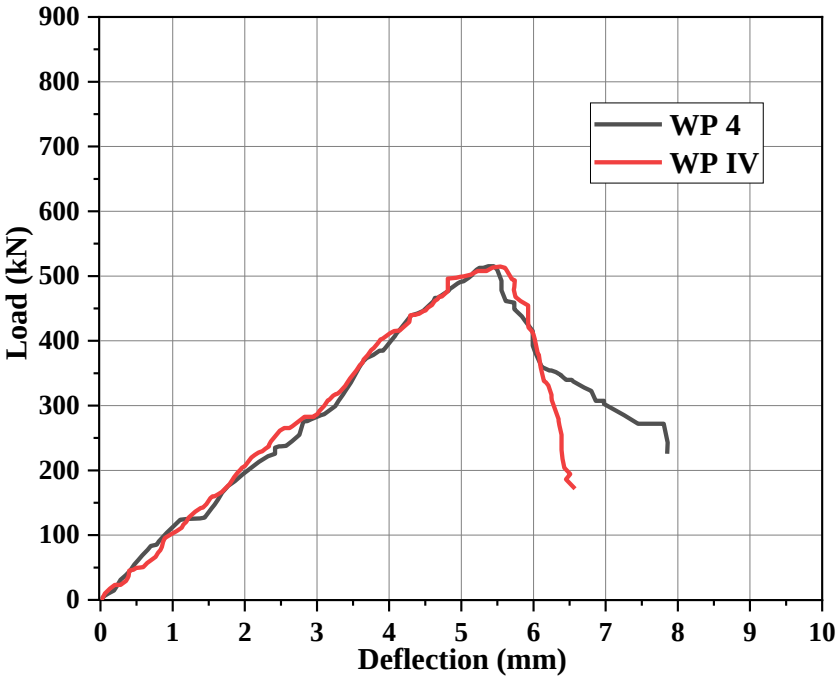

Figure 4. 31: Comparison of both specimen containing polyester biaxial geogrid (Sgi200)

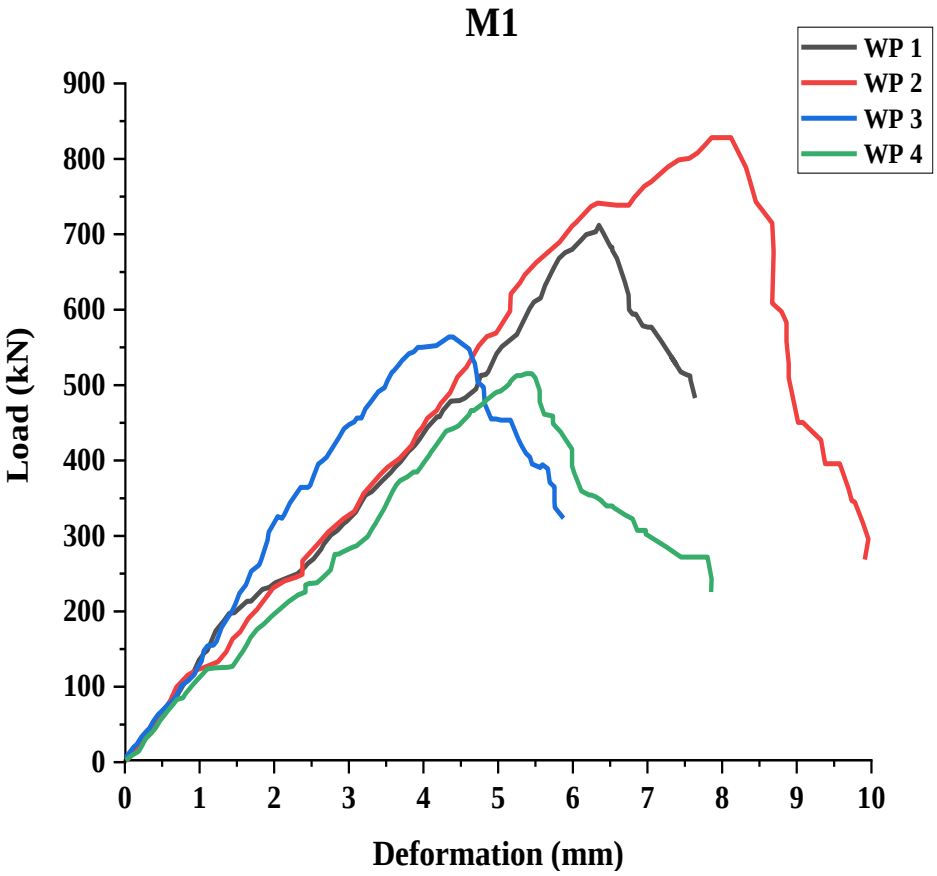

Figure 4. 32: Axial compresssion graph of all M1 specimens

Through a comparative analysis of mix M1 specimens, it has been observed that specimen WP 2 demonstrates a notable increase in strength, with a recorded improvement of 16.42% (Figure 4.32). The decrease in strength observed in the specimen containing PBG2 and PBG3 may be attributed to insufficient bonding between the layers of the same wythe. In the comparison of specimens within mix M2, it was observed that the load bearing capacity of specimen WP II exhibited a significant increase of 25.37% when compared to specimen WP I. In contrast, the compression load experienced a significant decrease in specimens WP III and WP IV. This reduction can be attributed to the bonding of the layer within the same wythe, where each layer had a thickness of 20 mm, resulting in a total wythe thickness of 40 mm. Additionally, the width of the strip also played a role in reducing the compression load. The present study conducted a comparative analysis between M1 mix (WP1) and M2 mix (WPI) to investigate their load bearing capacities. The findings of this research indicate a significant increase of 19.25% in the load bearing capacity of the M1 mix when compared to the M2 mix (Refer Figure 4.33). The PUG specimens have shown an additional increase of 10.78%, while the PBG2 specimens have exhibited an increase of 5.77%.

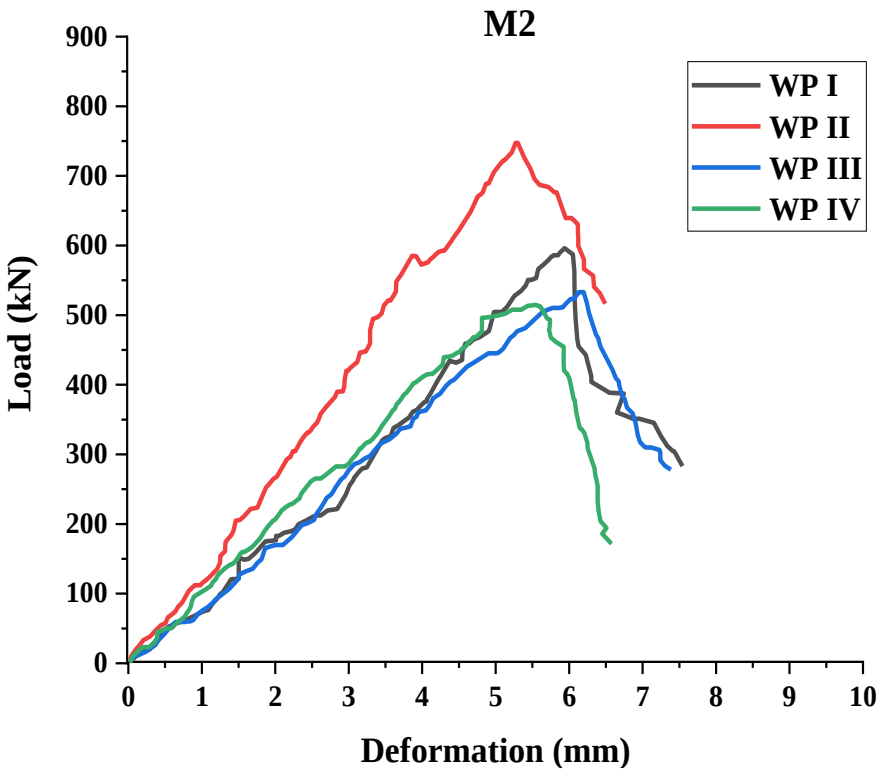

Figure 4. 33: Load vs Deformation for mix M1 and M2

4.4.2 Mode of Failure

Both the specimens, WP1 and WPI, exhibited local concrete crushing at the end beam joint upon application of axial compression force, ultimately leading to failure. The failure of specimen WP1 has been observed at the top capping, and concrete spalling has also been noticed, as illustrated in Figure 4.34(a). Cracks also developed throughout the wythe as can be clearly seen in Figure 4.34 (b). Crack widened as the load increased (Figure 4.34 (c)). The specimen WP I experienced longitudinal cracks and after achieving the peak load, spalling of concrete has also been observed (Figure 4.35). The two specimens showed composite behaviour, and once the maximum stress has been reached, vertical cracks appeared on the wythe. Axial compression failure and local concrete crushing has been observed in the WP 2 specimen. At a load of 250 kN, the initial crack appeared and subsequently extended vertically from the uppermost section to the lowermost section within the rear wythe. The crack promulgated almost in the middle. The cracks on both wythes at the centre of the panel indicate the specimen's composite character. Similar behaviour has been observed in specimen WP II under axial compression testing.

As shown in Figure 4.36, the crack in the specimen WP 3 began in the front wythe and close to the support, whereas in the opposite wythe, crack propagation was seen from the top to the bottom. The failure of WP3 specimen occurred at a lower load magnitude compared to the control specimen, WP1. The load value immediately decreases after reaching the peak load. The interlocking mechanism between PBG2 and the wythe may be responsible for the observed abnormalities. The inadequate bonding between the two layers of the same wythe is attributed to the width of the strip in PBG2, depicting the division of layers within the wythe. Synergistic effect of the wythe layers and weak bond establishment with concrete lead to lower peak load value.

An axial compression in-plane failure has been observed in WP III. The specimen WP III has exhibited similar behaviour to specimen WP 3. The only different feature of this specimen is the M2 mixture used in its casting, which has a lower compressive strength than the M1 mixture. Longitudinal cracks have been observed in the front wythe of the WP4 specimen and no crack on the back wythe has been observed. The top end beam of the WP IV specimen has undergone forced intrusion into the panel, as depicted in Figure 4.38. The welded wire mesh encountered buckling which can be seen in the Figure 4.13. The potential cause of the failure of the top support could be attributed to the PBG3 bond with the concrete and the bond between

the two layers of the same wythe. Concrete spalling has also been observed at the top support located at the back.

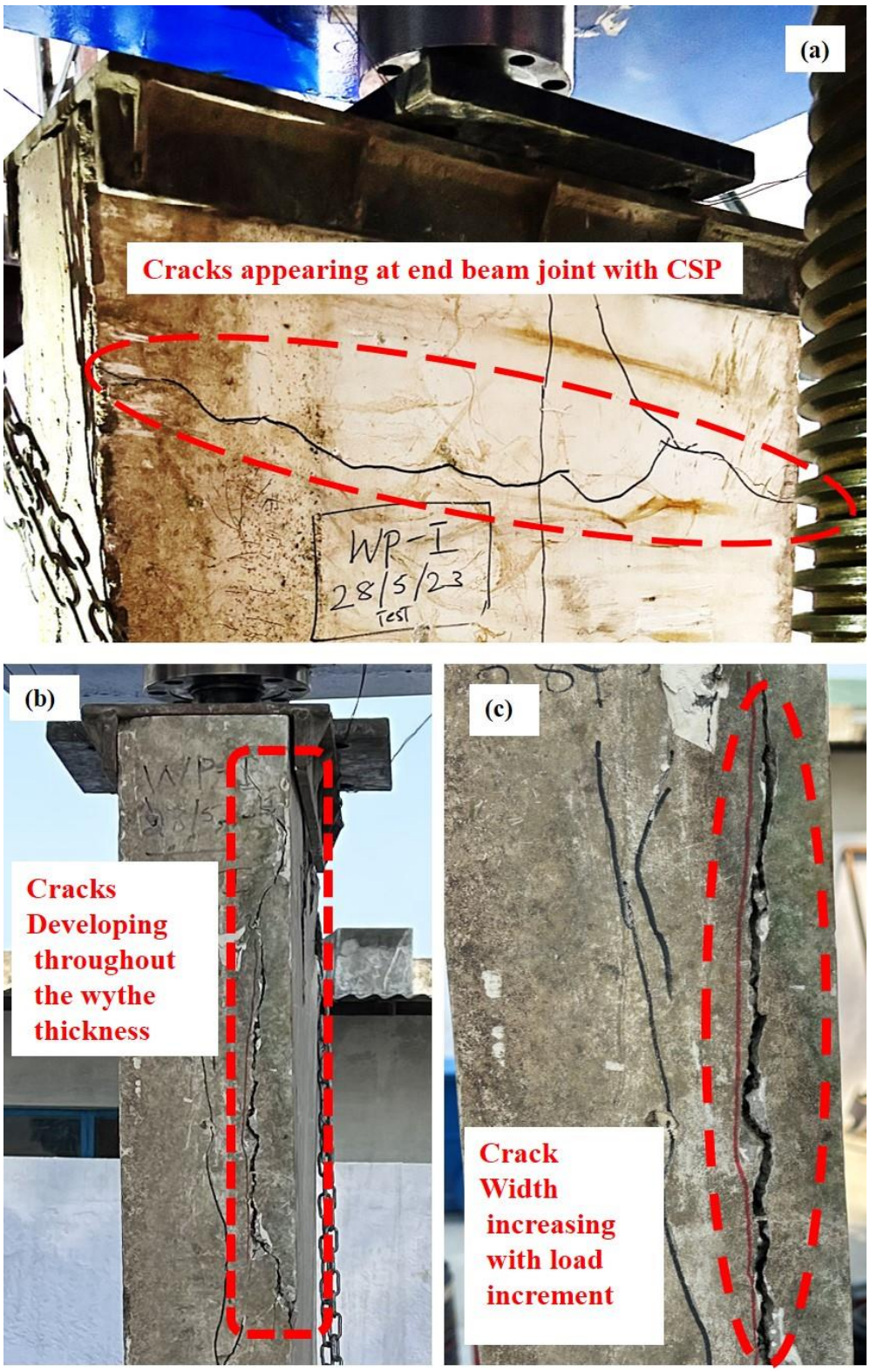

Figure 4. 34: Failure of WP1 (a) WP 1 specimen showing the cracks at the joint of top end beam with the concrete sandwich panel; (b) side profile of the specimen WP 1; (c) expansion of crack in post elastic region.

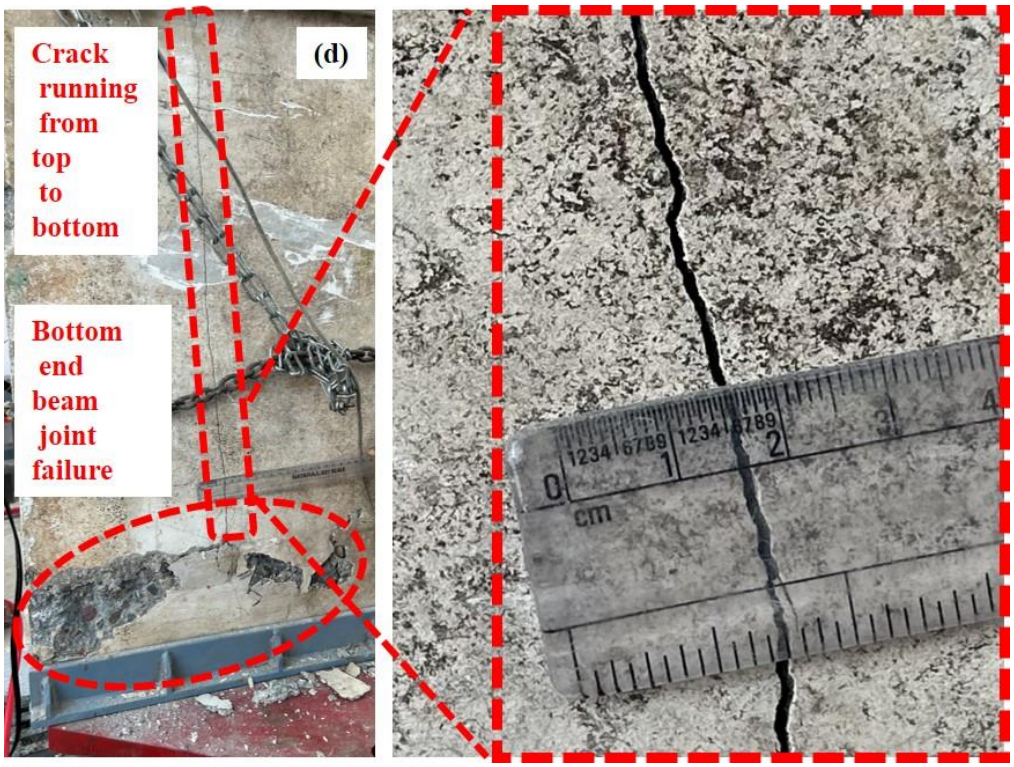

Figure 4. 35: WP I specimen showing the spalling of concrete at the bottom end beam and panel joint, and the magnified view of the longitudinal crack propagating in the middle of wythe.

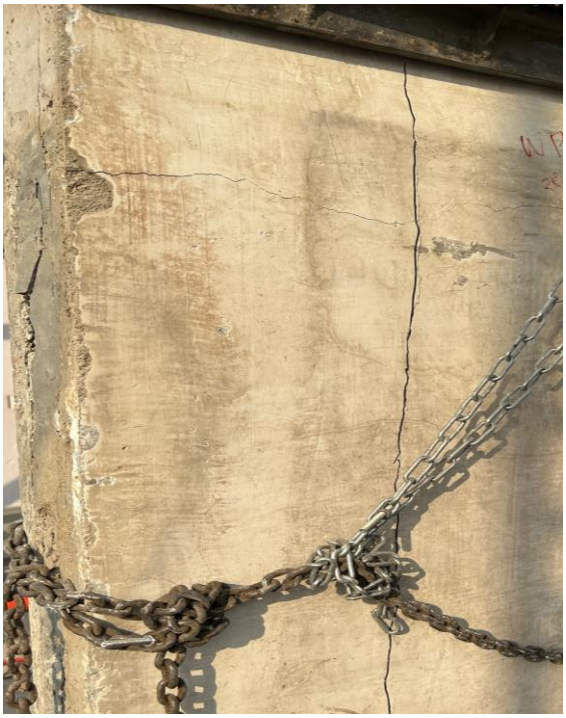

Figure 4. 36: Crack propagation in WP3 specimen under axial compression

Based on experimental observation, PBG could not increase load-bearing capacity because of the poor bonding between the two layers of concrete. Due to the more width of the PBG strip, it lead to partial bonding between the layers of a wythe. Hence leading to partial debonding of the layer while achieving the peak load. It is recommended to utilise polyester biaxial geogrids (PBG) with narrower strip widths or increased spacing between strips to enhance the interlayer adhesion of the concrete.

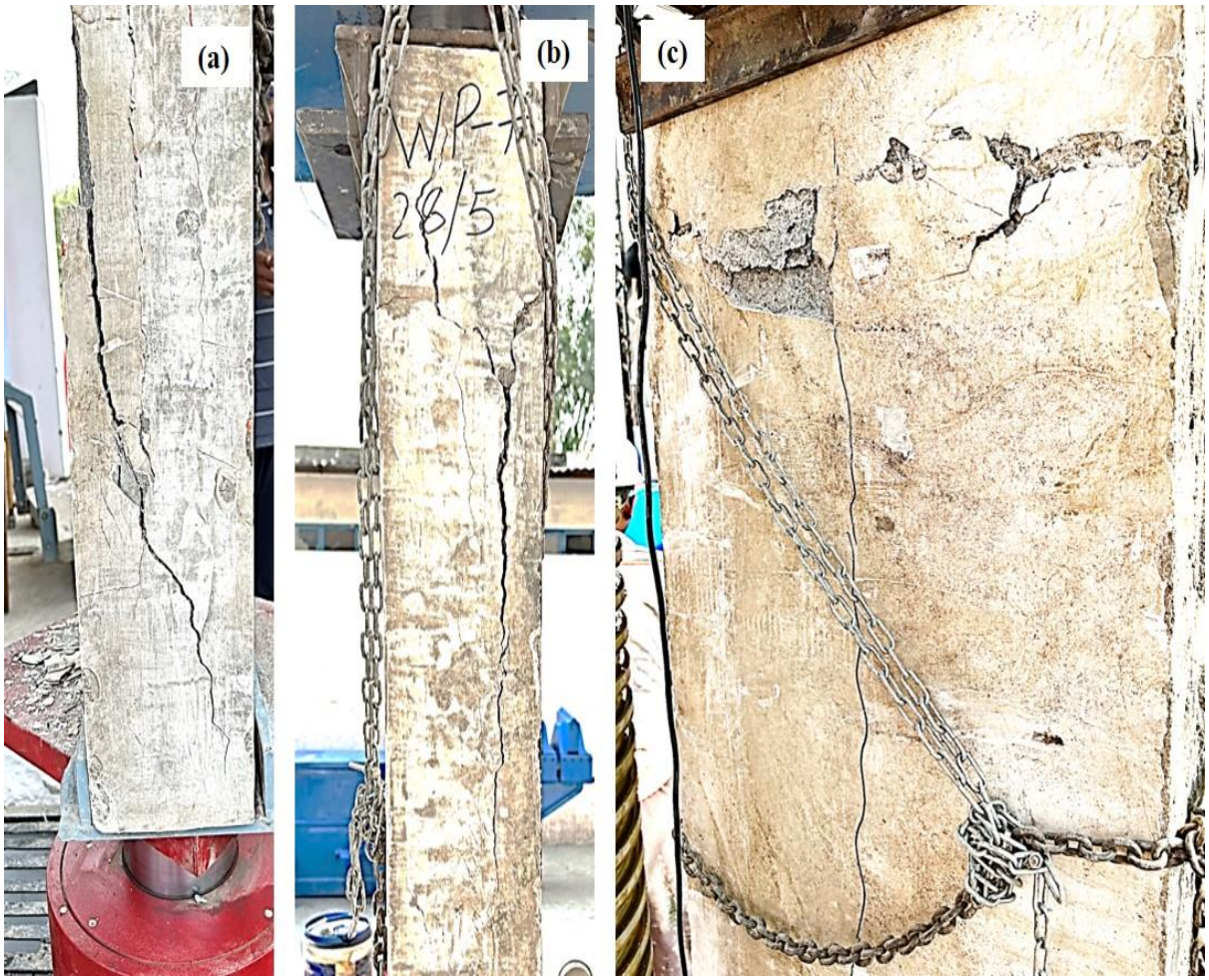

Figure 4. 37: Various wall panel failure (a) WP 2 specimen cracks are generated in front wythe and propagating to the back wythe; (b) WP II specimen showing the debonding of the wythe from the core after peak load is achieved; (c) WP 3 specimen cracks developing from middle top to bottom.

PUG is a stiff plastic material having thin strips (diameter = 4mm-5mm). While casting the wythe, the binding between the two layers of the same wythe is consistent, and the layers of the wythe act as one composite. The addition of plastic uniaxial geogrid (WP2 and WPII specimens) has enhanced the performance of concrete sandwich panels (Refer Figure 4.37).

Debonding failure has not been observed in the case of PUG and PBG2 specimens. PBG3 specimens achieved the peak load during the partial debonding. The horizontal crack width also signifies the behaviour of the geogrids incorporated in the concrete sandwich panel (Shelton et al., 2021).

4.4.3 Energy dissipation

The results in Table 4.8 demonstrate that adding geogrids as an extra reinforcement significantly improved the CSPs' load-bearing capacity, energy dissipation, ductility, and deflection ductility index. In contrast to the control specimen, the results reveal a gain of around 16.42 % in PUG (WP 2). This could be because grid confinement and welded wire mesh have a synergistic effect. Due to the partial debonding within the wythe, PBG3 (WP IV) has shown 15.95 % lower strength than the WP I.

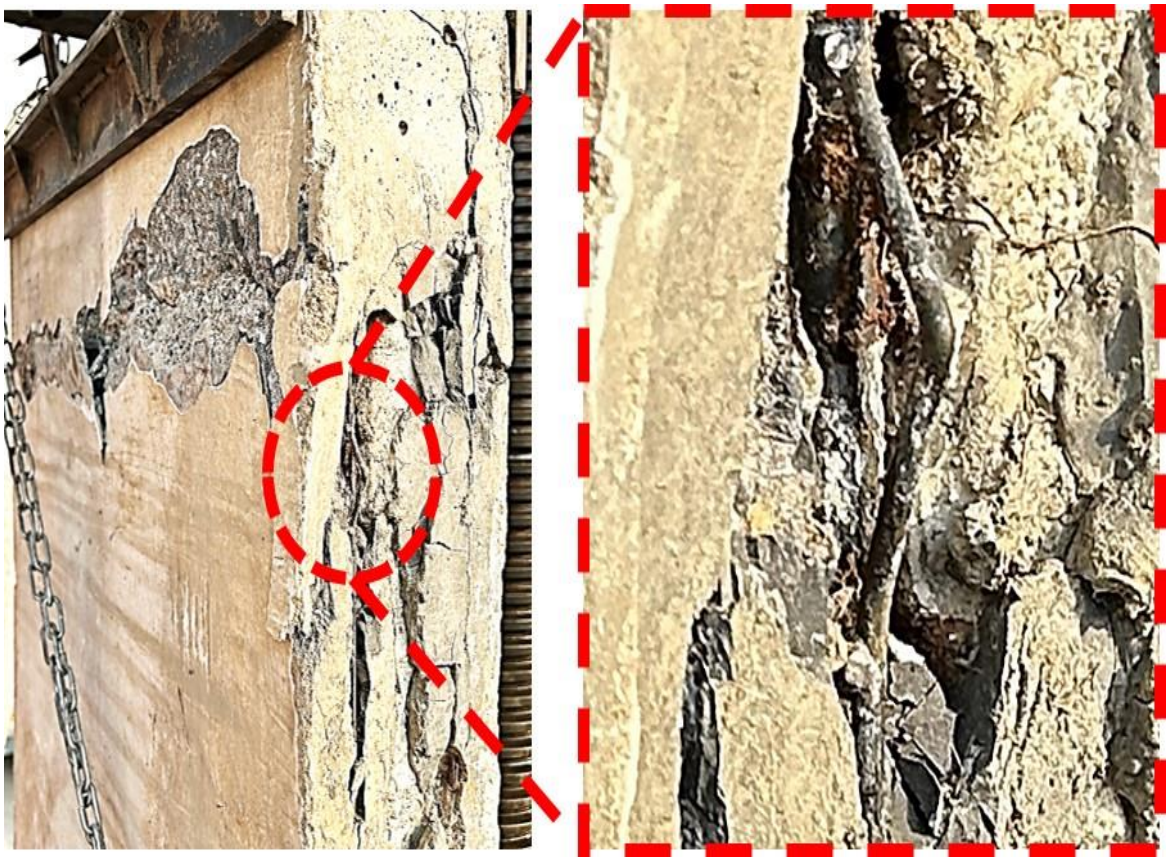

Figure 4. 38: WP 4 specimen experienced local crushing failure and bending of welded wire mesh can also be seen in the magnified figure.

The ductility of sandwich panels is one of the most essential variables for determining efficiency. The affinity of the panels to distort after they have yielded or dissipated energy is referred to as ductility. The capacity of a structure to tolerate substantial deformation in an inelastic condition is known as ductility (Spadea et al., 1998). The deflection ductility factor

(μΔ) is determined in this study; the ratio of ultimate deformation (Δu) to yield deformation (Δy). The energy absorption ductility (μE), is defined as the ratio of area under the curve of load-deformation up to the ultimate load (Eu) divided by the yield load (Ey) (Bastin & Sharma, 2017).

Energy dissipation capacity mentioned in Table 4.8, the deformation capacity has been calculated by computing the region under the load-deformation graph. More energy absorption implies more post-elastic deformation before the collapse, implying that CSP with greater energy dissipation capacity is undoubtedly ductile (Bastin & Sharma, 2017).

The energy dissipation of WP 2 is the highest among all the specimens, whereas WP3 has shown lowest energy dissipation value. This may be due to the debonding of the layer of wythe on one side.

4.4.4 Effect of mixes

The compressive strength results of mix M1 are superior to those of mix M2. The impact of these combinations can be readily recognised on the strength of the specimen. The load deformation curve of all the specimens indicates that the M1 mix specimen fared better than the M2 mix specimen.

4.4.5 Effect of geogrids

The inclusion of geogrids as supplementary reinforcement aims to augment the ductility of the concrete sandwich panel. It has been found from the load versus deformation curves that the specimen containing the geogrids exhibited greater deformation compared to the control specimen of either mix.

Additionally, the plastic uniaxial geogrid increased the strength significantly, while the polyester geogrid improved the ability to deform.

Closing Remark

The clear motive behind the testing of the concrete sandwich panels under different loading conditions is to enhance the strength and deformation capability. This has been achieved by the addition of geogrids to the concrete sandwich panel resulting in enhanced deformation capacity. This is also evident from the load versus deformation curves. Ductility has also been enhanced of concrete sandwich panel. The effect of mixes has also been studied and it has been observed that mix M1 is having high compressive strength which played a major role in the strength of the panel.

Table 4. 8: Strength and energy dissipation values of axial compression specimen

Panel Designation	**Yield load P_y (kN)**	**Ultimate load P_u (kN)**	**Deflection Δy (mm)**	**Δu (mm)**	**Deflection ductility factor $\mu\Delta = \Delta u/\Delta y$**	**Energy E_y (kN.mm)**	**E_u (kN.mm)**	**Energy ductility factor $\mu_E = E_u/E_y$**	**Energy dissipation (kN.mm)**	**Failure mode**
M1 (1:3)										
WP 1	482.88	711.23	4.55	6.34	1.41	1168.42	2248.82	1.92	2248.82	A
WP 2	635.89	828.08	5.30	7.85	1.48	1590.39	3490.44	2.19	3490.44	C
WP 3	491.17	563.75	3.39	4.39	1.29	846.32	1384.86	1.63	1384.86	C & D
WP 4	439.56	515.30	4.30	5.45	1.26	906.18	1462.65	1.61	1462.65	A
M2 (1:2:3)										
WP I	504.51	596.19	5.08	5.93	1.16	1175.02	1648.33	1.40	1648.33	A
WP II	519.40	747.45	3.48	5.30	1.52	818.28	1954.46	2.38	1954.46	B
WP III	399.04	532.95	4.32	6.19	1.43	818.51	1695.42	2.07	1695.42	B
WP IV	318.55	514.50	3.28	5.54	1.68	543.11	1530.82	2.81	1530.82	A

A: local crushing failure; B: axial compression failure; C: combined failure; D: Partial debonding of the layer

Chapter 5

Infill wall behaviour of concrete sandwich panels vs. brick masonry in a two-dimensional reinforced frame.

5.1 General

In the previous section, extensive testing has been conducted on the concrete sandwich panels to evaluate their performance under various loading conditions. The test results indicate that the panels have a higher load bearing capacity and improved ductility. This chapter focuses on the performance of concrete sandwich panels as infill walls in 2D RC frames under cyclic loading. An experimental assessment has been conducted to evaluate the effectiveness of the concrete sandwich panel as a potential substitute for brick masonry. A comparison is conducted between concrete sandwich panels and brick masonry as infill walls. In addition, we have conducted tests on a CSP frame with a door opening to evaluate its performance under cyclic loading. This section showcases the results of the in-plane cyclic tests. These results are thoroughly analysed by evaluating various performance indicators that describe the seismic behaviour of the structures. These indicators include: (i) the curves that show the relationship between the applied load and displacement during the cyclic tests, (ii) the modes in which the structures fail, (iii) the reduction in strength over time, (iv) the decrease in secant stiffness over time, (v) the measure of displacement ductility, and (vi) the capacity of the reinforced concrete frames to dissipate energy. Three frames were tested: Specimen "C" - a 2D RC frame with a concrete sandwich panel as an infill wall, Specimen "O" - a 2D RC frame with a concrete sandwich panel that includes a door opening, and Specimen "B" - a 2D RC frame with brick masonry as an infill wall.

5.2 Behaviour of brick masonry as infill wall (Specimen “B”)

The RC frame has been observed under quasi-static loading (Figure 5.1). The load displacement hysteresis curve (Refer Figure 5.2) explains the different parameters of the initial phase of loading. As this test has been performed in a displacement controlled environment, so the readings at every cycle has been noted. A total of 20 cycles per specimen has been

performed. The cyclic loading in this experiment employed a push-pull mechanism driven by an actuator. Each cycle comprised two distinct phases:

1. Forward motion (push): The actuator extended, applying a compressive force to the frame, pushing it away from its initial position (marked by the yellow line).
2. Backward motion (pull): The actuator retracted, applying a tensile force to the frame, pulling it back towards its initial resting position.

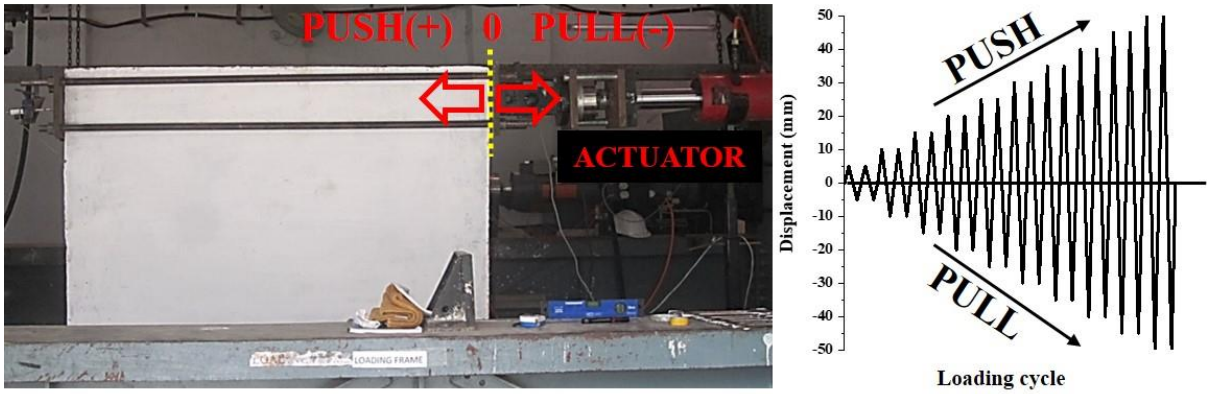

Figure 5. 1: Illustration of experiment with loading cycle

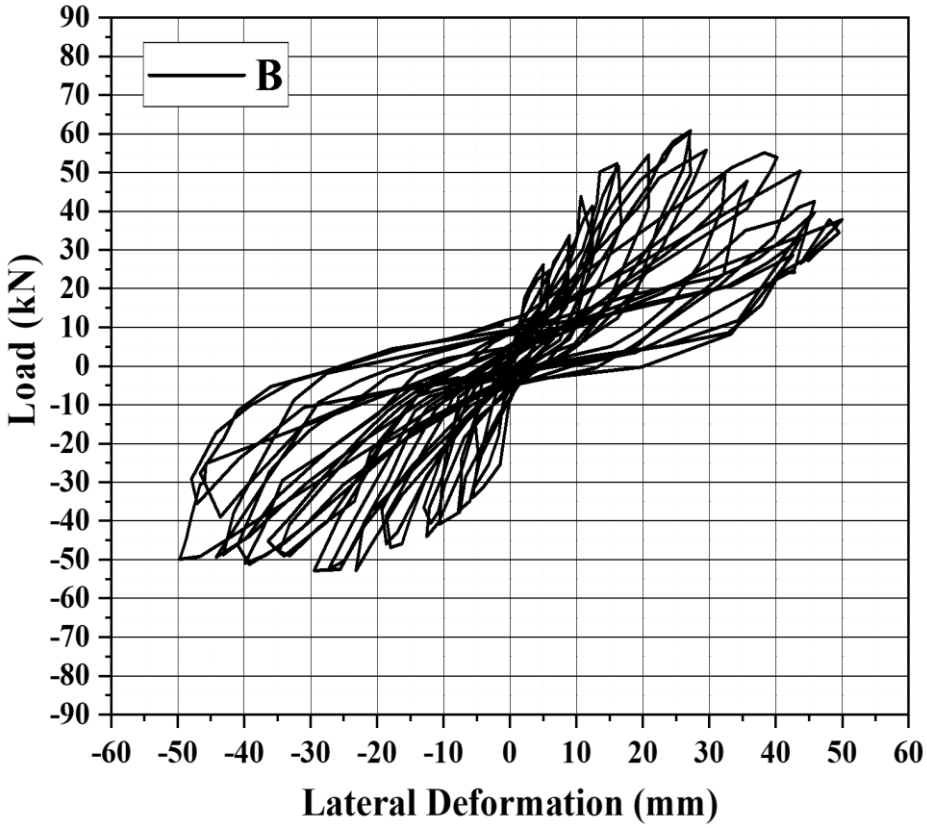

Figure 5. 2: Hysteresis curve of brick masonry infill wall in 2D RC frame (Specimen “B”)

During the first loading cycle, a controlled displacement of 5 mm (push) resulted in a load of 25 kN. Further upon reversing the direction for the subsequent cycle, the load at the same 5 mm displacement increased to 27.5 kN, indicating potential hysteresis (energy dissipation) in the frame. The experiment continued with another 5 mm push in the forward direction, reaching a load of 26.5 kN. Notably, during the following pull, the load at the same 5 mm displacement jumped to 35 kN, further suggesting the presence of hysteresis and potentially non-linear behaviour.

No crack is observed in the specimen in the first two cycles (5 mm each). In the third cycle the displacement is now increased to 10 mm from the initial starting point of zero displacement (as actuator ensured the displacement to be of exact measurement). Load values reached up to 35 kN in push cycle i.e. pushing the frame away from the loading point. While pulling back, the load achieved is 39 kN. As the deformation has been increasing with each cycle cracks are now starting to generate at the joints of mortar layer with brick. At higher cycles of displacement the cracks start to generate at the diagonally opposite corner of the loading. This diagonal cracking generating at the lower opposite corner while pushing and similar diagonal cracks are also observed while pulling back but this time its at the upper corner of the RC frame. The peak load achieved by the brick masonry is 61 kN. As the number of cycles exceed the value of 30 mm displacement the cracks in the beam column joint are also observed. Damage index is calculated so as to understand the limit of the cycles to be given for the RC frame.

5.3 Behaviour of concrete sandwich panel as infill wall (Specimen “C”)

In the quasi-static loading analysis of the RC frame (Figure 5.3), the load-displacement hysteresis curve provided valuable insights into various parameters during the initial loading phase. Conducted in a displacement-controlled setting with a meticulous recording of readings at each cycle. In the initial cycle, a 30 kN load has been achieved during the 5 mm push, while the load reached 36 kN during the pull. Subsequent cycles involved a forward displacement of 5 mm with a load of 31.5 kN in the push and 37 kN in the pull. Remarkably, no cracks were observed in the specimen during the first two cycles. Advancing to the second cycle with a 10 mm displacement, load values peaked at 47 kN during the push and 45 kN during the pull. Concurrently, as displacement increased with each cycle, the concrete sandwich panel have the welded wire mesh which added to the strength of the panel and also the dowel bars attached to the panel through the plinth beam gave the extra strength and the frame may have behaved more compositely when compared with brick masonry infill wall frame. Notably, at higher

cycles, no diagonal cracks manifested at diagonally opposite corners during both push and pull sequences. Specifically, only hair line cracks appeared at the edges where the concrete sandwich panel is attached to the column. The result of this analysis revealed a peak load of 83.5 kN (drift ratio of 1.59) sustained by the concrete sandwich panel as infill wall. Beyond 30 mm displacement cycles, micro cracks appeared all over the boundaries. In the extreme displacement cycles i.e. the 50 mm push and pull cycle underwent a flexural failure in the column near to the loading point. To quantify structural damage, a damage index has been calculated, shedding light on the cycle limits applicable to the RC frame.

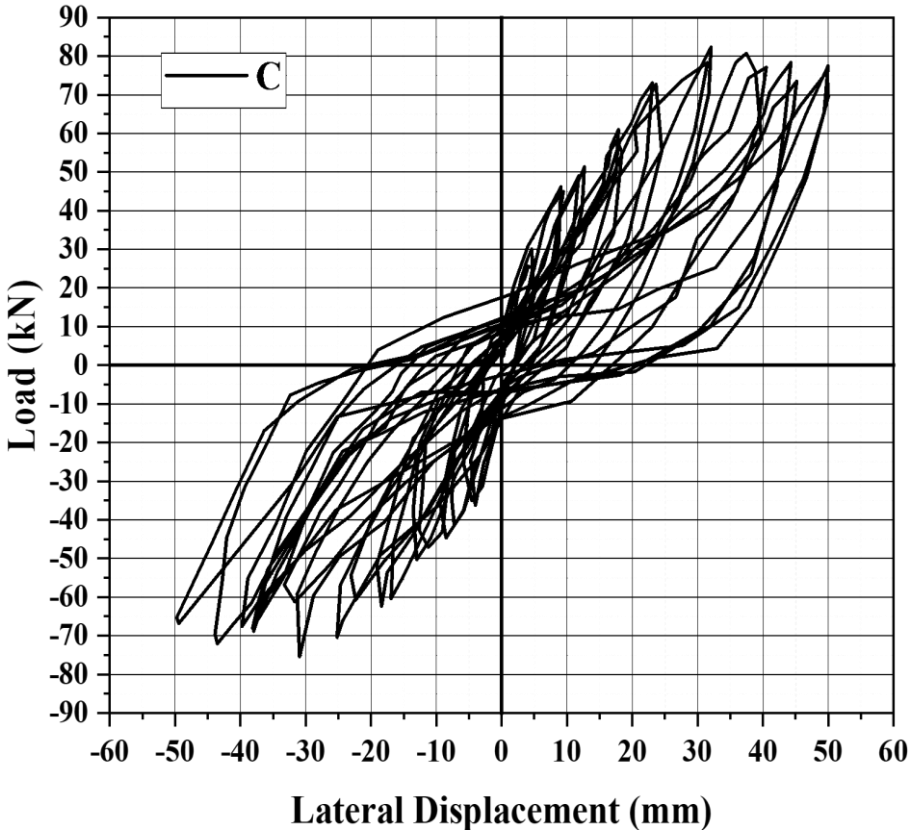

Figure 5. 3: Hysteresis curve of concrete sandwich panel in 2D RC frame (Specimen “C”)

5.4 Behaviour of CSP with a door opening as infill wall (Specimen “O”)

The quasi-static loading (Mugahed Amran et al., 2018)analysis of the RC frame involved meticulous recording of load-displacement hysteresis curves (Figure 5.4), revealing essential parameters. With a minimum of 10 cycles per specimen, initial cycles showed load achievements of 23 kN during a 5 mm push and 27 kN during pull. Notably, no cracks were observed in the first two cycles. Subsequent cycles exhibited increasing deformation, generating cracks at the corners of the door opening. This opening has been placed away from the loading point, so the corners of the door have been most affected due to the horizontal

irregularity. Hence the spalling of concrete as well as big cracks have been encountered as the displacements increased in each consecutive cycles. Peak load reached 70.5 kN at the displacement of 32 mm, accompanied by cracks cycle. Diagonal cracks emerged at opposite corners, transitioning from lower to upper corners in beam-column joints beyond 30 mm displacement cycles.

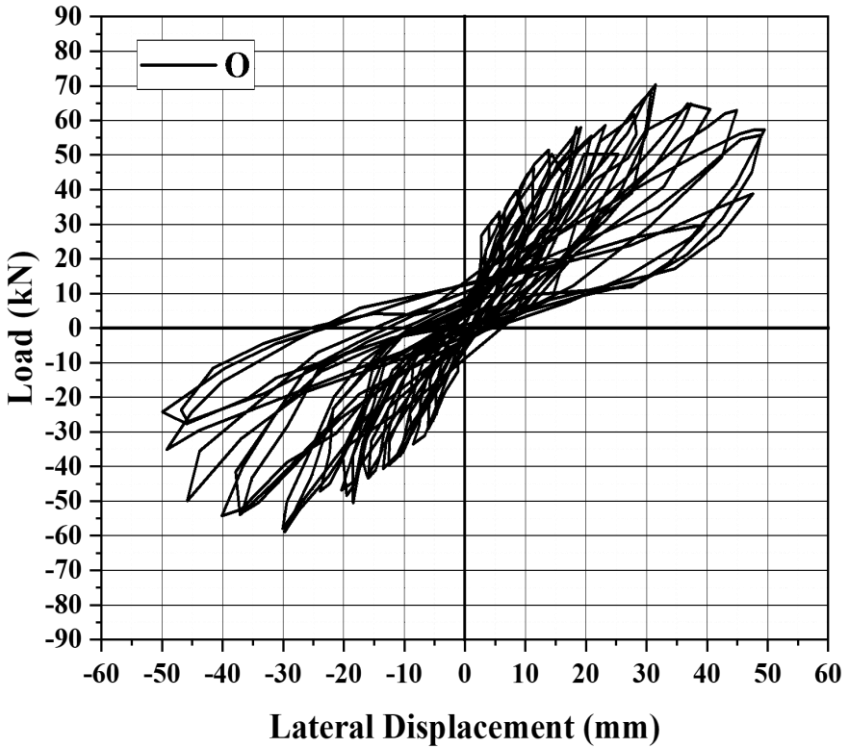

Figure 5. 4: Hysteresis curve of CSP with door opening in 2D RC frame (Specimen "O")

Flexural cracks have also been observed in the column near to the door opening, which explains the horizontal irregularity or the gap due to the door opening (Figure 5.11). As the displacement value surpasses the 40 mm mark spalling of concrete is seen at the bottom of the panel at the point where dowel bar is installed (Figure 5.13). At 50 mm displacement the concrete sandwich panel completely lost its contact with the frame and the failure is reached.

5.5 Push and pull analysis of frames

The hysteresis curves for lateral load versus displacement were obtained for specimens C, O, and B, as shown in Figure 5.3, Figure 5.4, and Figure 5.5, respectively. The directions of the hydraulic actuator can be categorised as either positive, when it applies a pushing force to the specimen, or negative, when it applies a pulling force to the specimen. Table 5.1 displays performance indicators derived from the curves of both push and pull cycles. These indicators include: (i) the maximum in-plane loads achieved during the first and second cycles, denoted

as , f_{max1} and f_{max2} respectively; (ii) the lateral displacement at which the maximum load levels occur, referred to as D_{Fmax} ($D_{Fmax1} \approx D_{Fmax2}$); and (iii) the initial elastic stiffness, k_{el}, which represents the linear-elastic phase of the cyclic behaviours observed (de Sousa et al. (2022).

Table 5. 1: Stiffness of all the three specimens for positive and negative directions

Specimen ID	Direction: positive				Direction: negative			
	k_{el} (kN/mm)	f_{max1} (kN)	f_{max2} (kN)	D_{Fmax} (mm)	k_{el} (kN/mm)	F_{max1} (kN)	F_{max2} (kN)	D_{Fmax} (mm)
C	3328	83.2	78	31	3750	-75	-61	-31.1
O	3500	70	68	32.4	3093	-58	-57	-29.5
B	3753	61	55	25	3600	-54	-53	-25

The lateral load-displacement graphs first exhibit linear/elastic behaviour, then become increasingly nonlinear as specimens crack and deteriorates. The brick infill wall and concrete sandwich panel give a substantial boost in rigidity and load bearing capability of the 2D frame. Similar observation were noted by de Sousa et al. (2022). Specimen B exhibited the highest elastic stiffness, so validating the significance of masonry infill walls in influencing the lateral performance of reinforced concrete frame structures, as corroborated by previous research (Akhoundi et al., 2018; Dautaj et al., 2018; Milheiro et al., 2016). Specimen B exhibited the highest lateral strength until about a 0.4% increase (5.1 mm) and a 0.8% decrease (-10.1 mm) in drift. The improved connection between the masonry wall and the reinforced concrete (RC) components supports these findings, particularly until the point where cracking begins in the masonry wall at a drift of 0.2%. Specimen C exhibited superior lateral strength compared to the damage threshold, particularly in the positive loading direction, with a more pronounced strength enhancement of approximately 30% compared to specimen B.

The load-displacement diagrams and data in Table 5.1 demonstrate that all specimens had symmetrical behaviour. The symmetry in the curves mostly arises from the initiation of damage during each cycle, which indicates the unique state of damage for each loading direction. The observed phenomenon is particularly evident in specimen "O", attributed to the presence of an opening in the concrete sandwich panel, leading to increased crack propagation at the corners of the opening.

5.6 Comparison of CSP as infill with brick masonry as infill wall

The specimen “C” having concrete sandwich panel as infill wall is being compared with the conventional material to build walls i.e. brick masonry, specimen “B”. The S-curve is being shown in Figure 5.5. From this curve it can be depicted that specimen “C” having concrete sandwich panel as infill wall has shown more ductile behaviour than its counterpart specimen “B”. The specimen “B” yielded at a deformation value of 26 mm (drift ratio = 2.1 %) whereas the specimen “C” yielded at 32.5 mm (drift ratio = 2.65 %). The test have been halted once the decrease in load is more than 10 %. These results show that the concrete sandwich panel has shown more ductility than its counterpart, Brick masonry.

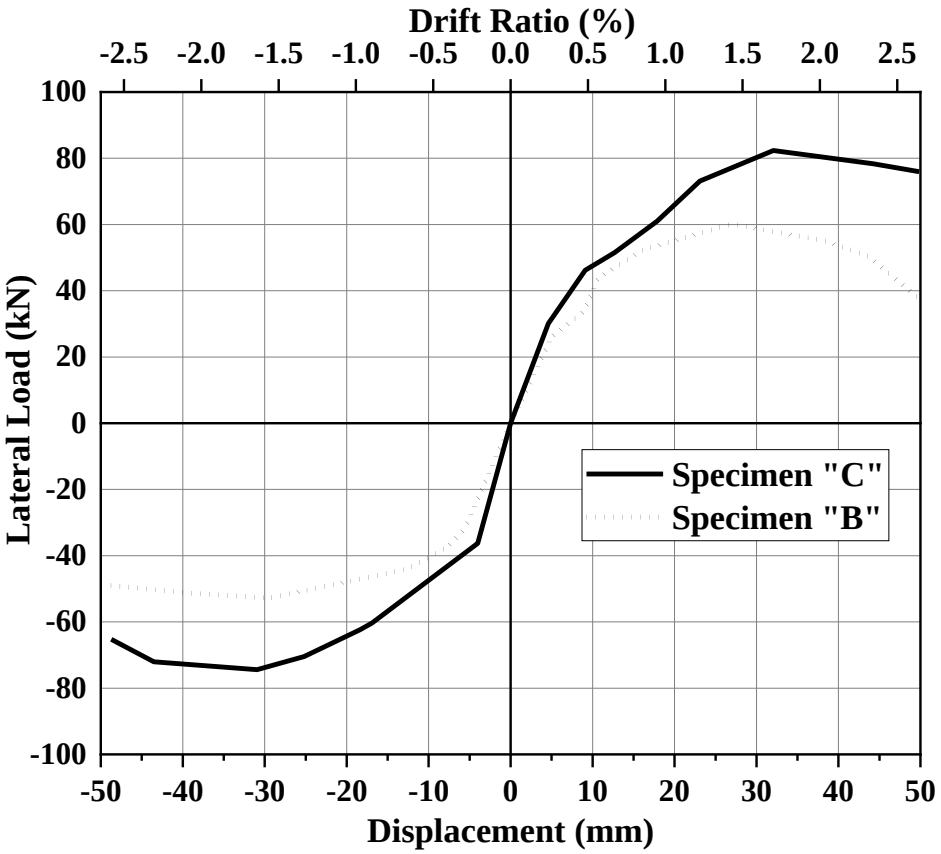

Figure 5. 5: S-curve comparison of 2D RC Frame with CSP as infill wall with brick masonry as infill wall

5.7 Comparison of CSP as infill with CSP with door opening as infill wall

The comparison of a concrete sandwich panel as infill wall with concrete sandwich panel having a door opening has intensified the research. This is due to the horizontal irregularity in the panel i.e. the door (Figure 5.6). Though the specimen “O” achieved the peak

load at 71 kN, with a corresponding deformation is 31.5 mm. The cracks at the corners of the opening clearly hints to the weak areas and the spalling of concrete with major cracks have been observed. Through this finding it can be observed that even if the panel has an horizontal irregularity, specimen “O” behaved stronger than the brick masonry. Flexural cracks on the loaded column hints that the horizontal irregularity has transferred the maximum load on to the RC frame. Major cracks and displacement of concrete sandwich panel with a door opening have also been observed.

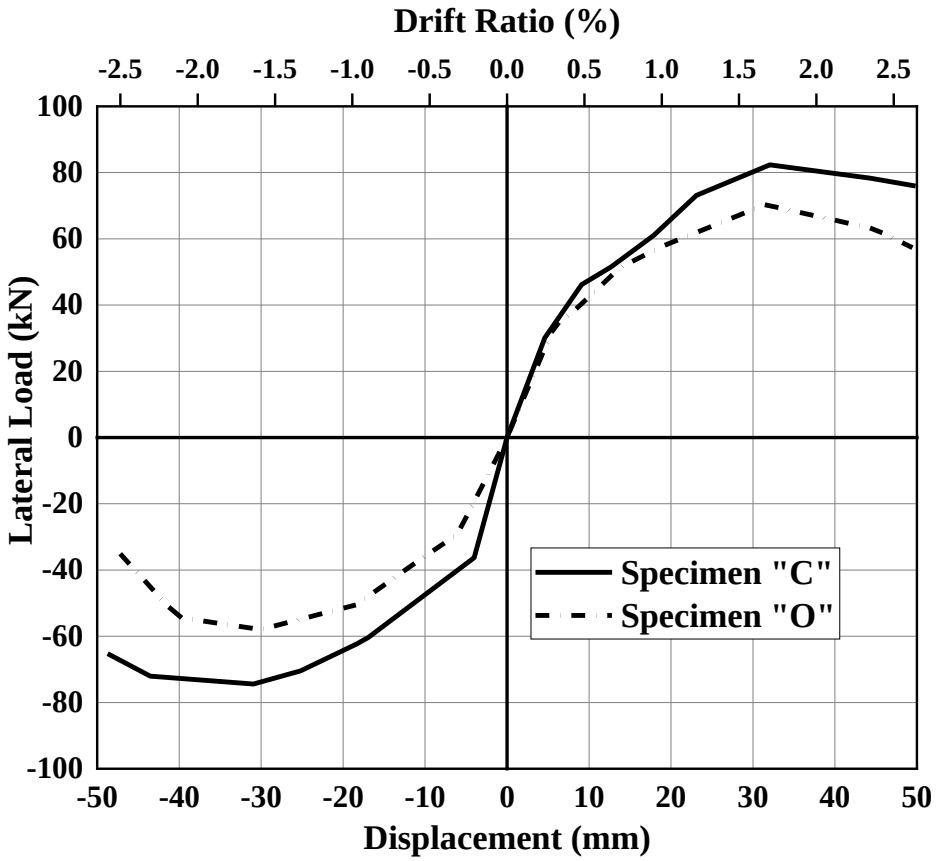

Figure 5. 6: S-curve comparison of 2D RC Frame with CSP as infill wall with concrete sandwich panel with a door opening as an infill wall

5.7 Analysis of the progression of damage and modes of failure

The damage evolution in the specimens is noted for different levels of lateral displacement. Specimen C gave the most rigid behaviour i.e. it showed the maximum stiffness and also the minimum ductility (Table 5.2). In specimen “O” it has been observed that cracks generated at the opening. Further propagation of cracks occurred at the corners of the opening. As the level of drift reached a higher percentage, the debonding of the panel with the 2D frame

has also been encountered at the corners. Moreover, in specimen B cracks occurred at the middle and started at the corner (Figure 5.8 and Figure 5.9). The spalling of mortar in the middle bricks is also observed. The cracks propagate through the mortar layer in between the bricks (Figure 5.10).

The cracking pattern observed in specimen C reveals that all flexural cracks are confined to the columns, with no significant cracks forming in the beams. The damage is most concentrated near the joints, leading to the formation of plastic hinges at both the bottom and top ends of the columns, with the damage being more pronounced at the bottom. The column exhibited flexural failure. The cracking pattern seen in specimen B can be described as follows: (i) Cracking began at approximately 0.4% drift, at the boundary between the reinforced concrete members and the masonry bricks. (ii) Diagonal cracking in the masonry wall started at around 0.2% drift and continued to increase steadily with each cycle (Figure 5.9). (iii) The plaster between the bricks began to delaminate at 0.5% drift, leading to a significant number of diagonal cracks in the wall (Figure 5.10). (iv) Further damage and diagonal cracking occurred in the infill walls when the drift of the reinforced concrete frame reached 1.1%. (v) At 2.1% drift, the cracks extended even closer to the corner (Figure 5.9).

Figure 5. 7: Specimen “C” having a flexural failure in column

Figure 5. 8: Diagonal cracks propagating from top left corner to middle in specimen “B”

Figure 5. 9: Cracks observed at lower end at 2.1% drift in specimen “B”

Finally, specimen O had the following cracking pattern and damage modes: (i) diagonal cracks form at the concrete sandwich panel's bottom corners at 0.2% drift; (ii) crack development in the upper-left corner of the opening (Figure 5.11). In Figure 5.12 it can be seen that cracks are propagating from weakest point in the infill wall i.e. opening, and from its corner, crack propagates to the corner of the RC frame. When the frame reaches the 20th cycle i.e. 2.65% drift, the uplifting of complete sandwich panel can be seen and dowel bar is exposed leading to a complete failure of the infill wall. Though the failure has been reached but the concrete sandwich panel is maintaining its composite nature which can be attributed to the reinforcement present in the panel. Moreover the cracks have been more prominent near the opening because it's away from the loading corner.

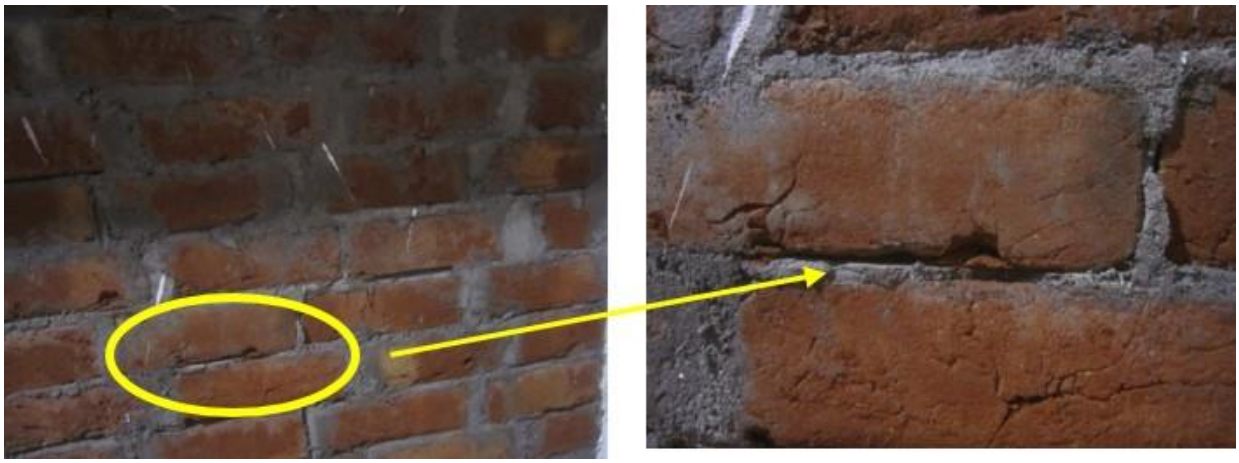

Figure 5. 10: Failure of Specimen "B" (a) Plaster delamination in brick masonry; (b) magnified view of the brick delamination with plaster and cracks developing in brick due to loading.

5.8 Strength degradation

From Figure 5.5 and Figure 5.6 it can be clearly seen that the specimen C showed the maximum strength as compared to conventional brick masonry infill (specimen B). The analysis indicates that the concrete sandwich panel used in specimen C as infill wall has been able to resist the quasi –static loading the most efficiently as there have been no major cracks in the panel and column failed in flexure at 2.65% drift (lateral displacement of 50 mm). Though the strength decreased once it reached its peak load i.e. 83.5 kN. Deterioration of strength increase with increasing drift. However, specimen O on the other hand showed quite phenomenon results and has also been found to be most ductile (Table 5.1). Strength degradation can be seen from the Figure 5.5 and Figure 5.6. With each successive cycle the deterioration increased, as can be seen from Figure 5.12 showing different push and pull cycles

and their respective cracks formed on the specimen. In the case of brick masonry it has been very linear as well as a very sudden decrease in load has been observed after the attainment of peak load. This can be due to the brick failure and their non-composite nature as brick wall is made up of several bricks bonded with mortar, whereas in CSP the welded wire mesh helps it to behave as a single unit. Hence the strength degradation is much more in specimen “B” than in specimen “C” and “O”.

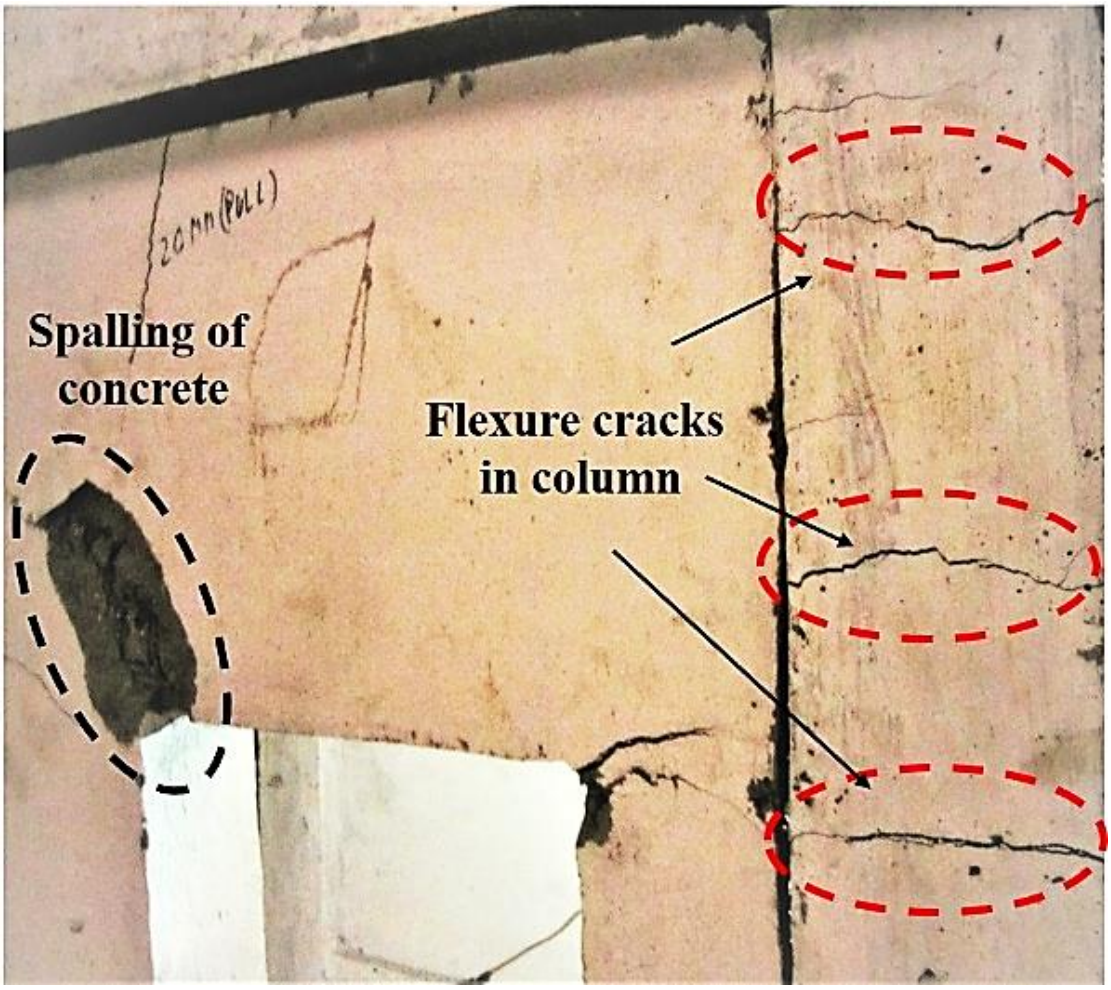

Figure 5. 11: Specimen “O” having developed flexure cracks in column and spalling of concrete at the corners of opening and reinforcement is also exposed.

5.9 Stiffness degradation

The decrease in the lateral secant stiffness, denoted by ks, is shown in Figure 5.14, together with the progression of the lateral drift. The secant stiffness is calculated by the slope of the straight line produced by the two points representing the peak loads for each cycle of the hysteretic responses (Figure 5.14). The observed stiffness degradation evolution indicates a gradual reduction in stiffness with increasing drift for all specimens. Specimen C when

compared with specimen O shows that the it is less stiff than specimen O (Figure 5.15). This is because of the extra reinforcement provided at the opening. As the drift advances specimen C which does not have any irregularity, clearly shows more secant stiffness. At approximately 0.75 % drift (lateral displacement = 7.5 mm) nearly the same secant stiffness as specimen O,

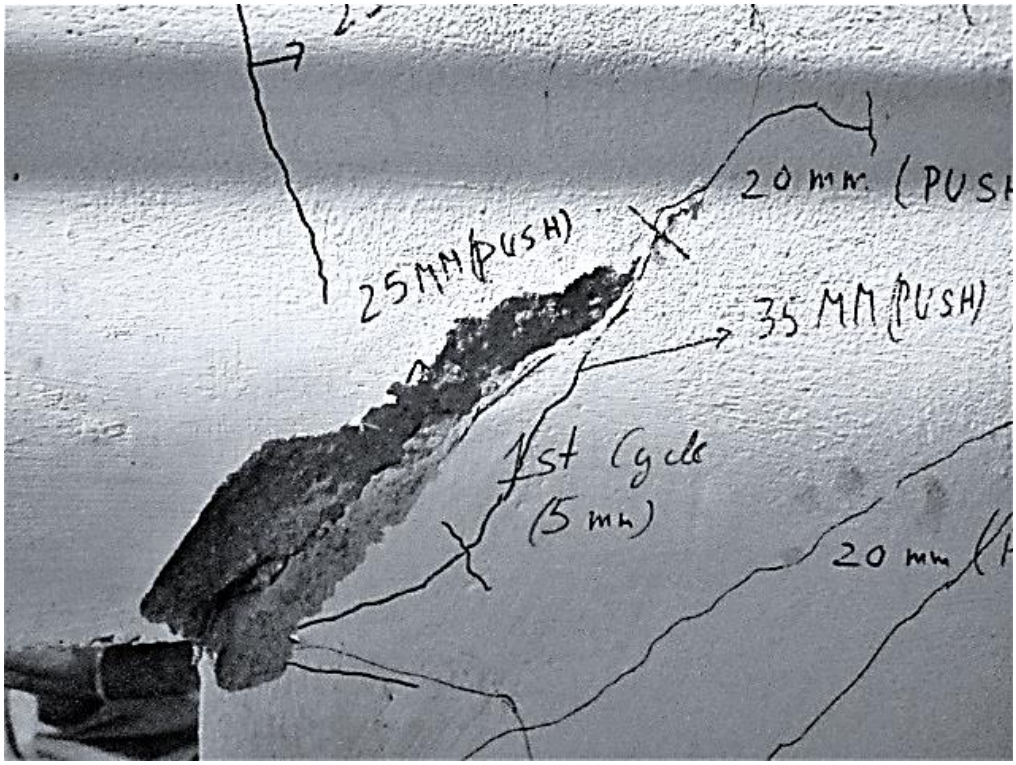

Figure 5. 12: Spread of cracks from opening corner to corner of frame

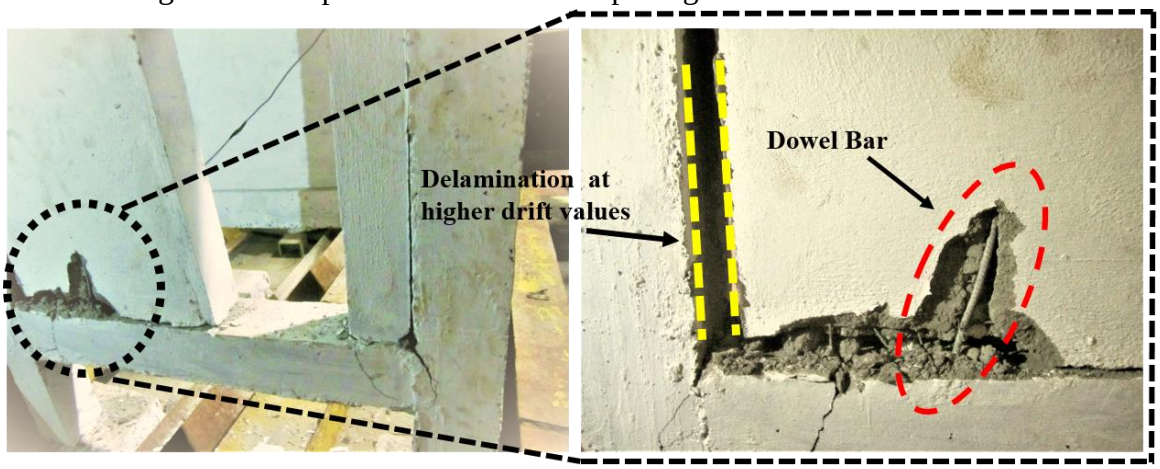

Figure 5. 13: Failure of Specimen "O" showing the delamination at 2.65% drift (50 mm) and the exposed dowel bar and reinforcement exposure with spalling of micro concrete.

the beam and column joint failed as flexure cracks develop both in beam as well as column. About this level of drift the cracks in brick masonry infill has started propagating from the top

corner of loading to the diagonally opposite corner. But due to the spalling of mortar layer, strength further decreased (Figure 5.15).

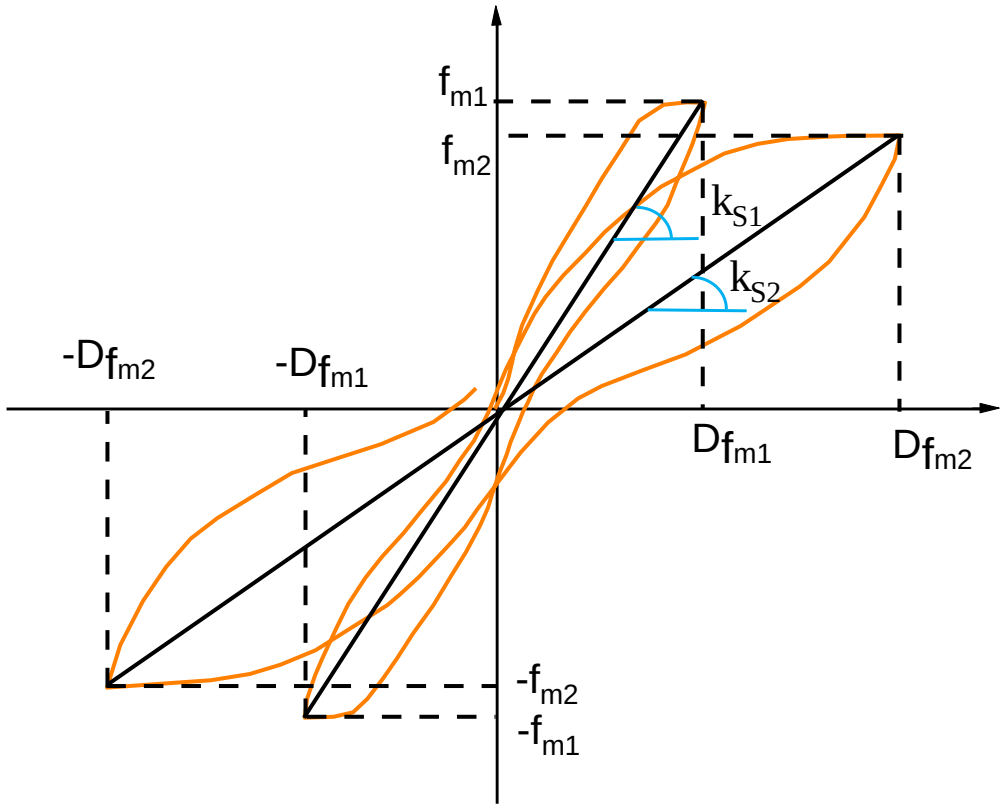

Figure 5. 14: Schematic illustration of stiffness degradation versus lateral drift (de Sousa et al., 2022)

5.10 Damage index

Park and Ang damage index (Park et al., 1987) says that the if the damage index value exceeds 1, than the test specimen i.e in this case 2D RC frame has reached its maximum failure point. The mathematical formula suggested by them was as follows:

$$D = \frac{\delta_M}{\delta_U} + \frac{\beta}{F_Y \times \delta_U} \int dE$$

Where, δ_M, the maximum displacement demand under is cyclic loading; δ_U is the ultimate displacement capacity, β is the strength degradation parameter, and its value for reinforced concrete structure is taken as "0.1" (I.Villemure & E.Ventura, 1995). F_Y is the yield load of the structure. With a value of 0 indicating no damage and a value of 1 indicating full destruction, the damage index [DI] may take on a range of 0-1 values.

The damage index became the indicator for the testing so as to understand when the loading can be stopped. As the loading can be exceeded from 50 mm cycle to a 100 mm cycle also.

Due to the damage index values, the test has to be stopped at 50 mm cycle as the DI value exceeded 1 (range of DI: 0-1). The damage index values of all the 2D RC Frames are mentioned in Table 5.2.

The values obtained in Table 5.2 clearly states that the deformation at various intervals corresponding to the drift ratios gives the damage index of all the three specimen. The values of the frame having brick masonry as infill has achieved the highest damage index values among all the three specimen. From this it can be interpreted that frame with concrete sandwich panel i.e. specimen "C" has been the most ductile in nature. This is also supported by the hysteresis loop (Refer Figure 5.3).

Table 5. 2: Damage index values of all the three 2D RC frames

S No.	Deformation (mm)	Drift Ratio	Damage Index		
			CSP as infill wall	CSP with door opening	Brick masonry
1	5	0.265	0.107	0.107	0.119
2	10	0.53	0.213	0.209	0.234
3	15	0.79	0.318	0.316	0.346
4	20	1.06	0.425	0.423	0.459
5	25	1.32	0.541	0.525	0.586
6	30	1.59	0.660	0.624	0.699
7	35	1.86	0.760	0.741	0.822
8	40	2.12	0.875	0.844	0.955
9	45	2.39	1	0.958	1.04
10	50	2.65	1.065	1.076	1.16

5.11 Displacement ductility

The performance of a structural system under seismic loading conditions is primarily determined by its ability to withstand significant deformations while retaining its load-bearing capacity, particularly in terms of lateral load resistance (Roosta & Liu, 2021). In order to evaluate a structure's ability to withstand significant deformations in the post-peak phase while retaining a substantial portion of its ultimate lateral load capacity, it is customary to calculate the displacement ductility factor and related parameters based on the structure's cyclic

response. The displacement ductility factor, μ, is determined by the ratio between the ultimate lateral displacement, Δ_u, and the displacement at yield point, Δ_y (Figure 5.16).

Table 5.3 displays the calculated values of Δy and Δu in both positive and negative directions, along with the resulting μ (average value derived from positive and negative directions). It is important to mention that specimen C showed 39.97 % more ductility than specimen B. This is due to the excessive stiffness due to the truss shaped shear connectors which helps in attaining more strength and compromising ductility. Whereas specimen O came out to be 5% more ductile than conventional brick masonry infill wall (Table 5.3).

5.12 Energy dissipation

The assessment of 2D frame behaviour involves a crucial aspect of post-yield response and its capacity for energy dissipation. The ductile response of the component is governed by the

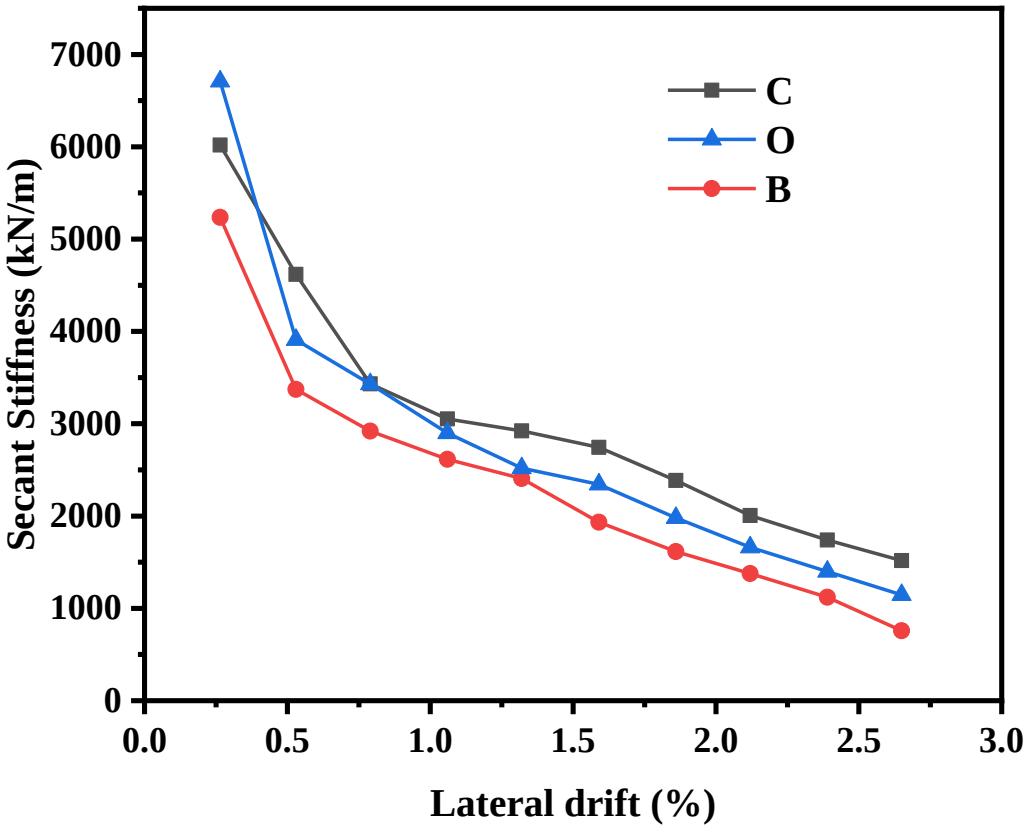

Figure 5. 15: Secant stiffness of all three specimens

larger energy dissipation in succeeding cycles as deformation increases after yielding. Conversely, the component exhibits brittle behaviour when the opposite is true. In this study, two different energy dissipation parameters are calculated: (a) the relative energy dissipation

(RED) parameter, which relates to the energy dissipation in each subsequent individual cycle, and (b) the cumulative energy dissipation (CED) parameter, which relates to the cumulative energy after each subsequent cycle (Table 5.3).

The yielding occurred in the specimen "C" in the 8th cycle whereas in Specimen O it occurred 6th cycle and in specimen B it occurred a bit earlier that is in 5th cycle due to the brittleness of the brick masonry and it is also deduced from the area of a hysteresis loop of the cycle. After the peak load has been attained specimen "C" being the most rigid showed the maximum energy dissipation (Figure 5.17 (a)), followed by Specimen O and least energy dissipation has been observed in specimen B. Figure 5.17 (b) illustrates the correlation between the wasted energy and the cumulative lateral deflection. The latter was obtained by summing the absolute values of the lateral displacements measured in all cycles. The dissipated energy has been calculated by determining the enclosed area under the hysteresis curves of the lateral applied load vs. displacement for each loading cycle, as shown in Figure 5.2.

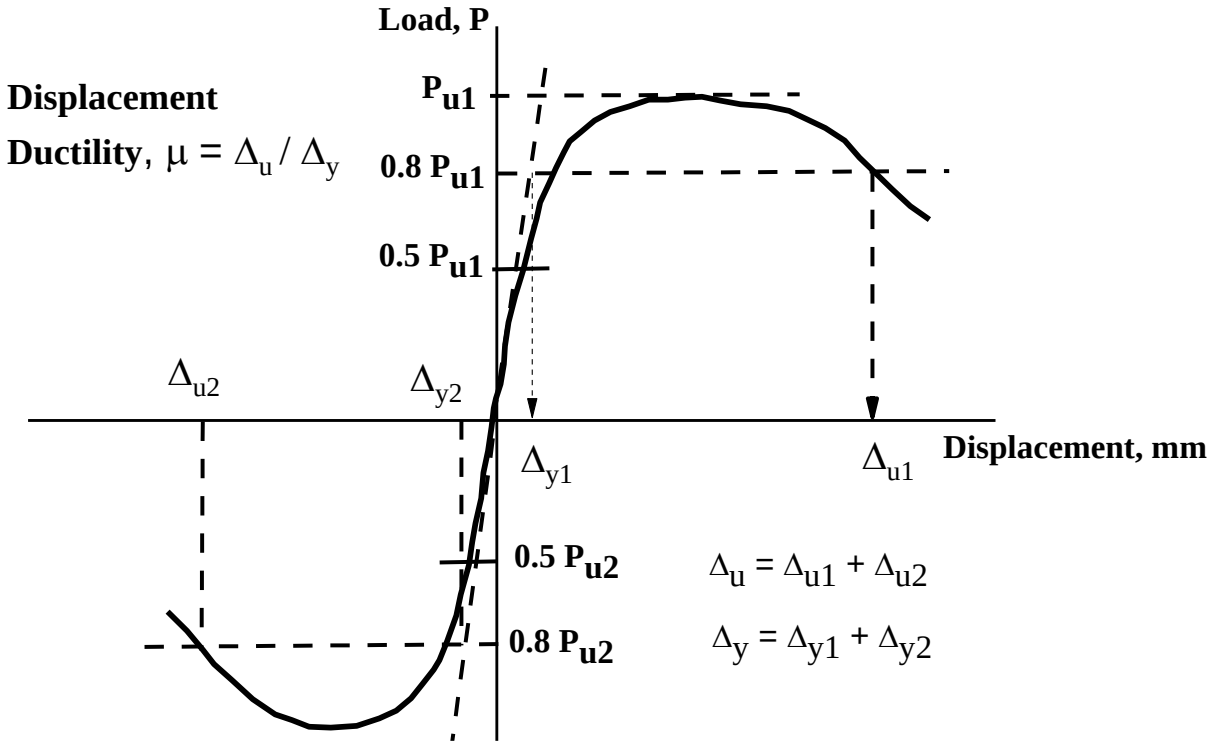

Figure 5. 16: Displacement Ductility factor curve

The energy dissipation capacity of specimen C and O was found to be significantly higher than that of specimen B, as evidenced by the obtained hysteretic curves. From Figure 5.17(b) it can be noticed that specimen C has been able to dissipate 66% more energy than specimen B. and specimen O has been able to dissipate 41.6% more energy than specimen B.

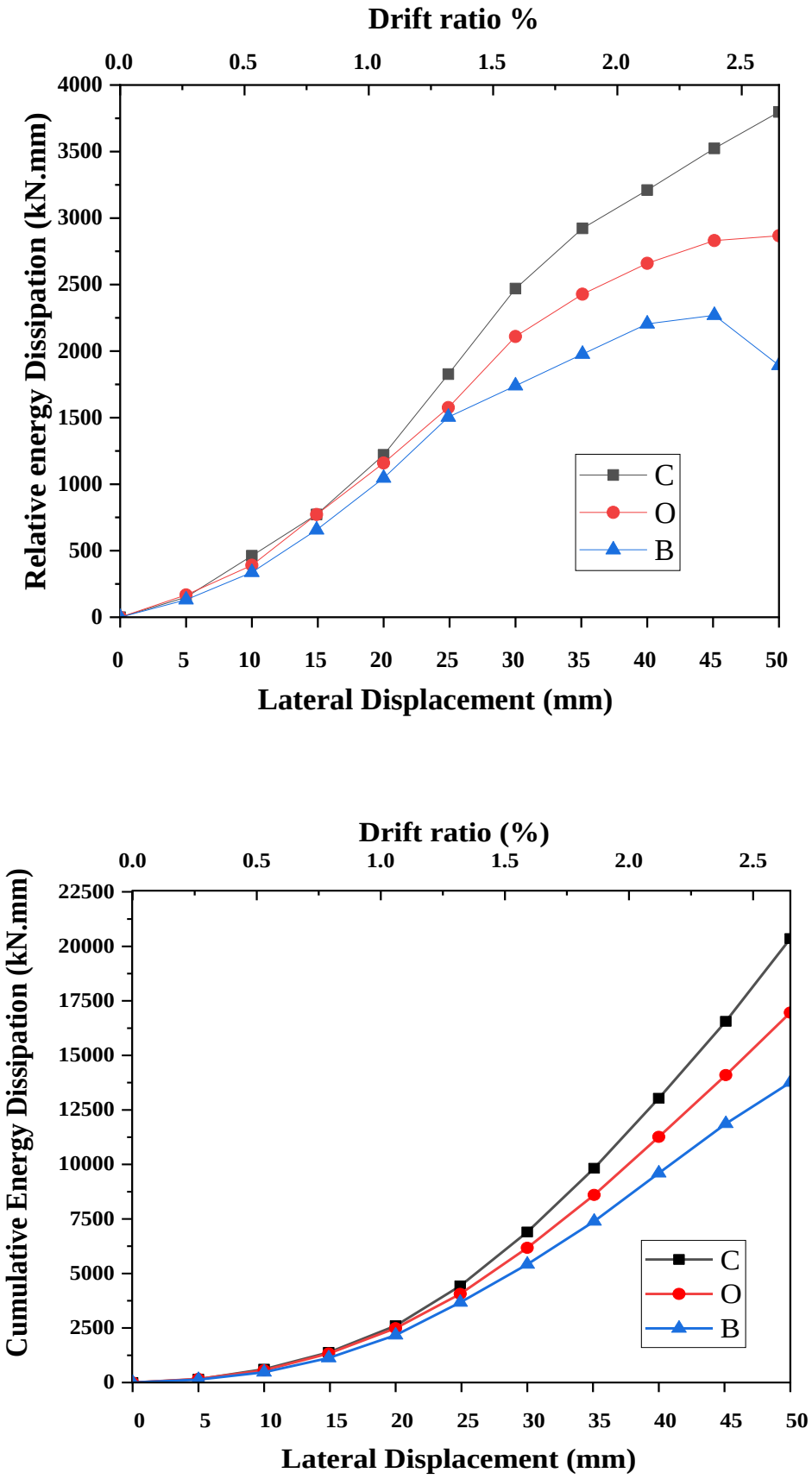

Figure 5. 17: (a) Relative energy dissipation; (b) Cumulative energy dissipation

Table 5. 3 : Test results of all test specimens

Specimen ID	Maximum				Ultimate				Displacement		Ductility
	Positive		Negative		Positive		Negative		Δ_y (mm)	Δ_u (mm)	$\mu = \Delta_u / \Delta_y$
	P (kN)	Δ_m (mm)	P (kN)	Δ_m (mm)	P (kN)	Δ_u (mm)	P (kN)	Δ_u (mm)			
C	83.5	35	78	35	75.94	50	65.23	50	5	50	10
O	70.33	30	57.96	30	57.35	50	35.09	50	3.5	50	14.28
B	60.16	25	52.81	30	37.84	50	49.03	50	3	50	16.66

Closing remarks

This chapter dealt with the comparison of brick masonry infill wall with the concrete sandwich panel as infill wall. It has been found that concrete sandwich panel can be a good replacement for brick masonry in terms of enhancing the structural capacity of the frame when subjected to seismic forces. Concrete sandwich panel with a door opening has also been tested under cyclic loading, which behaved better than the brick masonry infill wall. Hence it can be concluded that concrete sandwich panel is a better than brick masonry and can be used as infill wall in a RC frame.

Chapter 6

Finite-Element Analysis of Concrete Sandwich Panels

6.1 General

The Finite Element Analysis (FEA) of concrete sandwich panels is a complex computational method that is necessary for understanding the detailed structural response of these panels to different types of loads. These panels have a composite construction consisting of outer concrete facings that enclose a core substance. They have different mechanical reactions. Finite Element Analysis (FEA) allows for a thorough examination of the panels' behaviour when subjected to bending, diagonal shearing, and compression forces. This analysis provides a precise understanding of how stress is distributed, how the panels deform, and the mechanisms that lead to failure. The numerical simulation entails dividing the intricate geometry into smaller, more manageable pieces, enabling the implementation of constitutive models that accurately represent the material properties and nonlinear characteristics of concrete. Using this approach, examination of the complex interaction among the elements, separation between the surface and inner layers, localised formation of cracks, and the general integrity of the structure can be analysed.

The numerical analysis of the models has been carried out using the ANSYS software through the finite element model simulation. The modelling process includes selecting the appropriate elements to match the actual behaviour of the model components, loading states, and supports. The materials that make up the model include the various components of concrete sandwich panel.

6.2 Methodology of FEM analysis

The FEA models in ANSYS WORKBENCH were generated using an enhanced version of Static Structural Simulation, which utilises the FEA methodology. ANSYS requires the material properties, geometric dimensions, support requirements, and loading conditions for each node in order to solve equations for analysis. These equations are subsequently aggregated for all the degrees of freedom (DOF) within each element.

Figure 6.1 depicts the procedure of establishing a static structural model. The first stage is acquiring the requisite materials and comprehending their physical characteristics.

Subsequently, the geometric prototype is generated either through the utilisation of ANSYS Workbench's integrated sketching tool or by importing the geometry from CAD files, specifically SolidWorks in this instance. Once the geometry is finished, the system proceeds to generate a mesh and apply forces or displacement according to the type of analysis, whether it is load controlled or displacement controlled. Prior to solving the prototype, constraints are also implemented. Figure 6.1 illustrates the components involved in static structural analysis.

6.3 Geometry

The geometry was made in one of the CAD systems (solidworks) and imported to the ANSYS workbench. The imported geometry was than analysed by the FEM software. Once the geometry is accepted by the software than connections are established between the different materials of the geometry which in this case is concrete sandwich panel. Further to add to its complexity, another two layers of geogrids have been added as an additional reinforcement. Due to multiple number of layers in the geometry it is very important to define the contacts with precision.

These contacts will be the base for the geometry to go under meshing. If the contacts are not accurately defined than meshing of the geometry cannot be achieved.

The dimensions of the geometry have been taken as follows:

- Flexure specimen 1000 mm x 600 mm x 130 mm
- Diagonal shear specimen 600 mm x 600 mm x 130 mm
- Axial compression specimen 1000 mm x 600 mm x 130 mm

Two concrete layes are of 40 mm each and EPS is of 50mm thickness. The shear connector which are having truss shape are inclined at an angle of 70˚. The behaviour of sandwich panel completely depends on to the composite nature of the panel. The composite nature ensures that the load is transferred fully to the bottom layer and hence the failure type is noted. While performing in ANSYS workbench, this composite nature is ensured by the defined contacts and targets so as to know the behaviour of the panel.

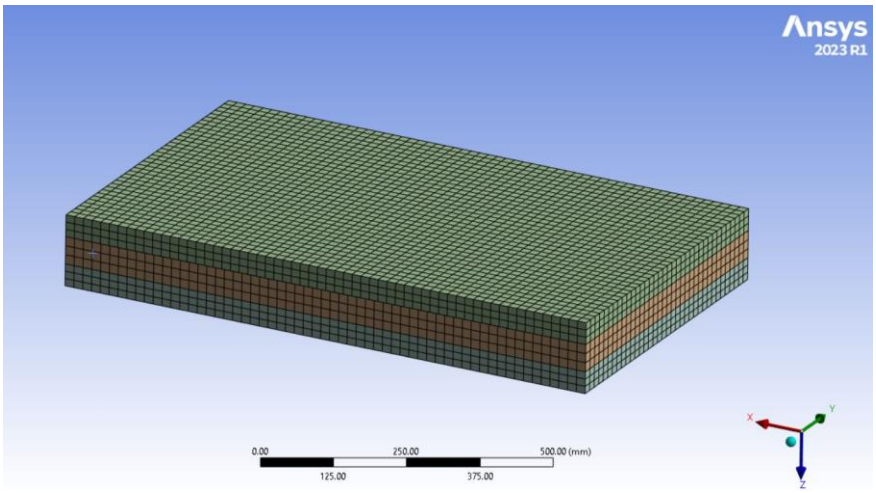

(a) Finite element meshing of Concrete sandwich panel

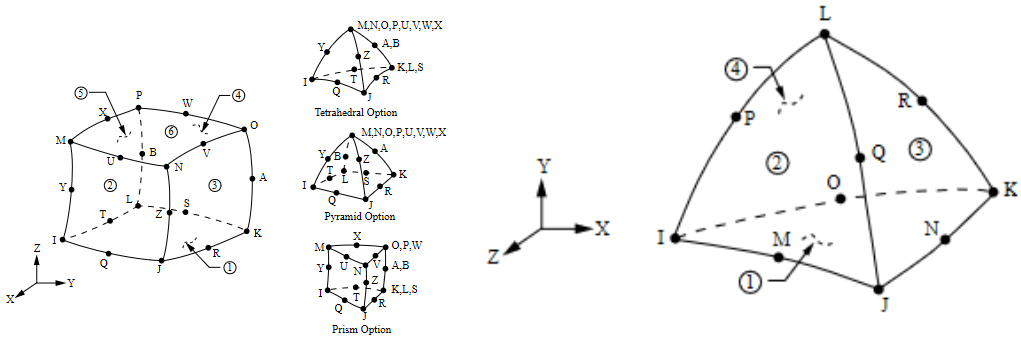

(b) Solid 186 and Solid 187 – 3D solids modeling. SAS (2013)

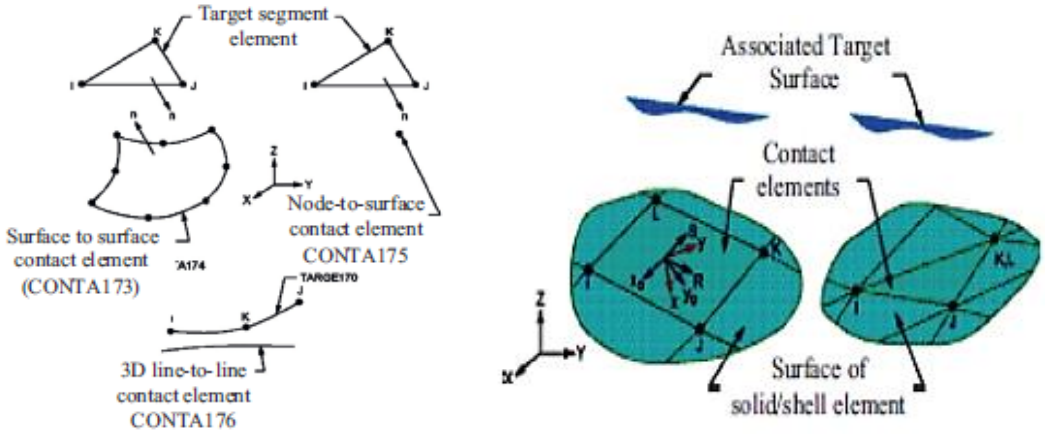

(c) TARGE170 and CONTA173 Geometry. SAS (2013)

Figure 6. 1: Pictorial representation of ANSYS FEM elements.

6.4 Cement matric (concrete) failure standards

The Finite Element Analysis (FEA) of the material is significantly influenced by the selection of mathematical equations used for the analysis and the input values of parameters in the solution model. Therefore, selecting a failure criterion is the initial step in studying the behaviour of cement matrices. The failure development of the cement matrix is intricate due to the heterogeneous nature of concrete, despite being treated as homogenous for analysis purposes. The force distribution in concrete occurs through the transfer of forces between individual grains or particles. Furthermore, the interfacial transition zone (ITZ) is created at the interface between the cement and aggregate, resulting in the concrete becoming softer once it reaches specific stress-strain thresholds. The selection of an appropriate concrete failure model is crucial for accurately representing the behaviour of the real environment. There are several failure criteria available, ranging from simple standards like the maximum tensile stress and maximum tensile strain criteria with only one restriction, to more complex criteria like the Mohr-Coulomb and Drucker-Prager criteria with two restrictions, and the William-Warnke criteria with three or five restrictions. Adding additional limitations enhances accuracy, but it unavoidably increases the level of complexity. William and Warnke (1974) introduced a widely respected prototype of a tri-axial failure plane for unconfined ordinary cement matrix, which is utilised for modelling concrete.

6.5 William and Warnke material prototype for concrete

Willam & Warnke (1975) prototype has the capability to predict the collapse of cement matric materials. The analysis includes the examination of both crushing and cracking failure mechanisms collectively. The prototype requires two resistance values to characterise deformation constraints: compression resistance to deformations (f_{ck}) and ultimate uniaxial tensile resistance, which are necessary to define a failure plane of concrete. The failure of the cement matrix can be determined by analysing the multiaxial stress condition. Figure 6.2 depicts a three-dimensional failure plane for the cement matrix.

The most remarkable aspect is that the primary stress has non-zero values in both the X and Y directions respectively. Figure 6.2 illustrates the three failure planes that correspond to distinct stress components in the direction of the stress plane. Specifically, it displays the predictions of stress on the σ_{xp} - σ_{yp} principal stress plane. The failure mode is contingent upon the sign of σ_{zp} (the magnitude of the primary stress in the Z-axis). For instance, if both σ_{xp} and σ_{yp} are

negative (indicating compression) and σ_{zp} is slightly positive (indicating tensile stress), cracking would be anticipated in a direction perpendicular to σ_{zp}. However, if σ_{zp} is equal to zero or has a slightly negative value, the cloth is considered to be crushed. The implementation of the William and Warnke material prototype in ANSYS requires the use of specific constant values that are dependent on the material attributes.

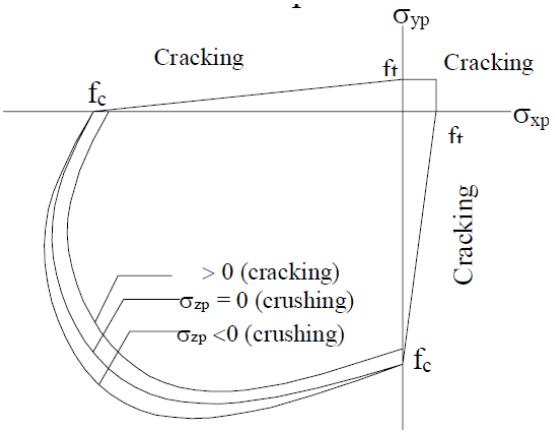

Figure 6. 2: Failure surface of concrete(Willam & Warnke (1975))

6.6 Prototype coefficients of concrete

In order to accurately simulate the cement matrix in Finite Element Analysis (FEA), it is necessary to have linear isotropic and multilinear isotropic material properties for the prototype. In ANSYS, the Von-Mises failure standard is commonly employed to represent the failure of cement matrix in multilinear isotropic materials. The Willam and Warnke prototype is also extensively used for this purpose.

$E_c = 5000\sqrt{f_{ck}}$ 6.1

The compression uniaxial stress-strain relationship for the cement matrix prototype can be derived using equations 6.1 to 6.5, as recommended by previous researchers.

$$f_{ck}=\frac{Ec}{1+\frac{\varepsilon}{\varepsilon_0}} \quad 6.2$$

$$\varepsilon_0 = \frac{2f'_c}{E_c} \quad 6.3$$

$$E_c = \frac{f}{\varepsilon} \quad 6.4$$

where:

f = stress at any strain ε, MPa

ε = strain at stress f_{ck}

ε_0= strain at the ultimate compression resistance to deformation f'_c

The implementation of the multilinear isotropic σ-ε requires the identification of the primary point on the curve for analysis. The essential need is to satisfy the proportionality restriction, also known as Hooke's Law.;

$$E = \frac{\sigma}{\epsilon} \quad 6.5$$

The utilisation of the multilinear curve facilitates the convergence of the Non-linear solution procedure. The value of stress vs strain is obtained from the formulae provided above. In order to implement the Willam and Warnke prototype in ANSYS WORKBENCH, it is necessary to have 9 constants (SAS, 2012). The 9 constants utilized in the analysis of the concrete wythe in the slab may be found in Table 4.

Table 6. 1: Values of coefficients used for analysis

S. No	Coefficient	Value
1	Open crack shear transfer coefficient	0.5
2	Closed crack Shear transfer coefficient	1
3	Tensile cracking σ in a uniaxial direction	4.5 MPa -slab panel and 2.4 MPa- wall panel
4	Crushing σ in a uniaxial direction	45 MPa -slab panel and 20 MPa- wall panel
5	Crushing σ for biaxial direction.	0
6	Ambiance hydrostatic	0
7	Value of ambiance hydrostatic σ state for Biaxial crushing σ.	0
8	Value of ambient hydrostatic σ state for Uniaxial crushing σ.	0
9	Value of Strength multiplier under the cracked tensile state.	0

- The recommended range for the open crack shear transfer coefficient, as proposed by Razaghi et al. (2005), is between 0.2 and 0.5. The input for the open crack shear transfer coefficient was set to 0.5.
- According to Razaghi et al. (2005), the suggested range for the shear transfer coefficient is from 0.0 (indicating a smooth fracture with total loss of shear transfer) to 1 (indicating

a rough crack with no loss of shear transfer). The input value for the shear transfer coefficient of a closed crack was set to 1.

- The value of Tensile cracking σ in the uniaxial direction was determined using the modulus of rupture and was inputted as 0.1 fck, equivalent to 4.5 MPa.
- The value of the crushing stress (σ) in the uniaxial direction was determined by the uniaxial unconfined compression resistance to deformation. It was set at 45 MPa to activate the cement matrix component's ability to crush, as explained by Kachlakev and Miller (2001).

Wolanski and B. (2004) utilised a value of 0 for factors ranging from 5 to 9 in order to address the ANSYS convergence issue.

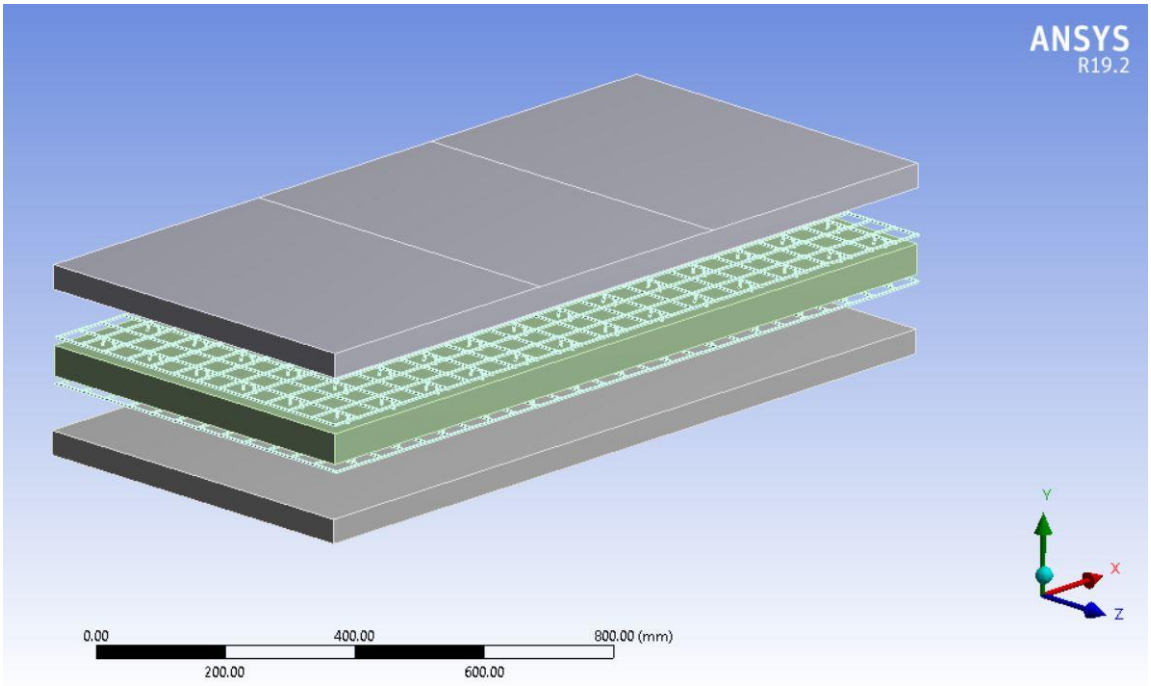

Figure 6. 3: Exploded view of CSP (Control)

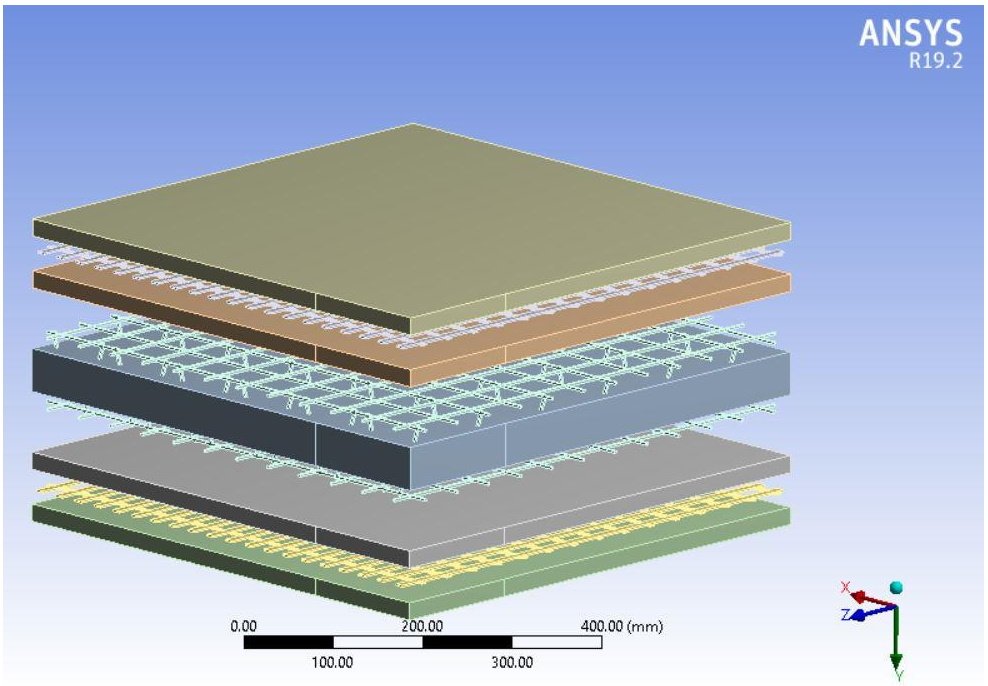

Figure 6. 4: Diagonal shear specimen with PBG (Exploded view)

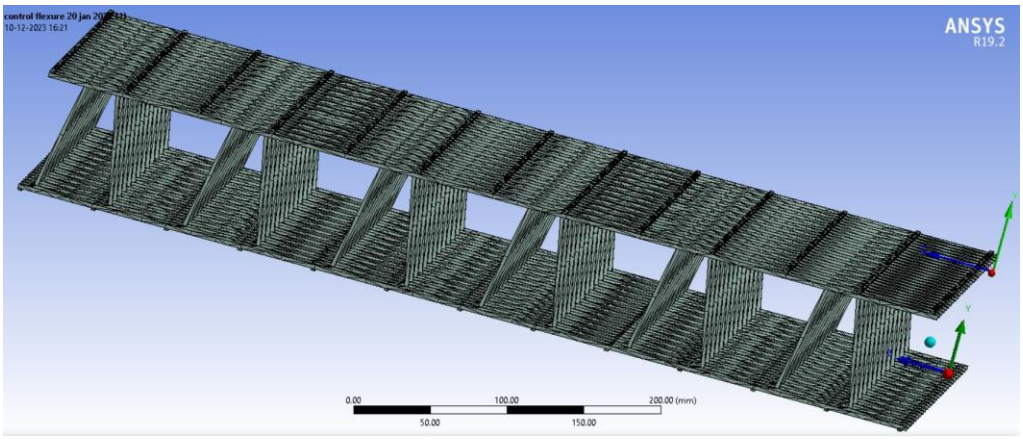

Figure 6. 5: WWM with shear connectors at an angle of 70˚

6.7 Meshing

The most crucial part of the simulation is to identify the complex areas in any geometry and giving the right type of the meshing results. The size of meshing is as per the requirement. Usually for simple type of geometries, “hex mesh” is used. The finer the mesh size, chances of more accurate result is possible. The coarser the mesh, more effective results are produced.

In this study, two types of meshing has been used

- Tetrahedron mesh

- Hex mesh

Further to enhance the total number nodes, meshing size can also be reduced in order to get accurate results. Results also vary on the basis of the material properties given to the software. In finite element analysis three-dimensional solid elements have been used in this study, to model concrete, while to quantify EPS, welded wire mesh and geogrid and concrete by defining its different coefficients using the modulus of elasticity, as well as defining the non-linear stress-strain curve of concrete. Also, these two elements have high stress capabilities, high elasticity, and great deformation.

SOLID186 which is a 20-node 3D brick element with three degrees of freedom at each node is used to model top and bottom concrete layers and a middle layer of EPS sheet. SOLID187 which is a 10-node 3D tetrahedron element having the capability to model irregular shapes used to model steel wire mesh and truss type shear connectors. TARGE170 and CONTA173 elements have been employed to represent contact of truss shaped shear connectors with wire mesh and the concrete surface. SURF154 is used to model surface effect of displacement coming from load in 3D structural prototype. The meshing and elemental representation are given in Figure 6.1.

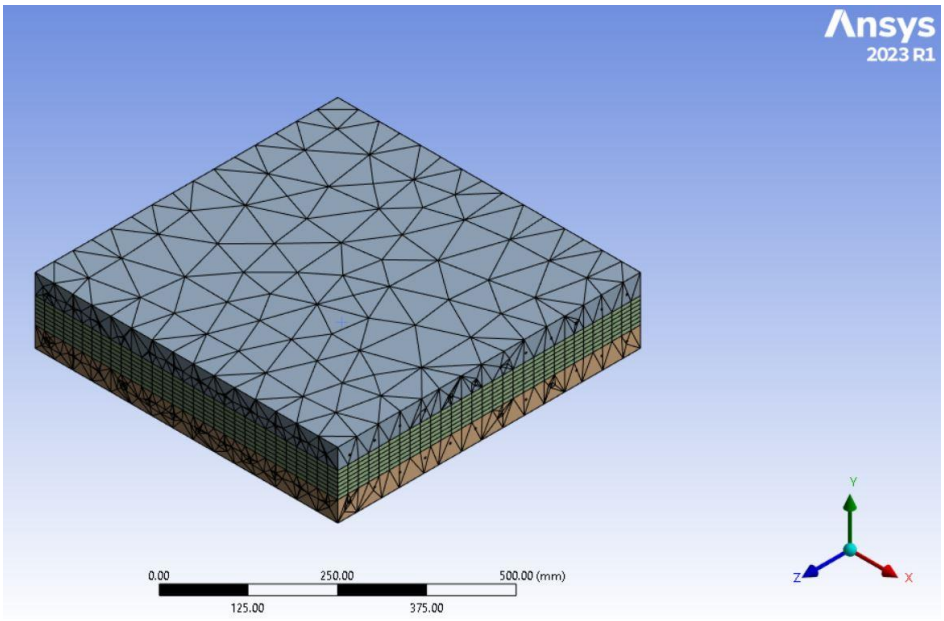

Figure 6. 6: Tetrahedral meshing (Top and Bottom) and hex meshing (Middle) on the EPS

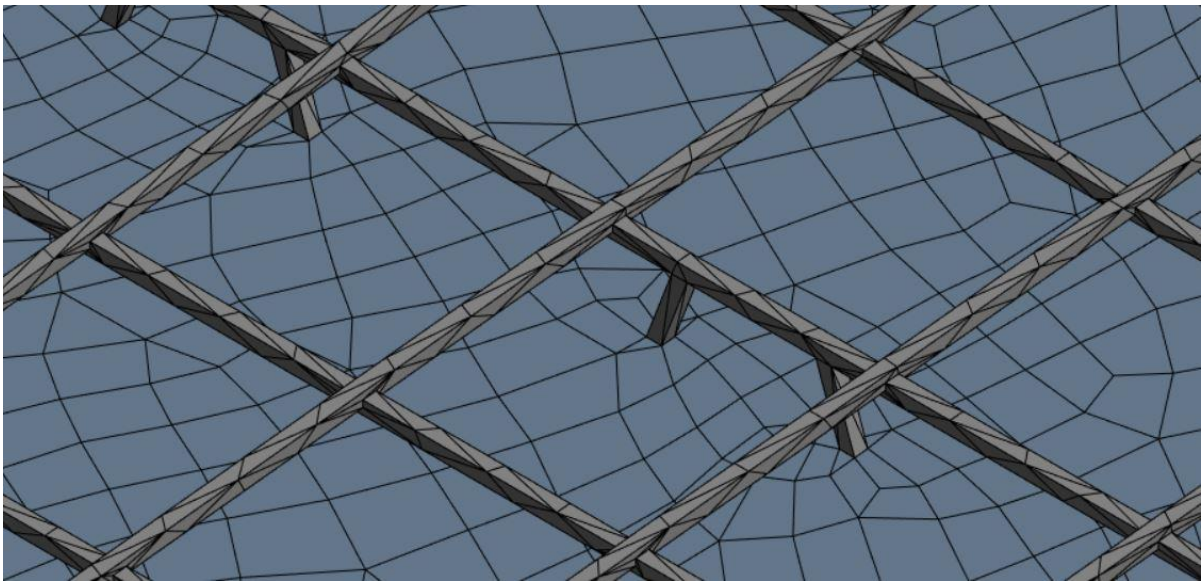

Figure 6. 7: Irregular Mesh at the conjunction of EPS and shear connector

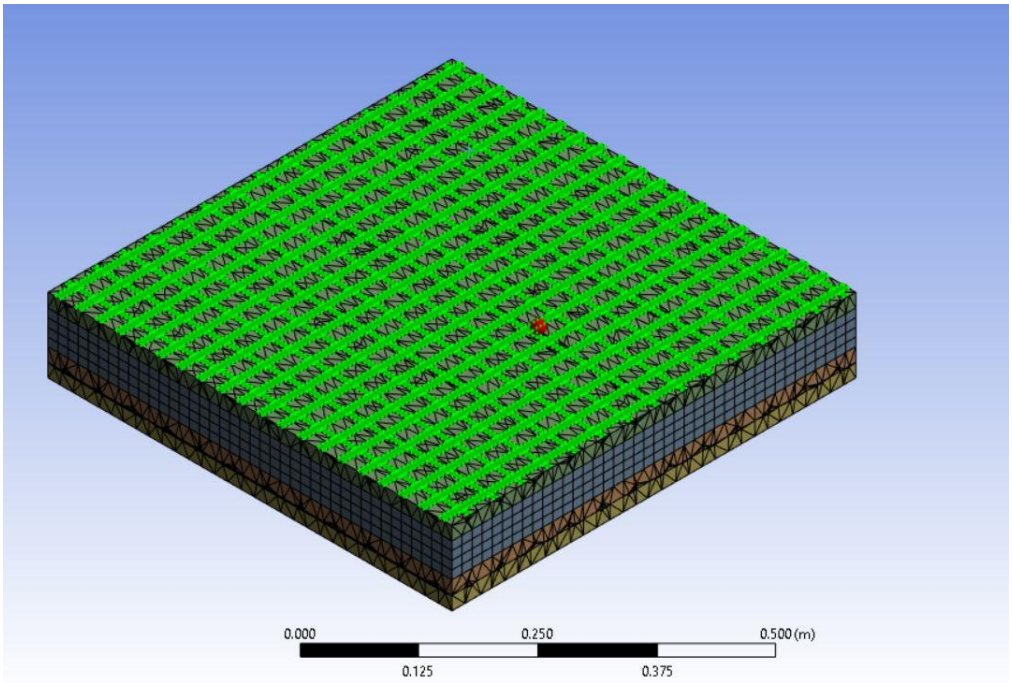

Figure 6. 8: Layer of polyester geogrid (Green colour)

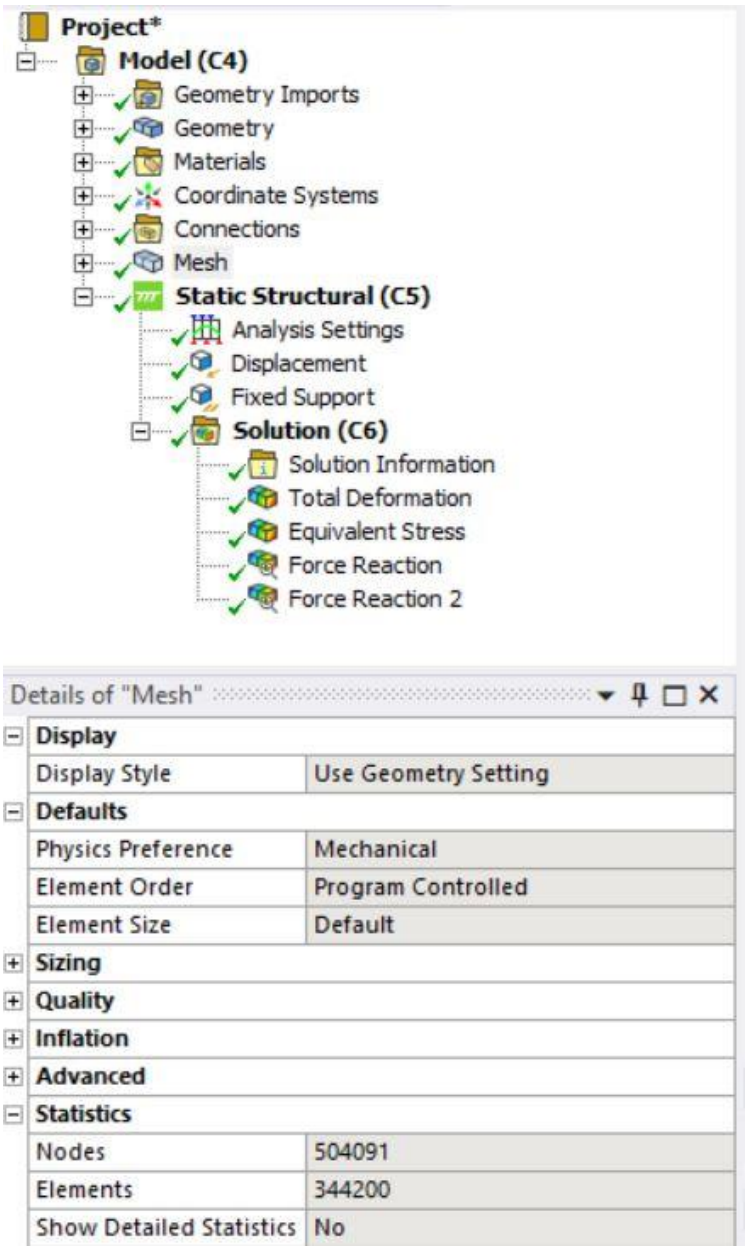

Figure 6. 9: Number of nodes and elements to solve for diagonal shear specimen

6.8 Boundary conditions

After the meshing the most critical work is to provide with the right type of boundary conditions. Boundary condition means the restrained side of the specimen is to be given the right selection of the forces. In this case in particular a four point bending test has been performed on the concrete sandwich panel and same has been done through the experimental testing. Assigning of loading conditions and defining the element to be used to solve the particular area or node.

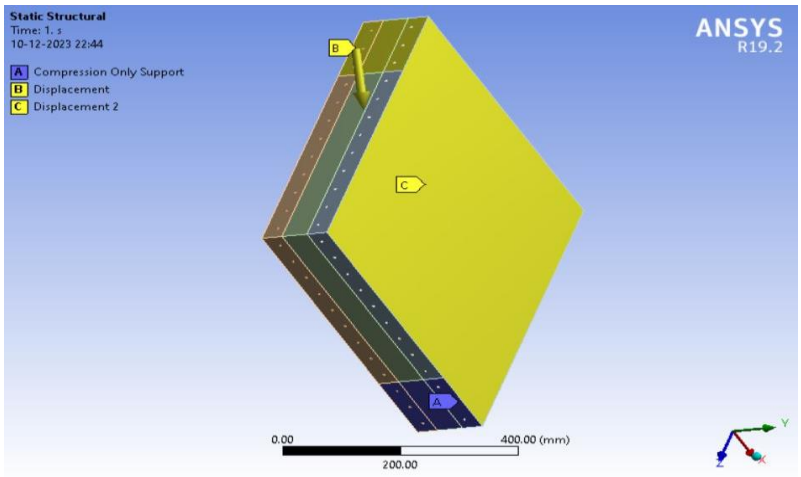

Figure 6. 10: Boundary condition (A, B and C) applied on diagonal shear test specimen

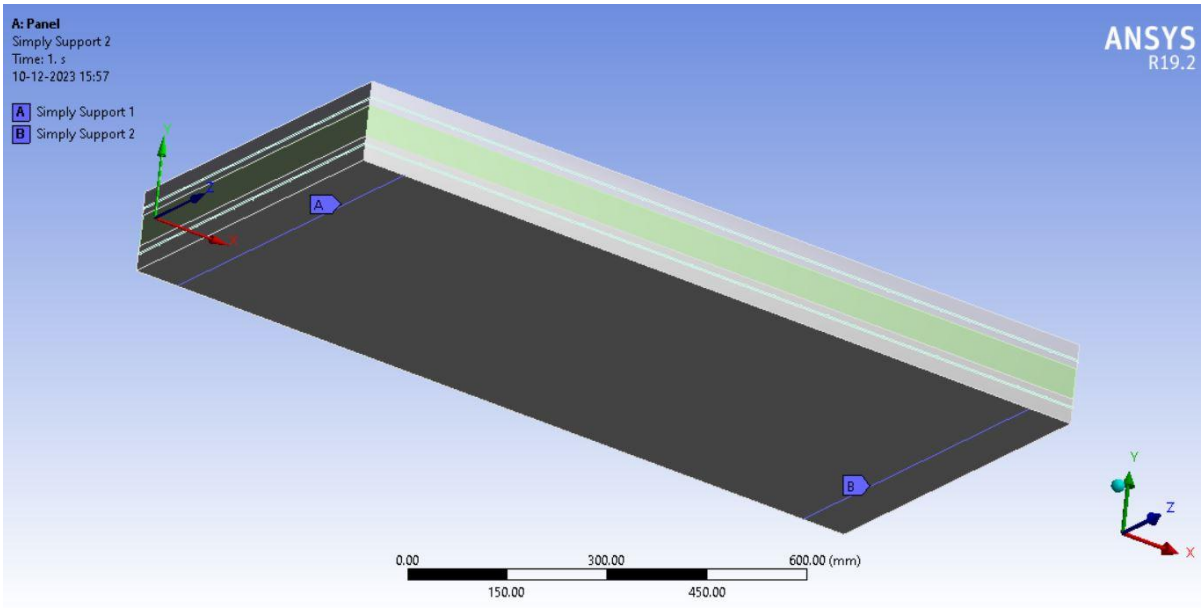

Figure 6. 11: Roller and pinned support (A and B) applied to the flexure specimen

6.9 Results and Discussions of FEM Analysis

The analysis of concrete sandwich panels is done as per the experimental tests. Displacement controlled analysis is done. In four-point bending the boundary condition, one side is applied as roller and the other side is hinged. The load-displacement curves are plotted and the validation of the experimental results is performed.

6.9.1 Force Vs Displacement Behaviour

The FEM analysis is performed by considering the non-linear behaviour of the panel. From the FEM, it is analysed that the cement matrix concrete sandwich panel failed by establishing inclined cracks that have a tendency to connect with the nearest support and loaded

point. It is also highlighted that the general failure of the panel is not governed by shear failure. Yet, it is found from the present study that the cement matrix of concrete sandwich panel failed by forming inclined cracks that have a tendency to link with the nearest support and loaded point. After the creation of the inclined cracks, when the functional force is amplified, the size of the inclined crack enlarged deprived of developing new flexural cracks in the slabs (Figure 6.1 and Figure 6.2).

For diagonal and axial compression loading cases the main load is taken by 40 mm thick concrete wythes present on both sides and the central EPS core has the least role in it. Initially, for all the specimens both the concrete wythe are experiencing compressive force but as the load increases the outer wythe experience tension and the inner wythe experiences compression. As a result of which outer wythe will experience under elongation and the inner wythe will experience under shortening deformation in axial loading. In both these loading cases, the load causes formation of weak zones and the area of these weak zone increases with the increment in load and ultimately this causes failure of the specimen. The failure is due to increment of stress of the element than that of the bearing capacity. In diagonal compression, one side of diagonal will go under tensile rupture and the other side of diagonal will go under compression crushing ultimately causes the failure of the panel (Figure 6.3 to Figure 6.8).

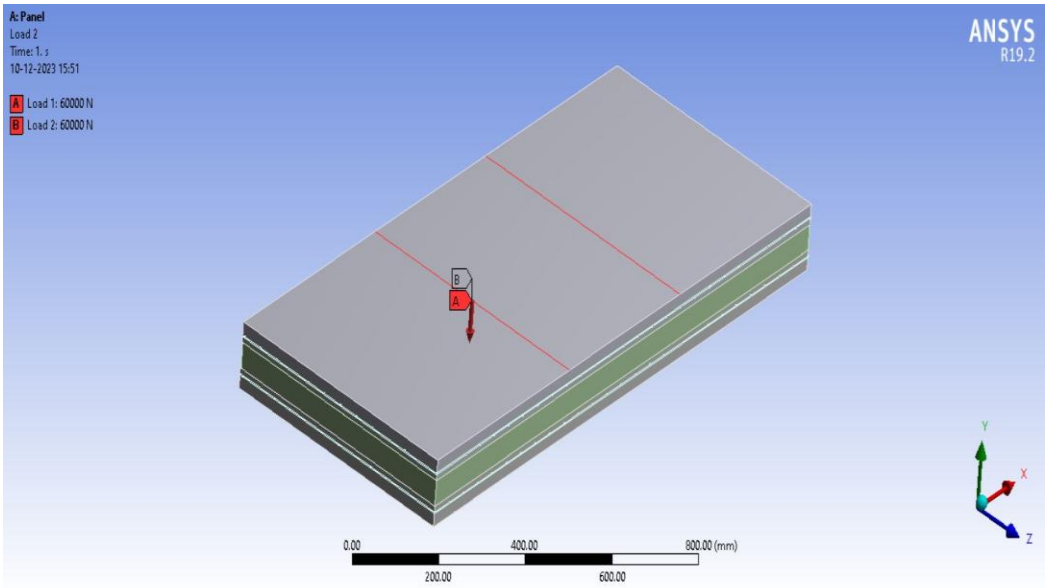

Figure 6. 12: Application of loading on CSP

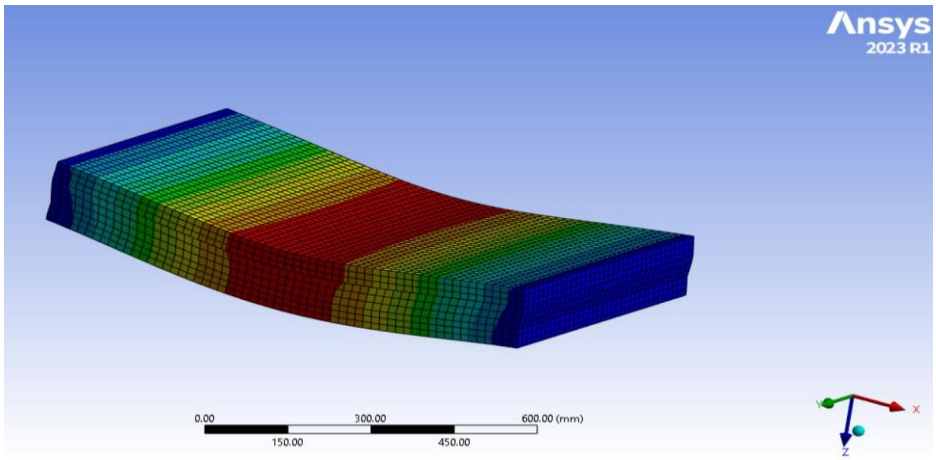

Figure 6. 13: Flexural failure of the CSP (FEM analysis)

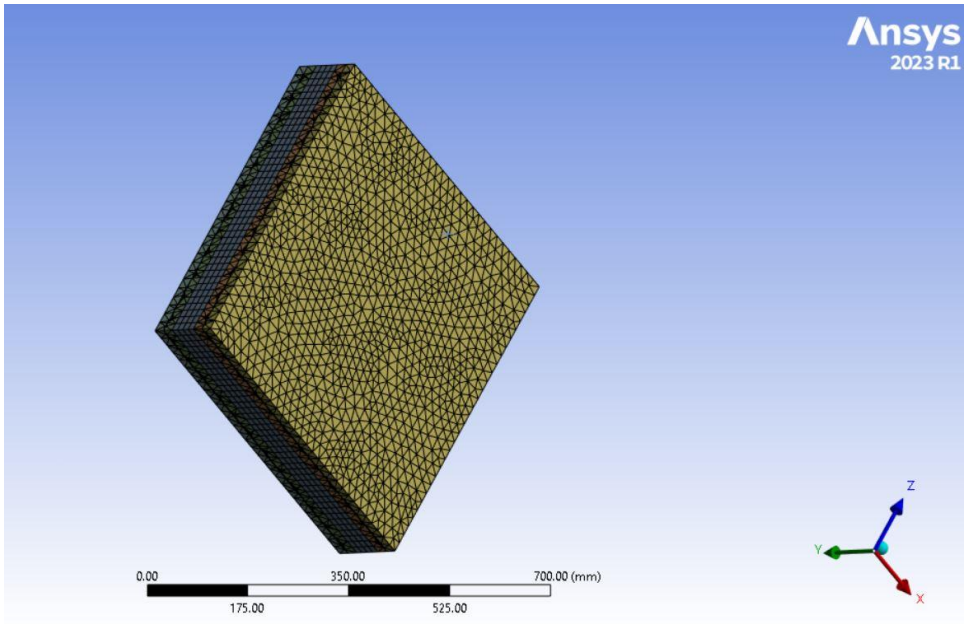

Figure 6. 14: Finer mesh size generated

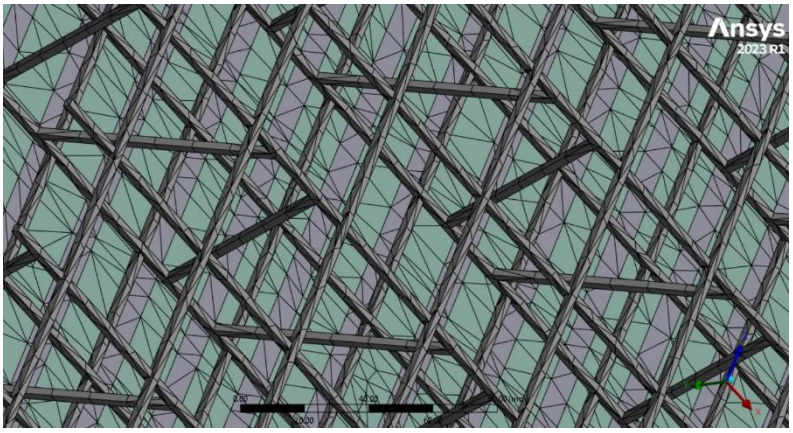

Figure 6. 15: Meshing of the welded wire and geogrid inside the CSP

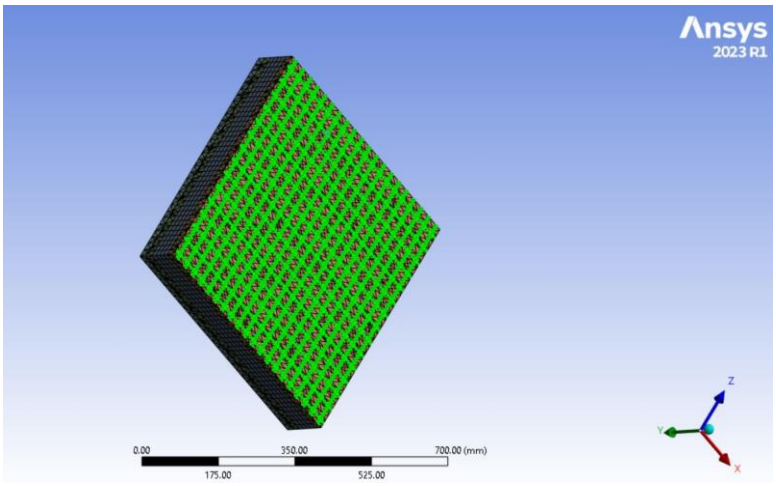

Figure 6. 16: Geogrid layer in CSP (Green Mesh)

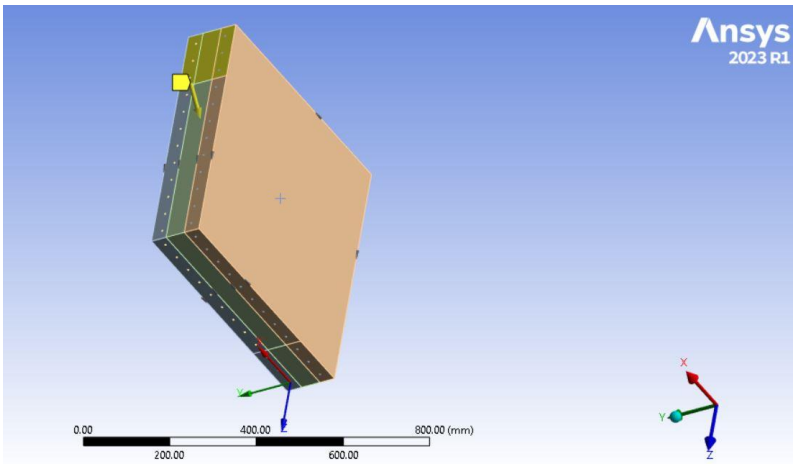

Figure 6. 17: Application of load on the diagonal shear specimen at the edges

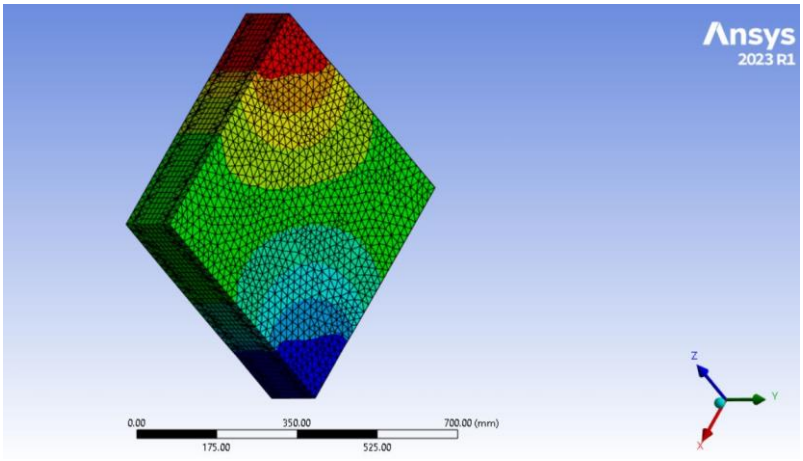

Figure 6. 18: In-plane failure of the specimen after the application of load at the top edge

6.9.2 Response of concrete sandwich panel under flexural loading

Based on the Finite Element Method (FEM) analysis, it can be inferred that the specimen SPC1S exhibits linear behaviour up to a force of 30 kN, but in experimental testing, this linear behaviour is observed up to a force of 25 kN. Figure 6.9 (a) shows that the red curve indicates the point at which the panel reaches its maximum elastic deformation. At this point, plastic hinges begin to form around a loading of approximately 27 kN. This phase marks the initiation of the first crack development. Subsequently, a subsequent augmentation in the applied load results in additional crack formation and expansion of pre-existing cracks, as illustrated in Figure 6.9 (a) at about 57kN. Ultimately, there comes a point where the panel becomes incapable of withstanding any stress and experiences failure (at around 61 kN). The FEM prototype exhibits more strength compared to the experimental prototype because to the controlled settings of the FEM analysis, which disregards factors such as micro-cracks, shrinkage, and potential creep effects. Furthermore, in experimental studies, the outcomes are contingent upon instrument calibrations and the composition of the casting material. Conversely, in the case of FEM analysis (an iterative process), the outcomes are contingent upon material properties, loading conditions, and the type of solver employed. Consequently, the prototype will exhibit increased rigidity. The error percentage between the experimental result (SPC1) and numerical analysis (SPC1S) is found to be 7.0%.

The results for the specimen containing plastic geogrid are shown in Figure 6.9 (b). It is observed that due to the presence of plastic uniaxial geogrid (PUG) the strength of the concrete sandwich panel has been enhanced (shown by red line in the graph) as seen in Figure 6.9 (b). SPGGS behaved linearly up to 30 kN whereas SPGG behaved linearly up to 22 kN. Peak load achieved in SPGGS is 79.56 kN which is 7.7% higher than SPGG. In the specimen containing polyester biaxial geogrid (PBG2) an abrupt increase in strength has been observed as the peak load value achieved is the highest among all the M1 specimens (Figure 6.9 (c)).

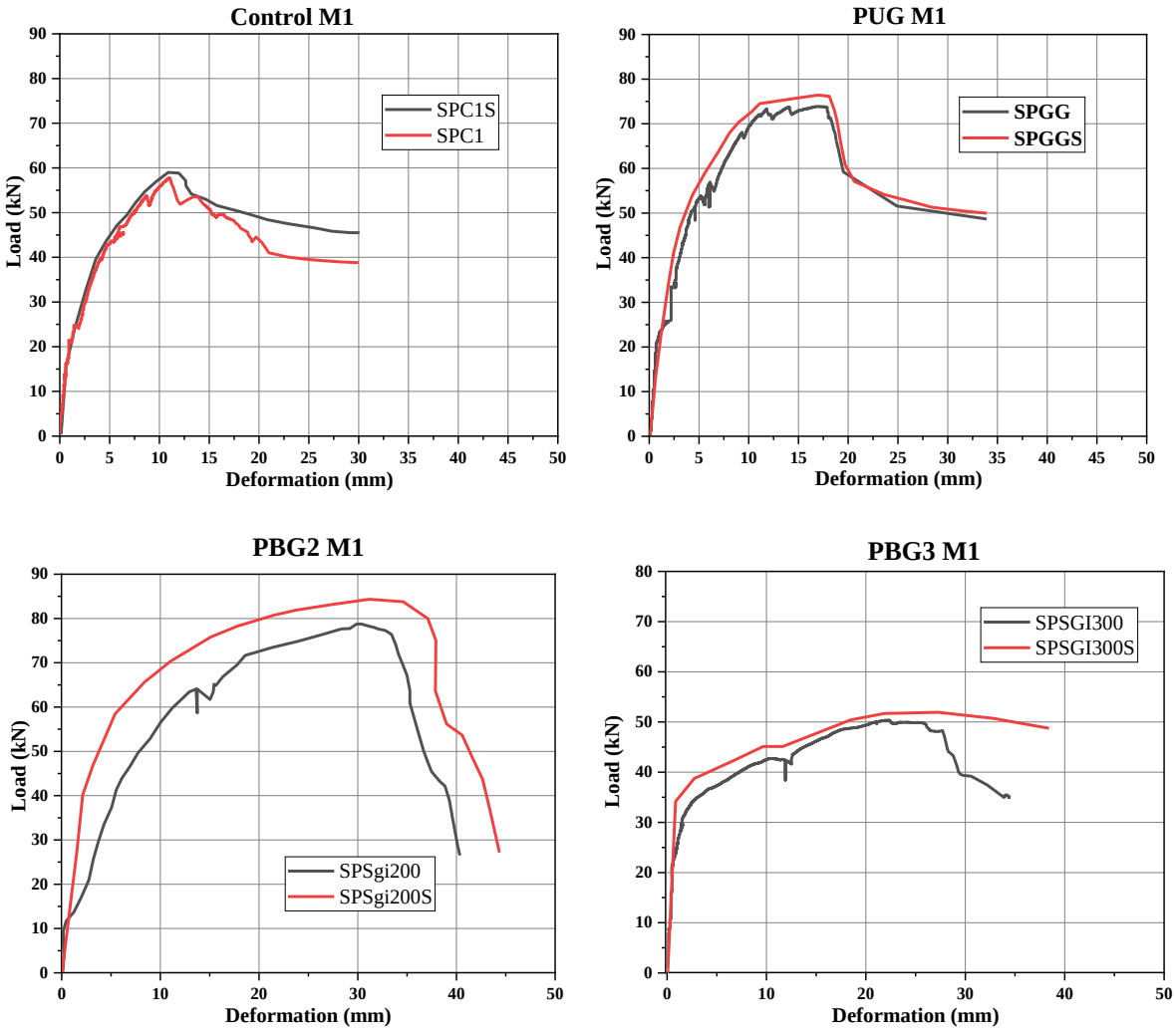

Figure 6. 19: Experimental results vs numerical modelling under flexural loading for mix M1; (a) Control specimen; (b) PUG; (c) PBG2; (d) PBG3

The percentage increase found to be is 9% (approximately) more than the SPSGi200 specimen. Similarly in case of PBG3 specimen (SPSGI300S) the peak load achieved is 6% more than the experimental (SPSGI300) value (Figure 6.9 (d)). When comparing all the M1 specimen results, SPSGi200 achieved maximum peak load (i.e. 85.23 kN) and can be recommended for practical application.

For the mix M2 it can be concluded that the specimen SP1CS behaves linearly up to 33.45 kN load whereas in case of experimental it is 20 kN. This difference in the values can be attributed to the controlled environmental testing in the FEM software, as the properties mentioned in the above paragraph which have been neglected while numerical modelling in ANSYS software. Similarly other three specimens behaved in a similar manner when compared with the experimental curves with an approximate increase of 5%- 10% in peak load values.

This further suggests that the numerical simulation is in good agreement with the experimental results.

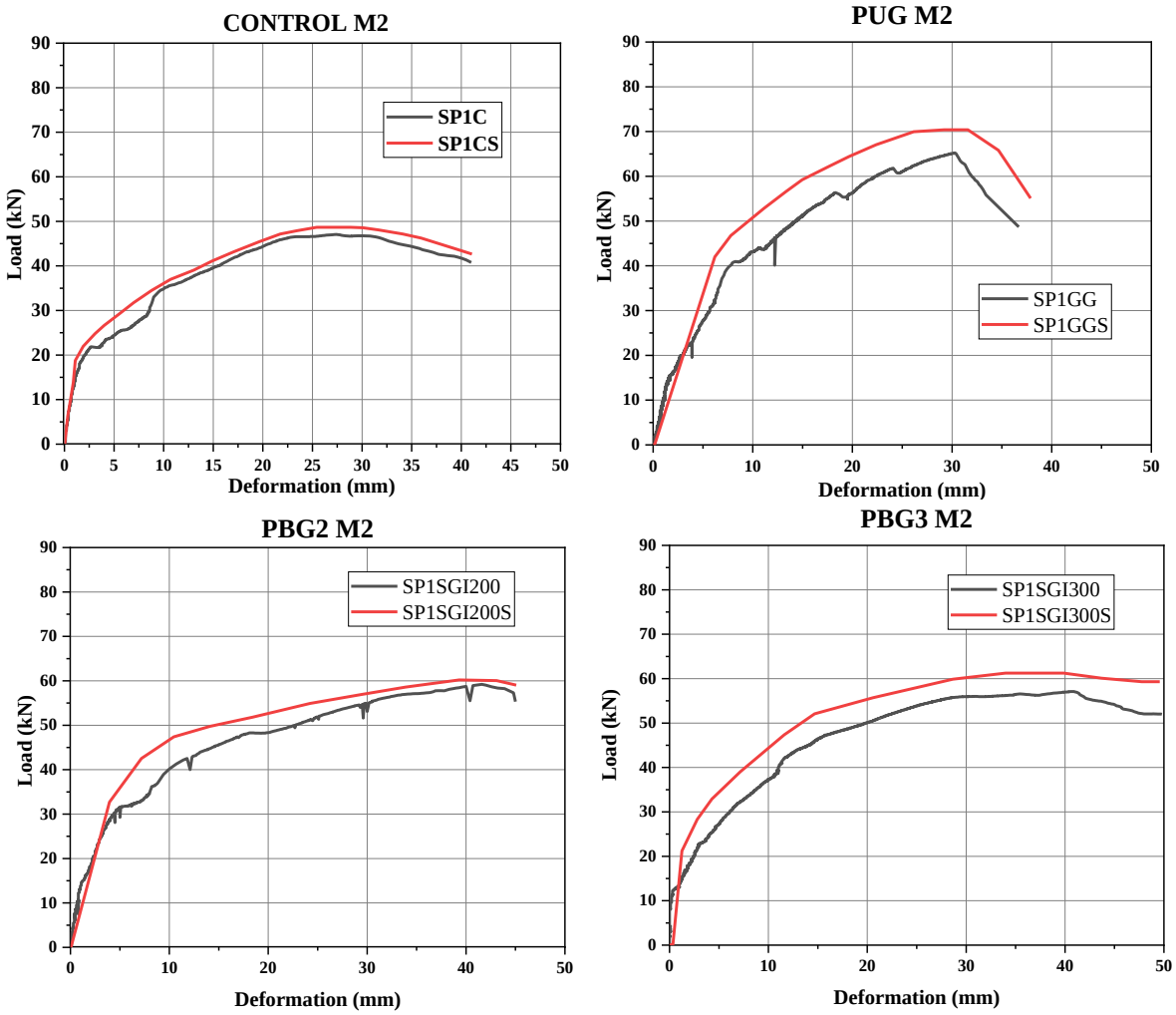

Figure 6. 20: Experimental results vs numerical modelling under flexural loading for mix M2;(a) control specimen; (b) PUG; (c) PBG2; (d) PBG3

6.9.3 Response of concrete sandwich panel under diagonal in-plane shear loading

Diagonal shear specimen has been under different loading conditions from the flexure specimen. This type of loading is also called in-plane shear loading. Figure 6.7 shows how the load is being applied and also demonstrates the boundary conditions applied. Figure 6.11 (a) shows the comparative graph of control specimen of mix M1 i.e. DS1C vs DS1CS. The graph clearly illustrates that the numerical modelling curve (red line) closely aligns with the experimental results, indicating a high level of agreement. Peak load achieved in the software analysis is 309 kN which is 5.46% more than experimental value (293 kN). Figure 6.11 (b)

PUG M1 represents the specimen containing plastic uniaxial geogrid, when compared with the experimental results gave almost the same result as the experimental specimen DS1GG.

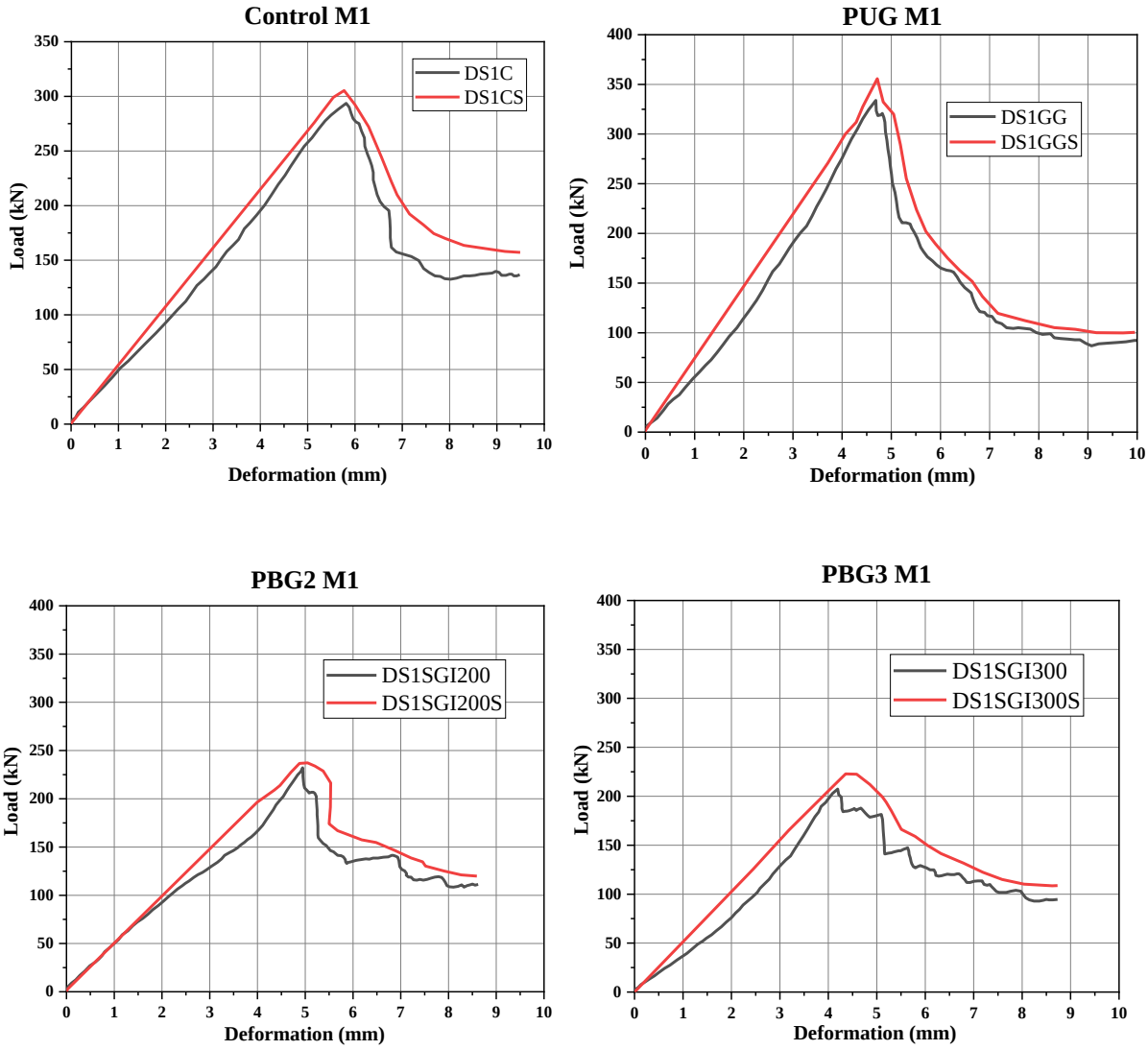

Figure 6. 21: Experimental results vs numerical modelling under diagonal shear loading for mix M1 (a) Control specimen; (b) PUG; (c) PBG2; (d) PBG3

The graph between polyester biaxial geogrid as an additional reinforcement in Figure 6.11 (c) and Figure 6.11(d) shows that initially upto elastic limit the behaviour of concrete sandwich panel is exactly the same as in experimental results. Upon reaching the plastic range, cracks begin to form in the specimen, indicating the deformation of the welded wire mesh and potential failure of the shear connectors. After achieving the peak load there is sudden drop which also suggests the debonding of the layer of the wythe from the core. Similar curve obtained in ANSYS validates the experimental results.

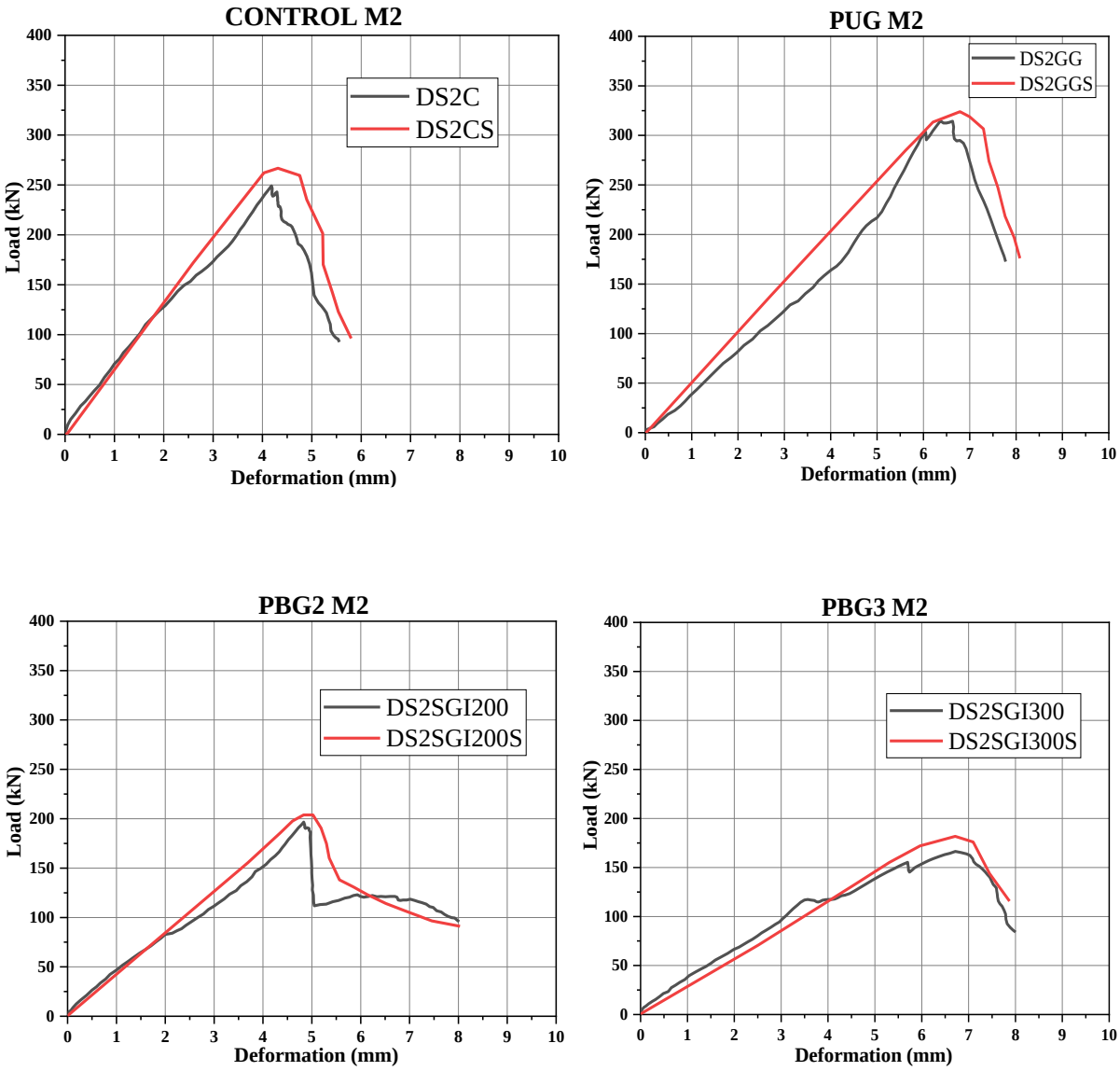

Figure 6. 22: Experimental results vs numerical modelling under diagonal shear loading for mix M2 (a) Control specimen; (b) PUG; (c) PBG2; (d) PBG3

In Figure 6.12 (a) it can be seen that the mix M2 has shown its effect on the concrete sandwich panel in the software analysis also as the compessive strength value of the mix M2 is lower than mix M1. It has shown very less deformation or it can also be said that brittle failure is encountered. After the introduction of the plastic uniaxial geogrid (depicted in Figure 6.12 (b)), there is a noticeable augmentation in both the maximum load and the amount of deformation. 8% increase in peak value is found in DS2CS specimen than DS2C. an increase of 6% is observed for the specimen containing PUG.

Similarly for the specimen DS2SGI200S, elastic behaviour is in complete synchronization with the experimental results but the post elastic behaviour is a bit different.

This diffference is due to the debonding of wythe in the experimnental testing. As in the software analysis boundary conditions make sure that no debonding occurs before the failure of the shear connectors. Debonding can only be expected after the major number of shear connector fails. Specimen DS2SGI300S behaved in accordance with the experimental results and validated them.

6.9.4 Response of concrete sandwich panel under axial compression loading

Axial compression loading is similar to the diagonal in-plane shear loading, the only difference is the area of contact at the loading increases. Specimen WP1S behaved approximately in the

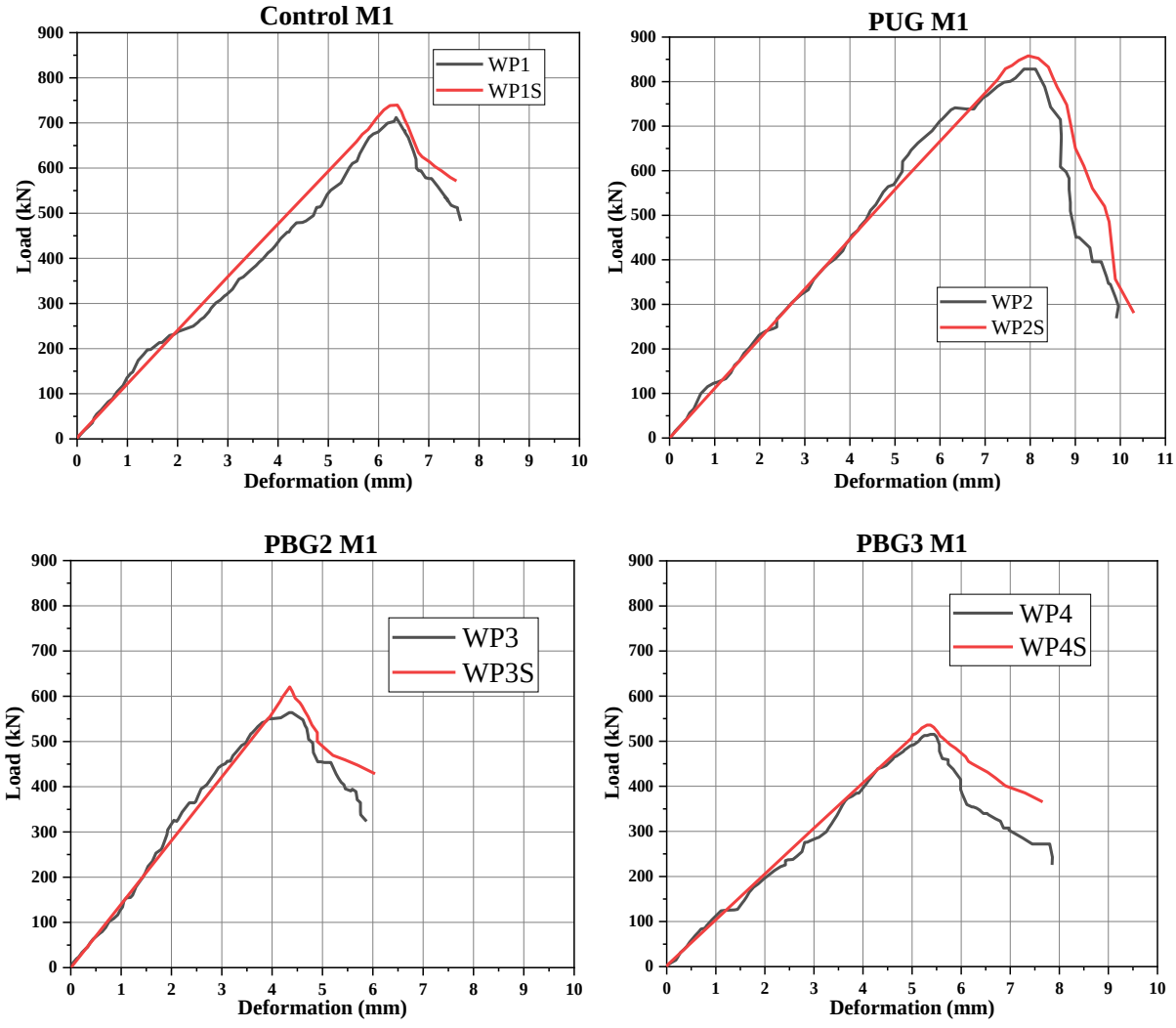

Figure 6. 23: Experimental results vs numerical modelling under axial compression loading for mix M1; (a) Control specimen; (b) PUG; (c) PBG2; (d) PBG3

similar manner as the specimen WP1. The peak loads achieved in the WP1S specimen is 4% more than the specimen WP1 (Figure 6.13 (a)). The post elastic behaviour showed that the

panel failed at the ultimate load of 580kN whereas the experimental specimen failed at the load of 480 kN. This can be said that the software analysis is showing 20% less ductile nature in post elastic region when compared with the experimental results. Specimen WP2S (Figure 6.13 (b)) showed the best results in terms of deformation and the behaviour at each instant when compared with the experimental results. WP3S and WP4S showed similar results as they both are incorporated with similar material and due to the less area of bond in between the wythe layers, it confirmed the experimental results (Figure 6.13 (c) Figure 6.13 (d)).

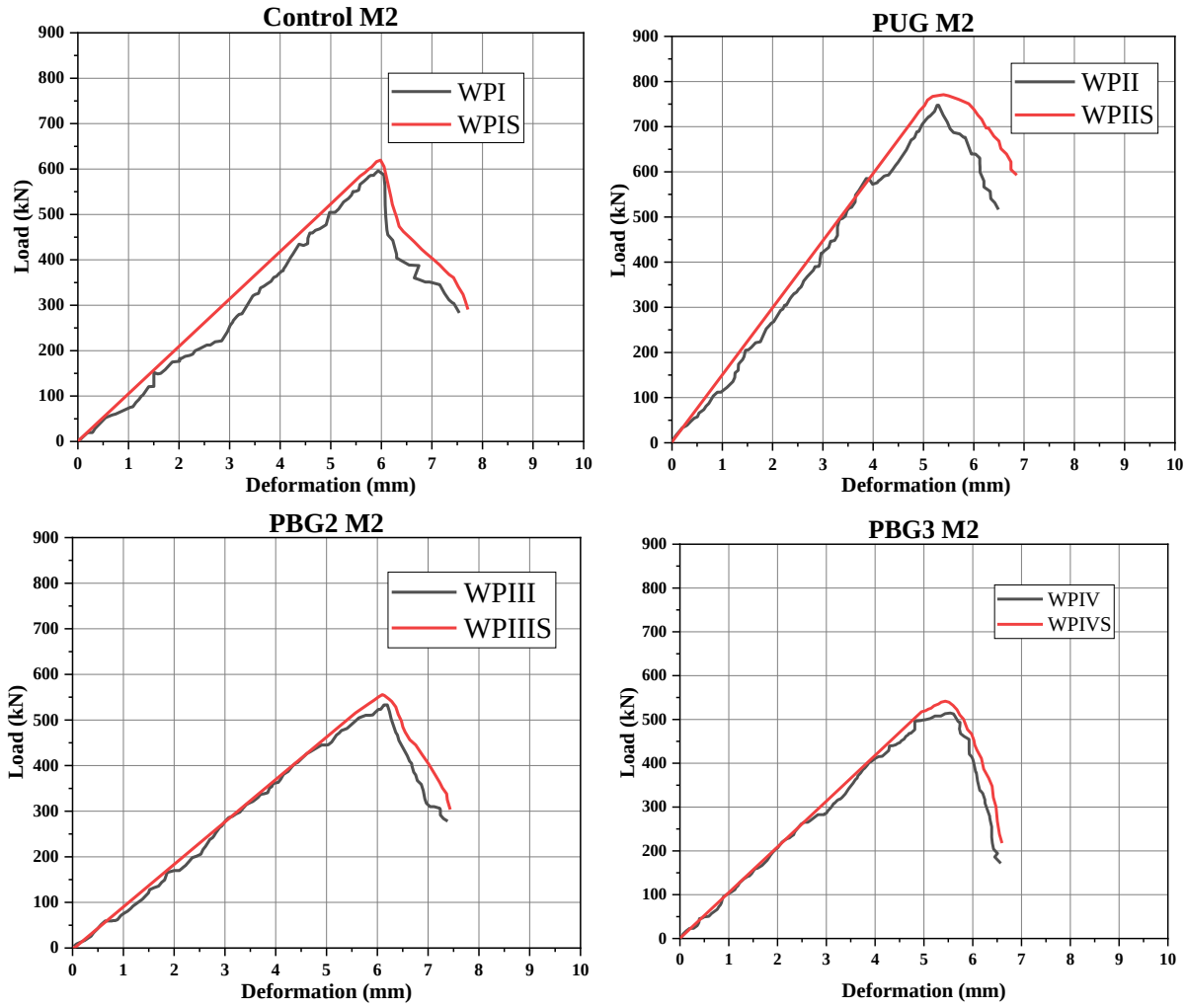

Figure 6. 24: Experimental results vs numerical modelling under axial compression loading for mix M2; (a) control specimen; (b) PUG; (c) PBG2; (d) PBG3

For the mix M2, it can be clearly seen that due to the less compressive strength of the micro concrete the control specimen showed the peak load value less than the mix M1 control specimen. WPIS specimen showed very less non-linear behaviour as the graph is almost a straight line but has been able to show the similar nature in post elastic region (Figure 6.14(a)).

Specimen WPIIS showed the maximum peak load among all the mix M2 specimen. This is due to the stiff plastic material of the PUG which added to its strength and gave an 6% increase in peak load (Figure 6.14(b)). The experimental results indicate that Specimen WP IIIS and WP IVS exhibit a high level of agreement.

Closing Remarks

This comparative analysis aims to validate and enhance numerical modelling methodologies for concrete sandwich panels. By improving the dependability of these techniques in forecasting structural performance, it will provide guidance for future design and analysis practices.

Chapter 7

Conclusions

This thesis investigates the performance of forty eight CSP specimens incorporated with various geogrid materials i.e. plastic and polyester geogrid (Sgi200 and Sgi300) under out of plane (flexure), horizontal in-plane shear loading and compression testing. Also, three 2D RC frames have also been tested under quasi static loading. A comparison of brick masonry as infill wall has been done with the concrete sandwich panel as infill wall. One of the 2D RC frame is also constructed with an opening in the concrete sandwich panel and the behaviour of the same has been noted. FEM analysis has also been performed to validate the experimental results of out-of-plane, in-plane and axial compression testing.

Behaviour of CSP under flexure loading

The geo-grid as additional reinforcement improves the specimen strength and also helps to increase deforming capability. The observed crack failure pattern clearly shows the tension resistant capacity effect of geo-grids. SPSgi200 specimen showed remarkable improvement in post-yield behavior and a 36.8% increase was observed in comparison to the peak load of SPC1. Moreover, the highest energy dissipation was also observed which is supported by the degree of composite action value i.e. 13.44 (highest among all specimen)

SPSgi300 showed a drastic change in post-yield behaviour i.e. in terms of ductility factor, it behaved 2.71 times better than SPC1. All specimen cast using M2 behaved well in the post elastic region which suggests that these specimens are more resilient. • SP1Sgi200 showed the highest energy dissipation capability (i.e. 1900 kN.mm) among all specimen, which again indicates the ductility behaviour is also more than other specimen.

The replacement of fine sand with stone dust in mix M1 showed the improvement in compressive strength results and M1 performed better than M2.

Behaviour of CSP under diagonal shear loading

The capacity for deformation that is perpendicular to the load has been improved by PUG. In the horizontal direction, this is also ensured by the size of the fracture width. The results were superior for the specimens containing PUG compared to those containing PBG2

and PBG3. Because of the usage of plastic uniaxial geogrid, the load bearing capacity in in-plane shear has greatly risen by 26%, and the shear capacity has increased by 13.7%.

It has been determined that specimens containing PBG2 and PBG3 are unable to produce results that are superior to those of the control specimen. As soon as the vertical crack propagated from top to bottom (when the max stress was achieved), the failure became brittle. Specimen containing polyester biaxial geogrid (PBG2 and PBG3) behaved in a non-composite manner. This is due to the width of strip and spacing between the strips of polyester biaxial geogrid. Hence partial debonding of the wythe within a wythe has been encountered.

The implementation of a geogrid (PUG) as additional reinforcement has been observed to enhance the strength and deformability of the specimen. The crack failure pattern that was observed provides evidence for the impact of geogrids' tension resistance capacity.

The observed increase in the energy dissipation capacity value indicates that the post-elastic behaviour of the M2 mix specimen has been augmented as a result of the inclusion of PUG. The specimens containing the polyester biaxial geogrid exhibited a significant alteration in post-yield behaviour. Specifically, the ductility factor was observed to be 43% superior to the control for M2 mix.

Behaviour of CSP under axial compression loading

The panel consisting of PUG gave the CSP enhanced values of peak load, whereas the addition of the PBG enhanced the deformation capacity of the wall panels. It has also been found that mix M1 played a significant role in enhancing the strength of the wall panels. In case of mix M2, the specimen containing PUG out performed its control specimen. On comparing both the control specimen (M1 and M2) it has been found that the specimen WP1 made with M1 showed better peak strength. The value of energy dissipation also approves that the specimen made with M1 have failed at higher dissipation energy values.

Behaviour of CSP as infill wall in 2D RC frame

The RC frame with the concrete sandwich panel exhibited the highest lateral strength. This has been the case for imposed lateral drifts that were greater than 0.5 % (deflection of 10.3 mm). 30% more strength than RC frame having brick masonry as infill. In terms of both lateral load bearing capacity and energy dissipation, the proposed concrete sandwich panel with and without opening, proved to be the superior alternative to the RC frame with conventional brick masonry infill wall.

Flexural cracks have been observed in the columns of the reinforced concrete frames with concrete sandwich panels, indicating the progression of damage. The employment of concrete sandwich panel resulted in increased damage, such as wider cracks and spalling of concrete cover, it also yielded a more dispersed pattern of cracks, with cracking propagation occurring in both beam and column members.

Behaviour of CSP simulated by FEA

Finite Element Method (FEM) analysis aligned well with experimental results, though some specimens exhibited debonding during testing. Overall, FEM results were consistently 10-12% higher than experimental values, indicating a trend of enhanced numerical simulation outcomes. The post-elastic behaviour demonstrated enhanced ductility in both experimental and numerical simulations, emphasizing the effectiveness of the proposed modifications in improving specimen performance.

Closing Remarks

The findings of this investigation on concrete sandwich panels indicate that this innovative method has the potential to serve as a viable alternative to traditional construction techniques. Further comprehensive testing and procedural analysis are required to enhance comprehension of the subject matter. The future entails the substitution of outdated construction methods with modern ones, and this study on the "Behaviour of Structurally Insulated Panels" represents a tiny advancement towards this goal.

Future scope

This research can be considered as picking up of a few stones near the sea, a whole sea of possibilities is still yet to be explored keeping in mind different parameters and materials and different loading conditions in the field of structurally insulated panels as it is going to replace the conventional . Further the numerical analysis of this these concrete sandwich panels can be very useful, a small analysis has been performed in this study using ANSYS. The addition of geogrids enhanced the load bearing and deformation capacity, but the economic consideration of such interdisciplinary fields of incorporation of material used in soil stabilization and using it in structure needs a detailed study, which can also be a part of future scope.

References

Ahmad, A., & Singh, Y. (2021). In-plane behaviour of expanded polystyrene core reinforced concrete sandwich panels. *Construction and Building Materials*, *269*, 121804. https://doi.org/10.1016/j.conbuildmat.2020.121804

Akhoundi, F., Vasconcelos, G., Lourenço, P., Silva, L. M., Cunha, F., & Fangueiro, R. (2018). In-plane behavior of cavity masonry infills and strengthening with textile reinforced mortar. *Engineering Structures*, *156*(December 2017), 145–160. https://doi.org/10.1016/j.engstruct.2017.11.002

Almasri, R., Alardhi, A., & Dilshad, S. (2021). Investigating the Impact of Integration the Saudi Code of Energy Conservation with the Solar PV Systems in Residential Buildings. *Sustainability*, *13*(6), 3384. https://doi.org/10.3390/su13063384

Arslan, M. E., Aykanat, B., Ayyıldız, M. A., Subaşı, S., & Maraşlı, M. (2022). Effects of basalt and glass fiber composites usage for strengthening on the cyclic behavior of brick infill walls. *Journal of Building Engineering*, *52*(January). https://doi.org/10.1016/j.jobe.2022.104405

Asteris, P. G. (2003). Lateral Stiffness of Brick Masonry Infilled Plane Frames. *Journal of Structural Engineering*, *129*(8), 1071–1079. https://doi.org/10.1061/(ASCE)0733-9445(2003)129:8(1071)

ASTM A370. (2004). Standard Test Methods and Definitions for Mechanical Testing of Steel Products. *ASTM International*, *01.03*(Rapproved), 1–48. https://doi.org/10.1520/A0370-16.2

ASTM E 519-02. (2002). Standard Test Method for Diagonal Tension (Shear) in Masonry Assemblages. *American Society for Testing Materials*, 5. https://doi.org/10.1520/E0519

ASTM E72. (2002). *Standard Test Methods of Conducting Strength Tests of Panels for Building*.

ASTM E519. (2020). *Standard Test Method for Diagonal Tension (Shear) in Masonry Assemblages*. 1–5. www.astm.org,

Bastin, D. R. A., & Sharma, U. K. (2017). A study on different techniques of restoration of fire damaged reinforced concrete flexural members. *Journal of Structural Fire Engineering*, *8*(2). https://doi.org/10.1108/JSFE-03-2017-0026

Behera, B., & Nanda, R. P. (2021). In-plane shear strengthening of brick masonry panel with geogrid reinforcement embedded in bed and bed-head joints mortar. *Engineering Structures*, *227*. https://doi.org/10.1016/j.engstruct.2020.111411

Benayoune, A. (2007). *Response of pre-cast reinforced composite sandwich panels to axial loading*. *21*, 677–685. https://doi.org/10.1016/j.conbuildmat.2005.12.011

BIS 383. (2016). *Coarse and Fine Aggregate for Concrete - Specification* (Issue January).

BIS 516. (1959). *Indian Standard Methods of Tests for Strength of Concrete*.

BIS 1124. (1974). *Indian Standard Method of Test for Determination of Water Absorption, Apparent Specific Gravity and Porosity of Natural Building Stones.*

Brodsky, A., & Yankelevsky, D. Z. (2017). Resistance of reinforced concrete frames with masonry infill walls to in-plane gravity loading due to loss of a supporting column. *Engineering Structures*, *140*, 134–150. https://doi.org/10.1016/j.engstruct.2017.02.061

Carbonari, G., Cavalaro, S. H. P., Cansario, M. M., & Aguado, A. (2013). *Experimental and analytical study about the compressive behavior of eps sandwich panels*. *63*, 393–402. https://doi.org/10.3989/mc.2013.01812

Chen, A., Norris, T. G., Hopkins, P. M., & Yossef, M. (2015). Experimental investigation and finite element analysis of flexural behavior of insulated concrete sandwich panels with FRP plate shear connectors. *Engineering Structures*, *98*, 95–108. https://doi.org/10.1016/j.engstruct.2015.04.022

Cheng, S., Yin, S., & Jing, L. (2020). Comparative experimental analysis on the in-plane shear performance of brick masonry walls strengthened with different fiber reinforced materials. *Construction and Building Materials*, *259*, 120387. https://doi.org/10.1016/j.conbuildmat.2020.120387

Chithambaram, S. J., & Kumar, S. (2017). Flexural behaviour of bamboo based ferrocement slab panels with flyash. *Construction and Building Materials*, *134*, 641–648. https://doi.org/10.1016/j.conbuildmat.2016.12.205

Choi, K.-B., Choi, W.-C., Feo, L., Jang, S.-J., & Yun, H.-D. (2015). In-plane shear behavior of insulated precast concrete sandwich panels reinforced with corrugated GFRP shear connectors. *Composites Part B: Engineering*, *79*, 419–429. https://doi.org/10.1016/j.compositesb.2015.04.056

CoDyre, L., & Fam, A. (2017). Axial Strength of Sandwich Panels of Different Lengths with Natural Flax-Fiber Composite Skins and Different Foam-Core Densities. *Journal of Composites for Construction*, *21*(5). https://doi.org/10.1061/(ASCE)CC.1943-5614.0000820

Colombo, I. G., Colombo, M., di Prisco, M., & Pouyaei, F. (2018). Analytical and numerical prediction of the bending behaviour of textile reinforced concrete sandwich beams. *Journal of Building Engineering*, *17*, 183–195. https://doi.org/10.1016/j.jobe.2018.02.012

Daniel Ronald Joseph, J., Prabakar, J., & Alagusundaramoorthy, P. (2019). Flexural Behavior of Concrete Sandwich Panels Under Punching Load and Four-Point Bending—Experimental and Analytical Study. In *Recent Advances in Structural Engineering, Volume 2: Select Proceedings of SEC 2016* (pp. 771–781). Springer. https://doi.org/10.1007/978-981-13-0365-4_66

Dautaj, A. D., Kadiri, Q., & Kabashi, N. (2018). Experimental study on the contribution of masonry infill in the behavior of RC frame under seismic loading. *Engineering Structures*, *165*(March), 27–37. https://doi.org/10.1016/j.engstruct.2018.03.013

de Sousa, C., Barros, J. A. O., & Correia, J. R. (2022). In-plane cyclic behaviour of RC frames strengthened with composite sandwich panels. *Engineering Structures*, *251*(November 2021), 113529. https://doi.org/10.1016/j.engstruct.2021.113529

Dey, V., Zani, G., Colombo, M., Di Prisco, M., & Mobasher, B. (2015). Flexural impact response of textile-reinforced aerated concrete sandwich panels. *Materials and Design*, *86*, 187–197. https://doi.org/10.1016/j.matdes.2015.07.004

Dong, Z., Deng, M., Dai, J., & Ma, P. (2021). Diagonal compressive behavior of unreinforced masonry walls strengthened with textile reinforced mortar added with short PVA fibers. *Engineering Structures*, *246*(February), 113034. https://doi.org/10.1016/j.engstruct.2021.113034

Einea, A. (1992). *Structural and thermal efficiency of precast concrete sandwich panel systems*. The University of Nebraska-Lincoln.

Einea, A., Salmon, D. C., Tadros, M. K., & Culp, T. (1994). A new structurally and thermally efficient precast sandwich panel system. *PCI Journal*, *39*(4).

Ferreira, S., Morais, M., Costa, V., Velosa, A., Vela, G., Teles, J., & Pereira, T. (2023). Modular sandwich panel system for non-loadbearing walls – Experimental mechanical, fire and acoustic testing. *Journal of Building Engineering*, *78*. https://doi.org/10.1016/j.jobe.2023.107642

Frankl, B. A. (2008). *Structural Behavior of Precast Prestressed Concrete Sandwich Panels Reinforced with CFRP Grid*.

Furtado, A., Rodrigues, H., & Arêde, A. (2015). Modelling of masonry infill walls participation in the seismic behaviour of RC buildings using OpenSees. *International Journal of*

Advanced Structural Engineering, *7*(2), 117–127. https://doi.org/10.1007/s40091-015-0086-5

Gara, F., Ragni, L., Roia, D., & Dezi, L. (2012). Experimental tests and numerical modelling of wall sandwich panels. *Engineering Structures*, *37*, 193–204. https://doi.org/10.1016/j.engstruct.2011.12.027

Ha, S. K., Yu, S. Y., & Kim, J. S. (2018). Experimental Study on Existing Reinforced Concrete Frames Strengthened by L-type Precast Concrete Wall Panels to Earthquake-Proof Buildings. *KSCE Journal of Civil Engineering*, *22*(9), 3579–3591. https://doi.org/10.1007/s12205-018-1197-x

Hafiza, E., Sameen, S., & Rahman, T. (2015). A Review on construction process of Ferrocement sandwich panel: Instigating an orderly approach in Bangladesh. *A Rev. Constr. Process Ferro Cem. Sandw. Panel Instigating an Orderly Approach Bangladesh*, *3*.

Halder, L., Chandra Dutta, S., Sharma, R. P., & Bhattacharya, S. (2021). Lessons learnt from post-earthquake damage study of Northeast India and Nepal during last ten years: 2021 Assam earthquake, 2020 Mizoram earthquake, 2017 Ambasa earthquake, 2016 Manipur earthquake, 2015 Nepal earthquake, and 2011 Sikkim earthquake. *Soil Dynamics and Earthquake Engineering*, *151*(September), 106990. https://doi.org/10.1016/j.soildyn.2021.106990

Hamed, E. (2016). Modeling, analysis, and behavior of load-carrying precast concrete sandwich panels. *Journal of Structural Engineering*, *142*(7), 04016036.

Hashemi, S. J. (2017). Effect of Concrete Sandwich Infill Panels with Opening on In-plane Behaviour of Steel Frames. *Concrete Research*, *10*(3), 5–18.

Hashemi, S. J., Razzaghi, J., Moghadam, A. S., & Lourenço, P. B. (2018a). Cyclic testing of steel frames infilled with concrete sandwich panels. *Archives of Civil and Mechanical Engineering*, *18*(2), 557–572. https://doi.org/10.1016/j.acme.2017.10.007

Hashemi, S. J., Razzaghi, J., Moghadam, A. S., & Lourenço, P. B. (2018b). Cyclic testing of steel frames infilled with concrete sandwich panels. *Archives of Civil and Mechanical Engineering*, *18*(2), 557–572. https://doi.org/10.1016/j.acme.2017.10.007

Hodicky, K., Sopal, G., Rizkalla, S., Hulin, T., & Stang, H. (2015). Experimental and numerical investigation of the FRP shear mechanism for concrete sandwich panels. *Journal of Composites for Construction*, *19*(5), 04014083.

Hopkins, P. M., Chen, A., & Yossef, M. (2017). Static and dynamic analyses of insulated concrete sandwich panels using a unified non-linear finite element model. *Engineering Structures*, *132*, 249–259.

Huang, C. J., Qian, C. H., & Song, X. B. (2020). Explicit nonlinear and plastic analysis model of steel–concrete–steel sandwich panels. *Journal of Constructional Steel Research*, *168*. https://doi.org/10.1016/j.jcsr.2019.105872

Humar, J. M., Lau, D., & Pierre, J. R. (2001). Performance of buildings during the 2001 Bhuj earthquake. *Canadian Journal of Civil Engineering*, *28*(6), 979–991. https://doi.org/10.1139/cjce-28-6-979

IS 456. (2000). *Plain and Reinforced Concrete - Code of Practice*.

IS : 2386 (Part I). (1963). Indian Method of test for aggregate for concrete. Part I - Particle size and shape. In *Indian Standards*.

IS 8112. (2013). Specification for 43 grade Ordinary Portland Cement. *Bureau of Indian Standards,New Delhi*, 17.

IS 10262. (2019). *Indian Standard Guidelines for concrete mix design proportioning* (Issue January).

IS 13935. (2009). *Seismic Evaluation, Repair and Strengthening of Masonry Buildings — Guidelines*.

IS13162. (1992). *Geotextiles- Method of test*.

Jagadish, K. S., Raghunath, S., & Nanjunda Rao, K. S. (2003). Behaviour of masonry structures during the Bhuj earthquake of January 2001. *Proceedings of the Indian Academy of Sciences, Earth and Planetary Sciences*, *112*(3), 431–440. https://doi.org/10.1007/BF02709270

Jensen, K., Al-Rubaye, S., Thomas, R. J., & Maguire, M. (2020). Mechanics-Based model for elastic Bending, Axial, thermal Deformations, and asymmetry of concrete composite sandwich wall panels. *Structures*, *23*, 459–471. https://doi.org/10.1016/j.istruc.2019.11.004

Jung, W. Y., & Aref, A. J. (2005). Analytical and numerical studies of polymer matrix composite sandwich infill panels. *Composite Structures*, *68*(3), 359–370. https://doi.org/10.1016/j.compstruct.2004.04.005

Kang, W.-H., & Kim, J. (2016). Reliability-based flexural design models for concrete sandwich wall panels with continuous GFRP shear connectors. *Composites Part B: Engineering*, *89*, 340–351.

Khatibi, S. H., Ghohani Arab, H., & Miri, M. (2023). The behavior of steel-concrete-steel sandwich composite beams with box-profile shear connectors: Experimental and numerical. *Structures*, *54*, 644–656. https://doi.org/10.1016/j.istruc.2023.05.054

Lameiras, R., Barros, J., Valente, I. B., & Azenha, M. (2013). Development of sandwich panels combining fibre reinforced concrete layers and fibre reinforced polymer connectors. Part I: Conception and pull-out tests. *Composite Structures*, *105*, 446–459.

Latour, M., D'Aniello, M., Landolfo, R., & Rizzano, G. (2021). Experimental and numerical study of double-skin aluminium foam sandwich panels in bending. *Thin-Walled Structures*, *164*. https://doi.org/10.1016/j.tws.2021.107894

Lee, A. J., Kelly, H., Jagoda, R., Rosenfeld, A., Stubee, E., Colaco, J., Gadgil, A., Akbari, H., Norford, L., & Van Burik, H. (2006). Affordable, safe housing based on expanded polystyrene (EPS) foam and a cementitious coating. *Journal of Materials Science*, *41*, 6908–6916.

Leng, Y.-B., & Song, X.-B. (2017). Flexural and shear performance of steel-concrete-steel sandwich slabs under concentrate loads. *Journal of Constructional Steel Research*, *134*, 38–52.

Mackechnie, J. R., Park, Y. S., Saevarsdottir, T., & Bellamy, L. (2007). Variable density precast concrete panel development. *23rd Biennial Conference of the Concrete Institute of Australia, Adelaide*, 795–801.

Manos, G. C., Melidis, L., Katakalos, K., Kotoulas, L., Anastasiadis, A., & Chatziastrou, C. (2021). Masonry panels with external thermal insulation subjected to in-plane diagonal compression. *Case Studies in Construction Materials*, *14*, e00538. https://doi.org/10.1016/j.cscm.2021.e00538

Manual for Expanded Polystyrene (EPS) Core Panel System and its field Application Sponsored By Ministry of Housing and Urban Poverty Alleviation , Government of India. (2017). *Ministry of Housing and Urban Poverty Alleviation, Government of India*, *June*.

Milheiro, J., Rodrigues, H., & Arêde, A. (2016). Evaluation of the contribution of masonry infill panels on the seismic behaviour of two existing reinforced concrete buildings. *KSCE Journal of Civil Engineering*, *20*(4), 1365–1374. https://doi.org/10.1007/s12205-015-0112-y

Mohamad, N., Wan, G., Abdullah, R., Aziz, A., Samad, A., & Mendis, P. (2017). Structural performance of FCS wall subjected to axial load. *Construction and Building Materials*, *134*, 185–198. https://doi.org/10.1016/j.conbuildmat.2016.12.133

Mousa, M. A., & Uddin, N. (2012). Structural behavior and modeling of full-scale composite structural insulated wall panels. *Engineering Structures*, *41*, 320–334.

Mugahed Amran, Y. H., Rashid, R. S. M., Hejazi, F., Abang Ali, A. A., Safiee, N. A., & Bida, S. M. (2018). Structural Performance of Precast Foamed Concrete Sandwich Panel Subjected to Axial Load. *KSCE Journal of Civil Engineering*, *22*(4), 1179–1192. https://doi.org/10.1007/s12205-017-1711-6

N. Jayaramappa. (2015). Study on the Behaviour of RC Bare Frame for Lateral Load. *International Journal of Engineering Research And*, *V4*(05). https://doi.org/10.17577/IJERTV4IS050519

Ngo, D. Q., & Nguyen, H. C. (2023). Experimental and numerical investigations of textile-reinforced concrete thin-wall panel bolted connections. *Case Studies in Construction Materials*, *19*. https://doi.org/10.1016/j.cscm.2023.e02229

O'Hegarty, R., Kinnane, O., Grimes, M., Newell, J., Clifford, M., & West, R. (2021). Development of thin precast concrete sandwich panels: Challenges and outcomes. *Construction and Building Materials*, *267*. https://doi.org/10.1016/j.conbuildmat.2020.120981

Padalu, P. K. V. R., Singh, Y., & Das, S. (2018). Experimental investigation of out-of-plane behaviour of URM wallettes strengthened using welded wire mesh. *Construction and Building Materials*, *190*, 1133–1153. https://doi.org/10.1016/j.conbuildmat.2018.09.176

Pantelides, C. P., Surapaneni, R., & Reaveley, L. D. (2008). Structural performance of hybrid GFRP/steel concrete sandwich panels. *Journal of Composites for Construction*, *12*(5), 570–576.

Proença, M., Neves e Sousa, A., Garrido, M., & Correia, J. R. (2020). Acoustic performance of composite sandwich panels for building floors: Experimental tests and numerical-analytical simulation. *Journal of Building Engineering*, *32*. https://doi.org/10.1016/j.jobe.2020.101751

Raj, S., Kumar, V. R., Kumar, B. H. B., Gopinath, S., & Iyer, N. R. (2015). Flexural studies on basalt fiber reinforced composite sandwich panel with profile sheet as core. *Construction and Building Materials*, *82*, 391–400.

Rao, G. A., & Poluraju, P. (2020). Cyclic behaviour of precast reinforced concrete sandwich slender walls. *Structures*, *28*, 80–92. https://doi.org/10.1016/j.istruc.2020.08.046

Ricci, I., Palermo, M., Gasparini, G., Silvestri, S., & Trombetti, T. (2013). Results of pseudo-static tests with cyclic horizontal load on cast in situ sandwich squat concrete walls. *Engineering Structures*, *54*, 131–149.

Rissman, J., Bataille, C., Masanet, E., Aden, N., Morrow, W. R., Zhou, N., Elliott, N., Dell, R., Heeren, N., Huckestein, B., Cresko, J., Miller, S. A., Roy, J., Fennell, P., Cremmins, B., Koch Blank, T., Hone, D., Williams, E. D., de la Rue du Can, S., … Helseth, J. (2020). Technologies and policies to decarbonize global industry: Review and assessment of mitigation drivers through 2070. *Applied Energy*, *266*(November 2019), 114848. https://doi.org/10.1016/j.apenergy.2020.114848

Ronald, J. D., Prabakar, J., & Alagusundaramoorthy, P. (2019). Experimental studies on through-thickness shear behavior of EPS based precast concrete sandwich panels with truss shear connectors. *Composites Part B*, *166*(November 2018), 446–456. https://doi.org/10.1016/j.compositesb.2019.02.030

Roosta, S., & Liu, Y. (2021). Behavior of concrete masonry infills bounded by masonry frames subjected to in-plane lateral loading – Experimental study. *Engineering Structures*, *247*(September), 113153. https://doi.org/10.1016/j.engstruct.2021.113153

Sadek, H., & Lissel, S. (2013). Seismic performance of masonry walls with GFRP and Geogrid Bed joint reinforcement. *Construction and Building Materials*, *41*, 977–989. https://doi.org/10.1016/j.conbuildmat.2012.07.005

Sagar, S. L., Singhal, V., & Rai, D. C. (2019). In-Plane and Out-of-Plane Behavior of Masonry-Infilled RC Frames Strengthened with Fabric-Reinforced Cementitious Matrix. *Journal of Composites for Construction*, *23*(1). https://doi.org/10.1061/(asce)cc.1943-5614.0000905

Sakr, M. A., El-Khoriby, S. R., Seleemah, A. A., Aboelnour, M. M., & Osama, B. (2021a). Experimental and numerical investigation on cyclic behavior of masonry infilled RC frames retrofitted with partially bonded CFRP strips. *Structures*, *33*(April), 2238–2252. https://doi.org/10.1016/j.istruc.2021.05.087

Sakr, M. A., El-Khoriby, S. R., Seleemah, A. A., Aboelnour, M. M., & Osama, B. (2021b). Experimental and numerical investigation on cyclic behavior of masonry infilled RC frames retrofitted with partially bonded CFRP strips. *Structures*, *33*, 2238–2252. https://doi.org/10.1016/j.istruc.2021.05.087

Salmon, D. C., & Einea, A. (1995). Partially Composite Sandwich Panel Deflections. *Journal of Structural Engineering*, *121*(4), 778–783. https://doi.org/10.1061/(ASCE)0733-9445(1995)121:4(778)

Serpilli, M., Clementi, F., & Lenci, S. (2021a). An experimental and numerical study on the in-plane axial and shear behavior of sprayed in-situ concrete sandwich panels. *Engineering Structures*, *232*. https://doi.org/10.1016/j.engstruct.2020.111814

Serpilli, M., Clementi, F., & Lenci, S. (2021b). An experimental and numerical study on the in-plane axial and shear behavior of sprayed in-situ concrete sandwich panels. *Engineering Structures*, *232*. https://doi.org/10.1016/j.engstruct.2020.111814

Shams, A., Stark, A., Hoogen, F., Hegger, J., & Schneider, H. (2015). Innovative sandwich structures made of high performance concrete and foamed polyurethane. *Composite Structures*, *121*, 271–279.

Shanker Singh, V., & Narayan Pandey, D. (2012). *Sustainable Housing: Balancing Environment with Urban Growth in India Climate Change and CDM Cell Rajasthan State Pollution Control Board Jaipur*. www.rpcb.nic.in

Shelton, J. S., Y, V. N., A, A. S., & Daniel, C. (2021). Experimental and analytical investigation of geo-grid confined RC beams with glass fiber reinforced concrete. *Structures*, *34*(June), 487–497. https://doi.org/10.1016/j.istruc.2021.08.002

Smakosz, Ł., & Tejchman, J. (2014). Evaluation of strength, deformability and failure mode of composite structural insulated panels. *Materials & Design (1980-2015)*, *54*, 1068–1082. https://doi.org/10.1016/j.matdes.2013.09.032

Spadea, G., Bencardino, F., & Swamy, R. N. (1998). Structural Behavior of Composite RC Beams with Externally Bonded CFRP. *Journal of Composites for Construction*, *2*(3), 132–137. https://doi.org/10.1061/(asce)1090-0268(1998)2:3(132)

Tomlinson, D., & Fam, A. (2016a). Analytical approach to flexural response of partially composite insulated concrete sandwich walls used for cladding. *Engineering Structures*, *122*, 251–266. https://doi.org/10.1016/j.engstruct.2016.04.059

Tomlinson, D., & Fam, A. (2016b). Combined Loading Behavior of Basalt FRP–Reinforced Precast Concrete Insulated Partially-Composite Walls. *Journal of Composites for Construction*, *20*(3). https://doi.org/10.1061/(asce)cc.1943-5614.0000611

United Nations. (2022, June 30). *India's urban population to stand at 675 million in 2035, behind China's 1 billion: U.N.*

Vishnu, B., Chauhan, A., Roy, D., & Sharma, U. K. (2017). Influence of various exposure conditions on the structural performance of sandwich wall panels. *Indian Concrete Journal*.

Willam, K. J., & Warnke, E. P. (1975). Constitutive models for the triaxial behavior of concrete. *Proceedings of the International Assoc. for Bridge and Structural Engineering*, *19*, 1–30.

World Bank. (2023). *India Urban Population 1960-2024*. https://www.macrotrends.net/countries/IND/india/urban-population#:~:text=Aggregation%20of%20urban%20and%20rural,a%202.15%25%20increase%20from%202020

Ye, X., Zhao, C., He, K., Zhou, L., Li, X., & Wang, J. (2021). Blast behaviors of precast concrete sandwich EPS panels: FEM and theoretical analysis. *Engineering Structures*, *226*. https://doi.org/10.1016/j.engstruct.2020.111345

Yuan, P., Xu, S., Liu, J., Su, Y., & Wu, C. (2023). Experimental and numerical study of blast resistance of geopolymer based high performance concrete sandwich walls incorporated with metallic tube core. *Engineering Structures*, *278*. https://doi.org/10.1016/j.engstruct.2022.115505

Zhao, C., Zhang, L., He, K., Chen, Y., & Li, X. (2023). Experimental and numerical study on the blast resistance of C-shaped doubled steel concrete slab (C-DSCS) with L-shaped connectors. *Engineering Structures*, *295*. https://doi.org/10.1016/j.engstruct.2023.116900

Zoppo, M. Del, Ludovico, M. Di, Balsamo, A., & Prota, A. (2019). In-plane shear capacity of tuff masonry walls with traditional and innovative Composite Reinforced Mortars (CRM). *Construction and Building Materials*, *210*, 289–300. https://doi.org/10.1016/j.conbuildmat.2019.03.133